Matter under Extreme conditions and Transport Coefficients of Hot and Dense matter

A thesis submitted in partial fulfilment of
the requirements for the degree of

Doctor of Philosophy

by

Aman Abhishek

(Roll. No. 14330001)

Under the supervision of

Prof. Hiranmaya Mishra

Senior Professor
Theoretical Physics Division
Physical Research Laboratory, Ahmedabad, India.

DISCIPLINE OF PHYSICS
INDIAN INSTITUTE OF TECHNOLOGY GANDHINAGAR
2019

to
My Family

Declaration

I declare that this written submission represents my ideas in my own words and where others' ideas or words have been included, I have adequately cited and referenced the original sources. I also declare that I have adhered to all principles of academic honesty and integrity and have not misinterpreted or fabricated or falsified any idea/data/fact/source in my submission. I understand that any violation of the above will be cause of disciplinary action by the Institute and can also evoke penal action from the sources which have thus not been properly cited or from whom proper permission has not been taken when needed.

Signature

Name: Aman Abhishek

(Roll No : 14330001)

Date:

Certificate

It is certified that the work contained in the thesis titled **“Matter under Extreme Conditions and Transport Coefficients of Hot and Dense Matter”** by Mr. Aman Abhishek(Roll No. 14330001), has been carried out under my supervision and that this work has not been submitted elsewhere for a degree.

Senior Prof. Hiranmaya Mishra,
Theoretical Physics Division,
Physical Research Laboratory,
Ahmedabad, India
(Thesis Supervisor)

Date:

Thesis Approval

The Thesis entitled

Matter under Extreme Conditions and Transport Coefficients of Hot and Dense Matter

by

Aman Abhishek
(Roll No. 14330001)

is approved for the degree of
Doctor of Philosophy

Examiner	**Examiner**
Supervisor	**Chairmain**

Date: ____________________
Place: ____________________

Acknowledgements

Several people have helped and supported me in doing the work towards this thesis. I would like to extend my gratitude and thank those people without whom this thesis would not have been possible.

First and foremost, I would like to thank my research supervisor Prof. Hiranmaya Mishra who introduced me to the very interesting field of Strong interactions and guided me through these five years. His expertise has helped me understand the subject with clarity and motivated me to pursue the research with curiosity. I am very grateful to him for the constant motivation, dedication, guidance, advice and help without which I would not have been able to do the research. His understanding of my academic and personal life helped me manage my work in a better way.

Besides my supervisor, I would like to thank my doctoral committee members Prof. Jitesh Bhatt and Prof. Namit Mahajan whose wider perspective as well as support and ecouragement helped me immensely in imporving my research work.

I am also very grateful to my collaborators Prof. Gastao Krein, Dr. Sabyasachi Ghosh, Dr. Santosh Kumar Das, Dr. Arpan Das, Ms. Pracheta Singha, Mr. Balbeer Singh and Mr. Deepak. It has been a pleasure and learning experience in discussing and working on physics with them.

I would also like to express my sincere thanks to the Director of PRL, the Dean, the Academic Committee members and Prof. Hiranmaya Mishra who as area chairman helped me in providing the necessary facilities to carry out the research work. I am also thankful to the head of the academic services Dr. Bhushit G. Vaishnav for his constant help.

I express my sincere gratitude to all the faculty members who had taught me during the course work including Prof. R. Rengarajan, Prof. J. Banerji, Prof. R. P. Singh, Prof. D. Angom, Dr. N. Mahajan, Dr. B. K. Sahoo, Dr. G. K. Samanta, Prof. R. Sekar, Dr. D. Chakrabarty, Dr. L. K. Sahu, Prof. P. Venkatakrishnan, Prof. N. Srivastava, Prof. S. K. Mathew, Dr. R. Bhattacharyya, Dr. B. Sivaraman and Dr. M. K. Srivastava. I would also like to thank Prof. S. Ganesh from astronomy division with whom I had done my project during the second semster of my coursework. I would also like to thank other professors from the theory division Prof. J. R. Bhatt, Dr. N. Singh and Dr. K. Patel for the useful physics discussions that we had during various seminars. I would also like to express my sincere gratitude to my teacher N. Islam who motivated me to study science.

I am thankful to all the staff members of our division, library, computer center, adminis- tration, dispensary, canteen, workshop and maintenance section of PRL for their assistance and support. I also take this moment to express my gratitude to the academic and administrative staff members of IIT Gandhinagar for helping with the registration procedures.

I thank my seniors Dr. Guruprasad Kadam, Dr. Bhaswar Chatterjee and Dr. Sreekanth. V. Lakkidi for various useful discussions.

Thanks to Vishnudath, who has been my roomate at PRL, for bearing with me all these years. I express my thanks to my friends and batch-mates Bhavesh, Bharti, Soumik, Niharika, Kiran, Anil, Nijil and Pradeep for all the enjoyable time we spent together and all the memorable trips we went to.

I am also grateful to all the fellow researchers from PRL for the numerous helps and the support that they have given at various times. Especially, I would like to mention Balbeer, Akanksha, Arpan, Suchismita, Alekha, Tripurari for all the discussions and memorable road trips. I always enjoyed conversations with Arko, Priyanka, Navpreet, Kumar, Jabir, Ali, Girish Kumar, Manu, Shraddha, Ikshu, Gaurav Jaiswal, Gaurav Tomar, Bhavya, Lakshmi R., Lakshmi S. Mohan, Luxmi Rani, Arun Pandey, Rukmani, Ashish, Arvind, Richa, Avdhesh, Tanmoy, Abhaya, Lata, Girish, Chandan, Ikshu, Shradha, Manu, Venkatesh, Nidhi, Soumya, Selva, Arun, Prasanna, Archita, Aarthy, Navpreet, Rupa, Kuldeep, Prahlad, Ashim, Oindrila, Sukanya, Surya, Ayon, Priyank, Anshika, Vishal, Deepak, Sudipta, Pravin and Hrushikesh. Kindly forgive if I have left out anyones name and please know that I am thankful to all of you.

Above all, I am immensely grateful to my parents and brother for everything that they have done for me.

Aman Abhishek

Abstract

In this thesis we investigate the properties of strongly interacting matter at extremely high temperatures and densities. The interactions of strongly interacting matter are governed by the laws of Quantum Chromodynamics(QCD) which is a gauge theory based on SU$(3)_c$ symmetry group. Standard model contains six strongly interacting quarks and eight gluons which bind together to form baryons such as protons, neutrons, etc and mesons such as pions, kaons, etc, collectively known as hadrons and make up the bulk of the observable universe. Strongly interacting matter exhibits peculiar features owing to the strong nature of its coupling, namely asymptotic freedom, confinement and spontaneous breaking of chiral symmetry.

Chiral symmetry refers to the symmetry of the lagrangian under chiral transformation. However the ground state of the system may not exhibit the symmetries of the Lagrangian. In such a case the symmetry of the theory is said to be spontanoeusly broken. In case of QCD the ground state of the system at low energies exhibits spontaneous breaking of chiral symmetry. Breaking of chiral symmetry results in mass generation and is responsible for most of the mass observed in universe since mass generated by higgs mechanism for stable quarks is small and heavy quarks are unstable against decay and hence not found in nature.

Asymptotic freedom refers to the fact that the strong coupling decreases with increasing energy and thus at very high energies the theory becomes weakly coupled. Weak coupling allows one to use usual methods of perturbation theory to make predictions about experiments and study the hot and dense matter created in heavy ion collisions. There have been considerable success in the use of perturbation theory to explain the experimental data obtained in heavy ion collisions. Despite the suc-

cesses there are may unresolved problems that remain. Predictions of the transport properties based on pQCD are in disagreement with experimental data and lattice QCD which suggests non-perturbative effects remain in the matter produced in heavy ion collisions for temperatures atleast few times the transition temperature. Other than high temperatures, the picture is also unclear at high densities. Lattice QCD, which is a first principle implementation of QCD has the sign problem and perturbative calculations are inapplicable due to large coupling for realistic densites, e.g. in the core of neutron stars or the dense matter produced in heavy ion collisions. Morever, it is also known that neutron stars have a very strong magnetic field. Origin of such high magnetic fields and its effect on hadronic matter is also a topic of active research. In view of these problems one turns to effective models which are based on phenomenological parameters and captures some of the basic properties of QCD. Two such popular models are Nambu Jona Lasinio model(NJL) and Polyakov Loop extended Quark Meson Model(PQM).

Nambu Jona Lasinio model was proposed by Yochiro Nambu and Jona Lasinio as a low energy phenomenological model of strong interactions. The model exhibits spontaneous chiral symmetry breaking and parameters of the model are fit to reproduce low energy hadronic spectrum. Gluons are absent in the model and the interaction is given by a four fermi point interaction. The model has been successfully applied to the study of strongly interacting matter both at high temperatures and high densities. Quark Meson Model(QM) is an extension of sigma model. Whereas in NJL model the degrees of freedom are quarks, QM model includes mesonic degrees of freedom such as pions. The mesonic degrees of freedom are coupled to quarks and themselves through self interaction.

Both Nambu Jona Lasinio and Quark meson model do not have gluons and they do not incorporate confinement. Due to confinement at low temperatures only color singlet hadrons are observed. To include the effect of confinement, QM model is extended by introducing a potential in terms of the polyakov loop which is the trace of the Wilson loop in temporal direction and is also coupled to quark. It is calculated in Lattice QCD which is a first principle calculation and is not restricted by strong values of the QCD coupling. Including the polyakov loop in the QM model suppresses the quark distribution functions, especially below the transition temperature. Thus it results in a statistical confinement of quarks in the sense that number density of quarks below the transition temperature is highly suppressed. This model is known as PQM model.

Using these two models we have studied the properties of matter under extreme conditions of temperature and densities. PQM is has been used to calculate the transport coefficients of hot matter created in heavy ion collision, namely the shear viscosity, bulk viscosity and thermal conductivity. Results have been obtained using kinetic theory and thermal averaging of scattering rates. Values obtained for the transport coefficients are consistent with experimental results and other phenomenological studies.

For quark matter at high densities and large background magnetic field, which is relevant for the interior of neutron stars, three flavor NJL model with determinant interaction has been used with background magnetic field to study color superconductivity at high densities. Constraints of charge neutrality have been imposed and resulting gapless modes have been studied. Impact of background magnetic field on the superconducting gap and neutrality conditions is also discussed.

Spontaneous spin polarization has been suggested as a possible mechanism for the origin of large magnetic fields in neutron stars. In order to study spotaneous spin polarization in quark matter, a three flavor NJL model with tensor interaction has

been used with non-zero current quark masses. Two independent spin polarization condensates arising from tensor interaction in three flavor NJL model, have been studied as a function of quark chemical potential. Magnetic field resulting from such condensates is estimated and found to be of expected order of magnitude.

Keywords: Quantum Chromodynamics, Chiral Symmetry, Confinement, Asymptotic Freedom, Heavy ion collisions, Transport coefficients, Color Superconductivity, Spin polarization, Quark matter

Contents

Acknowledgement v
Abstract v
List of Figures vii

1 Introduction **2**
1.1 Standard Model 2
1.2 Quantum Chromodynamics 4
1.2.1 Spontaneous Symmetry Breaking 4
1.2.2 Chiral Symmetry 5
1.2.3 Mass Generation : Higgs mechanism and Chiral Symmetry 7
1.2.4 Asymptotic Freedom 9
1.2.5 Confinement and Quark Gluon Plasma . . 10
1.3 Phase diagram of Quantum Chromodynamics . . 11
1.3.1 Transport properties 14
1.3.2 Strongly interacting matter at high densities: Color superconductivity 19
1.3.3 Spontaneous spin polarization in quark matter 21
1.4 Organization of thesis 23

2 Phenomenological Models and Mathematical Formalism **25**
2.1 Introduction 25
2.2 Nambu Jona Lasinio Model 26

2.2.1 Mesons in NJL model 27
2.3 Three flavor NJL model 29
2.3.1 Parameter for three flavor NJL model . . . 31
2.4 Polyakov loop extended Quark Meson Model . . . 34
2.4.1 Polyakov loop 34
2.4.2 Free energy in Quark meson model 37
2.4.3 Parameters of PQM model 39
2.4.4 Phase structure of Polyakov quark meson model 39
2.5 Boltzmann equation 45
2.6 Quark Matter in magnetic field 54

3 Transport Coefficients of Hot and Dense Matter 58
3.1 Introduction 58
3.2 Transport coefficients in relaxation time approximation 61
3.2.1 Relaxation time estimation- meson scatterings 62
3.2.2 Relaxation time estimation– Quark scatterings 64
3.2.3 Quark pion scattering and relaxation time 66
3.3 Results 68
3.3.1 Meson scatterings 68
3.3.2 Quark scatterings 72
3.4 Summary 78

4 Color Superconductivity in presence of background magnetic field 80
4.1 Introduction 80
4.2 The ansatz for the ground state 83
4.3 Evaluation of thermodynamic potential and gap equations 90
4.4 Results and Discussions 106

4.5 Summary 120

5 Spontaneous Spin Polarization in Quark Matter 124

5.1 INTRODUCTION 124

5.2 Formalism 127

5.3 Results and Discussions 133

5.3.1 Results with $F_8=\frac{F_3}{\sqrt{3}}$ 134

5.3.2 Results for independent F_3, F_8 139

5.3.3 Magnetic field due to spin polarization . . 139

5.4 Summary 140

6 Summary and Conclusions 148

7 Appendix 151

7.1 Appendix A 151

7.1.1 A. Evaluation of operator expectation values of some operators 151

7.2 Spontaneous Spin Polarization 154

7.2.1 Gap Equations 154

Bibliography 173

List of Publications 175

List of Figures

1.1 Fundamental particles in Standard Model. 3
1.2 Relative strengths of fundamental interactions. . . 3
1.3 4-loop running of QCD coupling with energy scale Q 9
1.4 Phase diagram of strongly interacting matter . . . 11
1.5 Heavy ion collision. 15
1.6 η/s for He, N_2, and H_2O and strongly interacting matter 17
1.7 Data on elliptic flow 17

2.1 M$_u$, M_s as a function of temperature at zero quark chemical potential. 33
2.2 M$_u$, M_s as a function of quark chemcial potential at zero temperature. 33
2.3 Variation of Polyakoc loop variable Φ and σ as a function of temperature at zero quark chemical potential. 40
2.4 Quark mass M, Pion mass M_π and Sigma mass M_σ at zero quark chemical potential. 41
2.5 Trace anomaly $\frac{(\epsilon-3p)}{T^4}$ at zero quark chemical potential. 41
2.6 Derivative of chiral order parameter. 43
2.7 Derivative of Polyakov loop variable multiplied by pion decay constant. 43
2.8 Temperature dependence of the velocity of sound at constant density. 44

3.1 Average relaxation time for pions (solid line) and sigma meson (dotted line). Only meson-meson scatterings are considered here. 68

3.2 Computations show mesonic contribution calculated using only meson-meson interactions. (a) : Shear viscosity to entropy ratio for $\mu = 0$. Present results 69

3.3 Average relaxation time for quarks arising from quark scattering. The solid curve corresponds to quark quark/antiquark scatterings with meson exchange. The dashed curve corresponds to including the effect of quark meson scatterings. Both the curves correspond to $\mu = 0$ case. 71

3.4 Different contributions for specific viscosity coefficients. η/s is shown in the left while ζ/s is shown on the right. In both the figures, ... 73

3.5 (a) : Shear viscosity to entropy ratio for $\mu = 0$. Present results are shown by solid lines. The dotted line correspond to results of NJL model of Ref. [1] , the short dashed 74

3.6 Average relaxation time of quarks and antiquarks for $\mu = 100$ MeV. The solid line correspond to the case of $\mu = 0$ MeV. 75

3.7 Viscosities for $\mu = 100$ MeV. The left figure shows η/s as a function of temperature for $\mu = 0$ MeV (solid line) and $\mu = 100$ MeV (dotted line). The right 76

3.8 Thermal conductivity in units of T^2 as a function of temperature for $\mu = 100$MeV. 76

4.1 Constituent quark masses and superconducting gap when charge neutrality conditions are not imposed. Fig.1-a shows the M_u at zero temperature as a function of quark chemical potential for different values of the magnetic field. Fig. 1-b shows the same for the strange quark mass M_s and the superconducting gap. 108

4.2 Baryon number density in units of nuclear matter density as a function of chemical potential for different strengths of magnetic field at zero temperature. 109

4.3 Critical chemical potential for chiral transition at zero temperature as a function of magnetic field . 110

4.4 Gaps without determinant interaction at zero temperature as a function of quark chemical potential. Solid curve refers to masses of u-d quarks, the dashed curve refers to the mass of strange quark and the dotted curve corresponds to the superconducting gap. 112

4.5 Constituent quark masses as a function of magnetic field for T=0. Fig.5-a shows the masses of the three quarks below the chiral transition for μ=200 MeV. Fig. 5-b shows the same for the masses along with the superconducting gap above the chiral transition for $\mu_q = 400$ MeV. 113

4.6 Constituent quark masses and superconducting gap when charge neutrality conditions are imposed. Fig.6-a shows the masses and superconducting gap at zero temperature as a function of quark chemical potential for magnetic field $\tilde{e}B = 0.1m_\pi^2$ Fig. 6-b shows the same for $\tilde{e}B = 10m_\pi^2$. . 113

4.7 Dispersion relation and the occupation number for condensing quarks at T=0,μ_q=340 MeV. Fig.7-a shows the dispersion relation for the condensing quarks for zeroth Landau level. The upper curve is for u quark and the lower curve corresponds to d quark dispersion relation. Fig. 7-b shows the occupation number as a function of momentum for $\tilde{e}B = 10m_\pi^2$. 115

4.8 Number densities of up and down quarks participating in the superconductivity for $\tilde{e}B = 0.1m_\pi^2$ (dashed line) and $\tilde{e}B = 10m_\pi^2$ (solid line) 118

4.9 Chemical potential μ_E and μ_8 for charge neutral quark matter. $|\mu_E|$ is plotted as a function of quark chemical potential μ_q for magnetic field $\tilde{e}B = 0.1m_\pi^2$ (Fig.9-a)and for $\tilde{e}B = 10m_\pi^2$ (Fig. 9-b). In Fig.9-a and Fig.9-b we have also plotted the mass of strange quarks and superconducting gap as a function of quark chemical potential to highlight the dependence of charge chemical potential on these two parameters. In the lower two plots, the color chemical potential μ_8 is plotted as a function μ_q for $\tilde{e}B = 0.1m_\pi^2$ (Fig 9-c) and for $\tilde{e}B = 10m_\pi^2$. 119

4.10 Population of different species for charge neutral quark matter for $\tilde{e}B = 0.1m_\pi^2$ (Fig. 10-a) and for $\tilde{e}B = 10m_\pi^2$ (Fig. 10-b). 121

4.11 Equation of state for $\tilde{e}B = 0.1m_\pi^2$ (dashed line) and $\tilde{e}B = 10m_\pi^2$ (solid line) 121

5.1 Constituent quark mass as a function of quark chemical potential at zero temperature in the presence and absence of 131

5.2 The figure shows the contour maps of the thermodynamics potential with the set 132
5.3 This figure shows the contour plots of the thermodynamic potential in $\sigma_s - F_3$ plane at zero temperature with 143
5.4 Left Plot: Dependence of constituent quark mass on the quark chemical potential at zero temperature in the presence as well as in the absence of spin polarization condensation 144
5.5 This figure shows the contour plots of the thermodynamic potential in $\sigma_s - F_3$ plane for finite temperature (T) 145
5.6 This figure shows the contour plots of the thermodynamic potential in $\sigma_s - F_3$ plane for zero temperature (T) and finite chemical 146
5.7 Plot (a), (b) and (c) show the variation of F_3 (red solid line) and F_8 (blue dotted line) with chemical potential where 147

Chapter 1

Introduction

1.1 Standard Model

As per our current understanding, nature is governed by four fundamental forces, namely Gravity, Electromagnetism, Weak interactions and Strong interactions. Gravity is responsible for the formations of structures in universe on the largest scales, i.e. solar system, galaxies, etc. Electromagnetism involves the phenomena of light matter interaction. It explains the formation of bound states such as atoms, emission and absorption of lights, lasers, etc. Weak interactions are responsible for decay processes such as neutron decay. Quantum Chromodynamics(QCD) is the theory of strong interactions, also known as colour force. It is the strongest of the four fundamental fources of nature. The three quantum theories, QED, Electroweak and QCD together form the Standard Model of particle physics [2]. Gravity [3], which works well on the scale of universe, is not presently understood as a quantum theory.

Fig. 1.1 shows the basic constituents of Standard Model. In the quantum picture of fundamental forces, the particles interact by exchanging bosonic particles. These are γ(photon) for

[1] https://www.u-tokyo.ac.jp/content/400021545.jpg

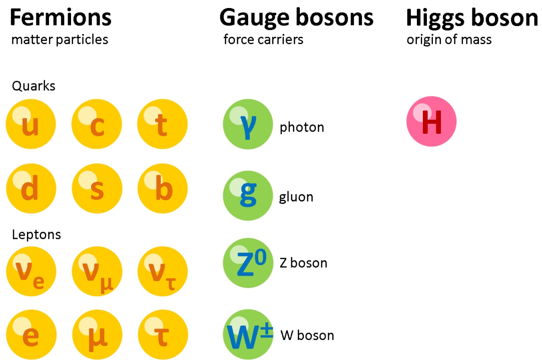

Figure 1.1: Fundamental particles in Standard Model.[1]

electromagnetic interactions, Z and W massive vector bosons for weak interaction and g, gluons for strong interactions. $e, \mu, \tau, \nu_e, \nu_\mu, \nu_\tau$ are the six leptons. e, μ and τ participate both in electromagnetic and weak interactions whereas ν_e, ν_μ, ν_τ participate only in weak interactions. Leptons do not participate in strong interactions. u, d, s, t, d, b are the six quarks. They participate in all three interactions. H is the Higgs boson, responsible for giving masses to the particles. However as we shall discuss later, most of the mass that we observe in the nature arises from strong interaction(color force) and not the Higgs mechanism.

Fundamental forces			
Force	Relative strength	Range/ m	Gauge - boson
Strong	1	10^{-15}	Gluon
Electromagnetic	1/137	Infinite	Photon
Weak	10^{-6}	10^{-18}	W^+, W^-, Z bosons
Gravitation	10^{-39}	Infinite	Graviton (predicted)

Figure 1.2: Relative strengths of fundamental interactions.[2]

Fig. 1.2 shows a rough comparision of the strengths of the four fundamental interactions. Strong interaction are about 38 orders of magnitude stronger than gravity. This introduces novel

[2]https://sites.google.com/a/pgscience.co.uk/physics/lessons/higher/higher-31-the-standard-model/312-interaction-of-particles

features in the interactions which are briefly discussed in following sections. QCD has been successfully applied in explaining the high energy deep inelastic scattering experiments as well as low energy hadronic physics. Also lattice QCD, which is the numerical implementation of QCD on computers has made predictions in agreement with observations.

1.2 Quantum Chromodynamics

Strong interaction is the force responsible for binding nucleons at the fundamental level and is described by Quantum Chromodynamics, which describes the interactions between quarks and gluons. Mathematically the strong force is described by the Lagrangian [4] :

$$\mathcal{L} = \bar{\Psi}(i\not{D} - ig\lambda^a \not{G}_a)\Psi + -\frac{1}{4}G^a_{\mu\nu}G^{\mu\nu}_a \tag{1.1}$$

Here Ψ is a $N_f \times 1$ column vector for N_f flavors. $G^a_{\mu\nu} = \partial_\mu A^a_\nu - \partial_\nu A^a_\mu + gf^{abc}A^b_\mu A^c_\nu$ is the gluon field strength tensor. λ^a are 3×3 generators of the $SU(3)_c$ in the fundamental representation. There are 8 such generators. A^μ_a are eight gauge fields. 'g' is the strong gauge coupling.

Two important non-perturbative properties of QCD are chiral symmetry breaking and confinement. We shall discuss both the properties in the following discussion. However before discussing these two important aspects of QCD we shall discuss in general the spontanoeus symmetry breaking.

1.2.1 Spontaneous Symmetry Breaking

Symmetry [4] in particle physics refers to a transformation of the fields which leave the Lagrangian invariant. As an example consider the following Lagrangian.

$$\mathcal{L} = \partial_\mu \Phi^\dagger \partial^\mu \Phi + (\Phi^\dagger \Phi)^2 \tag{1.2}$$

Under the transformation $\Phi \to e^{i\alpha}\Phi$, where α is a real number, the two terms in above Lagrangian transform as :

$$\Phi^\dagger \Phi \to \Phi^\dagger e^{-i\alpha} e^{i\alpha} \Phi = \Phi^\dagger \Phi \tag{1.3}$$

$$\partial_\mu \Phi^\dagger \partial^\mu \Phi \to \partial_\mu \Phi^\dagger e^{-i\alpha} e^{i\alpha} \partial^\mu \Phi = \partial_\mu \Phi^\dagger \partial^\mu \Phi \tag{1.4}$$

Clearly the two terms remain invariant and thus the Lagrangian also remains invariant. This is an example of a symmetry transformation. However it may so happen that a symmetry of the Lagrangian is not respected by the ground state(i.e. the lowest energy state) of the system. For example if the ground state has a non-zero expectation value $\langle 0|\Phi\Phi|0\rangle$, then the ground state is not invariant under the transformation $\Phi \to e^{i\alpha}\Phi$. Symmetry breaking is ubiquitous is physics. Other examples include transition from paramagnetic to ferromagnetic phase where spontaneous magnetisation breaks the rotational invariance of the Lagrangian. In superconductivity gauge symmetry is spontaneously violated resulting in photon gaining mass and Meissner effect. Symmetry breaking is ubiquitous in nature and is important in understanding the diverse phenomenon in nature.

1.2.2 Chiral Symmetry

In the massless limit a fermion like a quark has a definite value of helicity, which is the projection of spin angular momentum on the three momentum of the particle. A Dirac spinor can be written as :

$$\omega = \begin{pmatrix} \phi \\ \chi \end{pmatrix} \tag{1.5}$$

The Dirac equation for a free particle reads:

$$\begin{aligned} E\phi &= \sigma.p\phi + m\chi \\ E\chi &= -\sigma.p\chi + m\phi \end{aligned} \tag{1.6}$$

For a massless particle the above equations can be restated as :

$$\begin{aligned} (\sigma.p/|p|)\phi &= \phi \\ (\sigma.p/|p|)\chi &= -\chi \end{aligned} \tag{1.7}$$

These are nothing but the helicity eigenstates. Eq. 1.7 also show that for massless particles upper and lower component of the spinor are decoupled. $\omega_1 = \begin{pmatrix} \phi & 0 \end{pmatrix}^T$ is a particle with positive helicity while $\omega_2 = \begin{pmatrix} 0 & \chi \end{pmatrix}^T$ is particle with negative helicity.

Chirality is defined as the eigenvalue of γ_5, where $\gamma_5 = i\gamma_0\gamma_1\gamma_2\gamma_3$, and $\gamma_i's$ are the Dirac gamma matrices. In Dirac representation γ_5 is given as :

$$\gamma_5 = \begin{pmatrix} 1 & 0 \\ 0 & -1 \end{pmatrix} \tag{1.8}$$

In massless limit chirality is the same as helicity. However a massive spinor is not an eigenstate of chirality.

$$\gamma_5\omega = \begin{pmatrix} \phi \\ -\chi \end{pmatrix} \neq \lambda \begin{pmatrix} \phi \\ \chi \end{pmatrix} \tag{1.9}$$

Thus a mass term breaks chiral symmetry since it couples upper and lower components of Dirac spinor. Mathematically the chiral transformations is:

$$\Psi \to e^{i\beta\gamma_5}\Psi \tag{1.10}$$

Here β is angle of the transformation. The Lagrangian in Eq.(1) is invariant under transformation Eq.(2). However a mass term $\bar{\Psi}\Psi$ is not invariant under the transformation Eq.(2). It transforms as :

$$\bar{\Psi}\Psi \to \bar{\Psi}e^{2i\beta\gamma_5}\Psi \neq \bar{\Psi}\Psi \tag{1.11}$$

Even in the absence of such mass term the QCD ground state has a non-zero expectation value for the chiral condensate, which is the expectation value $\langle\bar{\Psi}\Psi\rangle$. Therefore even though the Lagrangian is invariant under chiral transformation, the QCD ground state is not invariant. This is known as spontaneous breaking of chiral symmetry. $\langle\bar{\Psi}\Psi\rangle$ expectation value acts like a mass term for the quarks.

1.2.3 Mass Generation : Higgs mechanism and Chiral Symmetry

Higgs mechanism provides the masses to particles of the standard model. Consider the following lagrangian involving a fermion ψ and boson ϕ

$$\mathcal{L} = \bar{\psi}i\partial\!\!\!/\psi + (\partial_\mu\phi)^2 - g\bar{\psi}\phi\psi + \frac{1}{2}\mu^2\phi^2 + \frac{\lambda}{4}\phi^4 \tag{1.12}$$

The above lagrangian decribes a fermionic field without a mass term and a bosonic field with a mass term with wrong sign. The potential for the scalar field ϕ has a minima at $\phi = v = \sqrt{\frac{-\mu^2}{\lambda}}$. Making the substitution $\phi \to v + \tilde{\phi}$ we get

:

$$\mathcal{L} = \bar{\psi} i \partial\!\!\!/ \psi + (\partial_\mu \tilde{\phi})^2 - gv\bar{\psi}\psi + g\bar{\psi}\tilde{\phi}\psi + \frac{1}{2}\mu^2(v+\tilde{\phi})^2 + \lambda(v+\tilde{\phi})^4 \tag{1.13}$$

One may notice that expanding the scalar field about the minima of the potential has generated a mass term for the fermion. This is in essence the mechanism of mass generation by Higgs.

However hadrons such as protons are much more heavy than the sum of the masses of the constituent quarks generated by Higgs mechanism. For example combined mass due to Higgs mechanism of the three quarks which make up the proton is only about 20 MeV whereas the mass of proton is about 930 MeV. Rest of the mass of hadronic matter comes from interactions between quarks and gluons which result in a non zero value of chiral condensate. Thus QCD is responsible for most of the mass of visible matter in the universe.

Realistically mass of light quarks, i.e. their mass from Higgs mechanism, is actually non-zero. This is suggested by Gell Mann Oakes Renner(GOR) relation which relates mass of pion with u and d quark current mass. If the current masses were zero, the pion mass would be vanish too, as expected of a goldstone boson of spontaneous chiral symmetry breaking. Moreover if the non-zero mass of quarks were responsible for the breaking of chiral symmetry, one would expect the existence of nuclear parity doublets. Such parity doublets are not observed in nature. Chiral symmetry breaking also imposes constraints on the low effective theories of hadrons which are successful in explaining experimental data. These arguments suggest that chiral symmetry is spontaneously broken.

1.2.4 Asymptotic Freedom

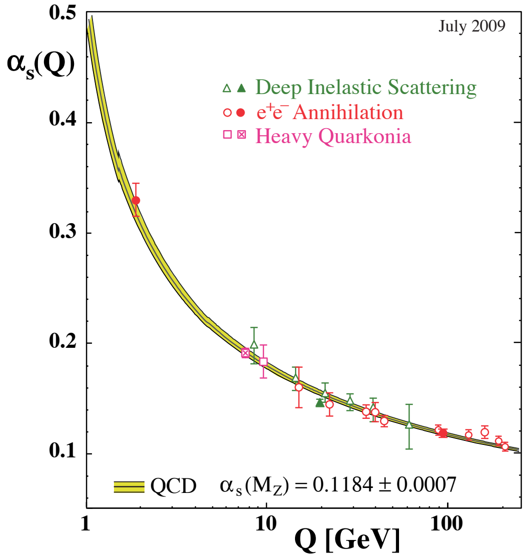

Figure 1.3: 4-loop running of QCD coupling with energy scale Q[3]

Another important property of QCD is asymptotic freedom. It refers to the fact that the strength of strong interaction decreases at high energies or short distances. QCD vacuum behaves like a dielectric. Just as in a dielectric the polarization of the medium modifies the electric charge, in QCD polarization of quantum fluctuations anti-screen the charge resulting in increasing charge density with distance. Mathematically this is represented by the beta function of QCD, which tells us how coupling varies with energy scale. At four loop the beta function is:

[3]http://pdg.lbl.gov/2011/reviews/rpp2011-rev-qcd.pdf

$$\alpha_s(\mu_R^2) = \frac{1}{b_0 t}\left(1 - \frac{b_1}{b_0^2}\frac{lnt}{t} + \frac{b_1^2(ln^2 t - lnt - 1) + b_0 b_2}{b_0^4 t^2}\right.$$
$$\left. - \frac{b_1^3(ln^3 t - \frac{5}{2}ln^2 t - 2lnt + \frac{1}{2}) + 3b_0 b_1 b_2 lnt - \frac{1}{2}b_0^2 b_3}{b_0^6 t^3}\right), t = ln\frac{\mu_R^2}{\Lambda^2} \tag{1.14}$$

Here N_c and N_f refer to the number of color and flavor repectively. Λ or Λ_{QCD} is the scale which sets non-perturbativity scale of QCD. It value is about 200 MeV. At energies high enough compared to λ_{QCD}, the theory is weakly coupled and perturbative techiques can be used. At low energies the coupling is strong and one requires non perturbative techniques such as Lattice QCD, QCD sum rules, effective theories like Chiral perturbation theory, phenomenological models such as NJL model, etc.

1.2.5 Confinement and Quark Gluon Plasma

Confinement refers to the fact that at low energies only color singlet asymptotic states are observed in QCD. Unlike QED where charge states such as ions, electrons, etc can exist in free state, in QCD all the charges combine in such a way that only colorless hadrons appear in the final state. However as the energy density increases, the coupling becomes weak and at sufficiently high energy densities the quark and gluons degrees of freedom which are confined into hadrons can become “free” over a macroscopic region. Such a macroscopic system where the degrees of freedom are quarks and gluons is known as quark gluon plasma. Such a state can form at both high temperatures which are obtained in relativistic heavy ion collisions and at high densities which may exist inside of neutron stars.

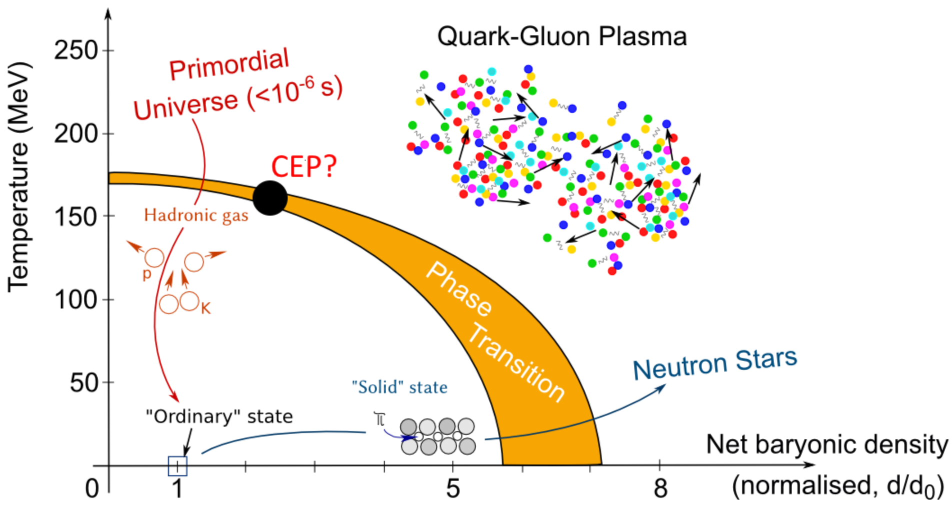

Figure 1.4: Phase diagram of strongly interacting matter. Baryon matter density has been normalised by nuclear matter density $d_0 = 0.17/\mathrm{fm}^3$.[5]

Having discussed the important properties of QCD we now discuss the phase diagram of QCD and the challenges in understanding the nature of strongly interacting system.

1.3 Phase diagram of Quantum Chromodynamics

A phase diagram of matter is a chart of the equilibrium phases as a function of thermodynamic variables such as temperature, chemical potential, etc. Fig. 5.2 shows the conjectured phase diagram of Quantum Chromodynamics [5]. It is conjectured because due to strong nature of coupling which prevents first principle calculations and lack of direct experimental measurements one doesn't have a established picture of phase diagram.

[5]https://compstar.uni-frankfurt.de/outreach/short-articles/the-qcd-phase-diagram-and-the-critical-end-point/

QCD has an intrinsic scale generated dynamically known as Λ_{QCD}. The value of Λ_{QCD} is about 200 MeV. Thus one expects phase transitions associated with energies $\sim \Lambda_{QCD}$. These energies roughly correspond to temperatures of $\sim 10^{12}$ K and densities of the order of $\sim 10^{15}$g/cm^3, which is also roughly the density of nucleon. Such high temperatures were present in the universe a few microsceonds after the big bang. High temperature are also obtained in collision of ultra relativistic particles at particle accelerators such as Relativistic Heavy Ion Collider(RHIC) and Large Hadron Collider(LHC). They reach center of mass energies of 200 GeV and 13 TeV respectively. These energies are much higher than the typical QCD scale and hence once expects transition from hadronic to quark gluon matter in these collisions. Indeed, there are hints of such a transition [6].

In high energy heavy ion collisions the number of particles produced is much higher than the initial quark access over antiquarks. Therefore these collisions have a vanishing baryon chemical potential. To study strongly interacting matter at densities few times the nuclear matter density(n_0=0.17 fm^{-3}) low energy collisions have been planned at facilities such as Nuclotron-based Ion Collider Facility(NICA), Facility for Antiproton and Ion Research(FAIR) and Japan Proton Accelerator Research Complex(J-PARC). Other than these experiments, high densities are also expected inside neutron stars which have density comparable to nuclear matter density. One may expect a phase transition to deconfined matter in the core of such stars.

QCD at zero baryon chemical potential is well studied. Lattice QCD, which is a first principle numerical implementation of QCD is applicable. Results of Lattice QCD are dependent on the number of flavors and colors. For N_c=3 and N_f=0, i.e. a pure glue theory, one gets a first order transition with $T_c \sim 270$ MeV. For three light flavors with realistic quark masses one gets a crossover with a pseudo-critical temperature T_c in the range 150 MeV - 200 MeV. Just above the critical temperature the system is expected to be strongly coupled and non-perturbative effects are important.

At finite densities the picture is less clear. Lattice QCD is not applicable due to sign problem associated with simulation in presence of finite chemical potential. The coupling at these densities is strong which prevents a perturbative analysis. Therefore one turns to chiral models and Taylor expansion in Lattice QCD to conjecture phase diagram at finite density. Such analysis suggest existence of a QCD critical end point (T_{cep},μ_{cep}). Beyond this point the hadron-quark transition is a first order transition. It is possible that this first order transition ends in another critical point (T_2,μ_2). Beyond this point the transition from nuclear superfluid to quark gluon matter is continous and there is no clear boundary between the two phases. This is known as the quark-hadron continuity.

At asymptotically high densities pQCD is applicable and analysis shows the ground state to be a color superconductor. Due to the fact there are more degrees of freedom available in QCD, namely color and flavor, there are several different superconducting states possible. Further different external conditions like charge neutrality(both color and electrical) affect the stability of phases and may favor phases with free energy which is not minimum. At asymptotic densisties the favoured state is Color-Flavor Locker(CFL) state in which color, flavor and spin degrees of freedom are correlated. Other possibility at intermediate densities is 2SC phase in which u and d quarks form cooper pairs while strange does not participate in superconductivity due to difference in fermi energies. Inhomogenous superconducting states where the order parameter varies over space are also known to exist, however the true ground state is unclear.

Effect of magnetic field [7] on QCD phase diagram has been of interest in recent investigations. This is so because it has been suggested that very strong magnetic fields of the order of hadronic scale may be produced in heavy ion collisions. Also neutron stars which are extremely dense environments are known to have strong surface magnetic fields which may be strong enough in the interior to affect hadronic properties. Also a magnetic field included in QCD Lagrangian can be studied in Lattice QCD as there is no sign problem like in the case of finite density. Lattice simulations show that at $T = 0$ the chiral condensate $\bar{\Psi}\Psi$ increases with magnetic field. This is also observed in chiral models. However at temperatures near the critical temperature the chiral condensate decreases with increase in magnetic field. This is contrary to results in chiral models.

Having discussed the phase diagram of QCD we now discuss briefly the three topics investigated in doing the work towards this thesis, namely transport properties, color superconductivity and spontaneous spin polarization.

1.3.1 Transport properties

Fig. 1.3.1 shows a typical collision of two nuclei in heavy ion collision. The two nuclei move in opposite direction at relativistic energies. The shaded region shows the overlap of the two nuclei. In ultra-relativistic heavy ion collisions the non-overlapping portion of the nuclei keep moving forward on their initial trajec-

[6] http://article.sapub.org/10.5923.j.jnpp.20140406.02.html

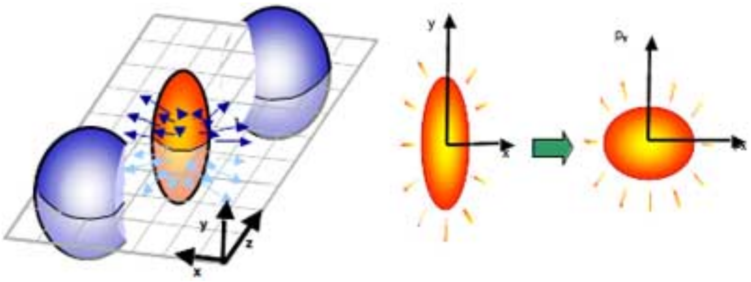

Figure 1.5: Heavy ion collision.[6]

tories. The overlapping region is in the shape of an almond and has geometrical anisotropy. This geometrical anisotropy results in pressure gradients which as the fireball evolves translates to momentum anisotropy. Differential distribution of final state particles can be written as:

$$E\frac{d^3N}{d^3p} = \frac{d^3N}{p_T dp_T dy d\phi} = \frac{d^2N}{p_T dp_T dy}\frac{1}{2\pi}\left[1+\sum 2v_n cos(n\phi)\right]$$

Here p_T is the transverse momentum, y is rapidity and ϕ is the azimuthal angle. In the second equality the azimuthal distribution is expanded in fourier series. The first two coefficients in the fourier series, v_1 and v_2 are the directed and elliptic flow. v_2 is the average of the particle distribution weighted with $cos(\phi)$. Thus it measures the spatial anisotropy in the final momentum of the particles which in turn is related to pressure gradients at initial times. Thus v_2, or the elliptic flow, is an important variable to study the initial stages of heavy ion collisions and deconfined matter which may be present in the initial stages.

The system produced in heavy ion collisions is studied using hydrodynamics which is a long wavelength description of the system near equilibrium. Based on initial conditions and equation of state(EoS), it predicts the space time evolution of a fluid. If a fluid in equilibrium is perturbed, then the perturbations result in gradients. The system responds by generation of currents which tend to bring system back to equilibrium which is characterized by transport coefficients. Transport properties of a system refers to the ability of system as to how a physical quantity, such as energy, momentum, charge, etc is transferred from one point to another. For example perturbation in density results in currents which can be mathematically stated as :

$$\rho \boldsymbol{v} = -D \nabla \rho$$

In the above equation ρ is the density and D is a the transport coefficient. It is a property of the system and determines how fast the perturbations in density diffuse. Some other examples include Ohm's law $\boldsymbol{J} = -\sigma \nabla \phi$ and heat conductivity $\boldsymbol{Q} = -\kappa \nabla T$. Viscosity tensor determines the flow of momentum in the presence of velocity gradients. These coefficients are important because they are collective effects originating from microscopic interactions and can be measured in experiments. Thus they relate the microscopic and macroscopic physics.

Transport coefficients are also important for charting the phase diagram of quantum chromodynamics as shown below. Fig. 1.6 shows the plot of the ratio of shear viscosity to entropy as a function of temperature for some common elements and strongly interacting matter. One may note that around the phase transitions the ratio shows minima. Thus one expects that study of transport coefficients can help in mapping the phase diagram of strongly interacting matter. As evident from Fig. 3 experiments show that the quark gluon plasma produced in those collisions is the most perfect fluid known.

[7] R A Laceyet al,Phys. Rev. Lett. 98, 092301 (2007)

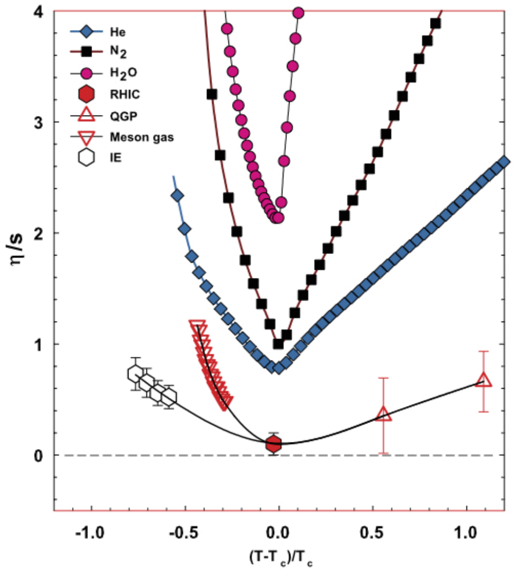

Figure 1.6: η/s for He, N_2, and H_2O and strongly interacting matter[7]

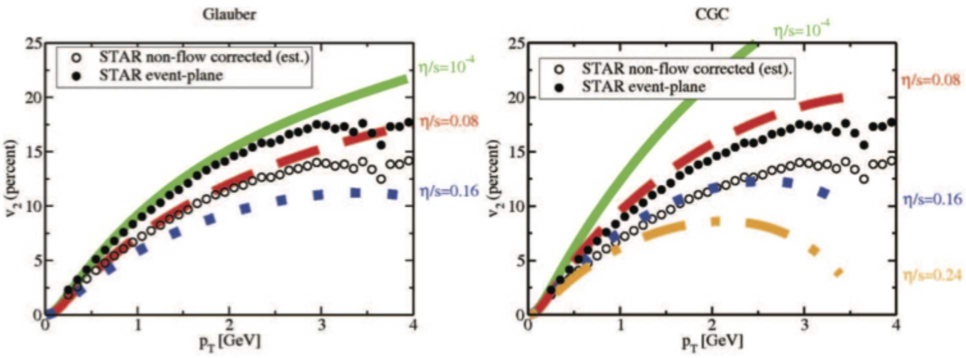

Figure 1.7: Data on elliptic flow[8]

Fig. 1.7 shows data on ellpitic flow as a function of transverse momentum along with hydro results. One finds that the elliptic flow is well explained by ideal hydrodynamics and viscous hydrodynamics with a small ratio of η/s. This suggests the im-

[8] M Luzum and P Romatschke,Phys. Rev.C78, 034915 (2008), Erratum,ibid.C79,039903 (2009)

portance of studying viscosity from a theoretical point of view. Investigations in perturbative QCD(pQCD)[8, 9, 10], which are valid in the limit $T >> \Lambda_{QCD}$ give following results :

$$\eta \sim \frac{T^3}{\alpha_s^2 ln\alpha_s^{-1}}, \zeta \sim \frac{\alpha_s^2 T^3}{ln\alpha_s^{-1}}$$

η/T^3 shows a rising behavior while ζ/T^3 shows a decreasing behavior. In the asymptotic limit QCD behaves like a conformal theory. Conformal theories have a vanishing ζ. Thus the above behavior of bulk viscosity is consistent in the limit $T >> \Lambda_{QCD}$. The ratio of shear viscosity to entropy has also been studied in the context of AdS/CFT duality[11] which indicate a universal lower bound on this ratio of $1/4\pi$. In this context it is intriguing that the ratio η/s obtained for QGP from experiments is close to the lower bound.

Transport coefficients for QGP have also been obtained from lattice QCD[12, 13, 14]. These calculations also suggest a small value of η/s and a rise in ζ/s close to transition temperature.

The expressions for shear viscosity, bulk viscosity and thermal conductivity are respectively[15]:

$$\boldsymbol{\eta} = \frac{1}{15T}\int \frac{d^3p}{(2\pi)^3}\frac{p^4}{E^2}\tau(E) f^{\mathrm{eq}}\left(\frac{E}{T}\right)$$

$$\boldsymbol{\zeta} = \frac{1}{9T}\int \frac{d^3p}{(2\pi)^3}\frac{\tau^a}{{E_a}^2}{f_a}^0\left(1+{f_a}^0\right)$$

$$\Bigg[p^2\left(1-3{v_n}^2\right) - 3{v_n}^2\left(M^2 - \mathrm{TM}\frac{\partial\ \mathrm{M}}{\partial\ \mathrm{T}} - \mu\mathrm{M}\frac{\partial\ \mathrm{M}}{\partial\ \mu}\right) + 3\left(\frac{\partial\ \mathrm{P}}{\partial\ \mathrm{n}}\right)_\epsilon\left(M\frac{\partial\ \mathrm{m}}{\partial\ \mu} - E\right.$$

$$\boldsymbol{\lambda} = (\frac{w}{nT})^2 \int \frac{d^3p}{(2\pi)^3} \frac{p^2}{3{E_a}^2} \tau_a(E_a)(t_a - \frac{nE_a}{w})^2 {f_a}^0 \left(1 + {f_a}^0\right)$$

In order to calculate these transport coefficients one needs to know the masses of the constituent quarks and mesons as well as the thermodynamic properties of the system. One also needs to know the scattering rates. We have used Polyakov extended quark meson(PQM) model to calculate these quantities. Polyakov loop allows one to include the effect of confinement in quark meson model by suppressing quark distributions below chiral transition. The masses of quarks and mesons are obtained from the thermodynamic potential. Scattering amplitudes are obtained from interaction terms in the PQM lagrangian. Relaxation time is obtained by thermal averaging the scattering rates. Once the relaxation time is calculated, the transport coefficients can be evaluated. Next we discuss color superconductivity.

1.3.2 Strongly interacting matter at high densities: Color superconductivity

From condensed matter physics it is known that a system of fermions with an attractive interaction is unstable with respect to formation of cooper pairs. If the interaction is attractive then it leads to a lowering of free energy of the system. The fermi sphere is unstable and system evolves to a new ground state. It was shown by Bardeen, Cooper and Schrieffer that in presence of an attractive interaction the ground state of such a system is a condensate of cooper pairs with the formation of gap near the fermi surface. The formation of such a gap in the energy spectrum leads to suppression of the scattering of fermions and leads to phenomenon of superconductivity.

In case of conventional superconductors in condensed matter physics it is the electrons which form the cooper pairs. Coulombic interaction between the electrons is repulsive. However the electrons also interact via exchange of phonons, which are vibrations in lattice. Phonon interactions generate an attractive force between the electrons and at low enough temperatures the phonon exchange is dominant over electromagnetic interaction leading to cooper instability and hence superconductivity. In case of QCD, due to the richer structure of color force, there exist a spin antisymmetric color anti-triplet channel in which quark-quark scattering is attractive. Thus one may expect cooper instability like phenomenon in strongly interacting dense matter.

Possibility of color superconductivity was suggested soon after QCD was established as theory of strong interactions [16]. Superconductivity in perturbative limit was studied in[17, 18]. Gap estimated in initial investigations was small, of the order of MeV, and therefore didn't generate much interest. However later it was suggested that the gap at intermediate densities could be much higher of the order of 100 MeV[19, 20]. Since critical temperature is also of the same order one expects that color superconductivity may be of relevance in neutron stars and even heavy ion collisions[21, 22, 23]. At intermediate densities superconductivity was studied in refs. [19, 20] within NJL type models and refs. [24, 25] in Instanton liquid model which also find similar order of magnitude gap. Realistically one expects the quark matter, if deconfined, to be color and electric charge neutral. Effects of such charge neutrality conditions were investigated in [26, 27, 28, 29]. Refs.[30, 31, 32, 33, 34, 35, 36] studied color superconductivity in background magnetic field.

In order to study color superconductivity in background magnetic field we employ Nambu-Jona Lasinio model with a diquark interaction term. The Hamiltonian is given as:

$$
\begin{aligned}
\mathcal{H} = & \psi^\dagger(-i\boldsymbol{\alpha}\cdot\boldsymbol{\nabla} - qBx\alpha_2 + \gamma^0 m)\psi \\
& - G_s \sum_{A=0}^{8}\left[(\bar{\psi}\lambda^A\psi)^2 - (\bar{\psi}\gamma^5\lambda^A\psi)^2\right] \\
& - G_D\left[(\bar{\psi}^c\gamma^5\epsilon\epsilon_c\psi)(\bar{\psi}\gamma^5\epsilon\epsilon_c\psi^c)\right] \\
& + K\left[det_f[\bar{\psi}(1+\gamma_5)\psi] + det_f[\bar{\psi}(1-\gamma_5)\psi]\right]
\end{aligned}
$$

To incorporate magnetic field one solves for Dirac equation with a background magnetic field and expands the spinors in terms of landau levels as follows

$$
\psi(\mathbf{x}) = \sum_n\sum_r \frac{1}{2\pi}\int d\mathbf{p}_{\not{x}}\left[q_r^0(n,\mathbf{p}_{\not{x}})U_r^0(x,\mathbf{p}_{\not{x}},n) + \tilde{q}_r^0(n,-\mathbf{p}_{\not{x}})V_r^0(x,-\mathbf{p}_{\not{x}},n)\right]e^{i\mathbf{p}_{\not{x}}\cdot\mathbf{x}_{\not{x}}}
$$

We assume a trial ground state with chiral and diquark condensate. With a trial ground state we can calculate the free energy of the system for a given value of magnetic field and quark chemical potential. All the calculations are restricted to zero temperature. Minimizing free energy gives us the gap equations for the masses and superconducting gap δ. Solving the gap equations self consistently gives the gaps as a function of chemical potential and magnetic field. Finally we discuss the phenomenon of spontaneous spin polarization.

1.3.3 Spontaneous spin polarization in quark matter

Magnetars are neutrons stars which have unusually high magnetic fields. Surface magnetic fields of magnetars can be as high as 10^{15} G. Inside the magnetic field could be even higher. Such large magnetic fields have been attributed to flux conservation during evolution of the star. However this hypothesis implies the radius of the resulting star to be smaller than the schwarzschild radius. Another explanation for the origin of ultra strong magnetic fields in neutron stars is sponatneous magnetisation in quark matter. Spontaneous polarization was studied in Ref. [37] with a one gluon exchange. The resulting magnetic field was estimated to be about 10^{17} G.

In the relativistic formalism spin polarization in dense quark matter can be studied using two spin condensates, axial vector condensate and tensor condensate. Axial vector condensate is the spatial component of axial vector $\psi^\dagger\Sigma^i\psi$ while the tensor condensate is $\psi^\dagger\gamma^0\Sigma^i\psi$. In the non-relativistic limit these two condensates are equivalent. Spontaneous spin polarization has been studied in effective models using these two condensates. In Ref. [38] spin polarization was studied with AV condensate along with color supercoductivity in NJL model. Ref. [39] has investigated spin polarization in one flavor NJL model in AV channel with a chiral condensate. Tensor spin polarization was studied in Refs. [40] with two flavors and in Ref. [41] with three flavors but zero current quark masses. Spin polarization in the two cases exhibit different properties. AV condensate shows co-existence with chiral condensate while it is zero in chirally symmetric phase. Tensor condensate on the other hand is zero in symmetry borken phase and acquires finite value in symmetry restored phase.

In the present work we have considered tensor condensate to study spin polarization in a 2+1 flavor NJL model with determinant interaction and finite current quark masses. By including finite current quark masses we can study the effect of spin condensate on the quark masses, specifically the mass of strange quark which is large in NJL type models even after chiral restoration for u and d quarks. This is also relevant in the case where charge neutrality is imposed as strange quarks also contribute to maintaining charge neutrality. Three flavor case is also interesting because one has to consider two different spin condensates corresponding to two diagonal generators $SU(3)_f$.

1.4 Organization of thesis

This thesis is organized as follows. In Chapter 1 we have given introduction to Standard Model of particle physics and Quantum Chromodynamics. Important features of Quantum Chromodynamics have been discussed along with the phase diagram of quantum chromodynamics. Understanding the phase diagram also motivates the study of properties of strongly interacting matter which forms the work done towards completion of this thesis.

In Chapter 2 we discuss the phenomenological models and frameworks used in studying the properties of hot and dense matter. We discuss two and three flavor Nambu-Jona Lasinio model which is used in study of color superconductivity and ferromagnetism in quark matter at high densities. Thereafter we discuss Polyakov loop extended quark meson model which we have taken to calculate transport properties of matter at high temperatures. We also discuss the derivation of transport coefficents using Boltzmann equation in Relaxation Time Approximation. Solution of Dirac equation in magnetic field is derived which is important for studying the phenomenon of color superconductivity in background magnetic field.

After dicussing the theoretical framework we discuss in detail the calculation of transport coefficients of hot and dense matter in Chapter 3. After deriving the thermodynamics of Polyakov loop extended quark meson model we use the results to calculate scattering rates and transport coefficients, namely shear viscosity, bulk viscosity and thermal conductivity, of quark matter. We present the results and discuss the implications.

In Chapter 4 we study the phenomenon of color superconductivity in three flavor quark matter with determinant interaction in the presence of a background magnetic field. Method of Bogoliubov transformation to study superconductivity is discussed. Quark masses and superconducting gap are derived for varying quark chemical potential and magnetic field. Electrical and color charge neutrality is discussed. Impositions of neutrality conditions lead to gapless modes. These modes and the effect of magnetic field on color superconductivity and phase diagram of QCD is discussed.

After studying transport coefficients and color superconductivity we present the work on spontaneous spin polarization in three flavor quark matter with determinant interaction in Chapter 5. Study of spontanoeus spin polarization is motivated by the need to understand origin of large magnetic fields in neutron stars. The thermodynamic potential is derived at a mean field level. Minimization of thermodynamic potential with respect to quark masses and spin polarization condensates results in gap equations which are solved self consistently. Variation of masses and spin polarization condensates as a function of quark chemical potential is discussed and magnetic field resulting from such polarization is estimated which is found to be of the order expeected in neutron stars.

Finally in Chapter 6 we conclude with the discussion of work done in the thesis and its implications.

Chapter 2

Phenomenological Models and Mathematical Formalism

2.1 Introduction

After discussing the nature of strongly interacting matter and its properties in Chapter 1, we now discuss some some theoretical frameworks employed in the work done in this thesis. In the next section we discuss two flavor Nambu Jona Lasinio (NJL)model which is a phenomenological model . After discussing two NJL model we extend the discussion to three flavor case which includes strange quark. This is relevant for study of color superconductivity and ferromagnetism. After discussing three flavor NJL model we introduce Polyakov loop extended quark meson model which combines the confining and chiral symmetry aspect of Quantum Chromodynamics. Polyakov loop results in a statistical confinement while Quark meson model is written on the principle of chiral symmetry and reproduces low energy hadronic physics well. After discussing the models used in calculating the properties of strongly interacting matter we discuss the transport coefficents which are derived using Boltzmann equation. Finally we discuss the solution of Dirac equation in magnetic field which s important for describing quarks in a background magnetic field.

2.2 Nambu Jona Lasinio Model

The strong coupling nature of Quantum Chromodynamics makes it diffcult to extract useful information such as masses of bound states like hadrons from the Lagrangian. It is possible to solve QCD on a computer but it is a computationally intensive task and has limitations at finite density. Some progress can be made by making use of taylor expansion in chemical potential. However results are limited to small chemical potential[42, 43, 44, 45]. Therefore one seeks simpler models of QCD which reproduce important properties of the full theory in certain limit and respects symmetries obeyed by QCD lagrangian. One such model is the Nambu Jona Lasinio model[46, 47, 48]. It was originally postulated in 1962 by Y. Nambu and G. Jona-Lasinio as a model of nucleons with a chiral invariant four fermi interaction. The model was successful in generating large masses for hadrons dynamically while incorporating chiral symmetry which forbids mass term in the lagrangian. Later after the discovery of quarks and gluons the doublet in the model was reinterpreted with up and down quarks. The Lagrangian for the model is :

$$\mathcal{L} = \bar{\psi}(i\partial\!\!\!/ - m)\psi + G(\bar{\psi}\psi)^2 + (\bar{\psi}i\gamma_5\boldsymbol{\tau}\psi)^2 \tag{2.1}$$

In the above lagrangian $\psi = \begin{pmatrix} u & d \end{pmatrix}^T$ is quark doublet. τ are pauli matrices acting in isospin space and G is a dimensionful constant. Dynamical generation of mass is obtained by considering the Dyson equation for quark propagator which leads to following gap equation :

$$M = m + 2iG\int \frac{d^4p}{(2\pi)^4} TrS(p) \tag{2.2}$$

Here $S(p) = \frac{1}{p\!\!\!/ - M}$ is the full quark propagator with dynamical mass M[49]. Taking the trace in color, spin and flavor space we get :

$$M = m + 8N_f N_c G i \int \frac{d^4p}{(2\pi)^4} \frac{M}{p^2 - M^2 + i\epsilon} \tag{2.3}$$

For large enough four fermi coupling G there exists a non-trivial solution to the above gap equation. Eq.(2.3) can be rewritten in terms of chiral condensate as:

$$\langle \bar{q}q \rangle = -\frac{M - m}{2G} \tag{2.4}$$

Since the NJL postulates a four point interaction vertex, the theory is non-renormalizable. This implies one requires a regularization cut off. This a parameter of the theory along with the coupling strength and quark mass m. These are fit to reproduce the correct low energy hadron spectrum. Another limitation of the model is that it does not include confinement.

2.2.1 Mesons in NJL model

In order to calculate the meson masses one evaluates the correlation of two currents in specific channels. Doing so leads to effective propagators for mesons in Random Phase Approximation(RPA)[50]. Considering the quark-antiquark T matrix in RPA approximation one gets :

$$T_M(q^2) = \frac{2G}{1 - 2G\Pi_M(q^2)} \tag{2.5}$$

Here meson polarization function $\Pi_M(q^2)$ is :

$$\Pi_M(q^2) = i\int \frac{d^4p}{(2\pi)^4} Tr[\mathcal{O}_M S(p+q)\mathcal{O}_M S(p)] \qquad (2.6)$$

Evaluating the traces and the gap equation we get following for scalar and pseudo-scalar channel respectively:

$$\begin{aligned}\Pi_\sigma(q^2) &= \frac{1}{2G}\left(1-\frac{m}{M}\right) - \frac{1}{2}\left(q^2-4M^2\right)I(q^2)\Pi_{\pi_a}(q^2)\\ &= \frac{1}{2G}\left(1-\frac{m}{M}\right) - \frac{1}{2}q^2 I(q^2)\end{aligned}$$

The integral $I(q^2)$ is :

$$I(q^2) = 4N_f N_c i\int \frac{d^4p}{(2\pi)^4}\frac{1}{[(p+q)^2-M^2+i\epsilon][p^2-M^2+i\epsilon]} \qquad (2.7)$$

The mass of meson of extracted from the pole position of mesonic propagator at zero three momentum $\boldsymbol{q} = \mathbf{0}$ as follows :

$$1 - 2GRe(\Pi_M(q^2 = {m_M}^2)) = 0 \qquad (2.8)$$

Quark and meson coupling is obtained by taking the derivative of polarization function at $q^2 = m_M^2$. The expression is :

$$g_{Mqq}^{-2} = \frac{d\Pi_M}{dq^2}|_{q^2=m_M^2} \qquad (2.9)$$

Pion decay constant is obtained from one pion to vacuum matrix element:

$$f_\pi q^\mu \delta_{ab} = g_{\pi qq} \int \frac{d^4p}{(2\pi)^4} Tr[\gamma^\mu \gamma_5 \frac{\tau_a}{2} S(p+q) i\gamma_5 \tau_b S(p)] \quad (2.10)$$

It can be shown that that the Goldberger-Treimann relation is satisfied [51].

$$g_{\pi qq} f_\pi = M + \mathcal{O}(m) \quad (2.11)$$

Further, to leading order in 'm', Gell-Mann-Oakes-Renner relation was also shown to be valid [52].

$$f_\pi^2 m_\pi^2 = -m\langle \bar{q}q\rangle + \mathcal{O}(m^2) \quad (2.12)$$

To solve the equations we need to know the value of m_0, G and Λ. These are obtained using the pion mass $m_\pi = 135.0$MeV[53], pion decay constant $f_\pi = 92.4$MeV[54] and chiral condensate $190 \leq - < \bar{u}u >^{1/3} \leq 260 MeV$MeV[55].

2.3 Three flavor NJL model

In the three flavor case addition of strange quark explicitly breaks chiral symmetry. This results in $\langle \bar{s}s\rangle \neq \langle \bar{u}u\rangle$. Lagrangian for the three flavor model is :

$$\begin{aligned}
\mathcal{L} &= \bar{q}(\partial\!\!\!/ - \hat{m})q + \mathcal{L}_{sym} + \mathcal{L}_{det} \\
\mathcal{L}_{sym} &= G \sum_{a=0}^{8} [(\bar{q}\lambda_a q)^2 + (\bar{q} i\gamma_5 \lambda_a q)^2] \\
\mathcal{L}_{det} &= -K[det_f(\bar{q}(1+\gamma_5)q) + det_f(\bar{q}(1-\gamma_5)q)]
\end{aligned} \quad (2.13)$$

In the above lagrangian q is the quark field with three flavors, m is the mass matrix. m_s is different from m_u and m_d

and breaks $SU(3)$ flavor symmetry explicitly. The L_{sym} term is written assuming $SU(3)_f$ symmetry as in case of two flavor model. Here λ_a are the Gell Mann matrices and $\lambda_0 = I$. L_{det} is the t'hooft determinant term. The determinant is taken in flavor space. It breaks $U(1)_a$ symmetry explicity. $U(1)_a$ symmetry is anomalous in QCD. This term is important for getting the masses of η and η' splitting correct in the three flavor model. In mean field approximation the lagrangian 2.13 can be written as :

$$\mathcal{L} = \bar{\psi}(i\partial\!\!\!/ - \hat{M} + \mu\gamma^0)\psi - 2g(\sigma_u^2 + \sigma_u^2 + \sigma_s^2) + 4K\sigma_u^2\sigma_s \quad (2.14)$$

Here we have neglected expectation value for pseudoscalar condensates. $\hat{M} = diag(M_u, M_d, M_s)$ is the diagonal mass matrix. Constituent masses for quarks are given by:

$$\begin{aligned} M_u &= m_u - 4g\sigma_u + 2K\sigma_u\sigma_s \\ M_d &= m_d - 4g\sigma_u + 2K\sigma_u\sigma_s \\ M_s &= m_s - 4g\sigma_s + 2K\sigma_u^2 \end{aligned} \quad (2.15)$$

One may note that since in the present study isospin symmetry between up and down quarks is not broken, σ_d=σ_u is substituted in all expressions. t'hooft term gives extra contribution to mass gap equations which mixes the flavors apart from usual flavor diagonal terms. Using imaginary time formalism we calculate the thermodynamic potential for the mean field lagrangian as:

$$
\begin{aligned}
\Omega(T,\mu,\sigma_u,\sigma_s) = -N_c \sum_{f=u,d,s} \int \frac{d^3p}{(2\pi)^3} \Bigg[\Big(E_{f+} + E_{f-} \Big) \\
+ T \ln \Big(1 + e^{-\beta(E_{f+}-\mu)} \Big) \\
+ T \ln \Big(1 + e^{-\beta(E_{f+}+\mu)} \Big) + T \ln \Big(1 + e^{-\beta(E_{f-}-\mu)} \Big) \\
+ T \ln \Big(1 + e^{-\beta(E_{f-}+\mu)} \Big) \Bigg] \\
+ 2g(\sigma_u^2 + \sigma_u^2 + \sigma_s^2) - 4K\sigma_u^2\sigma_s,
\end{aligned}
$$

The dispersion relations are :

$$
\begin{aligned}
E_{u\pm} &= \sqrt{p^2 + M_u^2} \\
E_{d\pm} &= \sqrt{p^2 + M_d^2} \\
E_{s\pm} &= \sqrt{p^2 + M_s^2}
\end{aligned}
$$

Minimizing the potential implies following gap equations:

$$
\frac{\partial \Omega}{\partial \sigma_u} = \frac{\partial \Omega}{\partial \sigma_d} = \frac{\partial \Omega}{\partial \sigma_s} = 0 \tag{2.16}
$$

Gap equations can have several roots, but the solution with the lowest value of thermodynamic potential is taken as the stable solution. Self consistent solution of above gap equations gives the masses as a function of chemical potential and temperature.

2.3.1 Parameter for three flavor NJL model

We begin the discussion with the parameterization of the model. The parameters to be fixed are the three current quark masses

(m_u, m_d, m_s), the scalar coupling (g), the determinant coupling K and the three momentum cut-off Λ to regularize divergent integrals. There are several parameter sets available for NJL model [49]. These fits are obtained using low energy hadronic properties such as pion decay constant and masses of pion, kaon and η' [56, 57, 58]. The determinant interaction is important as it breaks $U(1)_A$ symmetry and gives correct η mass. One may note that there is discrepancy in determination of the determinant coupling K. For example in Ref. [56] the value of the coupling differs by as much as 30 percent compared to value used in present work. This discrepancy arises due to difference in treatment of η' mesons with a high mass [49]. In fact, this leads to a nonphysical imaginary part for the corresponding polarization diagram in the η' meson channel. This is unavoidable because NJL is not confining and is unrealistic in this context. Within the above mentioned limitations of the model and the uncertainty in the value of the determinant coupling, we proceed with the present parameter set as given in Table (5.1) [49].

Parameters and couplings	**Value**
Three momentum cutoff (Λ)	$\Lambda = 602.3 \times 10^{-3}$ (GeV)
u quark mass (m_u)	$m_u = 5.5 \times 10^{-3}$ (GeV)
d quark mass (m_d)	$m_d = 5.5 \times 10^{-3}$ (GeV)
s quark mass (m_s)	$m_s = 140.7 \times 10^{-3}$ (GeV)
Scalar coupling (g)	$g = 1.835/\Lambda^2$
Determinant interaction (K)	$K = 12.36/\Lambda^5$

Table 2.1: Parameter set considered in this work for 2+1 NJL model apart from the tensor coupling G_T.

In Fig. ?? we have plotted masses as a function of quark

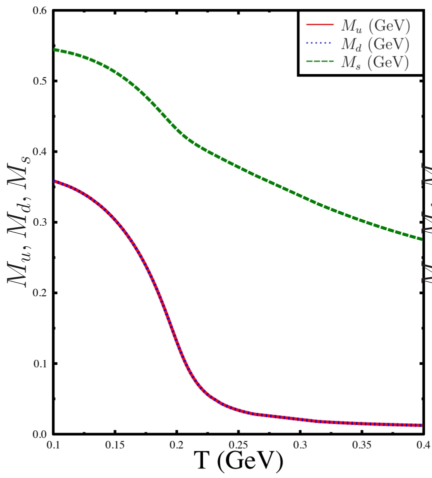

Figure 2.1: M_u, M_s as a function of temperature at zero quark chemical potential.

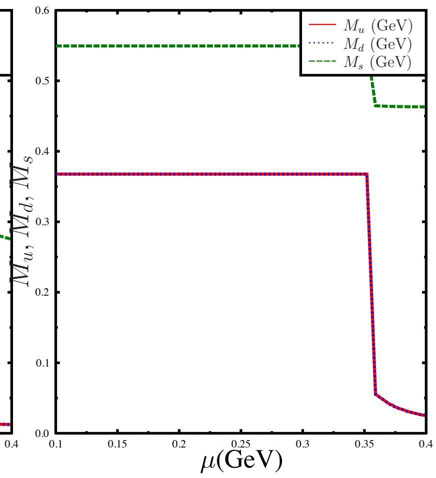

Figure 2.2: M_u, M_s as a function of quark chemcial potential at zero temperature.

chemical potential and temperature. At zero chemical potential and temperature the mass of u and d quarks is 367.6 MeV. As the temperature is increased at zero quark chemical potential the masses of quarks decrease. The decrease is maximum around T=180 MeV. However the transition from high to low quark masses is gradual which suggests a crossover. At temperatures higher than the chiral transition temperature u and d masses are small and asymptotically reach their current mass. The strange mass is large even beyond the transition temperature, bing about 350 MeV at T=300 MeV.

For vanishing temperatures the quark masses remain constant upto a critical quark chemical potential $\mu_c = \mu_q = 360$ MeV. Masses of up and down quarks in this phase is 367.6 MeV. Strange quark mass is about 549.4 MeV. At $\mu_q = \mu_c$ there is a sharp drop in quark masses suggesting a first order phase transition. Up and down quark masses decrease from 367.6 MeV to about 55 MeV while strange mass decreases from 549.4 MeV to 464.5 MeV. One may note here that the strange quark mass decreases as a result of determinant coupling to Up and down quark masses. Such drop in strange quark mass at $\mu_q = \mu_c$ is not observed without determinant coupling.

2.4 Polyakov loop extended Quark Meson Model

2.4.1 Polyakov loop

The Polyakov loop is a Wilson loop in temporal direction. It is defined as :

$$\mathcal{P}(\boldsymbol{x}) = \mathcal{P}exp(i \int_0^\beta d\tau A_0(\boldsymbol{x}, \tau)) \tag{2.17}$$

Here $\mathcal{P}$ is path ordering and $\mathrm{A}_0(\boldsymbol{x}, \tau)$ is time component of gauge field. Color trace of $\mathcal{P}(\boldsymbol{x})$ in the fundamental representation is creation operator of a quark at position $\boldsymbol{x}$. In the Polyakov gauge the temporal component of the gauge field is time independent, i.e. $A_0(\boldsymbol{x}, \tau) = A_0^c(\boldsymbol{x})$. Thus the Polyakov loop operator simplifies to :

$$\mathcal{P}(\boldsymbol{x}) = exp(i\beta A_0^c(\boldsymbol{x})) \tag{2.18}$$

Here $A_0^c(\boldsymbol{x}) = A_0^{(3)}(\boldsymbol{x})\tau_3 + A_0^{(8)}(\boldsymbol{x})\tau_8$. Above relation can be restated as:

$$A_0^c(\boldsymbol{x}) = -i(\partial_\beta \mathcal{P}(\boldsymbol{x}))\mathcal{P}^\dagger(\boldsymbol{x}) \tag{2.19}$$

Polyakov loop variable is the thermal expectation value of the Polyakov loop operator. It is defined as :

$$\Phi(\boldsymbol{x}) = \frac{1}{N_c} < tr_c \mathcal{P}(\boldsymbol{x}) >_\beta, \bar{\Phi}(\boldsymbol{x}) = \frac{1}{N_c} < tr_c \mathcal{P}^\dagger(\boldsymbol{x}) >_\beta \quad (2.20)$$

where the trace is taken in the fundamental representation. In the infinite mass limit the Polyakov loop variable acts as an order parameter for confinement-deconfinement transition. In the confined phase the free energy of system is infinite and Polyakov loop variable vanishes. In the deconfined phase free energy is zero and Polyakov loop has a finite value. This forms the polyakov criterion for confinement in pure gauge theory. Under a center symmetry transformation, polyakov loop variable transforms as :

$$\Phi \to z\Phi, z \in Z_{N_c} \quad (2.21)$$

Thus the confined phase is center symmetric while in deconfined phase center symmetry is broken. In the presence of dynamical quarks the free energy doesn't diverge anymore and hence the order parameter is always finite. Therefore in the presence of dynamical quarks polyakov loop is no longer an order parameter for confinement-deconfinement transition. The mean values of the Polyakov loop variables are determined by minima of the effective Polyakov loop potential obtained for pure glue theory in lattice QCD. In pure Yang mills theory one can write the potential as :

$$\frac{\mathcal{U}(\Phi, \bar{\Phi})}{T^4} = \frac{-b_2}{4}(|\Phi|^2 + |\bar{\Phi}|^2) - \frac{b_3}{6}(\Phi^3 + \bar{\Phi}^3) + \frac{b_4}{16}(|\Phi|^2 + |\bar{\Phi}|^2)^2 \quad (2.22)$$

By fitting thermodynamic potential to lattice results for pure yang mills thermodynamics, we get $b_3 = 0.75$, $b_4 = 7.5$ and temperature dependent b_2 as :

$$b_2(T) = a_0 + a_1\left(\frac{T_0}{T}\right) + a_2\left(\frac{T_0}{T}\right)^2 + a_3\left(\frac{T_0}{T}\right)^3 \tag{2.23}$$

Here $a_0 = 6.75$, $a_1 = -1.95$, $a_2 = 2.625$ and $a_3 = -7.44$. With this parameterization, the critical temperature is $T_0 = 270MeV$.

Quark meson model couples quark to hadronic degrees of freedom such as pions and sigma mesons. However the color symmetry group $SU(3)_c$ which is gauged in QCD is now a global symmetry and thus there are no gluons. Therefore we do not have confinement in the model. Since the model lacks confinement, contribution of quark degrees of freedom to quantities like EoS are non-zero at low temperatures which is unrealistic. However since the mass of quarks is much greater than that of pion, low temperature dynamics are dominated by mesons and results of chiral perturbation theory are reproduced. Furthermore the model shows chiral phase transition at realistic temperatures. By combining the polyakov loop and quark meson model one hopes to combine the confining properties of QCD with the chiral dynamics of quark meson model to achieve a more realistic EoS. The lagrangian for two flavor Polyakov extended quark meson model is given as:

$$\mathcal{L} = \bar{q}(i\not{D} - g(\sigma + i\gamma_5 \boldsymbol{\tau}.\boldsymbol{\pi}))q + \frac{1}{2}(\partial_\mu\sigma)^2 + \frac{1}{2}(\partial_\mu\boldsymbol{\pi})^2 - U(\sigma,\boldsymbol{\pi}) - \mathcal{U}(\Phi,\bar{\Phi}) \tag{2.24}$$

The gauge covariant derivative reads:

$$\not{D}(\Phi) = \gamma_\mu\partial_\mu - i\gamma_0 A_0(\Phi), A_\mu = \delta_{\mu 0}A_0 \tag{2.25}$$

The potential for mesons $U(\sigma, \boldsymbol{\pi})$ is defined as:

$$U(\sigma, \boldsymbol{\pi}) = \frac{\lambda}{4}(\sigma^2 + \boldsymbol{\pi}^2 - v^2)^2 - c\sigma \tag{2.26}$$

Here the term linear in sigma is responsible for explicit chiral symmetry breaking and giving finite mass to pions. Without this term the Lagrangian is exactly invariant under $SU(2)_L \times SU(2)_R$ transformation.

2.4.2 Free energy in Quark meson model

The free energy of the quark meson model is :

$$\Omega = \mathcal{U}(\Phi, \bar{\Phi}) + U(\sigma) + \Omega_{\bar{q}q}(\Phi, \bar{\Phi}, \sigma) \tag{2.27}$$

Mesonic potential is as given in Eq. 2.26. The contribution of quarks to the thermodynamic potential is:

$$\Omega_{\bar{q}q} = -2N_f T \int \frac{d^3p}{(2\pi)^3} tr_c[ln(1 + \mathcal{P}e^{-(E_p-\mu)/T}) + ln(1 + \mathcal{P}^\dagger e^{-(E_p+\mu)/T})] \tag{2.28}$$

The single quasiparticle energy is given as:

$$E_p = \sqrt{\boldsymbol{p}^2 + m_q^2} \tag{2.29}$$

After carrying out the color trace we get:

$$\begin{aligned}\Omega_{\bar{q}q} =& -2N_f T \int \frac{d^3p}{(2\pi)^3} (ln[1 + 3(\Phi + \bar{\Phi}e^{-(E_p-\mu)/T})e^{-(E_p-\mu)/T} + e^{-3(E_p-\mu)/T}] \\ &+ ln[1 + 3(\bar{\Phi} + \Phi e^{-(E_p+\mu)/T})e^{-(E_p+\mu)/T} + e^{-3(E_p+\mu)/T}])\end{aligned} \tag{2.30}$$

A cutoff Λ is not required since PQM model is renormalizable. For a given temperature T and chemical potential μ the value of σ and Polyakov loop variables Φ and $\bar{\Phi}$ are found by minimizing the thermodynamic free energy. Thus we get the gap equations :

$$\frac{\partial \Omega}{\partial \sigma} = \frac{\partial \Omega}{\partial \Phi} = \frac{\partial \Omega}{\partial \bar{\Phi}} = 0 \tag{2.31}$$

The σ and π masses are determined by the curvature of Ω at the global minimum

$$M_\sigma^2 = \frac{\partial^2 \Omega}{\partial \sigma^2}, \qquad M_{\pi_i}^2 = \frac{\partial^2 \Omega}{\partial \pi_i^2}. \tag{2.32}$$

These equations lead to the masses for the σ and pions given as

$$M_\sigma^2 = m_\pi^2 + \lambda(3\sigma^2 - f_\pi^2) + g_\sigma^2 \frac{\partial \rho_s}{\partial \sigma} \tag{2.33}$$

$$M_\pi^2 = m_\pi^2 + \lambda(\sigma^2 - f_\pi^2) + g_\sigma^2 \frac{\partial \rho_{ps}}{\partial \pi}. \tag{2.34}$$

Explicitly,

$$\frac{\partial \rho_s}{\partial \sigma} = \frac{6}{\pi^2} \int dpp^2 \left[\frac{g_\sigma p^2}{E(\mathbf{p})^3} \left(f_-(\mathbf{p}) + f_+(\mathbf{p}) \right) + \frac{M}{E(\mathbf{p})} \left(\frac{\partial f_-}{\partial \sigma} + \frac{\partial f_+}{\partial \sigma} \right) \right] \tag{2.35}$$

The derivatives of the distribution functions with respect to to the scalar field σ are given as

$$\frac{\partial f_-(\mathbf{p})}{\partial \sigma} = \frac{\beta g_\sigma^2 \sigma}{E(\mathbf{p})} \left[3{f_-}^2 - \frac{3e^{-3\beta\omega_-} + 4\bar{\phi}e^{-2\beta\omega_-} + \phi e^{-\beta\omega_-}}{1 + 3\phi e^{-\beta\omega_-} + 3\bar{\phi}e^{-2\beta\omega_-} + e^{-3\beta\omega_-}} \right] \tag{2.36}$$

and,

$$\frac{\partial f_+}{\partial \sigma} = \frac{\beta g_\sigma^2 \sigma}{E(\mathbf{p})} \left[3{f_+}^2 - \frac{3e^{-3\beta\omega_+} + 4\phi e^{-2\beta\omega_+} + \bar{\phi}e^{-\beta\omega_+}}{1 + 3\bar{\phi}e^{-\beta\omega_+} + 3\phi e^{-2\beta\omega_+} + e^{-3\beta\omega_+}} \right] \tag{2.37}$$

Similarly,

$$\frac{\partial \rho_{ps}}{\partial \pi} = \frac{6}{\pi^2} \int dp \frac{p^2}{E(\mathbf{p})} \left[f_-(\mathbf{p}) + f_+(\mathbf{p}) \right]. \qquad (2.38)$$

2.4.3 Parameters of PQM model

There are four parameters in the PQM model g, λ, v and c. They are obtained using spontaneous breakng of chiral symmetry, constituent quark mass in vacuum and PCAC relations. The expectation value $< \sigma >= f_\pi$, where f_π is the pion decay constant. The expectation value $< \boldsymbol{\pi} >$ of psuedoscalar fields is set to zero. Yukawa coupling g is fixed by vacuum quark mass as $g = m_q/f_\pi$. Partial conserved axial current gives $c = m_\pi^2 f_\pi$. Quartic coupling λ is fixed by sigma mass as $\lambda = (m_\sigma^2 - m_\pi^2)/(2f_\pi^2)$. Parameter v is fixed by minima of the mesonic potential as $v^2 =< \sigma >^2 -c/(\lambda < \sigma >)$. The values of the masses and decay constant are $m_\pi = 138MeV$, $m_\sigma = 600MeV$, $f_\pi = 93MeV$, $m_q = 300MeV$, $c = 1.77 \times 10^6 MeV^3$, $v = 87.6MeV$, $\lambda = 19.7$ and $g = 3.2$. T_0 is taken to be 192 MeV.

2.4.4 Phase structure of Polyakov quark meson model

In Fig. 2.4.4 we have plotted the variation of the chiral condensate and Polyakov loop variable as a function of temperature for $\mu_q = 0$. The chiral condensate has been normalized to 1. Since the baryon chemical potential is zero the polyakov loop variable and conjugate polyakov loop variable are equal. As temperature increases the value of chiral condensate remains nearly constant till about 150 MeV. From this point onwards the condensate starts decreasing and around 170 MeV it decreases rapidly. As temperature is further increased it decreases slowly but never vanishes. The Polyakov loop variable on the other hand increases with temperature. For small values of temperature the

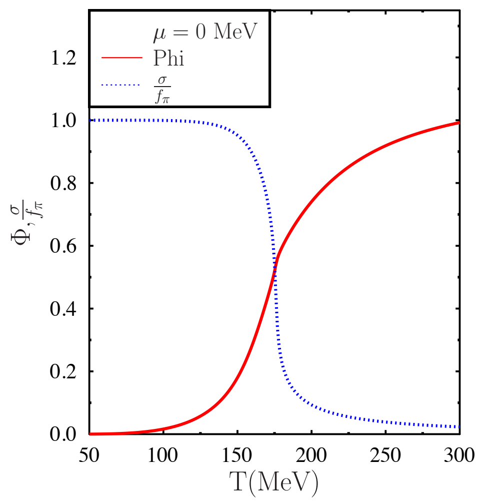

Figure 2.3: Variation of Polyakoc loop variable Φ and σ as a function of temperature at zero quark chemical potential.

polyakov loop variable is nearly zero. At high temperatures it reaches unity. One may note that polyakov loop variable exceeds unity in high temperature limit.

In Fig. 2.4.4 we have plotted the constituent quark mass and meson masses as a function of temperature for vanishing quark chemical potential. In chiral symmetry broken phase the pion mass, being the mass of goldstone mode, is approximately constant and varies only weakly with temperature. On the other hand mass of σ, which is about twice the constituent mass of quark, drops significantly near the transition temperature. Beyond the chiral transition temperature, since the chiral symmetry is restored, the masses of σ and π mesons become equal as they are chiral partners.

In Fig. 2.4.4 we have shown the trace anomaly as a function of temperature. From the plot we see that conformal symmetry

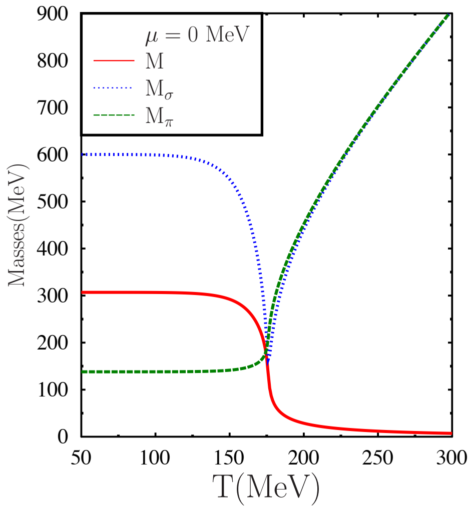

Figure 2.4: Quark mass M, Pion mass M_π and Sigma mass M_σ at zero quark chemical potential.

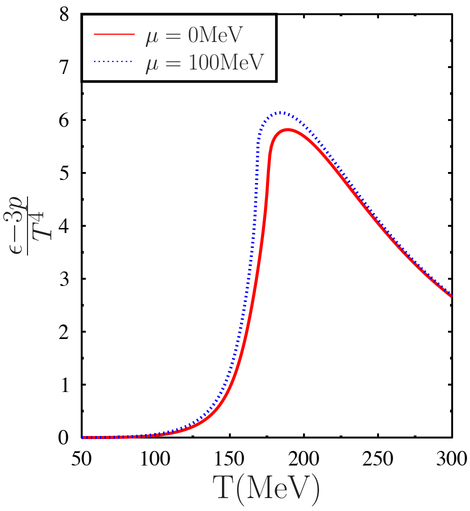

Figure 2.5: Trace anomaly $\frac{(\epsilon - 3p)}{T^4}$ at zero quark chemical potential.

is maximally broken near the transition temperature. The peak is found to increase with chemical potential. This is relevant for the computation of bulk viscosity.
Next in order to study the critical behavior and susceptibilities, one has to take higher derivatives of the thermodynamic potential with respect to order parameters. First order derivatives vanish to get solutions corresponding to minima of thermodynamic potential. Numerical differentiation is less accurate for higher order derivatives. We adopt a semi-analytic approach here. Numerics are used only for calculating final expressions.[**?**]. For example, to calculate the derivative of the order parameter X, $(X = \sigma, \phi, \bar{\phi})$ with respect to temperature is given by the equation

$$\frac{\partial}{\partial T}\left(\frac{\partial \Omega}{\partial X}\right)+\frac{\partial}{\partial \sigma}\left(\frac{\partial \Omega}{\partial X}\right)\frac{d\sigma}{dT}+\frac{\partial}{\partial \phi}\left(\frac{\partial \Omega}{\partial X}\right)\frac{d\phi}{dT}+\frac{\partial}{\partial \bar{\phi}}\left(\frac{\partial \Omega}{\partial X}\right)\frac{d\bar{\phi}}{dT}=0. \tag{2.39}$$

Thus we have a matrix equation of the type $\mathbf{A}\cdot\mathbf{Y}=\mathbf{B}$, where $\mathbf{A}$ is the coefficient matrix of the variables $\mathbf{Y}=\left(\frac{\mathbf{d}\sigma}{\mathbf{dT}},\frac{\mathbf{d}\phi}{\mathbf{dT}},\frac{\mathbf{d}\bar{\phi}}{\mathbf{dT}}\right)^{\mathbf{T}}$, and $\mathbf{B}$ is the matrix of derivatives of the thermodynamic potential involving explicit dependence on temperature, i.e., $\mathbf{B} = \left(-\frac{\partial}{\partial \mathbf{T}}(-\frac{\partial \mathbf{\Omega}}{\partial \sigma},-\frac{\partial \mathbf{\Omega}}{\partial \phi},-\frac{\partial \mathbf{\Omega}}{\partial \bar{\phi}})^{\mathbf{T}}\right)$.These matrix equations can be solved using Cramers rule. The coefficient matrix $\mathbf{A}$ is given by

$$\mathbf{A}=\begin{bmatrix}\Omega_{\sigma\sigma} & \Omega_{\sigma\phi} & \Omega_{\sigma\bar{\phi}}\\ \Omega_{\phi\sigma} & \Omega_{\phi\phi} & \Omega_{\phi\bar{\phi}}\\ \Omega_{\bar{\phi}\sigma} & \Omega_{\bar{\phi}\phi} & \Omega_{\bar{\phi}\bar{\phi}}\end{bmatrix} \tag{2.40}$$

with, $\Omega_{ab}=\frac{\partial^2\Omega}{\partial a\partial b}$ where a, b stand for σ, ϕ and $\bar{\phi}$. Similarly, to calculate the derivatives with respect to chemical potential, the coefficient matrix $\mathbf{A}$ remains the same while the matrix $\mathbf{B}$ will involve derivatives of the thermodynamic potential involving explicit dependence on the chemical potential.

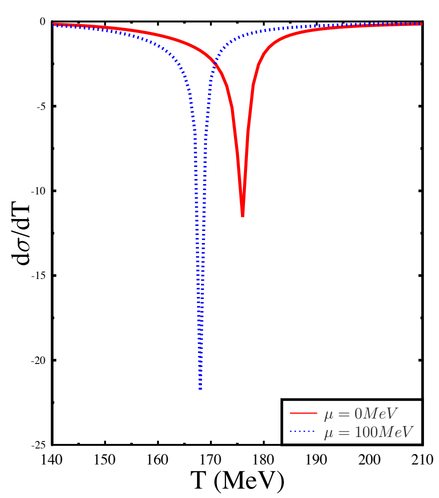

Figure 2.6: Derivative of chiral order parameter.

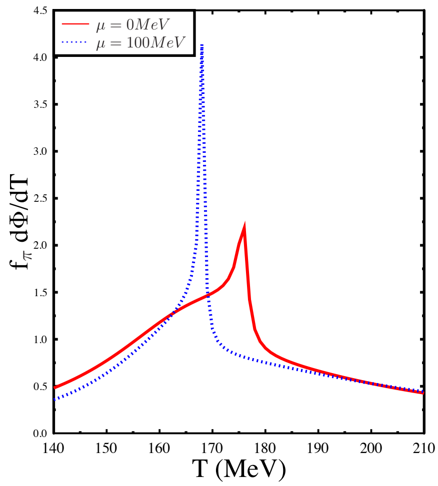

Figure 2.7: Derivative of Polyakov loop variable multiplied by pion decay constant.

Solving Eq. (2.39) this way, we have plotted the derivatives of the order parameters in Fig. 5.5. The critical temperature is defined by the position of the peaks of these derivatives of the order parameters. At zero chemical potential this occurs at $T_C \simeq 176$ MeV. Let us note that at T_C, the quark mass is $m_q = g_\sigma \sigma = 134$MeV, while the Polyakov loop variable $\phi \sim= 0.5$. Thus at the critical temperature the effect of interaction is significant. As chemical potential for the quarks increase the critical temperature decreases. With finite chemical potential the peaks also become sharper and at higher chemical potential the transition becomes a first order one. The critical point within this model occurs at $(T_c, \mu_c) = (155, 163)$ MeV.

The other thermodynamic quantity that enters into the transport coefficient calculation is the velocity of sound. The same

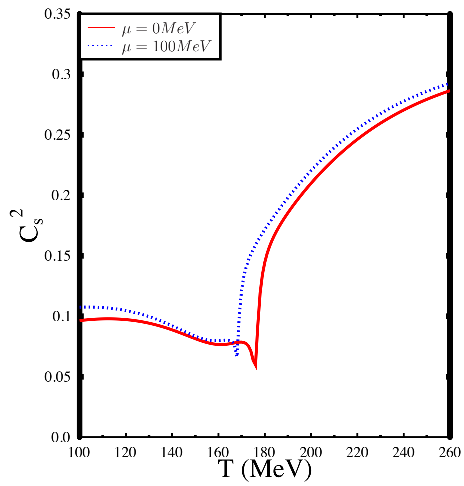

Figure 2.8: Temperature dependence of the velocity of sound at constant density.

at constant density is defined as

$$c_s^2 = \left(-\frac{\partial P}{\partial \epsilon}\right)_n = \frac{s\chi_{\mu\mu} - \rho\chi_{\mu T}}{T(\chi_{TT}\chi_{\mu\mu} - \chi_{\mu T}^2)} \tag{2.41}$$

where, P,the pressure, is the negative of the thermodynamic potential given in Eq. (4.59). Further, $s = -\frac{\partial\Omega}{\partial T}$ is the entropy density and the susceptibilities are defined as $\chi_{xy} = -\frac{\partial^2\Omega}{\partial x \partial y}$. The velocity of sound shows a minimum near the crossover temperature. Within the model, at low temperature when the constituent quarks start contributing to the pressure, their contribution to the energy density is significant compared to their contribution to the pressure leading to decreasing behavior of the velocity of sound until the crossover temperature, beyond which it increases as the quarks become light and approach the massless limit of $c_s^2 = \frac{1}{3}$. Such a dip in the velocity of sound is also observed in lattice simulation. As we shall observe later, this behavior will have important consequences for the behavior of bulk viscosity as a function of temperature. We might mention here that such a dip for the sound velocity was not observed for two-flavor NJL [59]. For the linear sigma model calculations such a dip was observed only for a large sigma meson mass [15].

2.5 Boltzmann equation

We follow a kinetic theory approach to study the transport coefficients of hot and dense matter[60, 15, 8, 9, 61, 62]. Each particle of given species is described by a phase space density distribution function nearly in equilibrium. Then the distribution function can be expanded as :

$$f(\boldsymbol{x},\boldsymbol{p},t) = f^0(\boldsymbol{x},\boldsymbol{p},t) + f^1(\boldsymbol{x},\boldsymbol{p},t) \tag{2.42}$$

Here $f^0(\boldsymbol{x},\boldsymbol{p},t)$ is the local equilibrium distribution function given as follows :

$$f^0(\boldsymbol{x},\boldsymbol{p},t) = \frac{1}{exp(\beta(x)(u_\nu(x)p^\nu \mp \mu(x))) + 1} \tag{2.43}$$

with $u_\mu = \gamma_\mu(1,\boldsymbol{u})$ being the four velocity, $\gamma_u = \sqrt{1-|\boldsymbol{u}|^2}$ is th elorentz factor, μ is the chemical potential and E=$\sqrt{\boldsymbol{p}^2+M^2}$ is the dispersion relation with medium dependent mass M. The Boltzmann equation for non-equilibrium distribution is :

$$\frac{\partial f_a}{\partial t} + \boldsymbol{v}_a.\nabla f_a - \nabla E_a.\nabla_p f_a = -C^a[f] \tag{2.44}$$

In the above equation index 'a' refers to a particular species of particle. Mass M being medium dependent can be differentiated with respect to spatial coordinates. Thus we can rewrite the above equation as :

$$\frac{p^\mu}{E_a}\partial_\mu f^a - \frac{M}{E^a}\frac{\partial M}{\partial x^i}\frac{\partial f^a}{\partial p^i} = -C^a[f] \tag{2.45}$$

In the above equation spatial and momentum gradients are assumed to be small. Also in this work the collision integral $C^a[f]$ on the right hand side contains only 2 →2 scatterings only. In relaxation time approximation(RTA) the collision integral for species 'a' contains non-equilibrium distribution only for species 'a' and equilibrium distribution for all other species. One may note that collision term $C^a[f_0]$ for equilibrium distribution f_0 is zero by detailed balance. Then the collision term can be written as:

$$C[f] = -f_a^1/\tau_a \tag{2.46}$$

τ_a is the relaxation time, or the inverse of scattering rate of species 'a'. It depends on energy of particle 'a'.

In order to derive transport coefficients within RTA approximation we consider the change in energy momentum tensor due to deviation from equilibrium of distribution functions. We consider energy momentum tensor $T^{\mu\nu}$ and quark four current J^μ as :

$$\begin{aligned} T^{\mu\nu} &= -pg^{\mu\nu} + wu^\mu u^\nu + \Delta T^{\mu\nu} \\ J_\mu &= nu_\mu + \Delta J_\mu \end{aligned} \tag{2.47}$$

p is the pressure and is a function of temperature and pressure, ϵ is the energy density and $w = \epsilon + p$ is enthalpy. u_μ is the four velocity of the fluid. $\Delta T^{\mu\nu}$ and ΔJ_μ are the dissipative parts defined in terms of viscosity and conductivity as follows:

$$\Delta T^{\mu\nu} = \eta\left(D^{\mu}u^{\nu} + D^{\nu}u^{\mu} + \frac{2}{3}\Delta^{\mu\nu}\partial_{\alpha}u^{\alpha}\right) - \zeta\partial_{\alpha}u^{\alpha},$$
$$\Delta J_{\mu} = \lambda\left(\frac{nT}{w}\right)^{2} D_{\mu}\left(\frac{\mu}{T}\right) \tag{2.48}$$

Here η, ζ and λ are the coefficients of shear viscosity, bulk viscosity and thermal conductivity respectively. $D_{\mu} = \partial_{\mu} - u_{\mu}u^{\alpha}\partial_{\alpha}$ is deriviative normal to u^{μ}. One may note that in the fluid rest frame D_0=0 an $D_i = \partial_i$.

In terms of distribution functions the energy momentum tensor and quark current can be written as:

$$T^{\mu\nu} = \sum_a \int d\Gamma^a \frac{p^{\mu}p^{\nu}}{E_a} f_a + g^{\mu\nu}V \tag{2.49}$$

$$J_{\mu} = \int \sum_a t_a \int d\Gamma_a \frac{p_{\mu}}{E_a} f_a \tag{2.50}$$

$d\Gamma_a = g_a \frac{d^3p}{(2\pi)^3}$ is the phase space measure and g_a is degeneracy for species 'a'. $p^{\mu} = (E_a, \boldsymbol{p})$ and $E_a = \sqrt{\boldsymbol{p}^2 + m^2}$. Second term in Eq. 2.49 is the "vacuum" energy density contribution giving a medium dependent mass. $t^a = \pm 1$ for particles and anti-particles. The distribution function here contains both the equilibrium and non-equilibrium part. Using the non-equilibrium part we can calculate the deviation in spatial part of energy momentum tensor as :

$$\delta T^{ij} = \sum_a \int d\Gamma^a \frac{p^i p^j}{E_a}\left(\delta f_a - f_a^0 \frac{\delta E_a}{E_a}\right) - \delta^{ij}\delta V \tag{2.51}$$

Since the mass is medium dependent, its variation is also taken into account. The variation in distribution function is given as :

$$\delta f_a = f_a(E_a, T, \mu) - f_a^0(E_a^0, T^0, \mu^0) = \delta \tilde{f}_a - \frac{\delta E_a}{T}(f_a^0(1 - f_a^0)) \tag{2.52}$$

Here the superscript ^{0} denotes equilibrium values. It is only the $\delta \tilde{f}_a$ which determines the transport coefficients.

Deviation in vacuum energy is obtained using gap equation as :

$$\delta V = \sum_a \int d\Gamma_a \frac{M}{E_a} f_a \delta M \tag{2.53}$$

Deviation in energy momentum tensor can now be written as :

$$\delta T^{ij} = \sum_a \int d\Gamma_a \frac{p^i p^j}{E^a} \delta \tilde{f} - \sum_a \int d\Gamma_a \frac{M}{E_a} f^a \left(1 + \frac{p^2(1 - f_a)}{3E_a T} + \frac{\boldsymbol{p}^2}{3E_a^2}\right) \delta M \tag{2.54}$$

Here we have made the substituted $p^i p^j \sim \frac{1}{3}\boldsymbol{p}^2$ and $\delta E_a = (M/E_a)\delta M$. Second term in the above equation vanishes. The result is :

$$\Delta T^{ij} = \sum_a \int d\Gamma_a \frac{p^i p^j}{E_a} \delta \tilde{f} \tag{2.55}$$

Similarly for quark four current we have

$$\Delta J^i = \sum_a t_a \int d\Gamma^a \frac{\boldsymbol{p}^i}{E_a} \delta \tilde{f} \tag{2.56}$$

In order to continue with the calculation we need to determine $\delta\tilde{f}^a$. This is achieved by using Boltzmann equation. The spatial and momentum space gradients are assumed to be small. Thus LHS of Eq. 2.45 is small due to assumption of small gradients. Therefore the non-equilibrium distributions f_a can be approximated by equilibrium distributions f_a^0 on the LHS of Eq. 2.45. We choose the local rest frame $u_\mu = (1, 0, 0, 0)$ in which velocity gradients are zero. The derivative of f_a^0 is given as :

$$\partial_\mu f_a^0 = -f_a^0(1 - f_a^0)\Big[-\frac{1}{T^2}(E_a - \mu_a) + \frac{1}{T}\partial_\mu(\pi_\nu u^\nu - \mu^\alpha)\Big] \tag{2.57}$$

E_a also depends on the spatial position through dependence of medium dependent mass M. Then the first term of Eq. 2.45 gives :

$$\frac{p^\mu}{E^a}\partial_\mu f_a^0 = \frac{f_a^0(1 - f_a^0)}{E^a}\Bigg[\frac{E^a}{T^2}p^\mu\partial_\mu T + p^\mu\partial_\mu\left(\frac{\mu^a}{T}\right) - \frac{1}{T}(p^\mu\partial_\mu E^a + p^\mu p^\nu\partial_\mu u_\nu)\Bigg] \tag{2.58}$$

Second term of Eq. 2.45 gives :

$$\frac{\partial f_a^0}{\partial p^i} = -f_a^0(1 - f_a^0)\frac{p_i}{E_a T} \tag{2.59}$$

In the local rest frame $\partial_\nu u^0 = 0$. Combining Eqs. 2.58 and 2.59 we get for the LHS of Eq. 2.45 :

$$\frac{f_a^0(1-f_a^0)}{E^a}\left[-E^a\partial_0\left(\frac{E^a-\mu^a}{T}\right)\frac{E^a p^i}{T}\left(\frac{\partial_i T}{T}-\partial_0 u_i\right)+p^i\partial_i\left(\frac{\mu^a}{T}-p^ip^j\partial_j u_i\right)\right] = - \tag{2.60}$$

Using energy momentum conservation and thermodynamic relations we can write :

$$\frac{df_a^0}{dt} = \frac{f_a^0(1-f_a^0)}{T}q^a(\beta,\mu) = -\frac{\delta\tilde{f}_a}{\tau_a} \tag{2.61}$$

$$\begin{aligned} q^a(T,\mu) = -\Bigg[&\frac{\partial T}{\partial t}\left(\frac{E^a-\mu^a}{T}-\frac{\partial E^a}{\partial T}\right) \\ &-\frac{\partial\mu}{\partial t}\left(\frac{\partial E^a}{\partial\mu}-t^a\right)+\frac{T}{E^a}\left(t^a-\frac{E^a n}{w}\right)p^i\partial_i\left(\frac{\mu}{T}\right) \\ &-\frac{p^ip^j}{2E^a}W_{ij}+\frac{\boldsymbol{p}^2}{3E^a}\partial_k u^k\Bigg] \end{aligned} \tag{2.62}$$

From above equation one can see that the Boltzmann equation relates the non-equilibrium distribution to variation in fluid velocity, temperature and chemical potential. Using energy momentum conservation and baryon number conservation one can relate the temporal derivatives of temperature and chemical potential with velocity gradients and speed of sound.

$$\begin{aligned} \partial_0 T &= -v_n^2 T\nabla.\boldsymbol{u} \\ \partial_0\mu &= -v_s^2\mu\nabla.\boldsymbol{u} \end{aligned} \tag{2.63}$$

Here v_n and v_s are speed of sound at constant number density and entropy respectively.

$$v_n^2 = \left(\frac{\partial P}{\partial \epsilon}\right)_n = \frac{\partial(p,n)}{\partial(\epsilon,n)} = \frac{s\chi_{\mu\mu} - n\chi_{\mu T}}{\frac{\partial \epsilon}{\partial T}\chi_{\mu\mu} - \frac{\partial \epsilon}{\partial \mu}\chi_{\mu T}}$$
$$v_s^2 = \left(\frac{\partial P}{\partial \epsilon}\right)_s = \frac{\partial(p,s)}{\partial(\epsilon,s)} = \frac{s\chi_{\mu T} - n\chi_{TT}}{\frac{\partial \epsilon}{\partial T}\chi_{\mu T} - \frac{\partial \epsilon}{\partial \mu}\chi_{TT}} \tag{2.64}$$

Using thermodynamic relation the above equations can be rewritten in following useful form as :

$$v_n^2 = \frac{s\chi_{\mu\mu} - n\chi_{\mu T}}{T(\chi_{\mu\mu}\chi_{TT} - \chi_{\mu T}^2)}$$
$$v_s^2 = \frac{n\chi_{TT} - s\chi_{\mu T}}{\mu(\chi_{\mu\mu}\chi_{TT} - \chi_{\mu T}^2)} \tag{2.65}$$

Variation in the distribution function can now be written as :

$$\frac{\delta \tilde{f}_a}{\tau_a} = -\frac{f_a^0(1-f_a^0)}{T} q^a(T,\mu) \tag{2.66}$$

$$q^a(T,\mu) = -Q_a(T,\mu,\boldsymbol{p}^2)\nabla.\boldsymbol{u} + \frac{T}{E_a} p^i \partial_i \left(\frac{\mu}{T}\right)\left(t_a - \frac{E_a n}{w}\right) + \frac{p^i p^j}{2T} W_{ij} \tag{2.67}$$

$Q_a(T,\mu,\boldsymbol{p}^2)$ is given as :

$$Q_a(T,\mu,\boldsymbol{p}^2) = -\left[v_n^2\left(-E_a + T\frac{\partial E_a}{\partial T} + \mu\frac{\partial E_a}{\partial \mu}\right) + \left(\frac{\partial P}{\partial n}\right)_\epsilon \left(\frac{\partial E_a}{\partial \mu} - t_a\right) + \frac{\boldsymbol{p}_a^2}{3E_a}\right] \tag{2.68}$$

Substituting Eq. 2.66 in Eq. 2.55 we get :

$$\delta T^{ij} = \sum_a \int d\Gamma \frac{p_a^i p_a^j}{T E_a} \tau_a f_a^0 (1 - f_a^0) q_a(\boldsymbol{p}, \beta, \mu) \tag{2.69}$$

Here the term in Eq. 2.67 proportional to gradient of $\frac{\mu}{T}$ vanishes by symmetry. Comparing with the disspative part of $\Delta T^{\mu\nu}$ in Eq. 2.55 we get :

$$\begin{aligned} \eta &= \frac{1}{15T} \sum_a \int d\Gamma_a \frac{\boldsymbol{p}_a^4}{E_a^2} (\tau_a f_a^0 (1 - f_a^0)) \\ \zeta &= -\frac{1}{3T} \sum_a \int d\Gamma_a \frac{\boldsymbol{p}_a^2}{E_a^2} (\tau_a f_a^0 (1 - f_a^0) Q_a) \end{aligned} \tag{2.70}$$

Similarly substituting $\delta \tilde{f}$ in Eq. 2.56. we get :

$$\delta J_i = \sum_a \int d\Gamma_a p^i \tau^a f_a^0 (1 - f_a^0) q^a(t, \mu) \tag{2.71}$$

Here the term proportional to $\frac{\mu}{T}$. Comparing with second equation in Eq. 2.48. the thermal conductivity is :

$$\lambda = \left(\frac{w}{nT}\right)^2 \sum_a \int d\Gamma^a \frac{p^2 \tau_a}{3E_a^2} \left(1 - \frac{t^a n E^a}{w}\right) f_a^0 (1 - f_a^0) \tag{2.72}$$

Q^a solutions in Eq. 2.68 should satisfy Landau Lifshitz conditions $u_\mu \Delta J^\mu = 0$ and $u_\mu u_\nu T^{\mu\nu} = 0$. The conditions in the local rest frame imply :

$$\begin{aligned}\Delta J_0 &= \sum_a \int d\Gamma_a t^a \delta f_a = 0 \\ \Delta T^{00} &= \sum_a \int d\Gamma_a E_a \delta f_a = 0\end{aligned} \tag{2.73}$$

Using Eq. 2.52, Landau Lifshitz conditions in relaxation time approximation can be written as :

$$\begin{aligned}\Delta J_0 &= \langle \tau^a Q^a(T,\mu) t^a g^a(T,\mu)\rangle = 0 \\ \Delta T^{00} &= \langle \tau^a Q^a(T,\mu) E^a g^a(T,\mu)\rangle = 0\end{aligned} \tag{2.74}$$

Here $g^a(T,\mu) = 1 - \frac{T(\frac{\partial E^a}{\partial T})_\sigma}{E^a - \mu^a + T(\frac{\partial \mu^a}{\partial T}_\sigma)}$. The derivatives at constant entropy are [63]:

$$\begin{aligned}\left(\frac{\partial E^a}{\partial T}\right)_\sigma &= \left(\frac{\partial E^a}{\partial T}\right)_\mu + \left(\frac{\partial E^a}{\partial \mu}\right)_T \left(\frac{\partial \mu}{\partial T}\right)_\sigma \\ \left(\frac{\partial \mu}{\partial T}\right)_\sigma &= \frac{1}{T}\left[\mu + \frac{1}{v_n^2}\left(\frac{\partial p}{\partial n}\right)_\epsilon\right]\end{aligned} \tag{2.75}$$

The notation $\langle \phi_a(p)\rangle$ stands for [62] :

$$\langle \phi_a(p)\rangle = \int d\Gamma[\phi_a(p) f_a^0 (1 - f_a^0)] \tag{2.76}$$

Landau-Lifshitz condition can also be satisfied by use of lagrange multipliers as follows [63, 62] :

$$\tau_a Q_a \rightarrow \tau_a Q_a - \alpha_n t^a - \alpha_e E^a \tag{2.77}$$

Substituting Eq. 2.77 in Eq. 2.74 we get :

$$\begin{aligned}
&\sum_a t_a \langle \tau_a Q_a \rangle - \alpha_n \sum_a \langle g^a \rangle - \alpha_e \sum_a \langle t^a E^a g^a \rangle = 0, \\
&\sum_a \langle E_a \tau_a Q_a \rangle - \alpha_n \sum_a \langle t^a E^a g^a \rangle - \alpha_e \sum_a \langle E_a^2 g^a \rangle = 0
\end{aligned} \tag{2.78}$$

Making the replacement Eq. 2.77 in Eq. 2.70 and using above two relations one gets bulk viscosity as :

$$\begin{aligned}
\zeta = &\frac{1}{9T} \sum_a \int d\Gamma^a \tau^a f_a^0 (1 - f_a^0) \\
&\left[\frac{\boldsymbol{p}^2}{E^a} - 3v_n^2 \left(E^a - T\frac{\partial E^a}{\partial T} - \mu \frac{\partial E^a}{\partial \mu} \right) + 3 \left(\frac{\partial P}{\partial n} \right)_\epsilon \left(\frac{\partial E^a}{\partial \mu} - t^a \right) \right]^2
\end{aligned} \tag{2.79}$$

Using the constraint $\Delta T^{0i} = 0$ in rest frame, one gets following expression for thermal conductivity as :

$$\lambda = \frac{1}{3} \left(\frac{w}{nT} \right)^2 \sum_a \int d\Gamma \frac{\boldsymbol{p}^2}{E_a^2} \tau^a \left(t^a - \frac{nE^a}{w} \right)^2 f_a^0 (1 - f_a^0) \tag{2.80}$$

2.6 Quark Matter in magnetic field

In order to solve Dirac equation in magnetic field we assume a magnetic field in z-direction $\boldsymbol{B} = B_0 \hat{\boldsymbol{z}}$. We choose the gauge $A_B^0 = A_B^y = A_B^z = 0, A_B^x = -yB_0$. Dirac equation for a particle of mass m and charge eQ in presence of magnetic field is :

$$
\begin{aligned}
i\frac{\partial\psi}{\partial t} &= \mathcal{H}_B\psi \\
\mathcal{H}_B &= \boldsymbol{\alpha}.\boldsymbol{\Pi} + \beta m
\end{aligned}
\tag{2.81}
$$

Here $\boldsymbol{\Pi} = -i\boldsymbol{\nabla} - e\boldsymbol{A}$ is the conjugate momentum. For stationary states we can write :

$$
\psi = e^{-iEt}\begin{pmatrix}\phi \\ \chi\end{pmatrix}
\tag{2.82}
$$

In this two component notation one can write equation 2.81 as :

$$
(E-m)\phi = \boldsymbol{\sigma}.(-i\boldsymbol{\nabla} - eQ\boldsymbol{A})\chi(E+m)\chi = \boldsymbol{\sigma}.(-i\boldsymbol{\nabla} - eQ\boldsymbol{A})\phi
\tag{2.83}
$$

Solving for ϕ we get :

$$
(E^2-m^2)\phi = \left[-\boldsymbol{\nabla}^2 + (eQ\boldsymbol{B})^2y^2 - eQ\boldsymbol{B}(2iy\frac{\partial}{\partial x} + \sigma_3)\right]\phi
\tag{2.84}
$$

Taking the solution to be of the form $\phi = e^{i\boldsymbol{p}.\boldsymbol{X}_{\not y}}f(y)$. There are in general two independent solutions for $f(y)$ which can be taken to be eigenstates of σ_z as follows :

$$
\begin{aligned}
f_+(y) &= \begin{pmatrix}F_+(y) \\ 0\end{pmatrix} \\
f_-(y) &= \begin{pmatrix}0 \\ F_-(y)\end{pmatrix}
\end{aligned}
\tag{2.85}
$$

The differential equation satisfied by F_s, where s is defined as eigenvalue $\sigma_z F_s = sF_s$, is :

$$\frac{d^2F_s}{dy^2} - (eQBy + p_x)^2 F_s + (E^2 - m^2 - p_z^2 + eQBs)F_s = 0 \quad (2.86)$$

Transforming to dimensionless variable $\zeta = \sqrt{e|Q|B}(y + \frac{p_x}{eQB})$, the above differential equation can be simplified as :

$$\left[\frac{d^2}{d\zeta^2} - \zeta^2 + a_s\right] F_s = 0 \quad (2.87)$$

Here $a_s = \frac{E^2 - m^2 - p_z^2 + eQBs}{e|Q|B}$. The form of the differential equation is known as Hermite's equation. The solutions exist for $a_s = 2\nu + 1$ for $\nu = 0, 1, 2, ...$ Energy eigenvalues are :

$$E^2 = m^2 + p_z^2 + (2\nu + 1)e|Q|B - eQBs \quad (2.88)$$

$$\begin{aligned} N_\nu e^{-\zeta^2/2} H_\nu(\zeta) &= I_\nu(\zeta) \\ N_\nu &= \left(\frac{\sqrt{e|Q|B}}{\nu! 2^\nu \sqrt{\pi}}\right)^{1/2} \end{aligned} \quad (2.89)$$

I_ν satisfy the following completeness relations :

$$\sum_\nu I_\nu(\zeta) I_\nu(\zeta_*) = \sqrt{e|Q|B}\delta(\zeta - \zeta_*) = \delta(y - y_*) \quad (2.90)$$

For $Q = -1$, energy eigenvalues are :

$$E_n^2 = m^2 + p_z^2 + 2neB \quad (2.91)$$

Except for $n = 0$, all other landau levels are two fold degenerate, for $s = 1, \nu = n - 1$ and $s = -1$, thus $\nu = n$. For $n = 0$ and $Q = -1$, $\nu = -\frac{1}{2}(1+s)$. As ν is non-negative, s = -1. Thus $n = 0$ is not degenerate. The positive energy solutions are :

$$\begin{aligned} f_+^{(n)}(y) &= \begin{pmatrix} I_{n-1}(\zeta) \\ 0 \end{pmatrix} \\ f_-^{(n)}(y) &= \begin{pmatrix} 0 \\ I_n(\zeta) \end{pmatrix} \end{aligned} \tag{2.92}$$

For $n = 0$, $I_{-1}(y) = 0$. We have determined the upper components of spinor Eq. 2.82. Lower two components can be obtained by solving Eq. 2.83. Positive energy solutions of Dirac equation are $e^{-ip.X_{\not{y}}} U_s(y, n, \boldsymbol{p}_{\not{y}})$. U_s are given as :

$$U_+(y, n, \boldsymbol{p}_{\not{y}}) = \begin{pmatrix} I_{n-1}(\zeta) \\ 0 \\ \frac{p_z}{E_n+m} I_{n-1}(\zeta) \\ -\frac{\sqrt{2neB}}{E_n+m} I_n(\zeta) \end{pmatrix}, U_-(y, n, \boldsymbol{p}_{\not{y}}) = \begin{pmatrix} 0 \\ I_{n-1}(\zeta) \\ -\frac{\sqrt{2neB}}{E_n+m} I_{n-1}(\zeta) \\ -\frac{p_z}{E_n+m} I_n(\zeta) \end{pmatrix} \tag{2.93}$$

Positron or negative energy solutions are :

$$V_-(y, n, \boldsymbol{p}_{\not{y}}) = \begin{pmatrix} \frac{p_z}{E_n+m} I_{n-1}(\tilde{\zeta}) \\ \frac{\sqrt{2neB}}{E_n+m} I_n(\tilde{\zeta}) \\ I_{n-1}(\tilde{\zeta}) \\ 0 \end{pmatrix}, U_-(y, n, \boldsymbol{p}_{\not{y}}) = \begin{pmatrix} \frac{\sqrt{2neB}}{E_n+m} I_{n-1}(\tilde{\zeta}) \\ -\frac{p_z}{E_n+m} I_n(\tilde{\zeta}) \\ I_{n-1}(\tilde{\zeta}) \\ 0 \end{pmatrix} \tag{2.94}$$

Chapter 3

Transport Coefficients of Hot and Dense Matter

3.1 Introduction

Having discussed the Polyakov loop extended quark meson model and kinetic theory formalism for transport coefficients in Chapter 2, we now discuss in detail the calculation of the transport coefficients. Transport coefficients of matter under extreme conditions of temperature, density or external fields are interesting for several reasons. In the context of relativistic heavy ion collisions, these properties enter as dissipative coefficients in the hydrodynamic evolution of the quark gluon plasma that is produced following the collision [64, 65, 66, 67, 68]. Indeed, an extremely low value of the shear viscosity-to-entropy ratio (η/s) is needed to successfully describe the collective dynamics of the quark gluon matter at high temperature and vanishing chemical potential to explain the elliptic flow data [69, 70, 71]. At intermediate densities, near the chiral phase transition, which is being probed at the Facility for anti-proton and Ion Research(FAIR) program at Geselleschaft fuer Schwerionenforschung(GSI) and the Nuclotron-based Ion Collider fAcility(NICA) program at Joint Institute for Nuclear Research(JINR) motivates us to understand the behavior of transport coefficients at finite chemical potential and temperature. motivates us to understand the behavior of transport coefficients at finite chemical potential and temperature. Further, in the low temperature and high-density regime, the matter could be in one of the possible types of color superconducting phases of which transport properties also need to be understood [72, 73]. The cooling of neutron stars at short time scales constrains the thermal conductivity [74] while the cooling through neutrino emission on a much larger time scales constrains the phase of the matter in the interior of the compact star [75, 76]. Further, the observable regarding the viscosity of the such matter is the r-mode instability. In the absence of viscous damping, the fluid in the rotating star becomes unstable to a mode that is coupled to gravity and radiates away the angular momentum of the star [77, 78, 79]. Apart from the wide variety of applications of the transport coefficients of strongly interacting matter, their temperature and chemical potential dependence may also be indicative of a phase transition.

Transport coefficients for QCD matter in principle can be calculated using Kubo formulation [80]. However, QCD is strongly interacting for both at energies accessible in heavy ion collision experiments as well as for the densities expected to be there in the core of the neutron stars making the perturbative estimations unreliable. Calculations using lattice QCD simulations at finite chemical potential is also challenging and is limited only to the equilibrium thermodynamic properties at small chemical potentials.

The understanding of the elliptic flow in relativistic heavy ion collisions using hydrodynamics with a low (η/s) and its connection to the conjectured lower bound $(\eta/s > 1/4\pi)$ using ADS/CFT correspondence [11] stimulated extensive investigation of this ratio for QCD matter. These have been studied using perturbative QCD [8, 9], transport simulations of the Boltzmann equation [81, 82], relaxation time approximation for solving the Boltzmann equations [1, 50, 59, 83, 62] and lattice simulation of QCD [14]. Most of these calculations have been performed at vanishing baryon density. The general variation of this ratio with temperature in most of these studies shows a minimum at the transition temperature. The numerical value of η at the minimum, however, differs by orders of magnitude. For example, Ref. [84, 85], Refs. [86, 87, 88] have predicted η of order 0.001 GeV^3, η=0.002-0.003 GeV^3 while Ref.[89] predicts a value of $\eta \simeq 0.4$ GeV^3. Further, the behavior of η/s shows a monotonic decrease with temperature in the Nambu-Jona-Lasinio (NJL) model in Ref. [90].

The bulk viscosity coefficient ζ has also been estimated in various effective models as well as in lattice QCD. The rise of the bulk viscosity coefficient near the transition temperature has been observed in these effective models such as chiral perturbation theory [91], quasiparticle models [60], linear sigma model [63], and the Nambu-Jona-Lasinio model [1, 59]. Large bulk viscosity of matter produced in relativistic heavy ion collisions can give rise to different interesting phenomenon such as cavitation where pressure vanishes and hydrodynamic description of evolution becomes invalid [92, 93, 94, 95]. Here, again, the numerical value of the bulk viscosity coefficients vary widely from 10^{-5} GeV^3 [96, 97] to 10^{-2} GeV^3 [1].

The other transport coefficient that is important at finite baryon density is the coefficient of thermal conductivity λ [98, 99, 100]. The effects of thermal conductivity in relativistic hydrodynamics has been discussed recently in Refs. [101, 100]. This coefficient has been evaluated in various effective models like the Nambu-Jona-Lasinio model using the Green-Kubo approach [102], relaxation time approximation [59] and the instanton liquid model [103]. The results, however, vary over a wide range of values, with $\lambda = 0.008$ GeV^{-2} as in Ref. [86] to $\lambda \sim 10$ GeV^{-2} as in Ref. [90] for a range of temperatures (0.12 GeV $<$T$<$ 0.17 GeV), which has been nicely tabulated in Ref. [104].

We shall attempt here to estimate these transport coefficients within an effective model of strong interaction, the Polyakov loop extended quark meson (PQM) model. It has become quite popular during last few years due to its close relationship with the linear sigma model that captures the chiral symmetry breaking aspect while being in agreement with the lattice QCD results for thermodynamics at vanishing baryon density. The physics of confinement is taken care of at least partially by coupling the quark field to the Polyakov loops so that quark excitations are suppressed below the transition temperature. Let us note that the transport coefficients like bulk viscosity apart from the distribution functions also depend upon the bulk thermodynamic quantities like velocity of sound. We wish to explore the effects of such nonperturbative properties on the transport coefficients.

The transport coefficients are evaluated within the relaxation time approximation of Boltzmann equation. The relaxation time is calculated by evaluating the scattering rates of the particles in the model, namely, the quarks and pion and sigma mesons, with their respective medium-dependent masses. The scattering processes considered here are meson scatterings as considered in Ref. [15], quark scattering through meson exchanges as in Refs. [1, 59, 90], and quark-meson scatterings. As we shall see in the following, each of these processes brings out distinct features for the transport coefficients. We would like to mention here that these coefficients have also been estimated using Kubo formulation through one-loop self-energies for quarks and mesons in a separate work [105].

We organize this chapter as follows. In the following section, we discuss the two-flavor PQM model thermodynamics. The reason is that the expressions for transport coefficients involve meson masses which are medium dependent. Further, some transport coefficients like the bulk viscosity involves bulk thermodynamical properties such as energy density, pressure and the velocity of sound. As the order parameters for chiral and confinement-deconfinement transitions are coupled, this leads to nontrivial relations for derivatives of the thermodynamic potential with respect to external parameters like chemical potential or temperature as the mean fields themselves are also medium-dependent. Furthermore, the implicit dependence of these mean fields/ order parameters are calculated here analytically to avoid possible numerical errors. In Sec. 2.2.1,2.2.2 and 2.2.3 we estimate relaxation time for different scatterings. In section 2.3.1 and 2.3.2 we present the results for relaxation time and transport coefficients. Finally, we summarize and draw the conclusions of the present investigation in section 2.4.

3.2 Transport coefficients in relaxation time approximation

We shall attempt here to estimate the transport coefficients in the relaxation time approximation where the particle masses are medium dependent. Such attempts were made earlier for the σ-model [15] as well as in the NJL model to compute the shear and bulk viscosity coefficients. Such an approach was also made to estimate the viscosity coefficients of pure gluon matter [61]. In all these attempts, the expressions for the viscosity coefficients were derived for vanishing chemical potential. Several attempts were made to estimate these coefficients with finite chemical potential with different Ansatze. These expressions were put on firmer ground by deriving the expressions when there are mean fields and medium-dependent masses in a quasiparticle picture [63]. The resulting expressions for the transport coefficients were manifestly positive definite as they should be. These expressions were derived explicitly for the NJL model [59]. We use the same expressions here for the transport coefficients. The shear viscosity coefficient is given by

$$\eta = \frac{1}{15T}\sum_a \int \frac{d\mathbf{p}}{(2\pi)^3}\frac{p_a^4}{E_a^2}\tau(E_a) f_a^0(1 \pm f_a^0) \tag{3.1}$$

where, the sum is over all the different species contributing to the viscosity coefficients including the antiparticles, and, τ^a is the energy-dependent relaxation time that we define in the following subsection. The coefficient of bulk viscosity is given by

$$\begin{aligned}\zeta &= \frac{1}{9T}\sum_a \int \frac{d\mathbf{p}}{(2\pi)^3}\frac{\tau^a}{{E_a}^2}{f_a}^0\left(1 \pm {f_a}^0\right)\Bigg[\mathbf{p}^2\left(1-3{v_n}^2\right)\\ &- 3{v_n}^2\left(M^2 - TM\frac{dM}{dT} - \mu M\frac{dM}{d\mu}\right)\\ &+ 3\left(\frac{\partial P}{\partial n}\right)_\epsilon\left(M\frac{dM}{d\mu} - E_a t^a\right)\Bigg]^2\end{aligned} \tag{3.2}$$

The thermal conductivity on the other hand is given by

$$\lambda = \left(\frac{w}{nT}\right)^2 \sum_a \int \frac{d\mathbf{p}}{(2\pi)^3} \frac{\mathbf{p}^2}{3E_a^2} \tau_a(E_a) \left(t_a - \frac{nE_a}{w}\right)^2 f_a^0(1 \pm f_a^0) \tag{3.3}$$

In the above expressions, f_a^0 is the equilibrium fermion/boson distribution functions depending upon the statistics with $(1 \pm f_a^0)$ being the Bose enhancement/ Fermi suppression factors and $t_a = +1,\ 1$ and 0 for the quark, antiquark, meson respectively. Further, $c_s^2 = \left(\frac{\partial p}{\partial \epsilon}\right)_n$ is the velocity of sound at constant density and $w = \epsilon + p$ is the enthalpy density.

3.2.1 Relaxation time estimation- meson scatterings

As may be noted, the expressions for the transport coefficients as in Eqs. (3.1,3.2,3.3), depend not only on bulk thermodynamic properties like energy density, pressure, velocity of sound but also on the energy-dependent relaxation time $\tau(E)$. In the following we shall first estimate the relaxation times involving meson exchanges similar to Ref. [15].

Using the Lagrangian Eq. (2.24), we calculate the relaxation time in PQM model by taking into account the following scattering amplitudes with the corresponding matrix elements being given as

$$M_{\sigma+\sigma\to\sigma+\sigma} = -6\lambda - 36\lambda^2 {f_\pi}^2 \left(\frac{1}{s - {m_\sigma}^2} + \frac{1}{t - {m_\pi}^2} + \frac{1}{u - {m_\pi}^2}\right) \tag{3.4}$$

$$M_{\boldsymbol{\pi}+\sigma\to\boldsymbol{\pi}+\sigma} = -2\lambda - 4\lambda^2 {f_\pi}^2 \left(\frac{3}{t - {m_\sigma}^2} + \frac{1}{u - {m_\pi}^2} + \frac{1}{s - {m_\pi}^2}\right) \tag{3.5}$$

$$M_{\boldsymbol{\pi}+\boldsymbol{\pi}\to\boldsymbol{\pi}+\boldsymbol{\pi}} = -2\lambda \left(\frac{s - {m_\pi}^2}{s - {m_\sigma}^2}\delta_{\rm ab}\delta_{\rm cd} + \frac{t - {m_\pi}^2}{t - {m_\sigma}^2}\delta_{\rm ac}\delta_{\rm bd} + \frac{u - {m_\pi}^2}{u - {m_\sigma}^2}\delta_{\rm ad}\delta_{\rm bc}\right) \tag{3.6}$$

$$M_{\boldsymbol{\pi}+\boldsymbol{\pi}\to\sigma+\sigma} = -6\lambda - 4\lambda^2 {f_\pi}^2 \left(\frac{3}{s - {m_\sigma}^2} + \frac{1}{t - {m_\pi}^2} + \frac{1}{u - {m_\pi}^2}\right) \tag{3.7}$$

The terms involving the propagators yield divergent integrals due to the poles in s and u channel which is known in the literature [15]. To regulate these integrals one can include a width for the mesons as evaluated in the next subsection (Eq. (3.20)). However, such a substitution violates crossing symmetry. Further, these terms are generated from the three-point vertices which are not taken into account in the mean field approximation used in solving the gap equations and the resulting equation of state. Hence, to be consistent with equation of state while maintaining crossing symmetry for the scattering amplitudes, we approximate the above scattering amplitudes by their limits when s, t and u are taken to be infinity and the scattering amplitudes reduce to constants [15]. Thus, the scattering amplitudes essentially reduce to constants. This allows us to compare our results with earlier work of [15] and study the effect of Polyakov loop and quarks within similar approximation.

The energy-dependent interaction frequency $\omega_a(E_a)$ for the particle specie 'a' arising from a scattering process $a, b \to c, d$, which is also the inverse of the energy-dependent relaxation time $\tau(E_a)$ is given by, with $d\Gamma_i = \frac{d\mathbf{p}_i}{2E_i(\mathbf{p})(2\pi)^3}$, [59]

$$\omega(E_a) \equiv \tau(E_a)^{-1} = \sum_b \int d\Gamma_b f_b^0 W_{ab}(s). \tag{3.8}$$

In the above, the summation is over all the particles except the species a with a, b as the initial state.

The quantity W_{ab} is dimensionless, Lorentz-invariant, and depends only on the Mandelstam variable s and is given by

$$\begin{aligned} W_{ab}(s) &= \frac{1}{1+\delta_{ab}} \int d\Gamma_c d\Gamma_d (2\pi)^4 \delta^4(p_a + p_b - p_c - p_d) \\ &\times \; |M|^2 (1+f_c)(1+f_d) \end{aligned} \tag{3.9}$$

In the above, we have included the Bose enhancement factors for the meson scattering. The quantity $W_{ab}(s)$ is related to the cross section by noting that, with t as the Mandelstam variable $t = (p_a - p_c)^2$,

$$\frac{d\sigma}{dt} = \frac{1}{64\pi s} \frac{1}{p_{ab}^2} |M|^2 \tag{3.10}$$

where, $p_{ab}(s) = 1/(2\sqrt{s})\sqrt{\lambda(s, m_a^2, m_b^2)}$, and the kinematic function $\lambda(x, y, z) = x^2 + y^2 + z^2 - 2xy - 2yz - 2zx$, is the magnitude of the 3-momentum of the incoming particle in the c.m. frame. In the c.m. frame, using the energy momentum-conserving delta function and integrating over the final momenta, we have

$$W_{ab}(s) = \frac{4\sqrt{s} p_{ab}(s)}{1+\delta_{ab}} \int_{t_{min}}^{t_{max}} dt \left(\frac{d\sigma}{dt}\right) (1 + f_c(E_c))(1 + f_d(E_d)). \tag{3.11}$$

where,

$$t_{max,min} = m_a^2+m_c^2-\frac{1}{2s}(s+m_a^2-m_b^2)(s+m_c^2-m_d^2)\pm\frac{1}{2s}\sqrt{\lambda(s,m_a^2,m_b^2)\lambda(s,m_c^2,m_d^2)}$$

In the limit of constant $|M|^2$, Eq. (3.11) reduces to

$$W_{ab}(s) = \frac{1}{1+\delta_{ab}}\frac{|M|^2}{16\pi\sqrt{s}p_{ab}}\left(t_{max}-t_{min}\right)(1+f_c(E_c))(1+f_d(E_d)) \quad (3.12)$$

and, the transition frequency or the inverse relaxation time is given as

$$\omega(E_a) \equiv \tau(E_a)^{-1} = \frac{1}{256\pi^3 E_a}\int_{m_b}^{\infty} dE_b\sqrt{E_b^2-m_b^2}f(E_b)|M|^2 \int_{-1}^{1}\frac{dx}{1+\delta_{ab}}\frac{1}{p_{ab}\sqrt{s}}\left(t_{max}-t_{min}\right).$$

In the above,

$$s = 2E_aE_b\left(1+\frac{m_a^2+m_b^2}{2E_aE_b}-\frac{p_ap_b}{E_aE_b}x\right)$$

To calculate e.g. the π^+ relaxation time (τ_{π^+}), we consider the scattering processes $\pi^+ + \pi^i \to \pi^+ + \pi^i$ ($i = +,-,0$) and, $\pi^+ + \sigma \to \pi^+ + \sigma$.

To get an order of magnitude of the average relaxation time, one can also calculate an energy averaged mean interaction frequency for a given species as $\bar{\omega}_a \equiv \bar{\tau}_a^{-1}$ as

$$\bar{\omega}_a = \frac{1}{n_a}\int\frac{d\mathbf{p}}{(2\pi)^3}\omega_a(E_a)f_a(E_a), \quad (3.13)$$

with

$$n_a = \int\frac{d\mathbf{p}}{(2\pi)^3}f_a(E_a). \quad (3.14)$$

3.2.2 Relaxation time estimation– Quark scatterings

We next consider the quark scattering within the model through the exchange of pion and sigma meson resonances. The approach is similar to Refs. [59, 50, 90] performed within NJL model to estimate the corresponding relaxation time for the quarks and antiquarks. The transition frequency is again given by Eq. (3.8), with the corresponding W_{ab} given as

$$W_{ab}^q(s) = \frac{2\sqrt{s(s-4m^2)}}{1+\delta_{ab}}\int_{t_{min}}^{0} dt\left(\frac{d\sigma}{dt}\right)\left(1-f_c(\frac{\sqrt{s}}{2},\mu)\right)\left(1-f_d(\frac{\sqrt{s}}{2},\mu)\right) \quad (3.15)$$

where,

$$\frac{d\sigma}{dt} = \frac{1}{16\pi s(s-4m^2)} \frac{1}{p_{ab}^2} |\bar{M}|^2 \tag{3.16}$$

with the corresponding suppression factors appropriate for fermions. For the quark scatterings, in the present case for two flavors we consider the following scattering processes:

$$u\bar{u} \to u\bar{u}, \quad u\bar{d} \to u\bar{d}, \quad u\bar{u} \to d\bar{d},$$

$$\begin{array}{lll} uu \to uu, & ud \to ud, & \bar{u}\bar{u} \to \bar{u}\bar{u}, \\ \bar{u}\bar{d} \to \bar{u}\bar{d}, & d\bar{d} \to d\bar{d}, & d\bar{d} \to u\bar{u}, \\ d\bar{u} \to d\bar{u}, & dd \to dd, & \bar{d}\bar{d} \to \bar{d}\bar{d}, \end{array}$$

One can use i-spin symmetry, charge conjugation symmetry and crossing symmetry to relate the matrix element square for the above 12 processes to get them related to one another and one has to evaluate only two independent matrix elements to evaluate all the 12 processes. We choose these, as in Ref. [50], to be the processes $u\bar{u} \to u\bar{u}$ and $u\bar{d} \to u\bar{d}$ and use the symmetry conditions to calculate the rest. We note, however, that, while the matrix elements are related, the thermal-averaged rates are not, as they involve also the thermal distribution functions for the initial states as well as the Pauli blocking factors for the final states. We also write down the square of the matrix elements for these two processes explicitly [59, 50]–.

$$\begin{aligned} |\bar{M}_{u\bar{u}\to u\bar{u}}|^2 &= g_\sigma^4 \bigg[s^2 |D_\pi(\sqrt{s},0)|^2 + t^2 |D_\pi(0,\sqrt{-t})|^2 (s-4m^2)^2 |D_\sigma(\sqrt{s},0)|^2 \\ &+ (t-4m^2)^2 |D_\sigma(0,\sqrt{-t})|^2 \\ &+ \frac{1}{N_c} Re\bigg(st D_\pi^*(\sqrt{s},0) D_\pi(0,\sqrt{-t}) + s(4m^2-t) D_\pi^*(\sqrt{s},0) D_\sigma(0,\sqrt{-t}) \\ &+ t(4m^2-s) D_\pi(0,\sqrt{-t}) D_\sigma^*(\sqrt{s},0) \\ &+ (4m^2-s)(4m^2-t) D_\sigma(0,\sqrt{-t}) D_\sigma^*(\sqrt{s},0) \bigg) \bigg]. \end{aligned} \tag{3.17}$$

Similarly, the same for the process $u\bar{d} \to u\bar{d}$ is given as [50]

$$\begin{aligned} |\bar{M}_{u\bar{d}\to u\bar{d}}|^2 &= g_\sigma^4 \bigg[4s^2 |D_\pi(\sqrt{s},0)|^2 + t^2 |D_\pi(0,\sqrt{-t})|^2 (s-4m^2)^2 |D_\sigma(\sqrt{s},0)|^2 \\ &+ (t-4m^2)^2 |D_\sigma(0,\sqrt{-t})|^2 \\ &+ \frac{1}{N_c} Re\bigg(-2st D_\pi^*(\sqrt{s},0) D_\pi(0,\sqrt{-t}) \\ &+ 2s(4m^2-t) D_\pi^*(\sqrt{s},0) D_\sigma(0,\sqrt{-t}) \bigg) \bigg]. \end{aligned} \tag{3.18}$$

The meson propagators $D_a(\sqrt{s},0)$, $(a=\sigma,\pi)$ is given by

$$D_a(\sqrt{s},\mathbf{0}) = \frac{i}{s - M_a^2 - iIm\Pi_{M_a}(\sqrt{s},\mathbf{0})} \tag{3.19}$$

In the above, the masses of the mesons are given by Eqs. (2.33) and (2.34) determined by the curvature of the thermodynamic potential. Further, in Eq. (3.19), $Im\Pi(\sqrt{s},0)$ which is related to the width of the resonance as $\Gamma_a = Im\Pi_a/M_a$ is given as [50]

$$Im\Pi_a(\omega,\mathbf{0}) = \theta(\omega^2-4m^2)\frac{N_cN_f}{8\pi\omega}\left(\omega^2-\epsilon_a^2\right)\sqrt{\omega^2-4m^2}\,(1-f_-(\omega)-f_+(\omega)) \tag{3.20}$$

with $\epsilon_a = 0$ for pions and $\epsilon_a = 2m$ for sigma mesons.

With the squared matrix elements for the quark scatterings given as above the transition frequency for the quark of a given species is

$$\omega_q(E_a) = \frac{1}{2E_a}\int d\pi_b f(E_b) W_{ab}^q. \tag{3.21}$$

3.2.3 Quark pion scattering and relaxation time

Next, we compute the contribution of quark meson scattering to the relaxation times for both mesons as well as quarks. One can argue that the dominant contribution comes from pions as their number is large compared to the sigma mesons both below and above T_c. Therefore, in the following we consider the quark-pion scattering only. The Lorentz-invariant scattering matrix element can be written as $\bar{U}(p_2)T_{ba}U(p_1)$, with $\bar{U}U = 2m_q$ and with p_1, p_2 denoting the initial and the final quark momenta, respectively, and q_1, q_2, being the momenta of the pions.

$$T_{ba} = \delta_{ba}\frac{1}{2}(q_1+q_2)^\mu\gamma_\mu(\delta_{ab}B^{(+)} + i\epsilon_{abc}\tau_c B^{(-)}) \tag{3.22}$$

where,

$$B^{(+)} = g_\sigma^2\left(\frac{1}{u-m_q^2} - \frac{1}{s-m_q^2}\right), \tag{3.23}$$

and

$$B^{(-)} = -g_\sigma^2\left(\frac{1}{u-m_q^2} + \frac{1}{s-m_q^2}\right). \tag{3.24}$$

Averaging over the spin and isospin factors, the matrix element square for the quark-pion scattering is given by

$$|\bar{M}|^2 = \frac{g_\sigma^4}{6}\left((s-u)^2 - t(t-4m_\pi^2)\right)\left(3B_+^2 + 2B_-^2\right) \tag{3.25}$$

The corresponding transition frequency is given by

$$\omega_{q\pi}(E_a) = \frac{1}{2E_a}\int d\pi_b f(E_b) W_{ab}^{(q-\pi)}. \tag{3.26}$$

where,

$$W_{ab}^{(q-\pi)} = \frac{1}{8\pi}\times\frac{1}{2\sqrt{s}p_0}\int dt|\bar{M}_{q-\pi}|^2(1-f_q)(1+f_\pi) \tag{3.27}$$

In the above $p_0^2 = (s+m_q^2-m_\pi^2)^2/(4s)-m_q^2$. The scattering will contribute to both the quark relaxation time as well as to the pion relaxation time using Eq. (3.26) with appropriate modification for the initial state.

Let us note that there are poles in the u channel in the quark pion scattering term beyond the critical temperature when the pion mass become larger than the quark mass. However, this is taken care of once we include the imaginary part of the quark self-energy in the propagators for the quarks in the calculation of the amplitude in Eqs. (3.23)-(3.24). The quark self-energy due to scattering with mesons can be written as [85]

$$\Sigma(p_0,\mathbf{p}) = m\Sigma_0 + \gamma\cdot\mathbf{p}\Sigma_3 - \gamma_0 p_0\Sigma_4. \tag{3.28}$$

so that the quark propagators get modified as

$$S(p_0,\mathbf{p}) = \frac{1}{\not{p}-m-\Sigma} = \frac{m(1+\Sigma_0)+\gamma_0 p_0(1+\Sigma_4)-\gamma\cdot\mathbf{p}(1+\Sigma_3)}{p_0^2(1+\Sigma_4)^2-\mathbf{p}^2(1+\Sigma_3)^2-m^2(1+\Sigma_0)^2}. \tag{3.29}$$

The imaginary part of the dimensionless functions Σ_j, $(j=0,3,4)$,i is given as

$$Im\Sigma_j(p_0,\mathbf{p}) = \frac{g^2}{32\pi p}d_j\int_{E_{min}}^{E_{max}} dE_f C_j[f_b(E_b)+f_-(E_f)+f_+(E_f)]. \tag{3.30}$$

In the above, $E_b = E_f + p_0$, $p_0 = \sqrt{\mathbf{p}^2+m^2}$ and $f_\pm$ are the distribution functions for the quarks/antiquarks, f_b is the meson distribution functions,and, C_js are the weight factors given as

$$C_0 = 1, C_3 = \frac{m_M^2-2m^2-2E_f p_0}{2\mathbf{p}^2}, C_4 = -\frac{E_f}{p_0}. \tag{3.31}$$

The integration limits are given by

$$E_{max,min} = \frac{1}{2m^2}\left[(m_M^2-2m^2)p_0 \pm |\mathbf{p}|m_M\sqrt{m_M^2-4m^2}\right] \tag{3.32}$$

Further, the degeneracy factors $d_{3,4}$ are 3 for pions and 1 for sigma while d_0 is -3 for pions and 1 for the sigma meson. To calculate the total relaxation

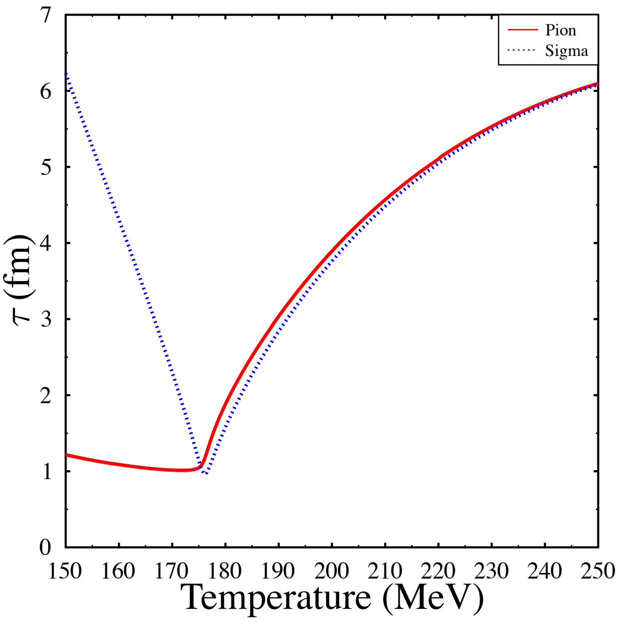

Figure 3.1: Average relaxation time for pions (solid line) and sigma meson (dotted line). Only meson-meson scatterings are considered here.

time for a quark of species 'a', we compute the total interaction frequency as $\omega_q^{total}(E_a) = \omega(E_a) + \omega_{q\pi}(E_a)$. One can define an average relaxation time for the quarks similar to Eq. (3.13) as $\bar{\tau}_q^{total} = \frac{1}{\bar{\omega}_q^{total}}$.

$$\bar{\omega}_q^{total} = \frac{1}{n_q} \int \frac{d\mathbf{p}}{(2\pi)^3} f_q(E) \omega_q^{total}(E) \tag{3.33}$$

3.3 Results

3.3.1 Meson scatterings

Let us first discuss the results arising from meson scattering alone. Using Eqs. (3.13), with constant $|M|^2$ as discussed, we have plotted the average relaxation times for the σ-meson and $\boldsymbol{\pi}$ mesons in Fig. 4.5. The relaxation times are minimum at the transition temperature. Because of larger mass of σ-mesons below the transition temperature, $\bar{\tau}_\sigma$ is much larger as compared to $\bar{\tau}_{\boldsymbol{\pi}}$. They become almost degenerate after the chiral transition as may be

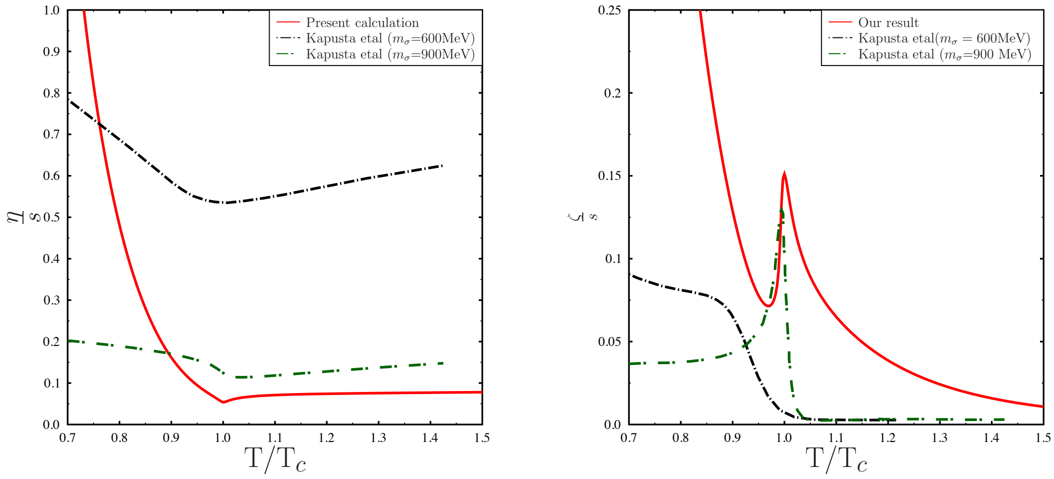

(a) (b)

Figure 3.2: Computations show mesonic contribution calculated using only meson-meson interactions. (a) : Shear viscosity to entropy ratio for $\mu = 0$. Present results are shown by solid lines. The two dot dashed curves correspond to results of linear sigma model of Ref. [15] corresponding two different masses for sigma mesons. (b): Bulk viscosity to entropy ratio for $\mu = 0$. Results for current calculations are shown by solid line. The other results correspond to Kapusta et.al. (short dashed) of linear sigma model with (m_σ=600 MeV), Kapusta et.al. (dash dot curve) for linear sigma model with m_σ=900 MeV [15]

.

expected from the behavior of their masses beyond the transition temperature. We may comment here that the particle with larger relaxation time dominates the viscosities as it can transport energy and momentum to larger distances before interacting. In Fig. 4.6 we have shown the behavior of the specific viscosities (normalized to entropy density) as a function of temperature. In Fig. 4.6(a), we have plotted the temperature dependence of the ratio η/s for $\mu = 0$. The behavior of this ratio is essentially determined by the behavior of the relaxation time. Similar to Fig. 4.5, η/s shows a minimum at the crossover temperature and the value at the minimum is about $\eta/s \sim 0.053$ which is slightly lower than the KSS bound of $1/4\pi$. We note that we have considered here only the contributions from meson scatterings. As we shall see later, inclusion of quark degrees of freedom increases the ratio. We have also compared with linear sigma model calculations [15] in which the quark as well as Polyakov loop contributions are not taken into account. The general behavior of the present calculations is similar to earlier calculations in the sense of having a minimum at the chiral crossover temperature. However, the magnitude of the ratio at the critical temperature is smaller compared to [15]. This is probably due to the fact that, the entropy density in the present calculations has contributions including those of gluon included through the Polyakov loop potential. The large entropy density, we believe, decreases the magnitude of the ratio.

In Fig. 4.6(b) the ratio of bulk viscosity to entropy is plotted which shows a maximum at the transition temperature. We have also plotted in the same figure the results without quarks and Polyakov loop potential. The present results show a distinct peak structure in the ζ/s ratio at the crossover temperature. Let us note that such a peak is expected as an effect of large conformality violation at the transition temperature as indicated in lattice simulations [14, 106]. In Ref. [15], a peak structure is seen for a heavier sigma meson ($m_\sigma = 900$MeV) which was interpreted as an effect of stronger self-coupling λ for higher M_σ. However, in the present case, this arises with quark and polyakov loop degrees of freedom even with a lighter $M_\sigma = 600$ MeV. The other characteristic feature of the present calculation is that, beyond the critical temperature the ratio ζ/s falls at a slower rate as compared to results of previous calculations. This has to do with the fact that velocity of sound approaches the ideal gas limit slowly as the effect of Polyakov loops on the quark distribution function remains significant beyond the critical temperature. In fact, at the transition temperature the value of the Polyakov loop remains about half its value of the ideal limit. Apart from this, the masses of mesons also get affected by the quark distribution functions significantly beyond the critical temperature. These non ideal effects lead to a slower decrease of the ratio beyond the critical temperature.

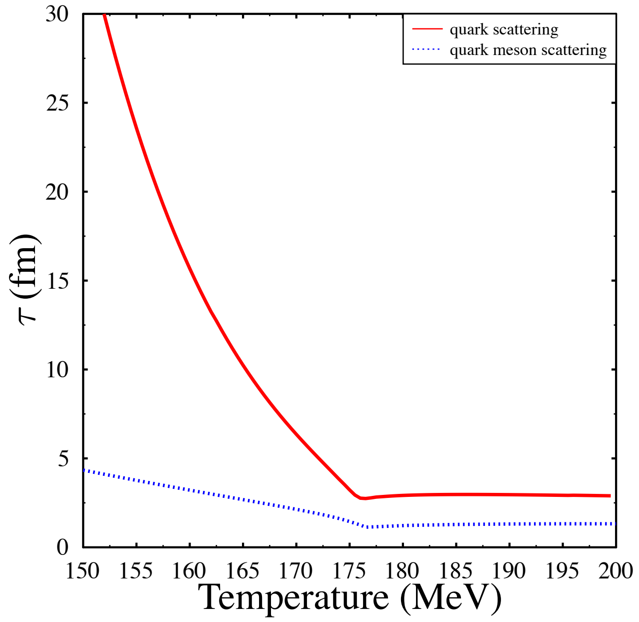

Figure 3.3: Average relaxation time for quarks arising from quark scattering. The solid curve corresponds to quark quark/antiquark scatterings with meson exchange. The dashed curve corresponds to including the effect of quark meson scatterings. Both the curves correspond to $\mu = 0$ case.

3.3.2 Quark scatterings

Next, we discuss quark scattering. In Fig. 4.7 we show the behavior of average relaxation time for quark scattering. The quark scattering through exchange of mesons is shown by the solid line in the figure. Let us recall that the average relaxation time is inversely proportional to the transition rate which is related to the cross section. The dominant contribution here comes from the quark-antiquark scattering from the s channels through propagation of the resonance states, the pions and the sigma mesons. The masses of the sigma meson decrease with temperature, becoming a minimum at the transition temperature, leading to an enhancement of the cross section. Beyond this, the cross section decreases due to the increase in the masses of the mesons. This, in turn, leads to a minimum in the relaxation time.

The average relaxation time for quarks including the quark meson scattering along with the quark scattering is shown as the dashed curve in Fig. 4.7. This curve lies below the quark quark scattering curve as there is additional contribution to the transition rate from the quark meson scattering. Below the critical temperature, the quark meson scattering dominates over the quark quark scattering due to the smaller mass of the pions as compared to the massive constituent quarks. Beyond the critical temperature, one would have expected the quark meson scattering contribution to be negligible because of the suppression due to the large meson masses. However, as was noted earlier, beyond the critical temperature, there are poles in the scattering amplitude in the u-channel for quark-pion scattering as the pion mass becomes larger than the quark masses. This is, however, regulated by the finite width of the quarks as calculated in Eq. (62). Nonetheless, the contribution of the quark pion scattering to the total quark interaction frequency $\omega_{q\pi}(\mathrm{E})$ is non-negligible beyond the critical temperature.

We next discuss the contribution of different scatterings to the specific shear viscosity η/s. The same is shown in Fig. 4.8(a) for vanishing chemical potential. The contribution from the mesons to the shear viscosity is arising from the meson scatterings only is shown by the green dashed curve while the effect of including the meson-quark scattering is shown by the maroon dotted curve. Similarly the quark contribution to this ratio η/s arising from quark quark scattering only is shown by the red solid line while the total contributions including the quark-pion scattering is shown by the blue dotted line. This also demonstrates the importance of the scattering of quarks and mesons to the total viscosity coefficient. The total contributions from both the quarks and mesons is shown as the black dashed curve in Fig. 4.8.

In a similar manner, various contributions to the specific bulk viscosity (ζ/s) coefficient are shown in Fig. 4.8(b). As may be observed, while no

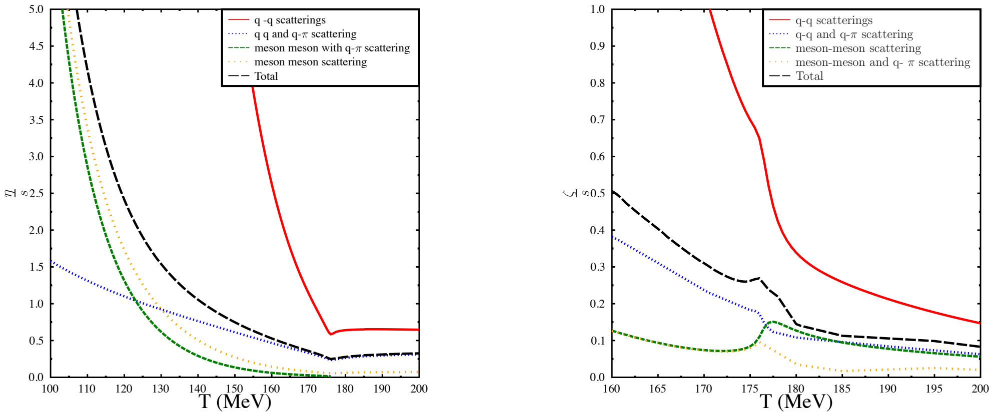

(a) (b)

Figure 3.4: Different contributions for specific viscosity coefficients. η/s is shown in the left while ζ/s is shown on the right. In both the figures, contributions from the quarks with relaxation time computed using only quark-quark scattering(red solid line) and also including quark-meson scattering(blue dotted line) are shown as a function of temperature. The contribution of the mesons due to meson-meson scattering (green dashed curve) and including meson-quark scattering (maroon short dashed curve) is also shown. The total contribution from the quarks and mesons are is shown by the black long dashed curve. All the curves correspond to $\mu = 0$ case.

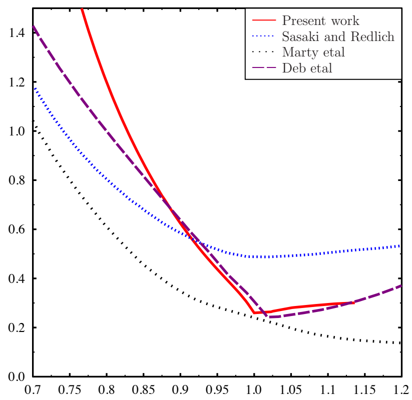

(a)

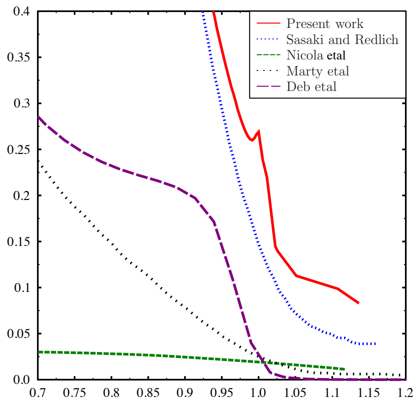

(b)

Figure 3.5: (a) : Shear viscosity to entropy ratio for $\mu = 0$. Present results are shown by solid lines. The dotted line correspond to results of NJL model of Ref. [1] , the short dashed curve correspond to results of Marty et.al. Ref. [90] and the long dashed curves correspond to results of Deb. et.al. Ref. [59]. (b): The results of Bulk viscosity to entropy ratio compared with other results in NJL models. The notation is similar to of (a).

peak structure is seen for this coefficient from the contributions arising from quarks scatterings only, such a structure is seen only when one includes the quark meson scattering. The total effect is shown as black dashed curve in Fig. 4.8(b).

In Fig. 4.9, we compare the present results with earlier works on the NJL model. As may be noted, in general, the behavior is similar regarding the shear viscosity-to-entropy ratio. Both NJL as well as the present calculations of the PQM model show the similiar behavior of having a minimum at the transition temperature as in Refs. [59, 1]. The results of Ref. [90], on the other hand, show a monotonic decrease with temperature. The bulk viscosity-to-entropy ratio, here however shows a much faster rise as the temperature is lowered below the critical temperature. In fact, both the specific viscosities rise much faster compared to NJL models below the critical temperature in the PQM model considered here. The reason could be due to the fact that the entropy density for PQM model is smaller compared to NJL models. The Polyakov loop decreases as temperature is lowered which leads to a suppression of quark distribution functions leading to decrease of en-

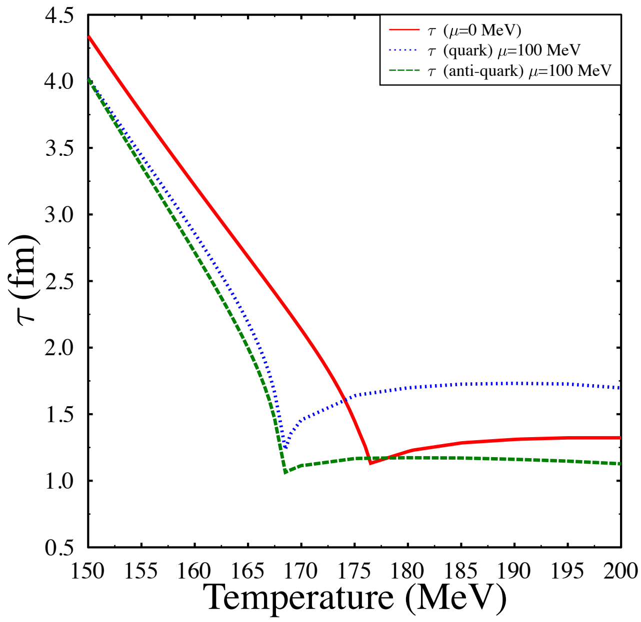

Figure 3.6: Average relaxation time of quarks and antiquarks for $\mu = 100$ MeV. The solid line correspond to the case of $\mu = 0$ MeV.

tropy density at a faster rate as compared to NJL model. Moreover, within the present approximation pions do not contribute to the thermodynamics here. Further, for temerature larger than the critical temperature, the bulk viscosity vanishes slowly with increase in temperature as compared to NJL model. This is due to the fact that the Polyakov loop variable takes its asymptotic values only at very high temperatures.

Next, we discuss about effect of finite chemical potential on the transport coefficients. To begin with let us note that the average relaxation time $\bar{\tau}_a$ as in Eq. (3.33) depends both on the transition rate and the density of the particles in the initial state. To this end, let us discuss the case of T>T$_c$. Here, the quark densities are larger than those of antiquarks. Further, the dominant contribution in this range of temperatures arises from $u\bar{d} \to u\bar{d}$ scatterings. As there are fewer antiquarks to scatter off, the average transition frequency of quark-antiquark scattering decreases. This leads to $\bar{\tau}_q(\mu) > \bar{\tau}_q(\mu = 0)$. On the other hand, for the antiquarks, there are more quarks to scatter off than compared to the case of $\mu = 0$. Hence, this leads to $\bar{\tau}_{\bar{q}}(\mu) < \bar{\tau}_{\bar{q}}(\mu = 0)$. This expected behavior is seen in Fig. 4.10. Next, let us consider the case T<T$_c$. In this case, the antiquark density is heavily suppressed due to constituent

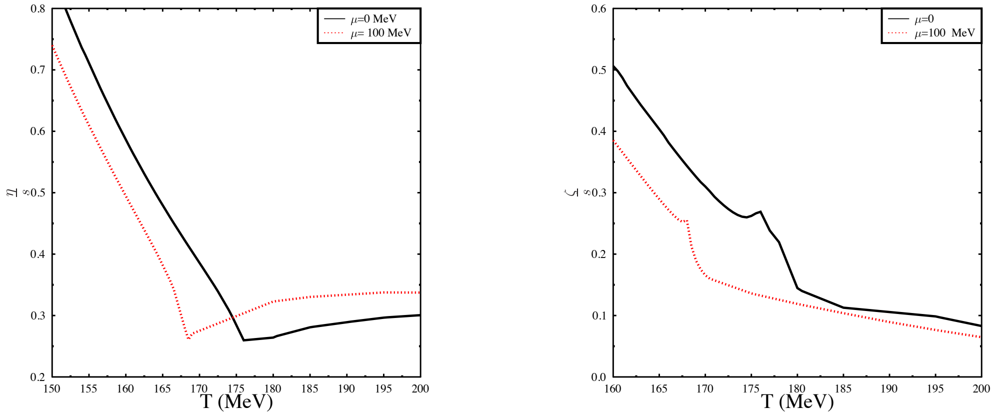

(a) (b)

Figure 3.7: Viscosities for $\mu = 100$ MeV. The left figure shows η/s as a function of temperature for $\mu = 0$ MeV (solid line) and $\mu = 100$ MeV (dotted line). The right figure shows the ratio ζ/s as a function of temperature.

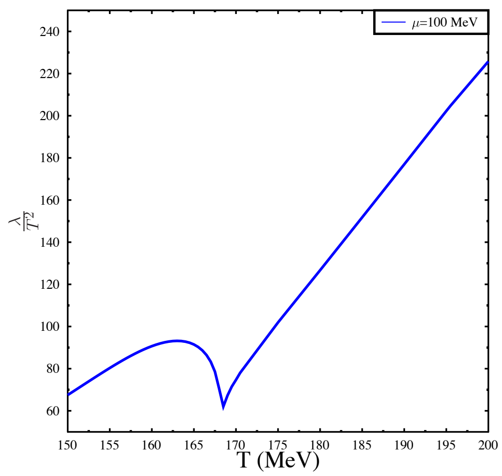

Figure 3.8: Thermal conductivity in units of T^2 as a function of temperature for $\mu = 100$MeV.

quark mass and the chemical potential and dominant contribution for quark relaxation time, therefore arises from quark-quark scatterings. This leads to $\bar{\tau}_q(\mu) < \bar{\tau}_q(\mu = 0)$. On the other hand, for the antiquarks, though their number density is smaller, their interaction frequency is enhanced both by the larger amplitude for $M_{u\bar{d}\to u\bar{d}}$ scattering and the larger number of quarks as compared to case at μ=0. This leads to $\bar{\tau}_{\bar{q}}(\mu) < \bar{\tau}_q(\mu = 0) < \bar{\tau}_{\bar{q}}(\mu = 0)$. This general behavior is reflected in the average relaxation time dependence on T in Fig. 4.10 below the critical temperature.

In Fig. 4.11, we have shown the results for the viscosities at $\mu = 100$ MeV. Fig. 4.11 (a) shows the variation of the specific shear viscosity (η/s) as a function of temperature for zero and finite chemical potential. The behavior of shear viscosity essentially follows that of the behavior of the relaxation time. η/s has a minimum at the critical temperature with $\eta/s|_{min} \sim 0.23$ ($\mu = 0$) due to suppression of the scattering cross section at higher temperature. At finite μ, the ratio is little higher as compared to the value at vanishing μ. This is due to two reasons. Firstly, the relaxation time at nonzero chemical potential is larger and, moreover, the quark density also becomes larger at finite chemical potential. At temperatures below the critical temperature and near the critical temperature,$\eta/s(\mu) < \eta/s(\mu = 0)$ as the relaxation time is lower. However, at lower temperatures, the meson scattering becomes significant and η/s for finite chemical potential becomes similar to that at vanishing chemical potential as is observed in the figure.

In Fig. 4.11(b), we have plotted the bulk viscosity-to-entropy ratio for $\mu = 0$ MeV and $\mu = 100$ MeV. It turns out that at finite μ the specific bulk viscosity is smaller than the value at $\mu = 0$ MeV. The reason for it is the fact that the dominating contribution to the finite μ arise from the term $M^2 - TM\frac{dM}{dT} - \mu M\frac{dM}{d\mu}$ in the expression for ζ/s in Eq. (3.2). This is due to the sharp variations of the order parameters at finite chemical potential as may be observed in Fig. 5.5. As this term contributes negatively to the expression for ζ, the specific bulk viscosity at finite μ is lower than that at $\mu = 0$ MeV.

In Fig. 3.8 , we have shown the results for thermal conductivity. We have plotted here the dimensionless quantity λ/T^2 as a function of temperature. We have plotted the results for $\mu = 100$MeV. As is well known, thermal conduction which involves the relative flow of energy and baryon number vanishes at zero baryon density. In fact, λ diverges as $1/n^2$ as may be expected from the expression given in Eq. (3.3). However, in the dissipative current, the conductivity occurs as λn^2 [107, 108] and the heat conduction vanishes for $\mu = 0$ [109]. On the other hand, in some cases, such as when pion number is conserved, heat conduction can be sustained by pions. In presece of a pionic chemical potential corresponding to a conserved pion number, thermal conductivity can be nonzero at vanishing baryonic chemical potential. This has been the basis for estimation of thermal conductivity at zero baryon density but finite pion density [86, 104, 96, 97]. However, in the present case, we consider the case of vanishing pion chemical potential and show only the contribution of quarks to thermal conductivity.

As expected from the behavior of the relaxation time, the specific thermal conductivity has a minimum at the critical temperature similar to Ref. [59] for the NJL model. The sharp rise of λ/T^2 can be understood by performing a dimensional argument to show that at very high temperature when chiral symmetry is is restored the integral increases as T^3 while the prefactor $w/(nT)$ grows as T^2 for small chemical potentials. Apart from this kinematic consideration, the integrand further is multiplied by $\tau(E)$ which itself is an increasing function of temperature beyond T_c. This leads to the sharp rise of the ratio λ/T^2 beyond the critical temperature. Below, the critical temperature, however, the ratio decreases which is in contrast to NJL results of Ref. [59]. The reason is twofold. First, the magnitude of the relaxation time decreases when quark meson scattering is included as compared to quark-quark scattering as shown in Fig. 4.7. Apart from this, in the integrand,the distribution functions are suppressed by Polyakov loops as compared to NJL model. As the antiquark densities are suppressed compared to quark densities at finite chemical potential, the high-temperature behavior is decided by the quark-quark scattering.

3.4 Summary

Transport coefficients of hot and dense matter are important inputs for the hydrodynamic evolution of the plasma that is produced following a heavy ion collision. In this chapter, we have investigated these cofficients taking into account the the nonperturbative effects related to chiral symmetry breaking as well as confinement properties of strong interaction physics within an effective model, the Polyakov loop extended quark meson coupling model. These coefficients are estimated using the relaxation time approximation for the solutions of the Boltzman kinetic equation.

We first calculated the medium-dependent masses of the mesons and quarks within a mean field approximation. The contribution of the mesons to the transport coefficients has been calculated through estimating the relaxation time for the mesons arising both from meson-meson scattering and meson-quark scattering. The contribution to the transport coefficients arises mostly from the meson scatterings at temperatures below the critical temperature, while above the critical temperature, the contributions arising from the quark scatterings become dominant. In particular, quark-meson scattering contributes significantly to the relaxation time for the quarks both below and above the critical temperature. The quark-pion scattering above the critical temperature gives significant contribution due to the pole structure of the corresponding scattering amplitude.

One important approximation in the present analysis is that the kinetic terms for the mesons are not modified at finite temperature and meson dispersion relation remains similar to those at the zero-temperature relativistic dispersion relation. The only temperature effect that remains in the meson dispersion lies in the temperature-dependent meson masses obtained through the curvature of the effective potential [110]. A more realistic approach would be to use effective field theory to have different dispersion relations for the mesons [111, 112, 113] depending upon their velocities and calculate the scattering processes to estimate the viscosities. However, such an approach is beyond the scope of present work in which we have restricted ourselves to thermal and density effects included in the masses and widths for the mesons.

In general, the effect of Polyakov loops lies in suppressing the quark contribution below the critical temperature. This leads to, in particular, the suppression of thermal conductivity at lower temperature arising from quark scattering. The effect of Polyakov loop also is significant near and above the critical temperature. Indeed, both the quark masses as well as Polyakov loop order parameter remain significantly different from their asymptotic values near the critical temperature.

Chapter 4

Color Superconductivity in presence of background magnetic field

4.1 Introduction

Having discussed transport properties of matter at high temperature, we now discuss the properties of quark matter at extreme densities in presence of large background magnetic field as relevant for the physics of neutron stars. Other than high temperature and density, effect of strong magnetic field on QCD vacuum structure has attracted recent attention. This is motivated by the possibility of creating ultra strong magnetic fields in non central collisions at RHIC and LHC. The strengths of the magnetic fields are estimated to be of hadronic scale [114, 115] of the order of $eB \sim 2m_\pi^2$ ($m_\pi^2 \simeq 10^{18}$ Gauss) at RHIC, to about $eB \sim 15m_\pi^2$ at LHC [115]. There have been recent calculations both analytic as well as with lattice simulations, which indicate that QCD phase diagram is affected by strong magnetic fields [116, 117, 118, 119].

In the context of cold dense matter, compact stars can be strongly magnetized. Neutron star observations indicate the magnetic field to be of the order of 10^{12}-10^{13} Gauss at the surface of ordinary pulsars [120]. Further, the magnetars which are strongly magnetized neutron stars, may have even stronger magnetic fields of the order of $10^{15} - 10^{16}$ Gauss [121, 122, 123, 124, 125, 126, 127]. Physical upper limit on the magnetic field in a gravitationally bound star is 10^{18} Gauss which is obtained by comparing the magnetic and gravitational energies using virial theorem [128]. This limit could be higher for self bound objects like quark stars [129]. Since the magnetic field strengths are of the order of QCD scale, this can affect both the thermodynamic as well as the hydrodynamics of such magnetized matter [130]. The phase structure of dense matter in presence of magnetic field along with a non zero chiral density has recently been investigated for two flavor PNJL model for high temperatures relevant for RHIC and LHC [117]. There have also been many investigations to look into the vacuum structure of QCD and it has been recognised that the strong magnetic field acts as a catalyser of chiral symmetry breaking [131, 132, 35, 36, 133, 134, 135, 136, 137, 138, 139]. The effects of magnetic field on the equation of state have been recently studied in Nambu Jona Lasinio model at zero temperature for three flavors and the equation of state has been computed for the cold quark matter [140, 141, 142] taking into account chiral condensate structure with quark-antiquark pair for the ground state.

On the other hand, color superconductivity is now an accepted conjectured state of cold and dense quark matter describing Cooper pairing of quarks of different colors and different flavors [19, 143, 144]. One can have a rigorous treatment of the phenomenon of such pairing using asymptotic freedom of QCD at very high densities. In its simplest form, when masses of the three quarks can be neglected compared to the chemical potential one can have the color flavor locked (CFL) phase[19, 143, 144]. However, to apply it to neutron star matter, the situation is more complicated as for the densities expected in the interior of neutron star, the masses of strange quarks cannot be neglected. Further, many nontrivial complications arise when beta equilibrium and charge neutrality conditions are imposed in such systems [145]. Since the well known sign problem prevents the first principle lattice simulations at finite chemical potentials, one has to rely on effective models at this regime of moderate densities. One model that has been extensively studied in this context has been the Nambu Jona Lasinio (NJL) model with contact interactions [49].

Of late, there has been a lot of attention on the investigation of color superconductivity in presence of magnetic field [30, 146, 147, 131, 35, 36, 33, 34]. Essentially, this is due to its possible application in the astrophysical situations as the densities in compact star cores are large enough to have possible superconducting phase as well as such compact stars can have strong magnetic field as mentioned above. Let us also mention here that although such systems can be color superconductors, these phases can be penetrated by a 'rotated' long range magnetic field. The corresponding rotated gauge field is a linear combination of vacuum photon field and the 8-th gluon field[148, 149]. These rotated magnetic fields are not subjected to Meissener effect. While the Cooper pair is neutral with respect to the magnetic field, the quark quasi particles have well defined charges. Therefore, the pairing phenomenon is affected by the presence of magnetic field. Initially, the effect of magnetic field on superconducting phase has been studied for CFL phase [30, 146, 147] where all the three quarks take part in the pairing dynamics. However, for realistic densities, such symmetric pairing is disfavored due to large strange quark mass that leads to large mismatch in the fermi surface. The condition of charge neutrality further complicates the pairing mechanism leading to gapless modes for homogeneous diquark pairing [150, 151]. Superconductivity for the two flavor quark matter in presence of magnetic field has been studied in Ref.s [35, 36, 152, 153, 154, 155] within NJL model. The effect of charge neutrality along with the interplay of chiral and superconducting condensates has been analyzed in Ref.s[152, 153, 154, 155] in this model. A complete three flavor analysis of magnetized dense quark matter including superconductivity has not been attempted so far. In the present investigation we include the effects of strange quarks that takes part in chiral condensation but not in the diquark channel in the magnetized quark matter. As we shall see, the strange quarks, similar to vanishing magnetic field case, play an important role for charge neutral matter and the resulting equation of state. Moreover, with the inclusion of a flavor mixing interaction term, the strange quark scalar condensate not only affects the light quark condensates but also the diquark condensates.

We organize this chapter as follows. In section 3.2, we discuss an ansatz state with quark-antiquark pairs related to chiral symmetry breaking, diquark and diantiquark pairs for the light flavors related to color superconductivity in in the presence of a magnetic field. We then generalize such a state to include the effects of temperature and density. In section 3.3, we consider the 3 flavor NJL model along with the so called the Kobayashi-Maskawa-t'Hooft (KMT) term – the six fermion determinant interaction term which breaks U(1) axial symmetry as in QCD. We use this Hamiltonian and calculate its expectation value with respect to the ansatz state to compute the energy density as well the thermodynamic potential for this system. We minimize the thermodynamic potential to determine the the ansatz functions and the resulting mass gap equations. These coupled mass and superconducting gap equations are solved and we discuss the results in section 3.4. We discuss here the results with and without constraints of charge neutrality. Finally we summarize and conclude in section 3.5. In the appendix we give some details of the derivation of the evaluation of expectation values of the order parameters.

4.2 The ansatz for the ground state

Let us first consider the ground state structure relevant for chiral symmetry breaking in presence of strong magnetic field [142]. We shall then modify the same relevant for color superconductivity. To make the notations clear, we first write down the field operator expansion for quarks with a current quark mass m and charge q in the momentum space in the presence of a constant magnetic field $\mathbf{B}$. We take the field direction to be along the z-axis. We choose the gauge such that the electromagnetic vector potential is given as $A_\mu(\boldsymbol{x}) = (0, 0, Bx, 0)$. The quark field operator expansion in presence of constant magnetic field is given as [142, 156]

$$\psi(\mathbf{x}) = \sum_n \sum_r \frac{1}{2\pi} \int d\mathbf{p}_{\not x} \left[q_r^0(n, \mathbf{p}_{\not x}) U_r^0(x, \mathbf{p}_{\not x}, n) + \tilde{q}_r^0(n, -\mathbf{p}_{\not x}) V_r^0(x, -\mathbf{p}_{\not x}, n) \right] e^{i\mathbf{p}_{\not x}\cdot\mathbf{x}_{\not x}}. \tag{4.1}$$

The sum over n in the above expansion runs from 0 to infinity. In the above, $\mathbf{p}_{\not x} \equiv (p_y, p_z)$, and, $r = \pm 1$ denotes the up and down spins. We have suppressed the color and flavor indices of the quark field operators. The quark annihilation and antiquark creation operators, q_r^0 and $\tilde{q}_r^0$, respectively, satisfy the quantum algebra

$$\{q_r^0(n, \mathbf{p}_{\not x}), q_{r'}^{0\dagger}(n', \mathbf{p}'_{\not x})\} = \{\tilde{q}_r^0(n, \mathbf{p}_{\not x}), \tilde{q}_{r'}^{0\dagger}(n', \mathbf{p}'_{\not x})\} = \delta_{rr'}\delta_{nn'}\delta(\mathbf{p}_{\not x} - \mathbf{p}'_{\not x}). \tag{4.2}$$

In the above, U_r and V_r are the four component spinors for the quarks and antiquarks respectively. The explicit forms of the spinors for the fermions with mass m and electric charge q are given by

$$U_{\uparrow}^{0}(x,\boldsymbol{p}_{\backslash\!\!\!x},n) = \begin{pmatrix} \cos\frac{\phi_0}{2}\left(\Theta(q)I_n+\Theta(-q)I_{n-1}\right) \\ 0 \\ \hat{p}_z\sin\frac{\phi_0}{2}\left(\Theta(q)I_n+\Theta(-q)I_{n-1}\right) \\ -i\hat{p}_\perp\sin\frac{\phi_0}{2}\left(\Theta(q)I_{n-1}+\Theta(-q)I_n\right) \end{pmatrix} \tag{4.3a}$$

$$U_{\downarrow}^{0}(x,\boldsymbol{p}_{\backslash\!\!\!x},n) = \begin{pmatrix} 0 \\ \cos\frac{\phi_0}{2}\left(\Theta(q)I_{n-1}+\Theta(-q)I_n\right) \\ i\hat{p}_\perp\sin\frac{\phi_0}{2}\left(\Theta(q)I_n-\Theta(-q)I_{n-1}\right) \\ -\hat{p}_z\sin\frac{\phi_0}{2}\left(\Theta(q)I_n-\Theta(-q)I_{n-1}\right) \end{pmatrix} \tag{4.3b}$$

$$V_{\uparrow}^{0}(x,-\mathbf{p}_{\backslash\!\!\!x},n) = \begin{pmatrix} \hat{p}_\perp\sin\frac{\phi_0}{2}\left(\Theta(q)I_n-\Theta(-q)I_{n-1}\right) \\ i\hat{p}_z\sin\frac{\phi_0}{2}\left(\Theta(q)I_{n-1}+\Theta(-q)I_n\right) \\ 0 \\ i\cos\frac{\phi_0}{2}\left(\Theta(q)I_{n-1}+\Theta(-q)I_n\right) \end{pmatrix} \tag{4.3c}$$

$$V_{\downarrow}^{0}(x,-\boldsymbol{p}_{\backslash\!\!\!x},n) = \begin{pmatrix} i\hat{p}_z\sin\frac{\phi_0}{2}\left(\Theta(q)I_n+\Theta(-q)I_{n-1}\right) \\ \hat{p}_\perp\sin\frac{\phi_0}{2}\left(\Theta(q)I_{n-1}-\Theta(-q)I_{n-1}\right) \\ -i\cos\frac{\phi_0}{2}\left(\Theta(q)I_n+\Theta(-q)I_{n-1}\right) \\ 0 \end{pmatrix}. \tag{4.3d}$$

In the above, the energy of the n-th Landau level is given as $\epsilon_n = \sqrt{m^2+p_z^2+2n|q|B} \equiv \sqrt{m^2+|\mathbf{p}^2|}$ with $\mathbf{p}^2 = p_z^2+\mathbf{p}_\perp^2$ so that $p_\perp^2 = 2n|q|B$, $\hat{p}_z = p_z/|\mathbf{p}|$, $\hat{p}_\perp = 2n|q|B/|\mathbf{p}|$. In Eq.s (4.3), $\cot\phi_0 = m/|\mathbf{p}|$. Clearly, for vanishing masses $\phi_0 = \pi/2$. The functions I_n's (with $n \geq 0$) are functions of $\xi = |qB|(x-p_y/|qB|)$ and are given as

$$I_n(\xi) = c_n \exp\left(-\frac{\xi^2}{2}\right) H_n(\xi) \tag{4.4}$$

where, $H_n(\xi)$ is the Hermite polynomial of the nth order and $I_{-1}=0$. The normalization constant c_n is given by

$$c_n = \sqrt{\frac{\sqrt{|q|B}}{n!2^n\sqrt{\pi}}}$$

The functions $I_n(\xi)$ satisfy the orthonormality condition

$$\int d\xi I_n(\xi)I_m(\xi) = \sqrt{|q|B}\,\delta_{n,m} \tag{4.5}$$

so that the spinors are properly normalized. The detailed derivation of these spinors and some of their properties are presented in the appendix of Ref.[142].

With the field operators now defined in terms of the annihilation and the creation operators in presence of a constant magnetic field, one can write down an ansatz for the ground state as in Ref.[142]. The ground state taken as a squeezed coherent state involving quark and antiquarks pairs. Explicitly, [151, 157, 158, 142]

$$|\Omega\rangle = \mathcal{U}_Q|0\rangle. \tag{4.6}$$

Here, $\mathcal{U}_Q$ is an unitary operator which creates quark–antiquark pairs from the vacuum $|0\rangle$ which in annihilated by the quark/antiquark annihilation operators given in Eq.(4.1). Explicitly, the operator, $\mathcal{U}_Q$ is given as [142]

$$\mathcal{U}_Q = \exp\left(\sum_{n=0}^{\infty}\int d\boldsymbol{p}_{\not z}\, q_r^{0i\dagger}(n,\boldsymbol{p}_{\not z})a^i_{r,s}(n,p_z)h^i(n,\boldsymbol{p}_z)\tilde{q}_s^{0i}(n,-\boldsymbol{p}_{\not z}) - h.c.\right) \tag{4.7}$$

In the above ansatz for the ground state, the function $h^i(n,p_z)$ is a real function describing the quark-antiquark condensates related to the vacuum realignment for chiral symmetry breaking to be obtained from a minimization of the thermodynamic potential. In the above equation, the spin dependent structure $a^i_{r,s}$ is given by

$$a^i_{r,s} = \frac{1}{|\mathbf{p}_i|}\left[-\sqrt{2n|q_i|B}\,\delta_{r,s} - ip_z\delta_{r,-s}\right] \tag{4.8}$$

with $|\mathbf{p}_i| = \sqrt{p_z^2 + 2n|q_i|B}$ denoting the magnitude of the three momentum of the quark/antiquark of i-th flavor (with electric charge q_i) in presence of a magnetic field. Summation over three colors is understood in the exponent of $\mathcal{U}_Q$ in Eq. (4.7). Clearly, a nontrivial $h_i(n,p_z)$ breaks the chiral symmetry.

It is easy to show that the transformation of the ground state as in Eq.(4.6) is a Bogoliubov transformation. With the ground state transforming as Eq.(4.6), any operator O^0 in the $|0\rangle$ basis transforms as

$$O = \mathcal{U}_Q O^0 \mathcal{U}_Q^\dagger \tag{4.9}$$

and, in particular, one can transform the creation and annihilation operators of Eq.(4.1) to define the transformed operators as above satisfying the same anticommuation relations as in Eq.(4.2).

$$\psi(\mathbf{x}) = \sum_n\sum_r \frac{1}{2\pi}\int d\mathbf{p}_{\not z}\left[q_r(n,\mathbf{p}_{\not z})U_r(x,n,\mathbf{p}_{\not z}) + \tilde{q}_r(n,-\mathbf{p}_{\not z})V_r(x,n,-\mathbf{p}_{\not z})\right]e^{i\mathbf{p}_{\not z}\cdot\mathbf{x}_{\not z}}, \tag{4.10}$$

with $q_r|\Omega\rangle = 0 = \tilde{q}_r^\dagger|\Omega\rangle$. In the above, we have suppressed the flavor and color indices. It is easy to see that the U,V spinors are given by exactly similar to spinors U_0, V_0 in Eq.(4.3) but with the shift of the function $\phi_0 \to \phi = \phi_0 - 2h$ with the function $h(\mathbf{k})$ to be determined by a minimization of free energy. As we shall see later, it is more convenient to vary $\phi(\mathbf{k})$ rather than $h(\mathbf{k})$. Let us note that with Eq.(4.10), the four component quark field operator gets defined in terms of the vacuum structure for chiral symmetry breaking given through Eq.(4.6) and Eq.(4.7) [159, 160] in presence of the magnetic field.

The chiral order parameter in the condensate vacuum $|\Omega\rangle$ can be evaluated explicitly using the field operator expansion given in Eq.(4.10) and is given by[142] (for i-th flavor)

$$I_s^i = \langle\Omega|\bar{\psi}^i\psi^i|\Omega\rangle = -\frac{N_c}{(2\pi)^2}\sum_n \alpha_n |q_i B| \int dp_z \cos\phi^i \tag{4.11}$$

This expression for the quark-antiquark condensate is exactly the same form as derived earlier in the absence of the magnetic field [161, 157] once one realizes that in presence of quantizing magnetic field with discrete Landau levels, one has [152, 153, 154]

$$\int \frac{d\mathbf{p}}{(2\pi)^3} \to \frac{|qB|}{(2\pi)^2}\sum_{n=0}^{\infty}\alpha_n \int dp_z.$$

Next, we would like to generalize the ansatz of Eq.(4.6) with quark-antiquark pairs in presence of magnetic field, to include quark-quark pairs for the description of the ground state as relevant for color superconductivity. However, few comments in this context are in order. It is known that in presence of color superconductivity, the diquark is electro-magnetically charged and the usual magnetic field will have a Meissener effect. However, a linear combination of the photon field and the gluon field given by $\tilde{A}_\mu = \cos\alpha A_\mu - \sin\alpha G^8_\mu$, still remains massless and is unscreened. For two flavor color superconductivity, $\cos\alpha = g/\sqrt{g^2 + e^2/3} \sim 1/20$ [148]. The electron couples to this rotated gauge field by the coupling $\tilde{e} = e\cos(\alpha)$.The quark field couples to the rotated gauge field through its rotated charge $\tilde{Q}$. In units of $\tilde{e}$, the rotated charge matrix in the flavor- color space is given by

$$\tilde{Q} = Q_f \otimes \mathbf{1}_c - \mathbf{1}_f \otimes \frac{T_c^8}{2\sqrt{3}} \tag{4.12}$$

. Thus, the $\tilde{e}$ charges of red and green u quarks is 1/2; red and green down and strange quarks is $-1/2$. The blue u-quark has $\tilde{Q}$ charge as $+1$, while the blue d and s quarks are $\tilde{Q}$ chargeless. We shall take the rotated U(1) magnetic field along the $z-$axis and spatially constant as before without the absence of superconductivity. The ansatz for the ground state with quark-antiquark condensate is now taken as, with i being the flavor index,

$$|\Omega\rangle_\chi = \exp \sum_{flav} (B_i^\dagger - B_i)|0\rangle. \tag{4.13}$$

The flavor dependent quark-antiquark pair creation operator for u-quark ($i = 1$) is given as, with $a = 1,2,3$ being the color indices for red,blue and green respectively

$$B_u^\dagger = \sum_{a=1}^{3}\sum_{n=0}^{\infty} \int d\boldsymbol{p}_{\not x}\, q_r^{1a}(n,\boldsymbol{p}_{\not x})^\dagger a_{r,s}^1(n,p_z) f^{1a}(n,\boldsymbol{p}_{\not x})\tilde{q}_s^{1a}(n,-\boldsymbol{p}_{\not x}) \tag{4.14}$$

while, for the down and strange quarks (i=2,3) the same is given as

$$\begin{aligned} B_i^\dagger &= \sum_{a=1}^{2}\sum_{n=0}^{\infty} \int d\boldsymbol{p}_{\not x}\, q_r^{ia}(n,\boldsymbol{p}_{\not x})^\dagger a_{r,s}^i(n,p_z) h^{ia}(n,\boldsymbol{p}_{\not x})\tilde{q}_s^{1a}(n,-\boldsymbol{p}_{\not x}) \\ &+ \int d\mathbf{p} q_r^{i3}(\mathbf{p})^\dagger (\sigma\cdot\hat{\mathbf{p}})_{rs} h^i(\mathbf{p})\tilde{q}_s^{i3}(-\mathbf{p}). \end{aligned} \tag{4.15}$$

The difference between the pair creation operator in Eqs.(4.14) and (4.15) lies on the contribution of the blue color. While the up blue quark has $\tilde{Q}$ charge, the blue quarks of down and strange quark are $\tilde{Q}$ neutral.

Next, we write down the ansatz state for having quark-quark condensates which is given by

$$|\Omega\rangle = U_d|\Omega\rangle_\chi \equiv \exp(B_d^\dagger - B_d)|\Omega\rangle_\chi. \tag{4.16}$$

In the above, $B_d^\dagger$ is the diquark (and di-antiquark) creation operator given as

$$\begin{aligned} B_d^\dagger = \sum_n \int dp_{\not x} \Big[& q_r^{ia}(n,p_{\not x})^\dagger r f(n,p_z) q_{-r}^{jb}(n,-p_{\not x},p_z) \\ & + \tilde{q}_r^{ia}(n,p_{\not x})^\dagger r f_1(n,p_z)\tilde{q}_{-r}^{jb}(n,p_{\not x})^\dagger \Big] \epsilon^{ij3}\epsilon^{3ab}. \end{aligned}$$

In the above, i,j are the flavor indices , a,b are the color indices and $r = \pm 1/2$ are the spin indices. The levi civita tensor ensures that the operator is antisymmetric in color and flavor space along with the fact that only u,d quarks with red and green colors take part in diquark condensation. The blue u,d quarks as well as the strange quarks (all the three colors) do not take part in the diquark condensation. The functions $f(n,p_z)$ and $f_1(n,p_z)$ are condensate functions associated with quark-quark and antiquark-antiquark condensates respectively. These functions are assumed to be independent of color and flavor indices. We shall give a post facto justification for this that these function depend upon the average energy and average chemical potentials of the quarks that condense.

To include the effects of temperature and density we next write down the state at finite temperature and density $|\Omega(\beta,\mu)\rangle$ through a thermal Bogoliubov transformation over the state $|\Omega\rangle$ using the thermofield dynamics (TFD) method as described in Ref.s [162, 163, 164, 142]. This is particularly useful while dealing with operators and expectation values. We write the thermal state as

$$|\Omega(\beta,\mu)\rangle = \mathcal{U}_{\beta,\mu}|\Omega\rangle = \mathcal{U}_{\beta,\mu}\mathcal{U}_Q|0\rangle, \tag{4.17}$$

where $\mathcal{U}_{\beta,\mu}$ is given as

$$\mathcal{U}_{\beta,\mu} = e^{\mathcal{B}^\dagger(\beta,\mu)-\mathcal{B}(\beta,\mu)},$$

with

$$\mathcal{B}^\dagger(\beta,\mu) = \sum_{n=0}^{\infty}\int d\boldsymbol{k}_{\not{x}}\Big[q_r^{ia}(n,k_{\not{x}})^\dagger\theta_-^{ia}(k_z,n,\beta,\mu)\underline{q}_r^{ia}(n,k_{\not{x}})^\dagger \\ + \tilde{q}_r^{ia}(n,k_{\not{x}})\theta_+^{ia}(k_z,n,\beta,\mu)\underline{\tilde{q}}_r^{ia}(n,k_{\not{x}})\Big].$$

In Eq.(4.18), the underlined operators are the operators in the extended Hilbert space associated with thermal doubling in TFD method, and, the color flavor dependent ansatz functions $\theta_\pm^{ia}(n,k_z,\beta,\mu)$ are related to quark and antiquark distributions as can be seen through the minimization of the thermodynamic potential.

All the functions in the ansatz in Eq.(4.17) are to be obtained by minimizing the thermodynamic potential. We shall carry out this minimization in the next section. However, before carrying out the minimization procedure, let us focus our attention to the expectation values of some known operators to show that with the above variational ansatz for the 'ground state' given in Eq.(4.17) these reduce to the already known expressions in the appropriate limits.

Let us first consider the expectation value of the chiral order parameter. The expectation value for chiral order parameter for the i-th flavor is given as

$$I_s^i = \langle\Omega(\beta,\mu)|\bar{\psi}_i\psi_i|\Omega(\beta,\mu)\rangle = \sum_{a=1}^{3} I_s^{ia} \tag{4.18}$$

These expectation values can be evaluated easily once we realize that the state $|\Omega(\beta,\mu)\rangle$ as in Eq.(4.17) is obtained through successive Bogoliubov transformations on the state $|0\rangle$ as in Eq.(4.13), Eq.(4.16). The details of evaluation for the different order parameters is relegated to the appendix. Explicitly, for the quarks that take part in superconductivity

$$I_s^{ia} = -\sum_n \alpha_n \frac{|q^{ia}B|}{(2\pi)^2}\int dp_z \cos\phi^{ia}\left(1 - F^{ia} - F_1^{ia}\right) \qquad (i,a=1,2) \quad (4.19)$$

where, $\alpha_n = (2-\delta_{n,0})$ is the degeneracy factor of the n-th Landau level (all levels are doubly degenerate except the lowest Landau level). Further,

$$F^{ia} = \sin^2\theta_-^{ia} + \sin^2 f\left(1 - \sin^2\theta_-^{ia} - |\epsilon^{ij}||\epsilon^{ab}|\sin^2\theta_-^{jb}\right) \qquad (4.20)$$

arising from the quarks which condense and

$$F_1^{ia} = \sin^2\theta_+^{ia} + \sin^2 f_1\left(1 - \sin^2\theta_+^{ia} - |\epsilon^{ij}||\epsilon^{ab}|\sin^2\theta_+^{jb}\right) \qquad (4.21)$$

arising from antiquarks which condense. Thus, the scalar condensates arising from quarks that take part in superconductivity depend both on the condensate functions in quark-antiquark channel (ϕ^i) as well as in quark-quark channel (f, f_1). Further, the thermal functions $\sin^2\theta_\pm^{ia}$, as we shall see later, will be related to the number density distribution functions.

Next, for the non-superconducting blue up quarks, the contribution to the scalar condensate is given by

$$I_s^{13} = -\sum_n \alpha_n \frac{|q^{1,3}|B}{(2\pi)^2}\int dp_z \cos\phi^{13}\left(1 - \sin^2\theta_-^{13} - \sin^2\theta_+^{13}\right). \qquad (4.22)$$

Let us note that in the limit of vanishing of the color superconducting condensate functions ($f, f_1 \to 0$), the contributions given in Eq.(4.19) reduce to Eq.(4.22) as they should [142].

Similarly, scalar condensate contribution from the charged strange quarks (red, green) is given by

$$I_s^{3a} = -\sum_n \alpha_n \frac{|q^{3a}|B}{(2\pi)^2}\int dp_z \cos\phi^{3a}\left(1 - \sin^2\theta_-^{3a} - \sin^2\theta_+^{3a}\right). \qquad (a=1,2) \qquad (4.23)$$

Finally, for the uncharged quarks i.e. blue down and blue strange quarks, the contributions to the scalar condensates are given by, for flavor i (i=2,3)

$$I_s^{i3} = -\frac{2}{(2\pi)^3}\int d\mathbf{k}\cos\phi^i\left(1 - \sin^2\theta_-^{i3} - \sin^2\theta_+^{i3}\right) \qquad (4.24)$$

Next, we write down the condensate in the superconducting channel which is given as

$$
\begin{aligned}
I_D &= \langle \bar{\psi}_c^{ia} \gamma^5 \psi^{jb} \rangle \epsilon^{ij} \epsilon^{3ab} \\
&= \frac{2}{(2\pi)^2} \sum_n \alpha_n |q_i B| \int dp_z \cos\left(\frac{\phi_1 - \phi_2}{2}\right) \Big[\sin 2f \left(1 - \sin^2\theta_-^1 - \sin^2\theta_-^2\right) \\
&+ \sin 2f_1 \left(1 - \sin^2\theta_+^1 - \sin^2\theta_+^2\right) \Big] \qquad (4.25)
\end{aligned}
$$

Let us note that the superconducting condensate also depends upon the chiral condensate functions $\phi(p_z)$ through the function $\cos\left(\frac{\phi_1-\phi_2}{2}\right)$ apart from the thermal distribution functions $\sin^2\theta_\pm^{ia}$. Further, this dependence vanishes when the u and d quark scalar condensates or equivalently the corresponding masses of the quarks are equal.

The other quantity that we wish to investigate is the axial fermion current density that is induced at finite chemical potential including the effect of temperature. The expectation value of the axial current density is given by

$$\langle j_5^3 \rangle \equiv \langle \bar{\psi}_i^a \gamma^3 \gamma^5 \psi_j^a \rangle.$$

Using the field operator expansion Eq.(4.10) and Eq.(4.3) for the explicit forms for the spinors, we have for the i-th flavor

$$\langle j_5^{i3} \rangle = \sum_n \frac{N_c}{(2\pi)^2} \int dp_x \left(I_n^2 - I_{n-1}^2\right) \left(\sin^2\theta_-^i - \sin^2\theta_+^i\right). \qquad (4.26)$$

Integrating over dp_y using the orthonormal condition of Eq.(4.5), all the terms in the above sum for the Landau levels cancel out except for the zeroth Landau level so that,

$$\langle j_5^{i3} \rangle = \frac{N_c |q_i| B}{(2\pi)^2} \int dp_z \left[\sin^2\theta_-^{i0} - \sin^2\theta_+^{i0}\right]. \qquad (4.27)$$

which is identical to that in Ref.[165] once we identify the functions $\sin^2\theta_\mp^{i0}$ as the particle and the antiparticle distribution functions for the zero modes (see e.g. Eq.(4.52) in the next section).

4.3 Evaluation of thermodynamic potential and gap equations

As has already been mentioned, we shall consider in the present investigation, the 3-flavor Nambu Jona Lasinio model including the Kobayashi-Maskawa-t-Hooft (KMT) determinant interaction. The corresponding Hamiltonian

Quark	e-charge	$\tilde{e}$-charge
u-red	$\frac{2}{3}$	$\frac{1}{2}$
u-green	$\frac{2}{3}$	$\frac{1}{2}$
u-blue	$\frac{2}{3}$	1
d-red	-$\frac{1}{3}$	$\frac{1}{2}$
d-green	-$\frac{1}{3}$	$\frac{1}{2}$
d-blue	-$\frac{1}{3}$	0
s-red	-$\frac{1}{3}$	$\frac{1}{2}$
s-green	-$\frac{1}{3}$	$\frac{1}{2}$
s-blue	-$\frac{1}{3}$	0

Table 4.1: Table: List of quarks and their electromagnetic and rotated charges

density is given as [49, 151, 142, 166]

$$\begin{aligned}
\mathcal{H} &= \psi^\dagger(-i\boldsymbol{\alpha}\cdot\mathbf{\Pi}) + \gamma^0\hat{m})\psi \\
&- G_s\sum_{A=0}^{8}\left[(\bar{\psi}\lambda^A\psi)^2 - (\bar{\psi}\gamma^5\lambda^A\psi)^2\right] \\
&+ K\left[det_f[\bar{\psi}(1+\gamma_5)\psi] + det_f[\bar{\psi}(1-\gamma_5)\psi]\right] \\
&- G_D\left[(\bar{\psi}\gamma^5\epsilon\epsilon_c\psi^C)(\bar{\psi}^C\gamma^5\epsilon\epsilon_c\psi)\right] \qquad (4.28)
\end{aligned}$$

where $\psi^{i,a}$ denotes a quark field with color 'a' ($a = r, g, b$), and flavor 'i' ($i = u, d, s$), indices. $\mathbf{\Pi} = -i(\nabla - i\tilde{e}\tilde{\boldsymbol{A}}\tilde{Q})$ is the canonical momentum in presence of the rotated U(1) gauge field $\tilde{A}_\mu$. When there is no superconductivity $A_\mu = \tilde{A}_\mu$ which is the usual massless photon field with the coupling to the quark field being given the electromagnetic charge eQ_f where, Q_f is diagonal matrix $(2/3, -1/3, -1/3)$. As mentioned in the previous section, when superconducting gap is non vanishing, the massless gauge field is given by $\tilde{A}_\mu = \cos\alpha A_\mu - \sin\alpha G^8_\mu$, where, $\cos\alpha = g/\sqrt{g^2 + e^2/3}$. We have taken here the standard convention of $SU(3)_c$ generators in the adjoint representation [148]. The $\tilde{Q}$ charges of the quarks are given in Table-I. It may also be relevant here to mention that, while we are taking into account combination of the photon and gluon field which is massless, the other orthogonal massive component, is either Meissener screened or nucleated into vortices [167].

The matrix of current quark masses is given by $\hat{m}$=diag$_f(m_u, m_d, m_s)$ in the flavor space. We shall assume in the present investigation, isospin symmetry with m_u=m_d. In Eq. (4.28), λ^A, $A = 1, \cdots 8$ denote the Gellmann matrices acting in the flavor space and $\lambda^0 = \sqrt{\frac{2}{3}}\,\mathbb{1}_f$, $\mathbb{1}_f$ as the unit matrix in the flavor space. The four point interaction term $\sim G_s$ is symmetric in $SU(3)_V \times SU(3)_A \times U(1)_V \times U(1)_A$. In contrast, the determinant term $\sim K$ which for the case of three flavors generates a six point interaction which breaks $U(1)_A$ symmetry. If the mass term is neglected, the overall symmetry is $SU(3)_V \times SU(3)_A \times U(1)_V$. This spontaneously breaks to $SU(3)_V \times U(1)_V$ implying the conservation of the baryon number and the flavor number. The current quark mass term introduces additional explicit breaking of chiral symmetry leading to partial conservation of the axial current. The last term in Eq.(4.28) describe a scalar diquark interaction in the color antitriplet and flavor antitriplet channel. Such a form of four point interaction can arise e.g. by Fierz transformation of a four point vector current-current interaction having quantum numbers of a single gluon exchange. In that case the diquark coupling G_D is related to the scalar coupling as $G_D = 0.75G_s$.

Next we evaluate the expectation value of the kinetic term in Eq.(4.28) which is given as

$$T = \langle\Omega(\beta,\mu)|\psi^{ia\dagger}(-i\boldsymbol{\alpha}\cdot\nabla - \tilde{q}^{ia}Bx\alpha_2)\psi^{ia}|\Omega(\beta,\mu)\rangle. \equiv \sum_{ia} T^{ia} \tag{4.29}$$

In the above the sum over the colors a and flavors i is understood. The color flavor dependent charges $\tilde{q}^{ia}$ for the quasi particles is given in Table I. To evaluate this, for non vanishing $\tilde{q}$ charges, we use Eq. (4.10) and the results of spatial derivatives on the functions $I_n(\xi)$ ($\xi = \sqrt{|q_i|B}(x - p_y/(|q_i|B))$).

$$\frac{\partial I_n}{\partial x} = \sqrt{|q^{ia}|B}\left[-\xi I_n + \sqrt{2n}I_{n-1}\right],$$

$$\frac{\partial I_{n-1}}{\partial x} = \sqrt{|\tilde{q}^{ia}|B}\left[-\xi I_{n-1} + \sqrt{2(n-1)}I_{n-2}\right]. \tag{4.30}$$

Using above, straightforward but somewhat tedious manipulations leads to the contribution arising from the quarks that take part in superconductivity, i.e. for color, flavor indices $i, a = 1, 2$,

$$T^{ia} = -\sum_{n=0}^{\infty}\alpha_n\frac{|\tilde{e}B|}{2(2\pi)^2}\int dp_z(m_i\cos\phi_i + |p_i|\sin\phi_i)(1 - F^{ia} - F_1^{ia}) \qquad (i, a = 1, 2). \tag{4.31}$$

where, we have defined $|p_i|^2 = p_z^2 + 2n|\tilde{q}B|$, ($\tilde{q} = \tilde{e}/2$). Here, the quark-antiquark condensate effects are encoded in the function ϕ_i while diquark and di-antiquark condensate effects are encoded in the functions F^{ia} and F_1^{ia} respectively as given in Eq.(4.20 and Eq.(4.21).

For the blue u-quark, which is charged but does not take part in diquark condensation the corresponding contribution to the kinetic term is given by

$$T^{13} = -\sum_{n=0}^{\infty} \alpha_n \frac{|\tilde{e}B|}{(2\pi)^2} \int dp_z (m_1 \cos\phi_1 + |p_1| \sin\phi_1)(1 - \sin^2\theta_-^{13} - \sin^2\theta_+^{13}) \tag{4.32}$$

The contribution of the charged strange quarks (with charges $\tilde{e}/2$) to the kinetic energy is given by, with $a = 1, 2$,

$$T^{3a} = -\sum_{n=0}^{\infty} \alpha_n \frac{|\tilde{e}B|}{2(2\pi)^2} \int dp_z (m_3 \cos\phi_3 + |p_3| \sin\phi_3)(1 - \sin^2\theta_-^{3a} - \sin^2\theta_+^{3a}). \tag{4.33}$$

Finally, the contribution from the $\tilde{e}$ -charge neutral quarks (blue d and blue s) is given as

$$T^{i3} = -\int \frac{d\mathbf{p}}{(2\pi)^3} \left(m_i \cos\phi_i + p \sin\phi_i\right) \left(1 - \sin^2\theta_-^{i3} - \sin^2\theta_+^{i3}\right) \qquad (i = 2, 3). \tag{4.34}$$

The contribution to the energy density from the the quartic interaction term in Eq. (4.28), using Eq. (4.18) turns out to be,

$$V_S \equiv -G_s \langle \Omega(\beta,\mu)| \sum_{A=0}^{8} \left[(\bar{\psi}\lambda^A\psi)^2 - (\bar{\psi}\gamma^5\lambda^A\psi)^2\right] |\Omega(\beta,\mu)\rangle = -2G_S \sum_{i=1,3} {I_s^i}^2, \tag{4.35}$$

where, $I_s^i = \langle\bar{\psi}_i\psi_i\rangle$ is the scalar quark-antiquark condensate given in Eq.(4.18). Further, in the above, we have used the properties of the Gellman matrices $\sum_{A=0}^{8} \lambda_{ij}^A \lambda_{kl}^A = 2\delta_{il}\delta_{jk}$.

Next, let us discuss the contribution from the six quark determinant interaction term to the energy expectation value. There will be six terms in the expansion of the determinant, each involving three pairs of quark operators of different flavors. These are to be 'contracted' in all possible manner while taking the expectation value. This means in the present context of having quark-antiquark and diquark condensates, one can contract a ψ with a $\bar{\psi}$ or ψ with a ψ . The former leads to condensates having quark-antiquark condensates $I_s^{(i)}$ while the latter leading to diquark condensates I_D. Further, for the case of quark-antiquark condensate contributions, the contracting ψ and $\bar{\psi}$ having the same color will lead to the dominant contribution while contracting similar operators with different colors will lead to a N_c suppressed contribution. Next coming to contributions arising from the diquarks, terms which are proportional to strange quark-antiquark condensate $\langle\bar{s}s\rangle$ will be dominant. These will have the contractions of strange quark-antiquarks having the same color. The rest four terms will be suppressed atleast by a factor N_c. Explicitly these two terms are given by $\sim \sum_h \bar{s}O^h s \left[\bar{u}\hat{O}^h u \times (\bar{d}\hat{O}^h d) - \bar{u}\hat{O}^h d \times (\bar{d}\hat{O}^h u)\right]$, where $h = \pm$ and $\hat{O}^{\pm} = (1 \pm \gamma_5)$. When contracted diquark wise, both the terms give identical contributions, except that the contribution of the second term will be of opposite sign as compared to the first term. This is a consequence of flavor antisymmetric nature of the diquark condensates. This leads to

$$V_{det} = +K\langle det_f[\bar{\psi}(1+\gamma_5)\psi] + det_f[\bar{\psi}(1-\gamma_5)\psi]\rangle = \frac{1}{3}|\epsilon_{ijk}|I_s^{(i)}I_s^{(j)}I_s^{(k)} + \frac{K}{4}I_s^{(3)}I_D^2$$

Next, the contribution from the diquark interaction is given by

$$V_D = -\langle G_D \left[(\bar{\psi}\gamma^5\epsilon\epsilon_c\psi^C)(\bar{\psi}^C\gamma^5\epsilon\epsilon_c\psi)\right]\rangle = -G_D I_D^2 \tag{4.36}$$

where, the diquark condensate I_D is already defined in Eq.(4.25).

To calculate the thermodynamic potential (negative of the pressure), we also have to specify the chemical potentials relevant for the system. Here, we shall be interested in the form of quark matter that might be present in compact stars that are older than few minutes so that chemical equilibration for weak interaction is satisfied. The relevant chemical potentials in such case are the baryon chemical potential $\mu_B = 3\mu_q$, the chemical potential μ_E associated with the electromagnetic charge, and, the color potentials μ_3 and μ_8. The chemical potential is a matrix that is diagonal in color and flavor space and is given by

$$\mu_{ij,ab} = (\mu\delta_{ij} + Q_{ij}\mu_E)\delta_{ab} + (T^3_{ab}\mu_3 + T^8_{ab}\mu_8)\delta_{ij} \tag{4.37}$$

Since, red and green color of a given flavor of quark is degenerate and the diquark is in blue direction in the color space , we can assume $\mu_3 = 0$. As mentioned earlier the flavor space charge $Q \equiv diag(2/3, -1/3, -1/3)$ which couples to the electromagnetic field A_μ.

The thermodynamic potential is then given by using Eq.s(4.29),(4.35),(4.36),(4.36) and with s being the entropy density,

$$\Omega = T + V_S + V_{det} + V_D - \langle\mu N\rangle - \frac{1}{\beta}s, \tag{4.38}$$

where we have introduced

$$\langle\mu N\rangle = \langle\psi^{ia\dagger}\mu_{ij,ab}\psi^{jb}\rangle = \sum_{i,a}\mu^{ia}\rho^{ia} \tag{4.39}$$

where, ρ^{ia} is the vector density $\rho^{ia} = \langle\psi^{ia\dagger}\psi^{ia}\rangle$. For the superconducting quarks this is given by

$$\rho^{ia} = \sum_n \frac{\alpha_n\tilde{e}B}{2(2\pi)^2}\int dp_z\left(F^{ia} - F_1^{ia}\right) \qquad (i, a = 1, 2) \tag{4.40}$$

while, for the blue u quark, the same is given by

$$\rho^{13} = \sum_n \frac{\alpha_n \tilde{e} B}{(2\pi)^2} \int dp_z \left(\sin^2\theta_-^{13} - \sin^2\theta_+^{13}\right). \tag{4.41}$$

For the charged strange quarks, this density is given by

$$\rho^{3a} = \sum_n \frac{\alpha_n \tilde{e} B}{2(2\pi)^2} \int dp_z \left(\sin^2\theta_-^{3a} - \sin^2\theta_+^{3a}\right) \qquad (a = 1, 2) \tag{4.42}$$

For the $\tilde{e}$-uncharged quarks (blue down and blue strange) , the vector density is given by

$$I_v^{i3} = \frac{2}{(2\pi)^3} \int d\mathbf{p} \left(\sin^2\theta_-^{i3} - \sin^2\theta_+^{i3}\right). \qquad (i = 2, 3) \tag{4.43}$$

Finally, for the entropy density $s = \sum_{i,a} s^{ia}$ where, s^{ia} is the entropy density for quarks of flavor i and color a. For the $\tilde{e}$-quarks, with charge $\tilde{q}^{ia}$, the phase space is Landau quantized and we have the entropy density given as [162, 163]

$$s^{ia} = -\sum_n \frac{\alpha_n |q^{ia}| B}{(2\pi)^2} \int dp_z \{(\sin^2\theta_-^{ia} \ln\sin^2\theta_-^{ia} + \cos^2\theta_-^{ia} \ln\cos^2\theta_-^{ia}) + (- \to +)\}. \tag{4.44}$$

On the other hand, for the uncharged (blue down and blue strange) quarks, the entropy density is given by

$$s^{i3} = -\frac{2}{(2\pi)^3} \int d\mathbf{p} \{(\sin^2\theta_-^{i3} \ln\sin^2\theta_-^{i3} + \cos^2\theta_-^{i3} \ln\cos^2\theta_-^{i3}) + (- \to +)\} \qquad (i = 2, 3). \tag{4.45}$$

Thus, the thermodynamic potential is now completely defined in terms of the condensate functions ϕ^i, $f(k)$ and the thermal distribution functions $\theta_\mp^{ia}$ which will be determined through a functional extremisation of the thermodynamic potential. Minimizing the thermodynamic potential with respect to the quark-antiquark condensate function $\phi_i(p)$ i.e. $\delta\Omega/\delta\phi_i = 0$ leads to,

$$\cot\phi^{ia} = \frac{(m_i - 4G_s I_s^i + K\epsilon^{ijk} I_s^j I_s^k + K/4 I_D^2 \delta_{i3})}{|p_{ia}|} \equiv \frac{M_i}{|p_{ia}|} \tag{4.46}$$

where, as earlier, we have defined $|p_{ia}| = \sqrt{p_z^2 + 2n|q_{ia}|B}$ and we have defined the constituent quark mass $M_i = m_i - 4G_s I_s^{(i)} + K|\epsilon_{ijk}| I_s^{(i)} I_s^{(j)} I_s^{(k)} + K/4 I_D^2 \delta^{i3}$. These expressions are actually self consistent equations for the constituent quark masses as scalar condensate $I_s^{(i)}$ as given in Eq.(4.18) involve M_i

through their dependence on ϕ_i. Explicitly, these mass gap equations are given as

$$M^u = m^u - 4G_s I_s^{(u)} + 2K I_s^{(d)} I_s^{(s)}, \tag{4.47}$$

$$M^d = m^d - 4G_s I_s^{(d)} + 2K I_s^{(u)} I_s^{(s)}, \tag{4.48}$$

$$M^s = m^s - 4G_s I_s^{(s)} + 2K I_s^{(d)} I_s^{(u)} + \frac{K}{4} I_D^2, \tag{4.49}$$

Let us note that while the color and flavor dependence on the quark-antiquark condensate functions ϕ^{ia} arises *only* from the momentum $|p_{ia}| = \sqrt{p_z^2 + 2n|\tilde{q}_{ia}|B}$ through the color flavor dependent $\tilde{q}$ charges, the constituent quark masses are color singlets and are given by the solutions of the self consistent equations Eq.(4.47)-Eq.(4.49). Further, the flavor mixing determinant interaction makes the masses of quark of a given flavor dependent upon the condensates of the other flavor quarks. This apart, the strange quark mass explicitly depends upon the diquark condensates through this determinant interaction. Note that for the two flavor superconductivity as considered here, the strange quark mass is affected explicitly by the superconducting gap given by the last term on the right hand side Eq.(4.49). Of course, there is implicit dependence on the superconducting gap in the second term through the functions F and F_1 (given in Eq.s (4.20) and (4.21)). Further, when chiral symmetry is restored for the light quarks i.e., when the scalar condensates for the non strange quarks vanish, still, the determinant term gives rise to a density dependent dynamical strange quark mass [166]. Such a mass generation is very different from the typical mechanism of quark mass generation through quark–antiquark condensates [168].

In a similar manner, minimizing the thermodynamic potential with respect to the diquark function $f(k)$ and di-antiquark function $f_1(k)$ i.e. $\frac{\delta\Omega}{\delta f(k)} = 0$ and $\frac{\delta\Omega}{\delta f_1(k)} = 0$ leads to

$$\begin{aligned} \tan 2f(k) &= \frac{2(G_D - \frac{K}{4} I_s^{(3)}) I_D}{\bar{\epsilon}_n - \bar{\mu}} \cos(\frac{\phi_1 - \phi_2}{2}) \equiv \frac{\Delta}{\bar{\epsilon}_n - \bar{\mu}} \cos(\frac{\phi_1 - \phi_2}{2}); \\ \tan 2f_1(k) &= \frac{\Delta}{\bar{\epsilon}_n + \bar{\mu}} \cos(\frac{\phi_1 - \phi_2}{2}) \end{aligned} \tag{4.50}$$

where, we have defined the superconducting gap Δ as

$$\Delta = 2\left(G_D - \frac{K}{4} I_s^{(3)}\right) I_D \tag{4.51}$$

and, $\bar{\epsilon} = (\epsilon_n^u + \epsilon_n^d)/2$, $\bar{\mu} = (\mu^{ur} + \mu^{dg})/2 = \mu + 1/6\mu_E + 1/\sqrt{3}\mu_8$, where, we have used Eq.(4.37) for the chemical potentials. Further, ϵ_n^i is the nth Landau level energy for the ith flavor with constituent quark mass M_i given as $\epsilon_n^i = \sqrt{p_z^2 + 2n|q_i|B + M_i^2}$. It is thus seen that the diquark condensate functions depend upon the *average* energy and the *average* chemical potential of the quarks that condense. We also note here that the diquark condensate functions depends upon the masses of the two quarks which condense through the function $\cos\big((\phi_1 - \phi_2)/2\big)$. The function $\cos\phi_i = M_i/\epsilon_n^i$, can be different for u,d quarks, when the charge neutrality condition is imposed. Such a normalization factor is always there when the condensing fermions have different masses as has been noted in Ref. [169] in the context of CFL phase.

Finally, the minimization of the thermodynamic potential with respect to the thermal functions $\theta_\pm^{ia}(\mathbf{k})$ gives

$$\sin^2\theta_\pm^{ia} = \frac{1}{\exp(\beta(\omega_{i,a} \pm \mu_{ia})) + 1}, \tag{4.52}$$

Various ω^{ia}'s $(i, a \equiv \text{flavor}, \text{color})$ are explicitly given as

$$\omega_{n\pm}^{11} = \omega_{n\pm}^{12} = \bar{\omega}_{n\pm} + \delta\epsilon_n \pm \delta_\mu \equiv \omega_{n\pm}^u \tag{4.53}$$

$$\omega_{n\pm}^{21} = \omega_{n\pm}^{22} = \bar{\omega}_{n\pm} - \delta\epsilon_n \mp \delta_\mu \equiv \omega_{n\pm}^d \tag{4.54}$$

for the quarks participating in condensation. Here,
$\bar{\omega_{n\pm}} = \sqrt{(\bar{\epsilon}_n \pm \bar{\mu})^2 + \Delta^2\cos^2(\phi_1 - \phi_2)/2}$. Further, $\delta\epsilon_n = (\epsilon_n^u - \epsilon_n^d)/2$ is half the energy difference between the quarks which condense in a given Landau level and $\delta\mu = (\mu_{ur} - \mu_{dg})/2 = \mu_E/2$ is half the difference between the chemical potentials of the two condensing quarks. For the charged quarks which do not participate in the superconductivity,

$$\omega_{n\pm}^{ia} = \epsilon_n^i \pm \mu^{ia}. \tag{4.55}$$

In the above, the upper sign corresponds to antiparticle excitation energies while the lower sign corresponds to the particle excitation energies.

Let us note that when the charge neutrality conditions are not imposed, the masses of u and d quarks will be almost the same but for the effect of the (rotated) magnetic field as the magnitude of the charges for red and green quarks are the same and that of the blue color is different. Since the chemical potentials of all the quarks are the same when charge neutrality is not imposed, all the four quasi particles taking part in diquark condensation will have (almost) the same energy $\bar{\omega}_{n-}$. On the other hand, when charge neutrality condition is imposed, it is clear from the dispersion relations given in Eq.(4.53), (4.54) that it is possible to have zero modes, i.e., $\omega^{ia} = 0$ depending upon the values of $\delta\epsilon_n$ and $\delta\mu$. So, although we shall have nonzero order parameter Δ, there will be fermionic zero modes or the gapless superconducting phase [170, 171].

Substituting the solutions for the quark-antiquark condensate function ϕ^i of Eq.(4.46), we have the solutions for the different quark-antiquark condensates i.e. I_s^{ia} given by, using equations Eq.(4.19), Eq.(4.22) and Eq.(4.23),

$$I_s^{ia} = -\sum_n \frac{\alpha_n}{(2\pi)^2}(\tilde{e}B/2)\int dp_z \frac{M_i}{\sqrt{p_z^2 + 2n(\tilde{e}B/2) + M_i^2}}\left(1 - F^{ia} - F_1^{ia}\right) \qquad (i, a = 1, 2)$$

$$I_s^{13} = -\sum_n \frac{\alpha_n}{(2\pi)^2}(\tilde{e}B)\int dp_z \frac{M_1}{\sqrt{p_z^2 + 2n(\tilde{e}B) + M_1^2}}\left(1 - \sin^2\theta_-^{13} - \sin^2\theta_+^{13}\right) \tag{4.56}$$

$$I_s^{3a} = -\sum_n \frac{\alpha_n}{(2\pi)^2}(\tilde{e}B/2)\int dp_z \frac{M_3}{\sqrt{p_z^2 + 2n(\tilde{e}B/2) + M_3^2}}\left(1 - -\sin^2\theta_-^{3a} - \sin^2\theta_+^{3a}\right) \qquad (a = 1, 2)$$

for the $\tilde{e}$ charged quarks while for the uncharged quarks (blue d and blue strange quarks),

$$I_s^{i3} = -\frac{2}{(2\pi)^3}\int d\mathbf{p} \frac{M_i}{i\sqrt{\mathbf{p}^2 + M_i^2}}\left(1 - \sin^2\theta_-^{i3} - \sin^2\theta_+^{i3}\right) \qquad (i = 2, 3) \tag{4.57}$$

Similarly, substituting the solutions for the diquark /di-antiquark condensate functions from Eq.(4.50) in Eq. (4.25), we have, with the usual notations,$\bar{\xi}_{n\pm} = \bar{\epsilon}_n \pm \bar{\mu}$ and $\bar{\omega}_{n\pm} = \sqrt{\xi_{n\pm}^2 + \Delta^2\cos^2(\phi_1 - \phi_2)/2}$,

$$\begin{aligned} I_D = {} & \frac{2}{(2\pi)^2}\sum_n \alpha_n |\tilde{e}B/2| \int dp_z \Delta \cos^2\left(\frac{\phi_1 - \phi_2}{2}\right) \\ & \left[\frac{1}{\bar{\omega}_{n-}}\left(1 - \sin^2\theta_-^1 - \sin^2\theta_-^2\right) + \frac{1}{\bar{\omega}_{n+}}\left(1 - \sin^2\theta_+^1 - \sin^2\theta_+^2\right)\right] \end{aligned} \tag{4.58}$$

Thus Eq.s(4.47)- (4.49) for the mass gaps, Eq.(4.51) for the superconducting gap and Eq.s (4.56)-(4.58) define the self consistent mass gap equation for the i-th quark flavor and the superconducting gap .

Next we discuss the thermodynamic potential. We substitute the solutions for the condensate functions Eq.(4.46), Eq.(4.50) in the expression for the thermodynamic potential Eq.(4.38) and use the gap equations Eq.s(4.47)-(4.49) and Eq.(4.51). The thermodynamic potential is then given by

$$\Omega_q = \Omega^{sc}_{1/2}+\Omega^{s}_{1/2}+\Omega_0+\Omega_1+4G_s\sum_i {I^i_s}^2-4KI^u_sI^d_sI^s_s+\frac{\Delta^2}{4G'_D}-\frac{K}{4}I^s_sI^2_D \quad (4.59)$$

where, we have defined, an effective diquark coupling $G'_D = G_D - \frac{K}{4I^s_s}$ in presence of the determinant term which mixes the flavors. Let us now discuss each of the terms in Eq.(4.59).The first term is the contribution from the quarks that take part in superconductivity i.e. the red and blue, u,d quarks. This contribution is given by

$$\begin{aligned}
\Omega^{sc}_{1/2} &= -2\sum_n \frac{\alpha_n(\tilde{e}B/2)}{(2\pi)^2}\int(\epsilon^u_n+\epsilon^d_n)dp_z \\
&+ 2\sum_n \frac{\alpha_n(\tilde{e}B/2)}{(2\pi)^2}\int\big((\bar{\xi}_{n-}+\bar{\xi}_{n+})-(\bar{\omega}_{n-}+\bar{\omega}_{n+})\big) \\
&- 2\sum_n\sum_{i=u,d}\frac{2\alpha_n(\tilde{e}B)/2}{(2\pi)^2\beta}\int dp_z \\
&\quad \big[\log(1+\exp(-\beta(\omega^i_{n-}-\mu_{ir})))+\log(1+\exp(-\beta(\omega^i_{n+}+\mu_{ir})))\big] \\
&\equiv \Omega^{sc}_{1/2,0}(T=0,\mu=0)+\Omega^{sc}_{1/2,med}(T,\mu) \qquad (4.60)
\end{aligned}$$

where, we have separated the contribution of the medium $\Omega^{sc}_{1/2,med}$ from $T = 0, \mu = 0$ contribution. Similarly, the $(\tilde{e})$ charged strange quark contribution to the thermodynamic potential is given by

$$\begin{aligned}
\Omega^{s}_{1/2} &= -2\sum_n \frac{\alpha_n(\tilde{e}B)/2}{(2\pi)^2}\int(\epsilon^s_n) \\
&- \sum_n\sum_{a=1,2}\sum_{s=\pm1}\frac{\alpha_n(\tilde{e}B)/2}{(2\pi)^2\beta}\int dp_z\,[\log(1+\exp(-\beta(\omega_{3a}+s\mu_{ia})] \\
&\equiv \Omega^s_{1/2,0}+\Omega^s_{1/2,med} \qquad (4.61)
\end{aligned}$$

The term Ω_1 in Eq.(4.59) arises from the blue colored u- quark with charge $\tilde{e}$ and is given as

$$\begin{aligned}
\Omega_1 &= -\sum_n \frac{\alpha_n(\tilde{e}B)}{(2\pi)^2}\int(\epsilon^u_n) \\
&-\sum_n\sum_{s=\pm1}\frac{\alpha_n(\tilde{e}B)}{(2\pi)^2\beta}\int dp_z\,[\log(1+\exp(-\beta(\omega_{33}+s\mu_{33})] \\
&\equiv \Omega^u_{1,0}+\Omega^u_{1,med}
\end{aligned}$$

Finally, the $\tilde{e}$ uncharged quarks' contributions to the thermodynamic potential Ω_0 is given by

$$\Omega_0 = -2\sum_{i=2,3}\int\frac{d\mathbf{p}}{(2\pi^3)}\epsilon^i(\mathbf{p}) - \frac{2}{(2\pi)^3\beta}\int d\mathbf{p}\sum_{s=\mp 1}[\log(1+\exp(-\beta(\omega_{23}+s\mu_{33})] \tag{4.62}$$

Now, all the zero temperature and zero chemical potential contributions of the thermodynamic potential in Eq.s(4.60)- (4.62) are ultraviolet divergent. This divergence also gets transmitted to the gap equations through the quark-antiquark as well as diquark condensates in equations Eq.(4.56), Eq.(4.56),Eq.(4.57)and Eq.(4.58). For the chargeless case, these can be rendered finite through a regularization with a sharp cut off in the magnitude of three momentum as is usually done in the NJL models. However, it is also seen that a sharp cutoff in the presence of magnetic field for charged particles suffers from cut-off artifacts since the continuous momentum dependence in two spatial dimensions are replaced by sum over discrete Landau levels. To avoid this, some calculations use a smooth parametrisation for the cutoff as e.g. in Ref.[117] . In the present work however we follow the elegant procedure that was followed in Ref. [140, 141] by adding and subtracting a vacuum (zero field) contribution to the thermodynamic potential which is also divergent. This manipulation makes e.g. the Dirac vacuum contribution in presence of magnetic field to a physically more appealing form by separating the same to a zero field vacuum contribution and a finite field contribution written in terms of Riemann-Hurwitz ζ function. The vacuum contribution to the energy density arising from a charged quark can be written as [142, 140, 141],

$$\begin{aligned}
&-\sum_{n=0}^{\infty}\frac{\alpha_n|q_iB|}{(2\pi)^2}\int dp_z\sqrt{p_z^2+2n|q_i|B+M_i^2} \\
=& -\frac{2}{(2\pi)^3}\int d\mathbf{p}\sqrt{\mathbf{p}^2+M_i^2} \\
-& \frac{1}{2\pi^2}|q_iB|^2\left[\zeta'(-1,x_i)-\frac{1}{2}(x_i^2-x_i)\ln x_i+\frac{x_i^2}{4}\right],
\end{aligned} \tag{4.63}$$

where, we have defined the dimensionless quantity, $x_i = \frac{M_i^2}{2|q_iB|}$, i.e. the mass parameter in units of the magnetic field. Further, $\zeta'(-1,x) = d\zeta(z,x)/dz|_{z=1}$ is the derivative of the Riemann-Hurwitz zeta function [172].

Using Eq.(4.63), the quark-antiquark condensate of $(\tilde{q})$ charged quarks can be written as

$$\begin{aligned}
\langle\bar{\psi}^{ia}\psi^{ia}\rangle &= -\frac{2}{(2\pi)^3}\int d\mathbf{p}\frac{M_i}{\sqrt{\mathbf{p}^2+M_i^2}} \\
&- \frac{M_i|q_iB|}{2\pi^2}\left[x_i(1-\ln x_i)+\ln\Gamma(x_i)+\frac{1}{2}\ln(\frac{x_i}{2\pi})\right]+I^{ia}_{s\ med} \\
&\equiv I^{ia}_{s\ vac}+I^{ia}_{s\ field}+I^{ia}_{s\ med} \qquad (4.64)
\end{aligned}$$

The first term, $I^{ia}_{s\ vac}$ can be explicitly evaluated with a cutoff Λ as

$$I^{ia}_{s\ vac}=\frac{M_i}{2\pi^2}\left[\Lambda\sqrt{\Lambda^2+M_i^2}-M_i^2\log\left(\frac{\Lambda+\sqrt{\Lambda^2+M_i^2}}{M_i}\right)\right]. \qquad (4.65)$$

The medium contribution to the scalar condensate from the superconducting part is

$$I^{ia}_{s\ med}=\sum_n\frac{\alpha_n(\tilde{e}B/2)}{(2\pi)^2}\int dp_z\frac{M_i}{\epsilon_n^i}\left(F^{ia}-F_1^{ia}\right), \qquad (4.66)$$

while, for the non superconducting blue u-quarks,

$$I^{13}_{s\ med}=\sum_n\frac{\alpha_n(\tilde{e}B)}{(2\pi)^2}\int dp_z\frac{M_1}{\epsilon_n^1}\left(\sin^2\theta_-^{13}-\sin^2\theta_+^{13}\right). \qquad (4.67)$$

Similarly, the contribution of the medium to the ($\tilde{q}$) charged strange quark-antiquark condensate is

$$I^{3a}_{s\ med}=\sum_n\frac{\alpha_n(\tilde{e}B/2)}{(2\pi)^2}\int dp_z\frac{M_3}{\epsilon_n^3}\left(\sin^2\theta_-^{3a}-\sin^2\theta_+^{3a}\right)\quad (a=1,2) \qquad (4.68)$$

In what follows, we shall focus our attention to zero temperature calculations. Using the relation $\lim_{\beta\to\infty}\frac{1}{\beta}\ln(1+\exp(-\beta\omega))=-\omega\theta(-\omega)$ and using Eq.s(4.60), Eq.(4.63), we have the zero temperature thermodynamic potential for the color superconducting quarks given as

$$\Omega^{sc}_{1/2}(T=0,\mu,B)=\Omega^{sc}_{1/2,0}(T=0,\mu=0)+\Omega^{sc}_{1/2,med}(T=0,\mu) \qquad (4.69)$$

with,

$$\Omega^{sc}_{1/2,0}(T=0,\mu=0)=-2\times2\sum_{i=u,d}G(\Lambda,M_i)-2\sum_{i=u,d}F(x_i,B) \qquad (4.70)$$

where we have defined the function $G(\Lambda, M)$ as

$$G(\Lambda, M) = \frac{1}{(2\pi)^3}\int_0^{\Lambda}\sqrt{\mathbf{p}^2+M^2}d\mathbf{p}$$
$$= \frac{1}{16\pi^2}\left[\Lambda\sqrt{\Lambda^2+M^2}(2\Lambda^2+M^2)\right. \tag{4.71}$$
$$\left. - M^4\log\left(\frac{\Lambda+\sqrt{\Lambda^2+M^2}}{M}\right)\right].$$

The prefactors in the first term correspond to color and spin degeneracy factors while the same in the second term correspond to the color degeneracy factor. The magnetic field dependent function, $F(x_i, B)$ with $x_i = M_i^2/|q_iB|$,

$$F(x_i) = \frac{1}{2\pi^2}|q_iB|^2\left[\zeta'(-1, x_i) - \frac{1}{2}(x_i^2 - x_i)\ln x_i + \frac{x_i^2}{4}\right], \tag{4.72}$$

The medium contribution from the superconducting quarks is given as

$$\Omega^{sc}_{1/2,med}(T=0,\mu) = 2\sum_{n=0}^{n_{max}}\frac{\alpha_n(\frac{\tilde{e}B}{2})}{(2\pi^2)}\int_0^{p_{zn}^{max}} dp_z\left[\bar{\xi}_{n-}+\bar{\xi}_{n+}-(\bar{\omega}_{n-}+\bar{\omega}_{n+})\right]$$
$$+ \sum_{n=0}^{n_{max}}\sum_{i=u,d}\frac{\alpha_n(\frac{\tilde{e}B}{2})}{\pi^2}\int_0^{p_{zn}^{max}} dp_z$$
$$\left[\quad \omega^i_{n-}\theta(-\omega^i_{n-}) + \omega^i_{n+}\theta(-\omega^i_{n+})\right]. \tag{4.73}$$

The three momentum cutoff Λ for the magnitude of momentum in the absence of magnetic field leads to the sum over the Landau level upto $n_{max} = \frac{\Lambda^2}{\tilde{e}B}$. Futher, the positivity of the magnitude of p_z, restricts the cutoff in $|p_z|$ as $p^n_{z,max} = \sqrt{\Lambda^2 - n\tilde{e}B}$ for a given value of n of the Landau level.

The contribution of the blue up quark to the thermodynamic potential $\Omega_1 = \Omega_{1,0} + \Omega_{1,med}$ with

$$\Omega_{1,0}(T=0,\mu=0) = -2G(\Lambda, M_u) - F(x_u, B) \tag{4.74}$$

and

$$\Omega_{1,med}(T=0,\mu) = \sum_{n=0}^{n^u_{max}}\frac{\alpha(\tilde{e}B)}{(2\pi^2)}$$
$$\left[\mu_{ub}\sqrt{\mu_{ub}^2 - M_{nu}^2} + M_{nu}^2\log\left(\frac{\mu_{ub}+\sqrt{\mu_{ub}^2-M_{nu}^2}}{M_{nu}}\right)\right]$$

where $M_{nu} = \sqrt{M_u^2 + 2n\tilde{e}B}$ is the n^{th} Landau level mass for up quark and $n^u_{max} = Int\left[\frac{\mu_{ub}^2 - M_u^2}{2\tilde{e}B}\right]$ is the maximum number of Landau level consistent with the zero temperature distribution function.

The $\tilde{e}$ charged strange quark contribution to the thermodynamic potential $\Omega^s_{1/2} = \Omega^s_{1/2,0} + \Omega^s_{1/2,med}$, with

$$\Omega^s_{1/2,0}(T = 0, \mu = 0) = -2 \times 2G(\Lambda, M_s) - 2F(x_s, B) \tag{4.75}$$

and

$$\Omega_{1/2,med}(T = 0, \mu) = 2 \sum_{n=0}^{n^s_{max}} \frac{\alpha(\frac{\tilde{e}B}{2})}{(2\pi^2)} \left[\mu_{sr}\sqrt{\mu_{sr}^2 - M_{ns}^2} + M_{ns}^2 \log\left(\frac{\mu_{sr} + \sqrt{\mu_{sr}^2 - M_{ns}^2}}{M_{ns}}\right)\right]$$

where, $M_{ns} = \sqrt{M_s^2 + 2n\tilde{e}B}$ is the n^{th} Landau level mass for the s-quarks. Further, the sum over the Landau levels is restricted to $n^s_{max} = Int\left[\frac{\mu_{sr}^2 - M_s^2}{\tilde{e}B}\right]$ arising from the distribution function at zero temperature $\theta(\mu - \epsilon_n)$.

For the uncharged quarks, i.e. blue down and strange quarks we have, $\Omega_0 = \Omega_{0,0} + \Omega_{0,med}$ with

$$\Omega_{0,0}(T = 0, \mu = 0) = -2\sum_{i=d,s} G(\Lambda, M_i) \tag{4.76}$$

and for the medium part, with $p_{fi} = \sqrt{\mu_i^2 - M_i^2}$,

$$\Omega_{0,med}(T = 0, \mu) = 2\sum_{i=d,s} H_i(\mu_{i3}, p_{fi}). \tag{4.77}$$

In the above H_i is the medium contribution from a single charge less flavor given as

$$H_i(\mu, p_f) = \frac{1}{16\pi^2}\left[p_{fi}\mu_i(p_{fi}^2 + \mu_i^2) - M_i^4 \log\left(\frac{\mu^i + p_{fi}}{M^i}\right)\right] \tag{4.78}$$

Next, we write down the expressions for the condensates at zero temperature, that are needed to compute the thermodynamic potential in Eq.(4.59). This is already given by Eq.(4.64). Here, we write down explicitly the zero temperature limit for the same. The scalar condensate for,say, u-quarks is given as

$$I^u_s = I^u_{s\,vac} + I^{ur}_{s\ \ med} + I^{ug}_{s\ \ med} + I^{uba}_{s\ \ med} + \sum_{a=1}^{3} I^{field-u}_s(x_{ua}) \tag{4.79}$$

The vacuum contribution $I^u_{s\;vac}$ is already given in Eq.(4.65).

The scalar condensate medium contribution from the superconducting red up and green up quarks are given as

$$I^{ur}_{s\;\;med} = I^{ug}_{s\;\;med} = -\sum_{n=0}^{n_{max}} \frac{\alpha_n(\tilde{e}B/2)}{(2\pi)^2} \int dp_z \frac{M_u}{\epsilon^u_n} \left(F^{ur} - F^{ur}_1\right) \tag{4.80}$$

The expressions for the distribution functions F^{ia} and F^{ia}_1 is already given in Eq.s (4.20)-(4.21) in terms of the diquark condensate functions and the thermal distribution functions.In the zero temperature limit, the distribution functions for e.g. u- quarks become

$$F^{ur} = \frac{1}{2}\left(1 - \frac{\bar{\xi}_{n-}}{\bar{\omega}_{n-}}\right)\left(1 - \theta(-\omega^d)\right) \tag{4.81}$$

and

$$F^{ur}_1 = \frac{1}{2}\left(1 - \frac{\bar{\xi}_{n+}}{\bar{\omega}_{n+}}\right). \tag{4.82}$$

The blue up quark contribution to the scalar condensate is given by

$$I^{ub}_{s\;\;med} = -\sum_{n=0}^{n^u_{max}} \frac{2M\alpha_n\tilde{e}B}{(2\pi)^2} \log\left(\frac{p^{max}_z + \sqrt{p^{max2}_z + M^2_{nu}}}{M_{nu}}\right) \tag{4.83}$$

As in Eq.(4.75) here we have defined the n-th Landau level mass for the blue up quark as $M^2_{nu} = M^2_u + 2n|\tilde{e}B|$. The magnetic field contribution to the scalar condensate for the up quarks of a given color 'a' is given by

$$I^{field-u}_s(x_{ua}) = -\frac{M_u|q_aB|}{2\pi^2}\left[x_a(1-\ln x_a) + \ln\Gamma(x_a) + \frac{1}{2}\frac{x_a}{2\pi}\right] \tag{4.84}$$

where, $x_a = M^2_u/2|q_aB|$ and $q_a = 1/2\tilde{e}$ for red and green colors and $\theta_a = \tilde{e}$ for blue color up quarks.

In an identical manner, the scalar condensates for the down and strange quarks I^d_s, I^s_s can be written down with appropriate changes for the charges and the masses. The diquark condensate $4I_D$ is given in Eq.(4.58) where the zero temperature limit can be taken by replacing the distribution functions $\sin^2\theta^i = \theta(-\omega^i)$, $(i = u, d)$. Thus the thermodynamic potential gets completely defined for the quark matter in presence of magnetic field.

In the context of neutron star matter, the quark phase that could be present in the interior, consists of the u,d,s quarks as well as electrons, in weak equilibrium

$$d \to u + e^- + \bar{\nu}_{e^-}, \tag{4.85a}$$

$$s \to u + e^- + \bar{\nu}_{e^-}, \tag{4.85b}$$

and,

$$s + u \to d + u, \tag{4.85c}$$

leading to the relations between the chemical potentials μ_u, μ_d, μ_s, μ_E as

$$\mu_s = \mu_d = \mu_u + \mu_E. \tag{4.86}$$

The neutrino chemical potentials are taken to be zero as they can diffuse out of the star. So there are *two* independent chemical potentials needed to describe the matter in the neutron star interior which we take to be the quark chemical potential μ_q and the electric charge chemical potential, μ_e in terms of which the chemical potentials are given by $\mu_s = \mu_q - \frac{1}{3}\mu_e = \mu_d$, $\mu_u = \mu_q + \frac{2}{3}\mu_e$ and $\mu_E = -\mu_e$. In addition, for description of the charge neutral matter, there is a further constraint for the chemical potentials through the following relation for the particle densities given by

$$Q_E = \frac{2}{3}\rho_u - \frac{1}{3}\rho_d - \frac{1}{3}\rho_s - \rho_E = 0. \tag{4.87}$$

The color neutrality condition corresponds to

$$Q_8 = \frac{1}{\sqrt{3}} \sum_{i=u,d,s} \left(\rho^{i1} + \rho^{i2} - 2\rho^{i3}\right) = 0 \tag{4.88}$$

In the above, ρ^{ia} is the number density for quarks of flavor i and color a. In particular, the number densities of the condensing quarks are given as

$$\rho^{ia} = \frac{1}{(2\pi)^2} \sum_n \frac{\tilde{e}B}{2} \int dp_z (F^{ia} - F_1^{ia}), (i, a = 1, 2) \tag{4.89}$$

where, F^{ia}, F_1^{ia} are defined in Eq.s (4.20), and Eq.(4.21) respectively in terms of the condensate functions and e.g. for zero temperature is given explicitly in Eq. (4.81) for up red quarks. For the blue colored quarks, the same for the up blue quarks is given by

$$\rho^{ub} = \frac{1}{2\pi^2} \sum_{n=0}^{n_{max}^u} \alpha_n \tilde{e}B \sqrt{\mu_{ub}^2 - M_u^2 - 2n\tilde{e}B} \tag{4.90}$$

while, for the $\tilde{e}$ uncharged d quarks,

$$\rho^{db} = \frac{(\mu_{db}^2 - M_d^2)^{3/2}}{3\pi^2} \tag{4.91}$$

For the charged strange quarks the number densities are given by

$$\rho^{sr} = \rho^{sg} = \frac{1}{(2\pi)^2}\sum_{n=0}^{n^s_{max}} \alpha_n \tilde{e}B\sqrt{\mu_{sr}^2 - M_s^2 - n\tilde{e}B} \tag{4.92}$$

while, for the $\tilde{e}$ uncharged blue strange quarks,

$$\rho^{sb} = \frac{(\mu_{sb}^2 - M_s^2)^{3/2}}{3\pi^2} \tag{4.93}$$

The electron number density is given by

$$\rho_E = 2\frac{1}{2\pi^2}\sum_{n}^{n_{maxe}} \alpha_n(\tilde{e}B\sqrt{\mu_E^2 - 2n\tilde{e}B}) \tag{4.94}$$

To discuss the pressure in the context of matter in the core of the neutron star, one also have to add the contribution of the electrons to the thermodynamic potential. Since we shall describe the system as a function of $\tilde{e}B$, we shall take the approximations $\tilde{e} \sim e$, $A_\mu \sim \tilde{A}_\mu$ to a good approximation as the mixing angle is small. The corresponding thermodynamic potential for the electrons is given by

$$\Omega_e = \frac{\tilde{e}}{4\pi^2}\sum_{n=0}^{n^e_{max}} \alpha_n \left[\mu_E^2 - 2n\tilde{e}B\log\left(\frac{\mu_E + \sqrt{(\mu_e^2 - 2n\tilde{e}B)}}{\sqrt{2n\tilde{e}B}}\right)\right]. \tag{4.95}$$

where, $n^e_{max} = \frac{\mu_E^2}{2|\tilde{e}B|}$. Thus the total thermodynamic potential or the negative of the pressure is given as

$$\Omega = \Omega_q + \Omega_e \tag{4.96}$$

The thermodynamic potential (Eq. (4.96)), the mass and superconducting gap equations Eq.(4.47),Eq.(4.48) ,Eq.(4.49) and Eq.(4.51), along with the charge neutrality conditions, Eq.(4.87), Eq.(4.88) are the basis for our numerical calculations for various physical situations that we shall discuss in in detail in the following section.

4.4 Results and Discussions

We begin the discussions with the parameters of the NJL model. The model parameters are the three current masses of quarks, namely m$_u$,m$_d$ and m$_s$ and the couplings G$_s$, G$_d$ and the determinant coupling K. This apart, one additional parameter, the momentum cut off Λ, is also required to regularize the divergent integrals which are characteristic of the four point interaction of NJL models. Except for the diquark coupling G_d, there are several parameter sets for the couplings derived from fitting of the meson spectrum and chiral condensate [56, 57, 58]. The diquark coupling is not known from fitting since one does not have a diquark spectrum to fit with. Fierz transforming quark-antiquark term gives the relation G_d=0.75 G_s. Although not precise, many other references use this value. The parameters used in our calculations are m_u=5.5 MeV, m_d=5.5 MeV, m_s=140.7 MeV for the current quark masses, the momentum cutoff $\Lambda = 602.5MeV$ and the couplings G_s Λ^2 =1.835 and $K\Lambda^5$=12.36 as have been chosen in Ref.[58]. After choosing the light current quark mass m_u=m_d=5.5 MeV, the remaining four parameters are chosen to fit vacuum values of pion decay constant f_π, masses of pion, kaon η'. With this set of parameters the η meson mass is underestimated by about 6 percent and leads to u and d constituent mass in vacuum to be about 368 MeV. The strange mass is about 549 MeV at zero temperature and density. The determinant interaction is responsible for $U(1)_A$ anomaly and getting the correct eta mass. Further, this interaction also mixes the various gap equations and affects the superconducting gap significantly as we shall see. However, we must point out that there is a large discrepancy in the determination of this six fermion interaction coupling K. E.g. in Ref.[56] the parameter $K\Lambda^5$ differs by as large as 30 percent as compared to the value chosen here. This discrepancy is due to the difference in the treatment of η' mesons with a high mass[49]. Infact, this leads to an unphysical imaginary part for the corresponding polarization diagram in the η' meson channel. This is unavoidable because NJL is not confining and is unrealistic in this context. Within the above mentioned limitations of the model and the uncertainty in the value of the determinant coupling, we proceed with the present parameter set which has already been used for phase diagram of dense matter in the Refs.[173, 174, 49] and for neutron star matter in Ref.[175].

We begin our discussion for the simpler case where the charge neutrality conditions are not imposed. In this case, the electrical and color charge chemical potential are set to zero so that all the quarks have same potential μ_q. In this case we have to solve four gap equations, three for the constituent masses Eq.s(4.47,4.48,4.49) and the fourth for the superconducting gap Eq.s(4.51,4.58). For given values of quark chemical potential and magnetic field we solve the gap equations self consistently. Few comments regarding solving these gap equations may be in order. We solve the gap equations at T=0. For non-vanishing magnetic fields, all the landau levels for the medium part up to a cutoff, n_{max}=$\frac{\sqrt{\mu^2-M_i^2}}{2\tilde{e}B}$ for each flavor i, are taken into account. Near the μ_c, the critical chemical potential, there can be multiple

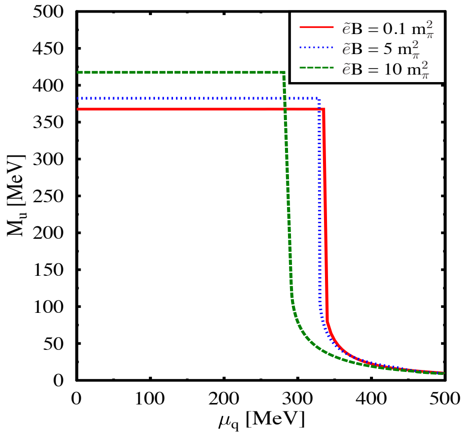

Fig. 1-a

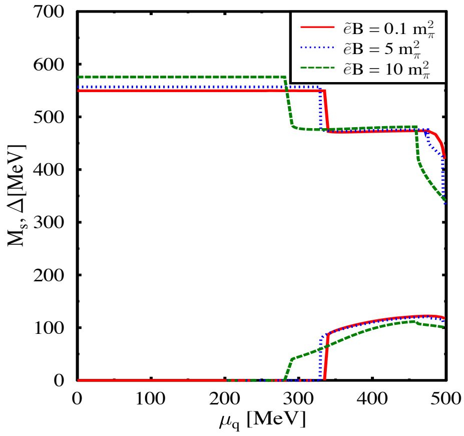

Fig.1-b

Figure 4.1: Constituent quark masses and superconducting gap when charge neutrality conditions are not imposed. Fig.1-a shows the M$_u$ at zero temperature as a function of quark chemical potential for different values of the magnetic field. Fig. 1-b shows the same for the strange quark mass M$_s$ and the superconducting gap.

solutions for the gap equations. We have chosen the solutions which have the lowest thermodynamic potential.

In Fig.5.2 , we have shown the variation of the masses as a function of quark chemical potential μ_q for three different values of magnetic fields, $\tilde{e}$B=0.1m_π^2,5 m_π^2,10 m_π^2. The results for $\tilde{e}B = 0.1m_\pi^2$ reproduce the vanishing magnetic field results. As the chemical potential increases, the masses remain constant upto a critical value of quark chemical potential μ_c and the superconducting gap remains zero. At the critical chemical potential there is a first order phase transition and the constituent masses drop sharply from their vacuum values and the superconducting gap becomes non-zero. For vanishing magnetic field, the isospin symmetry for the light quarks is unbroken and the constituent masses of u and d quarks are degenerate. The critical chemical potential,μ_c, is about 340 MeV for (almost) vanishing magnetic field. In this case, the up and the down quark masses decrease from their vacuum values of about 368 MeV to about 80 MeV. The strange mass being coupled to other gaps via determinant interaction also decreases from 549 MeV to 472 MeV when this first order transition happens for the light quarks. However, since this μ_c is still less than the strange mass its density

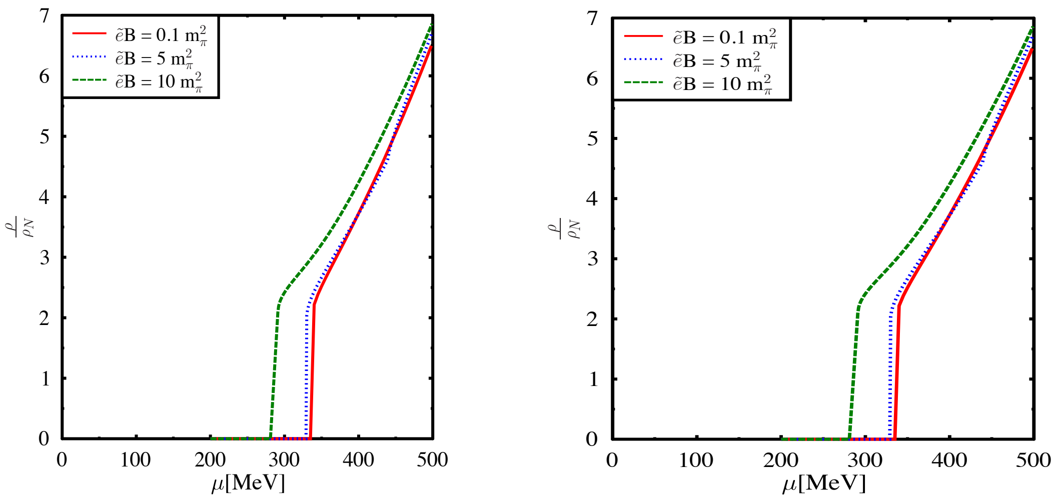

Figure 4.2: Baryon number density in units of nuclear matter density as a function of chemical potential for different strengths of magnetic field at zero temperature.

remains zero. The superconducting gap rises from 0 MeV to 88.0 MeV at μ_c. As the chemical potential is increased beyond μ_c, the superconducting gap shows a mild increase reaching a maximum value of 122 MeV at around $\mu_q \sim 475$ MeV. Beyond this value of μ, the strange quark mass starts decreasing rapidly. This leads to the effective diquark coupling $G'_D = G_D + \frac{K}{4}\langle\bar{s}s\rangle$ decreasing resulting in a decrease in the superconducting gap with increasing chemical potential.

In Fig.5.3, we have plotted the total baryon number density in units of nuclear matter density(ρ_N=0.17/fm^{-3}) as function of quark chemical potential. For vanishing magnetic field, at the critical chemical potential $\mu_c \sim 340$ MeV, the baryon density jumps from 0 to $0.38 fm^{-3}$ which is about 2.2 times the nuclear matter density.

Upon increasing the magnetic field, as seen in Fig.5.2, the vacuum constituent quark masses increase due to magnetic catalysis at zero density. It may also be observed here that the μ_c for chiral transition for the light quarks decreases with the magnetic field. Such a phenomenon is known as inverse magnetic catalysis at finite chemical potential.[176]. Let us note that in the superconducting phase the $\tilde{e}$ charges of the u and d quarks are identical in

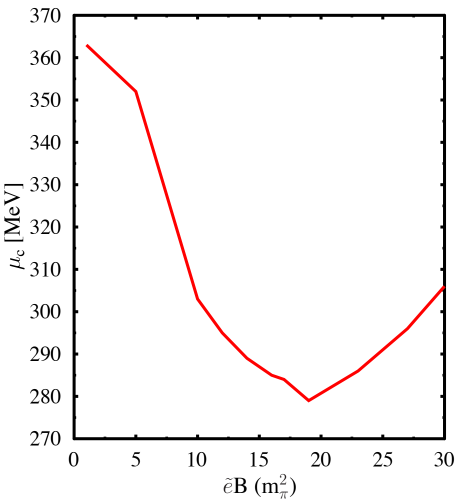

Figure 4.3: Critical chemical potential for chiral transition at zero temperature as a function of magnetic field

magnitude while that of unpaired blue quark are different for u and d quarks. This results in the color summed scalar condensate I_s^u and I_s^d to be different in presence of magnetic field. This leads to difference in constituent masses for the light quarks. For $\tilde{e}$B=10 m_π^2 the u mass in the chiral symmetry broken phase increases by about 13.6 percent and strange mass by about 4.7 percent. The critical chemical potential decreases from about 340 MeV to about 291 MeV. As seen in the plot, the superconducting gap decreases and the peak value decreases from 122 MeV to 111 MeV. As may be seen from Eq.(4.51) and Eq.(4.58), the superconducting gap depends upon the effective diquark coupling G$'_D$ = G$_D$-$\frac{K}{4}I_s^s$. With increase in magnetic field the effective coupling G$'_D$ has a slight increase in magnitude as the strange quark condensate increases with magnetic field. Therefore, one would have expected an increase in Δ with magnetic field. However, the variation in Δ due to the magnetic field is essentially decided by Eq.(4.58). From here also one would have expected an increase in Δ with magnetic field as $\tilde{e}B$ occurs in the numerator in Eq.(4.58). Infact, this behavior is actually seen for high magnetic field, where, only the lowest Landau level contributes to the integral in Eq.(4.58). For moderately strong magnetic fields, contributions of the higher Landau levels become relevant for the behavior of gap with magnetic field. As long as the contribution of higher Landau levels are non vanishing, the gap equation can support solution for the gap that decreases with magnetic field. We may point out that $\tilde{e}B$=5 m$_\pi^2$ and 10 m$_\pi^2$ the cut off for Landau levels n$_{max}$ equals 3 and 1 respectively. For $\tilde{e}B \geq 20$ m$_\pi^2$ only the lowest Landau level contributes to the integral in Eq.(4.58) and the gap increases with magnetic field. One may also note that at higher magnetic fields the charge asymmetry between the u and d quark becomes apparent in their masses as expected. At $10m_\pi^2$ the difference is about 3.4 percent and at $15m_\pi^2$ its about 5.7 percent at lower chemical potentials.

One may note that below the critical chemical potential μ_c the u quarks have higher mass compared to d quarks as all the three colors are charged for u quarks while for the d quarks, the blue color is chargeless. However beyond the critical chemical potential the u quark has a lower mass compared to d quarks. This is because with magnetic field the medium contribution to chiral condensate increases. This increase is same for the condensing pairs of u and d quarks but different for the blue quarks. The blue up quark has charge $\tilde{e} = 1$ whereas it is zero for down blue quark. Therefore the medium contribution from up quark is more than down quark and it reduces the condensate for up quark and consequently its mass too. As we shall see later, imposing charge neutrality requires the d quark chemical potential to be much higher compared to u quarks to balance their larger positive charge. This forces the d quark mass to be smaller compared to u quark mass above critical chemical potential . This results in an opposite behavior for the u and d quark masses with chemical potential, beyond μ_c when charge neutrality condition is imposed vis a vis when such condition is not imposed.

As may be observed from Fig.5.3, the baryon number density increases with magnetic field for a given chemical potential. This is because for the magnetic fields considered here, the symmetry is restored for lower chemical potential at higher magnetic field. Thus for a given chemical potential beyond the critical chemical potential the masses become smaller for higher magnetic field leading to larger baryon number density. This is consistent with inverse magnetic catalysis. One may note however that for very large fields, there is magnetic catalysis of chiral symmetry breaking in the sense that critical chemical potential increases with magnetic field. In Fig.5.5 we show the behavior of μ_c as a function of magnetic field. It is observed that μ_c is minimum for $\tilde{e}B$=$19m_\pi^2$.

To examine the effect of flavor mixing determinant interaction, we show in Fig.5.6, the variation of the masses and the superconducting gap without the determinant interaction. As expected, without the mixing of flavors the strange mass remains unaffected when u and d quark masses decrease. This is significantly different behavior compared to Fig.5.2 where the strange mass decreases by about 74 MeV beyond μ_c when there is a first order transition

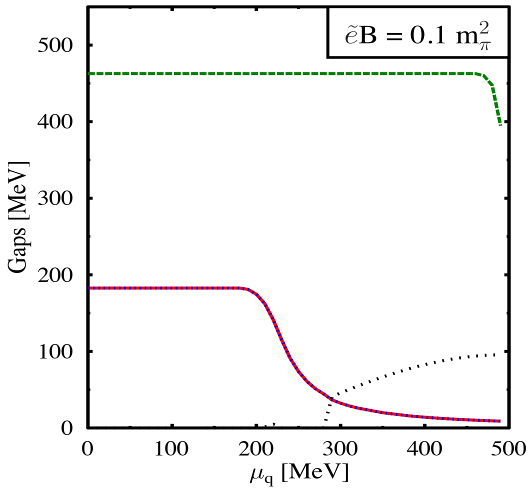

Figure 4.4: Gaps without determinant interaction at zero temperature as a function of quark chemical potential. Solid curve refers to masses of u-d quarks, the dashed curve refers to the mass of strange quark and the dotted curve corresponds to the superconducting gap.

for the light quarks. This also affects the superconducting gap. The superconducting gap is smaller as the effective diquark coupling decreases without the determinant interaction term.

In Fig.4.5 we show the variation of the gaps as a function of the magnetic field for μ=200 MeV and μ=400 MeV. μ=200 MeV is less than the critical μ_c for any value of magnetic field considered here. Hence the constituent masses are high and the superconducting gap is zero. We find that the masses increase monotonically with the magnetic field. At $\tilde{e}$B=10 m_π^2, the u mass increases by 14 percent of its zero field value while strange mass increases by 5 percent. Similarly for μ=400 MeV which is larger than the critical chemical potential for magnetic fields considered here, one also has finite superconducting gap. However, in this case it is observed that the u and d masses decrease slowly and monotonically with magnetic field while strange quark mass remains almost constant. The superconducting gap shows an oscillatory behavior with increase in magnetic field. The oscillatory behavior is associated with the discontinuous changes in the density of states due to Landau quantization and is similar to de Hass van Alphen effects for magnetized condensed matter system.

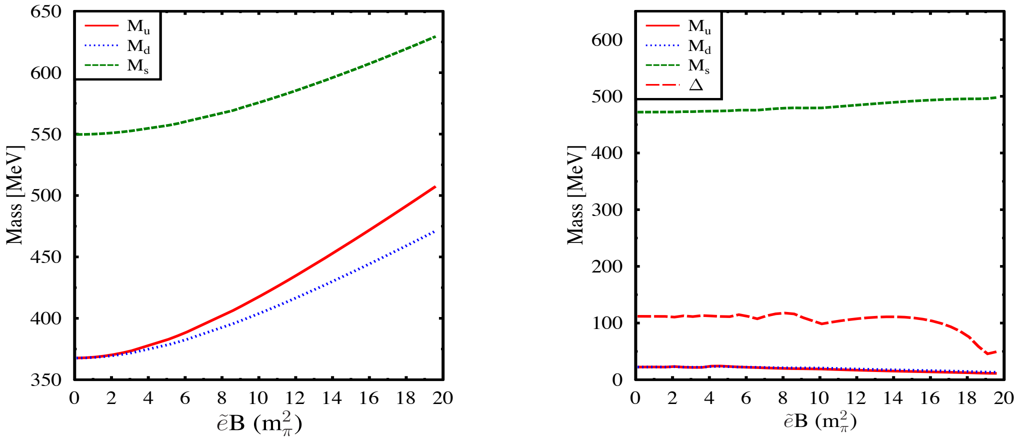

Fig. 5-a

Fig.5-b

Figure 4.5: Constituent quark masses as a function of magnetic field for T=0. Fig.5-a shows the masses of the three quarks below the chiral transition for μ=200 MeV. Fig. 5-b shows the same for the masses along with the superconducting gap above the chiral transition for $\mu_q = 400$ MeV.

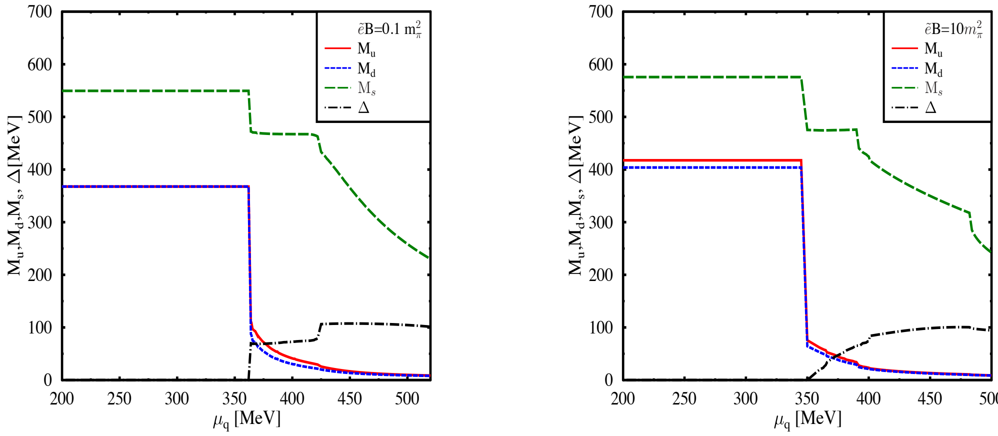

Fig. 6-a

Fig.6-b

Figure 4.6: Constituent quark masses and superconducting gap when charge neutrality conditions are imposed. Fig.6-a shows the masses and superconducting gap at zero temperature as a function of quark chemical potential for magnetic field $\tilde{e}B = 0.1m_\pi^2$ Fig. 6-b shows the same for $\tilde{e}B = 10m_\pi^2$.

Charge neutral magnetized quark matter

Next we discuss the consequences of imposing charge neutrality conditions($Q_E = 0$,$Q_8 = 0$). In Fig. 4.6 we show the results for the masses and the superconducting gaps for strength of the external magnetic field $\tilde{e}B = 0.1m_\pi^2$ (Fig 6-a) and $\tilde{e}B = 10m_\pi^2$ (Fig. 6-b). For small magnetic field($\tilde{e}B = 0.1m_\pi^2$) the masses in symmetry broken phase are the same as before but the critical chemical potential is now shifted to around $\mu_c = 364MeV$ as compared to $\mu_c = 335MeV$ when the condition is not imposed. At the transition point with neutrality the u quark mass decreases from 367 MeV to 111 MeV and the down quark mass from 367 MeV to 87 MeV. Charge neutrality requires d quark number densities to be higher as compared to u quarks. Let us note that near the critical chemical potential there are multiple solutions of the gap equations. The solution which is thermodynamically preferred when charge neutrality condition is not imposed may no longer be the preferred solution when the constraint of charge neutrality is imposed [151]. The strange quark mass is higher than the chemical potential at the chiral restoration so its density is zero. However due to the determinant interaction the strange mass decreases at the chiral restoration from 549 MeV to 472 MeV. At still higher chemical potential the strange quark density becomes non-zero and strange quark also helps in maintaining charge neutrality. The critical baryon density when charge neutrality is imposed is however similar to case when neutrality is not imposed. Specifically $\rho_c \sim 2.25\rho_0$ with charge neutrality while $\rho_c \sim 2.26\rho_0$ without charge neutrality despite the fact that μ_c is higher ($\mu_c = 364$ MeV) for the charge neutral matter compared when such charge neutrality condition is not imposed ($\mu_c = 335$ MeV). This is because the constituent masses at the transition is large ($M_u \sim 111MeV$ and $M_d \sim 87MeV$) for charge neutral case compared to ($M_u \sim M_d \sim 85MeV$) without charge neutrality condition. For $\tilde{e}B = 0.1m_\pi^2$, at the chiral transition $\mu_c = 364MeV$ the superconducting gap increases from zero to 69 MeV. As the chemical potential is further increased the superconducting gap increases to 80 MeV till $\mu = \mu_1 \sim 420$ MeV where it shows a sudden jump to 106 MeV. This happens when the gapless modes cease to exist as explained below. As magnetic field is increased to $\tilde{e}B = 10m_\pi^2$, as may be observed in Fig.6-b, the critical chemical potential μ_c for the charge neutral matter decreases to 350 MeV similar to the case without charge neutrality condition with inverse magnetic catalysis. The superconducting gap on the other hand becomes smaller. One can also observe that unlike vanishingly small magnetic field case, the superconducting gap increases smoothly with chemical potential from zero initial value to 73 MeV at $\mu = \mu_1 \sim 400$ MeV where it again jumps to a value of 83 MeV.

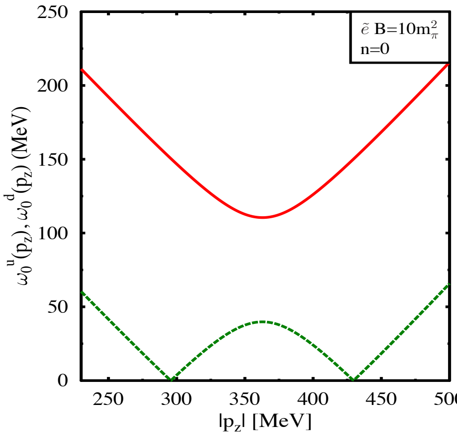

Fig. 7-a

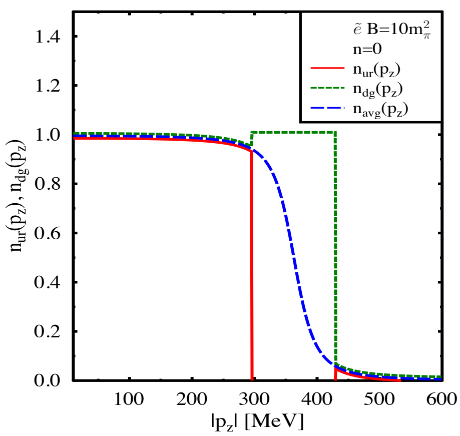

Fig.7-b

Figure 4.7: Dispersion relation and the occupation number for condensing quarks at T=0,μ_q=340 MeV. Fig.7-a shows the dispersion relation for the condensing quarks for zeroth Landau level. The upper curve is for u quark and the lower curve corresponds to d quark dispersion relation. Fig. 7-b shows the occupation number as a function of momentum for $\tilde{e}B = 10m_\pi^2$.

Gapless modes

In the region between μ_c and μ_1 the system shows gapless mode which we discuss now in some detail. Without magnetic field this has earlier been seen for charge neutral matter [150, 151].

As discussed earlier, from the dispersion relations for Landau levels for the superconducting matter as given in Eq.(4.53) and Eq.(4.54), it is possible to have zero modes depending upon the values of $\delta\mu$ and $\delta\epsilon_n$. These quantities are not independent parameters bu are dependent dynamically on the charge neutrality condition and the gap equations. For charge neutral matter, near μ_c, the d-quark number density is larger so that $\delta\mu = \mu_E/2$ is negative. This renders $\omega_n^u(p_z) > 0$ for any value of momentum p_z. On the other hand, for $\delta\mu$ negative, ω_n^d can vanish for some values of p_z. This defines the fermi surfaces for the superconducting d quarks. It is easy to show that the excitation energy of nth Landau level ω_n^d for the condensing d quarks vanishes for momenta $|p_{zn}|= \sqrt{\mu_\pm^2 - 2n\tilde{e}B}$. Here $\mu_\pm$=$(\bar{\mu} \pm \sqrt{\delta\mu^2 - \Delta^2})\theta(\delta\mu - \Delta)$. Thus higher Landau levels can also have gapless modes so long as $\sqrt{\mu_\pm^2 - 2n\tilde{e}B}$ is non-negative. Gapless modes occur when the chemical potential difference $\delta\mu$ is greater than the superconducting gap. In Fig.7-a, we have plotted the dispersion relation i.e. the excitation energy as a function of momentum for the lowest Landau level for the condensing quarks for μ_q =340 MeV and magnetic field $\tilde{e}B = 10m_\pi^2$. The superconducting gap turns out to be Δ =35.3 MeV and $\delta\mu$ =-74.5 MeV. The dispersion for the d quarks is given as $\omega_{0-}^d = \bar{\omega}_{0-} - \delta\epsilon + \delta\mu$ while the same for u-quark is given as $\omega_{0-}^u = \bar{\omega}_{0-} + \delta\epsilon - \delta\mu$. The average chemical potential is $\bar{\mu}$= 366 MeV. Far from the pairing region, $|p_z| \sim \bar{\mu} = 366 MeV$ the spectrum looks like usual BCS type dispersion relation. Of the two excitation energies, ω_0^u shows a minimum at $p_z = \bar{\mu}$ with a value $\omega_{0-}^u(|p_z| = \bar{\mu}) \sim \Delta - \delta\mu = 110$ MeV. On the other hand, ω_{0-}^d vanishes at momenta $|p_z| = \mu_\pm$. In this breached pairing region one has only unpaired d-quarks and no u-quarks. This can be seen explicitly as below.

The number densities of u quarks participating in condensation is given by

$$\rho_{sc}^u = \rho^{ur} + \rho^{ug} = \sum_n \frac{\alpha_n \tilde{e}B}{(2\pi)^2} \int dp_z \left[\frac{1}{2}\left(1 - \frac{\bar{\zeta}_{n-}}{\bar{\omega}_{n-}}\right)\left(1 - \theta(-\omega_n^d)\right) - \frac{1}{2}\left(1 - \frac{\bar{\zeta}_{n+}}{\bar{\omega}_{n+}}\right)\right] \tag{4.97}$$

This is because $\omega_{n_-}^u = \bar{\omega}_{n_-} - \delta\mu + \delta\epsilon$ is always positive as $\delta\mu$=$\frac{\mu^u - \mu^d}{2}$ is negative and the theta function $\theta(-\omega_n^u)$ does not contribute. Similarly the density of d-quarks participating in condensation is given by

$$\rho^d_{sc} = \rho^{dr} + \rho^{dg} = \sum_n \frac{\alpha_n \tilde{e} B}{(2\pi)^2} \int dp_z$$
$$\left[\theta(-\omega^d_n) + \frac{1}{2}\left(1 - \frac{\bar{\zeta}_{n-}}{\bar{\omega}_{n-}}\right)\left(1 - \theta(-\omega^d_n)\right) - \frac{1}{2}\left(1 - \frac{\bar{\zeta}_{n+}}{\bar{\omega}_{n+}}\right)\right]$$

For positive ω^d_{n-}, the θ-function contributions vanishes and the distribution functions are the BCS distribution function. On the other hand, when $|p_z| \in [P_{n-}, P_{n+}]$, ω^d_n is negative leading to ρ^u_{sc} to vanish but for the anti-particle contribution. In this region of momenta, ρ^d_{sc} is unity. We have plotted in Fig. 7-b the occupation number of the up and down quarks that take part in condensation as a function of the magnitude of momentum p_z i.e. the integrands of Eq.(4.97) and Eq.(4.98) respectively for the lowest Landau level. It is easy to see from Eq.(4.97) and Eq.(4.98) e.g. for the lowest Landau level, that except for the interval (μ_-, μ_+), the distribution function is like the BCS distribution function. This is shown by the blue long-dashed line. The u-quark distribution is shown by the red solid line while the d-quark distribution is shown by the green short dashed line. Indeed, except for the interval (μ_-, μ_+), all the three curves overlap with each other. In the 'gapless' momentum region, the u-quark occupation vanishes while d-quark occupation is unity. This leads to fact that the momentum integrated distribution function for the condensing u and d quarks are not the same for the gapless region unlike the usual BCS phase. We have plotted the number densities for the u- and d- quarks in Fig.4.8 which shows a fork structure in the gapless region.

Gapless modes have been considered earlier for two flavor quark matter both with[155, 152, 153, 154] and without magnetic field [150, 151]. However it has been shown[177, 178] that in QCD at zero temperature the gapless 2SC phases are unstable. This instability manifests itself in imaginary Meissner mass of some species of the gluons. Finite temperature calculations[179] show that at some critical value of temperature the instability vanishes. This value may range from few MeV to tens of MeV. The instability of the gapless phases indicate that there should be other phases of quark matter breaking translational invariance e.g. inhomogenous phase of quark matter like crystalline color superconductivity[180, 181]. One may note that these considerations apply to the case without magnetic field and may change in presence of strong magnetic field.

In Fig.4.9, we have plotted the electric and color chemical potentials μ_E and μ_8 to maintain the electric and color charge neutrality conditions given

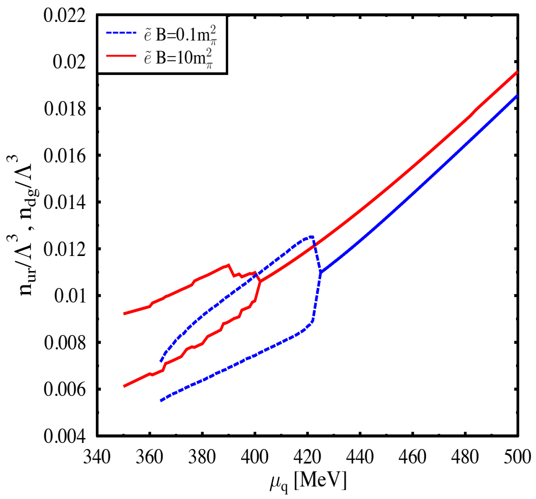

Figure 4.8: Number densities of up and down quarks participating in the superconductivity for $\tilde{e}B = 0.1m_\pi^2$ (dashed line) and $\tilde{e}B = 10m_\pi^2$ (solid line)

in Eq.(4.87) and Eq.(4.88) as a function of quark chemical potential. For 2+1 flavor matter, strange quarks play an important role in maintaining charge neutrality. As the the quark chemical potential increases, $|\mu_E|$ increases to maintain charge neutrality. When the chemical potential becomes large enough for strange quarks to contribute to densities, they also help in maintaining charge neutrality. This leads to decrease in electron density or the corresponding chemical potential $|\mu_E|$. This behavior is reflected in Fig. 9-a and 9-b as the initial slow rise of the $|\mu_E|$. However, as $|\mu_E|$ increases, the difference $\delta\mu = -\mu_E/2$ also increases and at μ_1, the condition $\delta\mu > \Delta$ for gapless modes to exist ceases to be satisfied. At the gapless to BCS transition point, the u-quark number density increases while that of d-quarks decreases and both become equal as in the usual BCS pairing phase. This leads to an increase in the positive electric charge density. To maintain electrical charge neutrality, the electron density increases at this point. Therefore gapless to BCS transition is accompanied with an increase in $|\mu_E|$. On the other hand, at higher densities when strange quarks start contributing to the density, it is accompanied with a drop in $|\mu_E|$ as strange quarks help in maintaining the charge neutrality along with the electrons. It turns out that for $\tilde{e}B = 0.1m_\pi^2$, the strange quarks densities become non vanishing after the gapless to BCS transition. This leads to the continuous

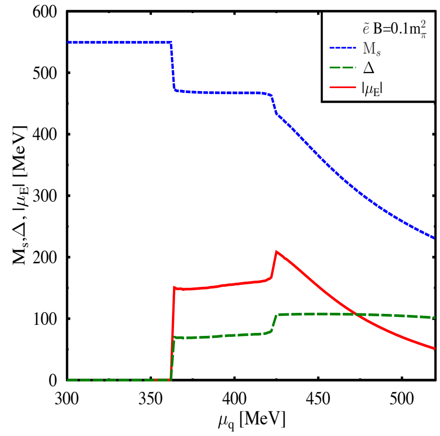

Fig. 9-a

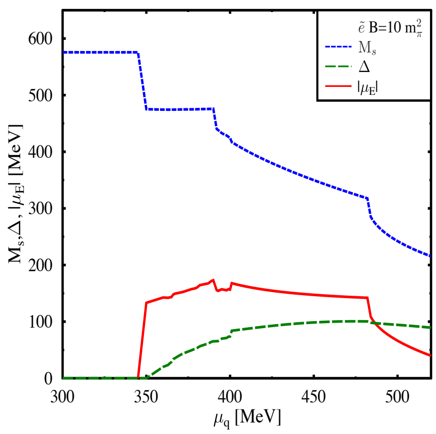

Fig.9-b

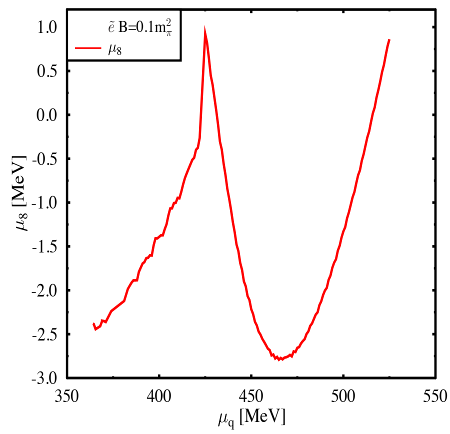

Fig. 9-c

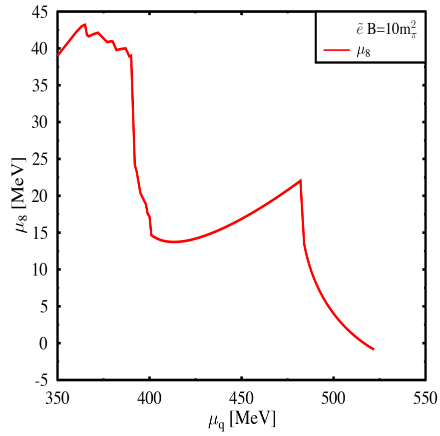

Fig.9-d

Figure 4.9: Chemical potential μ_E and μ_8 for charge neutral quark matter. $|\mu_E|$ is plotted as a function of quark chemical potential μ_q for magnetic field $\tilde{e}B = 0.1m_\pi^2$ (Fig.9-a)and for $\tilde{e}B = 10m_\pi^2$ (Fig. 9-b). In Fig.9-a and Fig.9-b we have also plotted the mass of strange quarks and superconducting gap as a function of quark chemical potential to highlight the dependence of charge chemical potential on these two parameters. In the lower two plots, the color chemical potential μ_8 is plotted as a function μ_q for $\tilde{e}B = 0.1m_\pi^2$ (Fig 9-c) and for $\tilde{e}B = 10m_\pi^2$.

decrease in the $|\mu_E|$ in the BCS phase as seen in Fig. 9-a. On the other hand, for larger fields, e.g. $\tilde{e}B = 10m_\pi^2$, chiral transition occurs at a lower μ_c due to magnetic catalysis and the strange quark density starts becoming non vanishing at lower chemical potential. This leads to a decrease in $|\mu_E|$ at $\mu = 392$MeV as may be seen in Fig.9-b. At $\mu = 400$ MeV, there is the transition from the gapless to BCS phase and is accompanied with a rise in $|\mu_E|$ as discussed above. Beyond $\mu = 400$ MeV, $|\mu_E|$ starts decreasing monotonically as strange quark density increase.

In Fig.9-c and Fig.9-d, we have plotted the color chemical potential μ_8. For weak field case, μ_8 is rather small (few MeVs) compared to both the electric chemical potential as well as the quark chemical potential which are two orders of magnitude larger. For small field, the difference in densities of red and green quarks and the blue quarks essentially arises because of the difference in the distribution functions. This results in a small but finite net color charge. To maintain color neutrality one needs a small μ_8 . On the other hand, at large magnetic field, the net color charge difference become larger as the $\tilde{e}$ charges of red and green quarks and that of blue quarks are different. This requires a somewhat larger μ_8 to maintain color neutrality as seen in Fig.9-d. In Fig.4.10 we have plotted the number densities of each species for the charge neutral matter for two different magnetic fields. As may be clear from both the plots the electron number densities gets correlated with the strange quark number densities.

Finally, we discuss the equation of state (EOS) for different magnetic fields. In Fig.4.11 we have plotted pressure as a function of energy for $\tilde{e}$B=$0.1m_\pi^2$ and $10m_\pi^2$. One can observe that the EOS become stiffer with increase in magnetic field. This can be understood as follows. For $\mu < \mu_c$, the thermodynamic potential contribution from the field as in Eq. (4.70), Eq.(4.74), Eq.(4.75) is dominant and decreases with increase in magnetic field. This leads to a higher pressure for higher magnetic field. As the chemical potential increases, for $\mu > \mu_c$, the medium contribution become dominant. As the masses decrease with magnetic field, the medium contribution increases with magnetic field. Moreover, the field contributions also leads to an increase in pressure. Both these effects make the resulting EOS stiffer at higher magnetic field as may be seen in Fig.4.11.

4.5 Summary

We have analyzed here the effect of magnetic field and neutrality conditions on the chiral as well as diquark condensates within the framework of a three flavor NJL model. The methodology uses an explicit variational construct

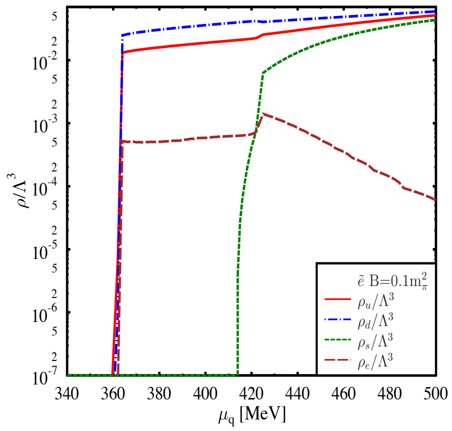

Fig. 10-a

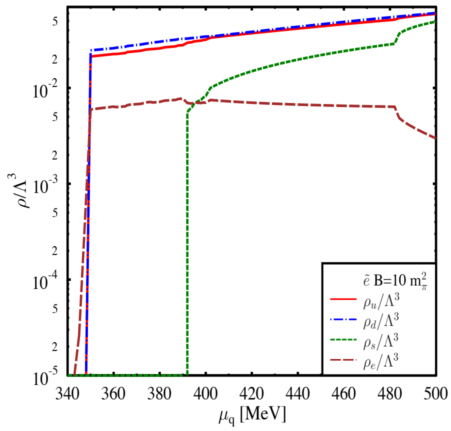

Fig.10-b

Figure 4.10: Population of different species for charge neutral quark matter for $\tilde{e}B = 0.1m_\pi^2$ (Fig. 10-a) and for $\tilde{e}B = 10m_\pi^2$ (Fig. 10-b).

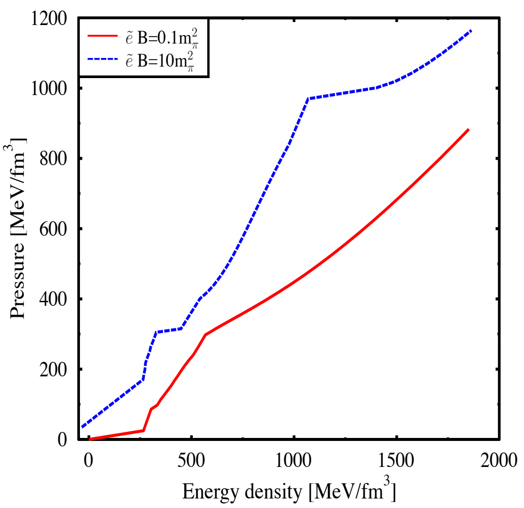

Figure 4.11: Equation of state for $\tilde{e}B = 0.1m_\pi^2$ (dashed line) and $\tilde{e}B = 10m_\pi^2$ (solid line)

for the ground state in terms of quark-antiquark pairing for all the three flavors as well as diquark pairing for the light quarks. A nice feature of the approach is that the four component quark field operator in presence of magnetic field could get expressed in terms of the ansatz functions that appears for the description of the ground state. Apart from the methodology being different, we also have new results. Namely, the present investigations have been done in a three flavor NJL model along with a flavor mixing six quark determinant interaction at finite temperature and density and fields within the same framework. In that sense it generalizes the two flavor superconductivity in presence of magnetic field considered earlier in Ref.s[152, 153, 154, 35, 36, 30, 146, 147] and Ref.[155]. The gap functions and the thermal distribution functions could be determined self consistently for given values of the temperature, the quark chemical potential and the strength of magnetic field.

For the charge neutral matter the chiral transition is a first order transition and we observe inverse magnetic catalysis at finite density. The chiral condensate for strange quark affects the u-d superconductivity through the flavor mixing determinant interaction. The effective diquark coupling increases in presence of strange quark condensates. On the other hand the diquark condensates contribute to the mass of the strange quark through the determinant interaction. Inverse magnetic catalysis is observed for magnetic fields upto 19 m_π^2. Beyond it magnetic catalysis is observed for chiral symmetry breaking [176].

At finite densities, the effects of Landau quantization get manifested in the oscillation of the order parameters similar to the de Hass van Alphen effect for magnetization in metals. However, in the present case of dense quark matter, the order parameters, the masses and the superconducting gap themselves are dependant on the strength of magnetic fields which leads to a non periodic oscillation of the order parameter.

Imposition of charge neutrality condition for the quark matter leads to gapless modes even in presence of magnetic field. The superconducting gaps in gapless modes are smaller compared to the gaps in the BCS phase. The transition from gapless to BCS phase is a sharp transition. Difference in the gap in the two phases at this transition decreases with magnetic field. For charge neutral matter the strange quark plays an important role in maintaining the charge neutrality. This leads to a depletion of electron density at higher chemical potential where strange quarks start to contribute to the densities. The resulting equation of state becomes stiffer with magnetic field.

This completes our investigation of color superconductivity in three flavor quark matter with background magnetic field. In the next chapter we study possible origin of large magnetic fields in neutron stars due to spontaneous spin polarization.

.

Chapter 5

Spontaneous Spin Polarization in Quark Matter

5.1 INTRODUCTION

At high densities relative to nuclear saturation density and low temperature exotic phases of QCD can exist, e.g. two flavor color superconducting phase (2SC), color-flavor locked phase (CFL), crystalline color superconductor, etc. Such high densities occur in the interior of neutron stars. Due to very low temperature and high baryon density, in the interior of a neutron star various QCD phases may be realized, e.g. deconfined quark matter [182, 183], meson condensation in hadronic phase[184], two flavor color superconducting phase, color-flavor locked phase [185, 48, 186] etc.

Further, compact objects like neutron stars can be strongly magnetized. Observations indicate that the magnetic field strength at the surface of pulsars can be of the order of $10^{12} - 10^{13}$ Gauss [187, 120]. Strongly magnetized neutron stars (magnetars) may have even stronger magnetic fields $\sim 10^{15} - 10^{16}$ Gauss [121, 122, 123, 124, 125, 126]. Using virial theorem and comparing the magnetic field energy and gravitational energy, one can estimate the physical upper bound on the strength of the magnetic field for a gravitationally bound star to be of the order 10^{18} Gauss[187, 120]. For self bound objects like quark stars this bound can be even higher [129]. The physical origin of the very strong magnetic field in the magnetars require reconsideration of the common understanding that the magnetic field of a neutron star is originated from the progenitor star [188]. Since quark matter can possibly be present at high densities, inside the neutron stars, presence of quark ferromagnetic phase in high density quark matter has also been suggested as possible explanation of large magnetic field associated with magnetars [37, 189, 38]. As a possible solution to this problem, author in Ref.[37] examined the possible existence of spin-polarized deconfined quark matter using one gluon exchange interaction between quarks in Fermi liquid theory within Hartree-Fock approximation. Taking the idea as proposed in the Ref.[37], spin polarization in the quark matter has been well explored in the subsequent literature. In general, a collective spin polarization of charged quarks can give rise to ferromagnetic nature of quark matter at high density, hence the spin of the fermions play the crucial role in determining the possibility of ferromagnetic nature of dense quark matter. It has been shown that in non-relativistic framework there is no possibility of spin polarization in normal nuclear matter[190]. On the contrary, using relativistic Hartree-Fock approximation, possibility of spin polarization at asymptotic high density has been suggested in Ref.[191, 192]. It is important to note that the relativistic framework may be more suitable than the non-relativistic approach to understanding the existence of spin polarization. But in any case to explore spin polarization in quark matter at a high density or baryon chemical potential a relativistic approach is very natural.

In relativistic framework "spin density" can be expressed in two different ways, first by the spatial component of the axial vector (AV) mean field, $\psi^\dagger\Sigma^i\psi \equiv -\bar{\psi}\gamma_5\gamma^i\psi$, constructed out of the fermionic field (quarks)ψ and axial vector combination of Dirac gamma matrices; second by tensor Dirac bilinear (T) $\psi^\dagger\gamma^0\Sigma^i\psi \equiv -\bar{\psi}\sigma^{12}\psi$. Although AV and T type mean fields are different in the massless limit of fermions, it has been shown that they are equivalent in nonrelativistic approximation [189]. Coexistence of the spin polarization and color superconductivity has been studied using the AV interaction for quark matter in NJL model [38]. The interplay between the spin polarization and chiral symmetry breaking at finite density for a single quark flavor using AV mean field has also been studied within NJL model in Ref.[39]. In Ref.[39], it has been shown that for one flavor, spin polarization is possible at finite density and zero temperature provided the ratio of the couplings of the axial vector channel and the pseudo scalar channel satisfies some lower bound. It has been argued in Ref.[39] that due to the interplay between spin polarization and chiral symmetry for a certain value of chemical potential, spin polarization appears due to the large dynamical quark masses generated by spontaneous chiral symmetry breaking. Interestingly it was also shown that spin polarization plays an important role in changing the value of the dynamical mass and at a very high density, both dynamical quark mass and spin polarization vanish in the chiral symmetric phase. Although in Ref.[37] author introduced the idea of quark spin polarization using one gluon exchange interaction, in the NJL model studies, AV mean field has been used. Due to the Fierz transformation, one can get AV channel interaction between quarks from one gluon exchange interaction, but the tensor Dirac bilinear representation of "spin density" operator does not appear in the Fierz transformation of the one gluon exchange interaction. Hence at asymptotically high densities where one gluon exchange interaction in perturbative QCD is applicable, spin polarization cannot be studied using the T channel interaction. But for moderate densities near chiral phase transition density perturbative QCD is not applicable and one can use QCD inspired low energy effective models e.g. NJL model. NJL model is not directly related to perturbative one gluon exchange interaction. In this model AV or T channel interactions are not written keeping in mind the perturbative nature of QCD and some nonperturbative effects can give rise to tensor channel interaction. Hence spin polarization in the tensor channel, which can be different from the AV channel can be studied within the NJL model. In fact, the tensor channel opens up a completely different point of view in looking into the spin polarization problem of quark matter at moderate densities e.g. in two flavour NJL model spin-polarized phase can be shown to be present in the chiral restored phase where the dynamical quark mass is zero [40, 193]. This result is different than the result obtained in Ref.[39], where spin polarization is not present in chiral restored phase. Since the manifestation of the AV and T channel interaction is different, the interplay between the AV and T type spin-polarized phases becomes interesting to study along with the other phases expected to arise in high baryon density region of the QCD phase diagram [38, 194, 39, 40, 195, 196, 197].

In this chapter we discuss the interplay between the spin polarization condensate ($\langle\bar{\psi}\Sigma^i\psi\rangle$) and the scalar chiral condensate ($\langle\bar{\psi}\psi\rangle$) in (2+1) flavor NJL model using only tensor(T) type interaction for spin polarization. Most of the earlier works used some simplified approximation to study the interplay between spin polarization and other high density phases, which includes single flavor NJL model [39], SU(2) flavor NJL model [40, 195], SU(3) flavor NJL model [198] with zero current quark mass etc. However, for a more realistic situation one should consider (2+1) flavor NJL model with different current quark mass of strange and non-strange quarks. This apart, the structure of ferromagnetic condensation for (2+1) flavor NJL model is qualitatively different from that of two flavor NJL model as inherently two different kinds of spin polarizations are possible which are associated with the diagonal generators of the SU(3) flavour group. Behaviour of these spin polarization condensates as function of temperature and quark chemical potential (μ) has been discussed extensively. Since the spin polarization condensates are also related to the quark-antiquark scalar condensates, it is evident that the spin polarization condensates affect the constituent mass of the quarks. In this work spin polarization condensates due to the tensor type interaction appear in the chiral symmetry restored phase and the quark masses, specifically strange quark masses, are strongly affected by the spin polarization condensates in the chiral symmetric phase.

This chapter is organized as follows. We first discuss the formalism of 2+1 flavour NJL model in the presence of tensor type interactions in section 4.1. In section 4.2 derivation of the thermodynamic potential is discussed in a mean field approach. Once the thermodynamic potential is derived one can get the gap equations to solve for the condensates. After the formalism important results and the corresponding discussion are given in 4.3. Finally in section 4.4 we summarize the work on spontaneous spin polarization.

5.2 Formalism

In order to study the spin polarization due to tensor channel interaction for realistic $(2+1)$ flavor and $SU(3)$ color quarks we start with the following NJL Lagrangian density [194, 49],

$$\mathcal{L} = \bar{\psi}\left(i\partial\!\!\!/ - \hat{m}\right)\psi + \mathcal{L}_{sym} + \mathcal{L}_{det} + \mathcal{L}_{tensor} + \mu\bar{\psi}\gamma^0\psi, \tag{5.1}$$

where $\psi = (u, d, s)^T$ is the three flavor quark field and the diagonal current quark matrix is $\hat{m} = \mathrm{diag}_f(m_u, m_d, m_s)$. In this work we have assumed that due to isospin symmetry in the non strange quark sector $m_u = m_d$. Strange quark mass m_s is different from the other light quark masses. Difference between the strange and non strange quark masses explicitly breaks the $SU(3)$ flavor symmetry. μ is the quark chemical potential. In literature different chemical potential for the strange and nonstrange quarks have been considered, but the phase diagram has no qualitative difference. In this case we are assuming that the quark chemical potential of the strange and nonstrange quarks are same. Following the representations of different interaction terms as given in Ref.[49], in general one considers,

$$\mathcal{L}_{sym} = g\sum_{a=0}^{a=8}\left[\left(\bar{\psi}\lambda_a\psi\right)^2 + \left(\bar{\psi}i\gamma_5\lambda_a\psi\right)^2\right]. \tag{5.2}$$

This term has been constructed keeping in mind the $U(3)_L \times U(3)_R$ chiral symmetry for three flavor case and it can be generalized to any number of flavours N_f. The interaction term $\mathcal{L}_{sym}$ represents four point interaction, where $\lambda_0 = \sqrt{2/3}I_f$ and λ_a, $a = 1, ...(N_f^2 - 1)$ are the generators of $SU(N_f)$. In the present case I_f is 3×3 identity matrix and λ_a for $a = 1, ...8$ are the Gell-Mann matrices.

The interaction term $\mathcal{L}_{det}$ in Eqn.(5.1) is 't Hooft determinant interaction term. This term breaks $U(1)$ axial symmetry explicitly and also successfully describes the nonet meson properties[199, 56, 200]. It can be expressed as,

$$\mathcal{L}_{det} = -K\det{}_f[\bar{\psi}(1+\gamma_5)\psi + h.c] \tag{5.3}$$

In this interaction term determinant is taken in the flavour space. This term represents maximally flavour-mixing $2N_f$ point interaction for N_f quark flavours. For two flavour NJL model this term does not introduce any new dynamics because for two flavour case it gives four Fermi interaction which is already there. But for three or more flavours this term generates new type of interaction, e.g. for three flavour case it gives rise to six point interaction term. The tensor interaction which is responsible for spin polarization is given as [194, 198],

$$\mathcal{L}_{tensor} = \frac{G_T}{2}\sum_{a=3,8}\left(\bar{\psi}\Sigma_z\lambda_a\psi\right)^2, \qquad \Sigma_z = \begin{pmatrix} \sigma_z & 0 \\ 0 & \sigma_z \end{pmatrix}, \tag{5.4}$$

where σ_z is the third Pauli matrix. Here we have assumed polarization along the z-axis. Note that $\mathcal{L}_{tensor}$ is not invariant under chiral symmetry, rather one requires to add a similar term with γ^5 matrix to make the tensor interaction symmetric under chiral symmetry. Since we are not considering any condensation involving γ^5, we have omitted the term which ensures chiral invariance for the tensor interaction. Thus the total Lagrangian with finite chemical potential becomes,

$$\begin{aligned}\mathcal{L} = &\bar{\psi}\left(i\partial\!\!\!/ - \hat{m}\right)\psi + g\sum_{a=0}^{a=8}\left(\bar{\psi}\lambda_a\psi\right)^2 - K\det{}_f[\bar{\psi}(1+\gamma_5)\psi + h.c] \\ &+ \sum_{a=3,8}\frac{G_T}{2}\left(\bar{\psi}\Sigma_z\lambda_a\psi\right)^2 + \mu\bar{\psi}\gamma^0\psi.\end{aligned} \tag{5.5}$$

In the mean field approximation expanding the operators around their expectation values and neglecting higher order fluctuations, we obtain,

$$\begin{aligned}
&(\bar{u}u)^2 \simeq 2\langle\bar{u}u\rangle\bar{u}u - \langle\bar{u}u\rangle^2 = 2\sigma_{ud}\bar{u}u - \sigma_{ud}^2 \\
&\left(\bar{d}d\right)^2 \simeq 2\langle\bar{d}d\rangle\bar{d}d - \langle\bar{d}d\rangle^2 = 2\sigma_{ud}\bar{d}d - \sigma_{ud}^2 \\
&(\bar{s}s)^2 \simeq 2\langle\bar{s}s\rangle\bar{s}s - \langle\bar{s}s\rangle^2 = 2\sigma_s\bar{s}s - \sigma_s^2 \\
&\left(\bar{\psi}\Sigma_z\lambda_3\psi\right)^2 \simeq 2\langle\bar{\psi}\Sigma_z\lambda_3\psi\rangle\left(\bar{\psi}\Sigma_z\lambda_3\psi\right) - \langle\bar{\psi}\Sigma_z\lambda_3\psi\rangle^2 = 2F_3\left(\bar{\psi}\Sigma_z\lambda_3\psi\right) - F_3^2 \\
&\left(\bar{\psi}\Sigma_z\lambda_8\psi\right)^2 \simeq 2\langle\bar{\psi}\Sigma_z\lambda_8\psi\rangle\left(\bar{\psi}\Sigma_z\lambda_8\psi\right) - \langle\bar{\psi}\Sigma_z\lambda_8\psi\rangle^2 = 2F_8\left(\bar{\psi}\Sigma_z\lambda_8\psi\right) - F_8^2,
\end{aligned}$$

where the chiral condensates or the quark-antiquark condensates are $\langle \bar{u}u \rangle = \langle \bar{d}d \rangle \equiv \sigma_{ud}$, $\langle \bar{s}s \rangle \equiv \sigma_s$ and the spin polarization condensates are $F_3 = \langle \bar{\psi}\Sigma_z\lambda_3\psi \rangle$ and $F_8 = \langle \bar{\psi}\Sigma_z\lambda_8\psi \rangle$. We can write the mean field Lagrangian as,

$$\mathcal{L} = \bar{\psi}\left(i\partial\!\!\!/ - \hat{M} + G_T F_3 \Sigma_z \lambda_3 + G_T F_8 \Sigma_z \lambda_8 + \mu\gamma^0\right)\psi - 2g\left(\sigma_{ud}^2 + \sigma_{ud}^2 + \sigma_s^2\right)$$
$$+ 4K\sigma_{ud}^2\sigma_s - \frac{G_T}{2}F_3^2 - \frac{G_T}{2}F_8^2,$$

where, $\hat{M} \equiv \mathrm{diag}(M_u, M_d, M_s)$, with effective masses,

$$\begin{aligned} M_u =& m_u - 4g\sigma_{ud} + 2K\sigma_{ud}\sigma_s \\ M_d =& m_d - 4g\sigma_{ud} + 2K\sigma_{ud}\sigma_s \\ M_s =& m_s - 4g\sigma_s + 2K\sigma_{ud}^2. \end{aligned}$$

For a given system at finite temperature and finite chemical potential most important quantity for the understanding of the thermodynamic behaviour or the phase structure, is the thermodynamic potential. Once the thermodynamic potential for this model is known, thermodynamic quantities can be extracted using Maxwell relations. The thermodynamic potential for the Lagrangian as given in Eqn.(5.6) in the grand canonical ensemble at a finite temperature and finite chemical potential can be given as:

$$\begin{aligned} \Omega(T,\mu,\sigma_{ud},\sigma_s,F_3,F_8) =& - N_c \sum_{f=u,d,s} \int \frac{d^3p}{(2\pi)^3}\Bigg[\left(E_{f+} + E_{f-}\right) \\ &+ T\ln\left(1 + e^{-\beta(E_{f+}-\mu)}\right) + T\ln\left(1 + e^{-\beta(E_{f+}+\mu)}\right) \\ &+ T\ln\left(1 + e^{-\beta(E_{f-}-\mu)}\right) + T\ln\left(1 + e^{-\beta(E_{f-}+\mu)}\right)\Bigg] \\ &+ 2g(\sigma_{ud}^2 + \sigma_{ud}^2 + \sigma_s^2) - 4K\sigma_{ud}^2\sigma_s + \frac{G_T}{2}F_3^2 + \frac{G_T}{2}F_8^2, \\ =& - \frac{6}{4\pi^2}\sum_{f=u,d,s}\int_0^{\Lambda} dp_T \int_0^{\sqrt{\Lambda^2 - p_T^2}} p_T dp_z \Bigg[\left(E_{f+} + E_{f-}\right) \\ &+ T\ln\left(1 + e^{-\beta(E_{f+}-\mu)}\right) + T\ln\left(1 + e^{-\beta(E_{f+}+\mu)}\right) \\ &+ T\ln\left(1 + e^{-\beta(E_{f-}-\mu)}\right) + T\ln\left(1 + e^{-\beta(E_{f-}+\mu)}\right)\Bigg] \\ &+ 2g(\sigma_{ud}^2 + \sigma_{ud}^2 + \sigma_s^2) - 4K\sigma_{ud}^2\sigma_s + \frac{G_T}{2}F_3^2 + \frac{G_T}{2}F_8^2 \end{aligned}$$

where $N_c = 3$ is the number of colors, transverse momentum $p_T = \sqrt{p_x^2 + p_y^2}$ and the single particle energies are,

$$E_{u+} = \sqrt{p_z^2 + \left(\sqrt{p_T^2 + M_u^2} + G_T\left(F_3 + \frac{F_8}{\sqrt{3}}\right)\right)^2}$$
$$E_{u-} = \sqrt{p_z^2 + \left(\sqrt{p_T^2 + M_u^2} - G_T\left(F_3 + \frac{F_8}{\sqrt{3}}\right)\right)^2}$$
$$E_{d+} = \sqrt{p_z^2 + \left(\sqrt{p_T^2 + M_d^2} + G_T\left(F_3 - \frac{F_8}{\sqrt{3}}\right)\right)^2}$$
$$E_{d-} = \sqrt{p_z^2 + \left(\sqrt{p_T^2 + M_d^2} - G_T\left(F_3 - \frac{F_8}{\sqrt{3}}\right)\right)^2}$$
$$E_{s+} = \sqrt{p_z^2 + \left(\sqrt{p_T^2 + M_s^2} + G_T\frac{2F_8}{\sqrt{3}}\right)^2}$$
$$E_{s-} = \sqrt{p_z^2 + \left(\sqrt{p_T^2 + M_s^2} - G_T\frac{2F_8}{\sqrt{3}}\right)^2}$$

Thermodynamic behaviour of the condensates can be found by solving the gap equations, which can be found from the stationary conditions (for details see Appendix),

$$\frac{\partial\Omega}{\partial\sigma_{ud}} = \frac{\partial\Omega}{\partial\sigma_s} = \frac{\partial\Omega}{\partial F_3} = \frac{\partial\Omega}{\partial F_8} = 0 \tag{5.6}$$

Gap equations can have several roots, but the solution with the lowest value of thermodynamic potential is taken as the stable solution.

NJL model Lagrangian in (3+1) dimension has operators which have mass dimension more than four, thus it can shown to be a non-renormalizable theory [201]. Thus the divergence coming from the three momentum integral of the vacuum part can not be removed by the renormalization prescriptions. The model predictions inevitably depend on the regularization procedures and parameter dependence in each regularization method has been reported in Ref.[202, 203]. In this work we have considered the most frequently used 3D momentum cutoff regulation scheme to regularize the divergence in Eq.(5.6) for thermodynamic potential.

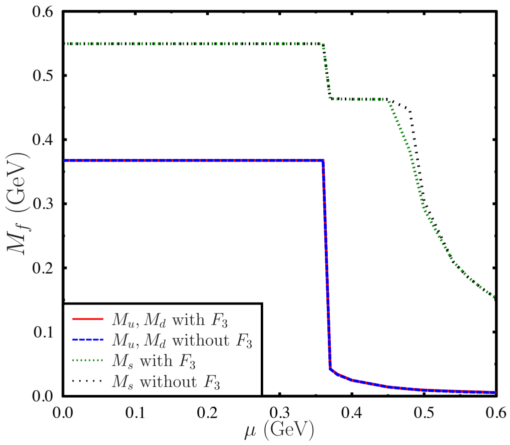

Figure 5.1: Constituent quark mass as a function of quark chemical potential at zero temperature in the presence and absence of spin polarization condensation. Red-solid line and green-dotted line represent non strange and strange quark mass in the presence of spin polarization condensate F_3. Blue-dashed line and black-dotted line represents non strange and strange quark constituent mass in the standard 2+1 flavor NJL model in the absence of any spin polarization condensate. Sharp jump in the value of M_u and M_s near $\mu = 0.360$ GeV indicates the first order chiral phase transition. In this case we have considered the tensor interaction coupling to be $G_T = 2g$. Comparing green and the black lines for strange quark it is clear that non zero value of spin condensate affects strange quark mass. However, the non strange quark masses are almost unaffected due to the presence of spin polarization condensate. For $G_T = 2g$ non zero value of F_3 appears only near 0.480 GeV which is away from the chiral phase transition critical chemical potential, hence in this case the chiral phase transition is unaffected by the presence of spin polarization.

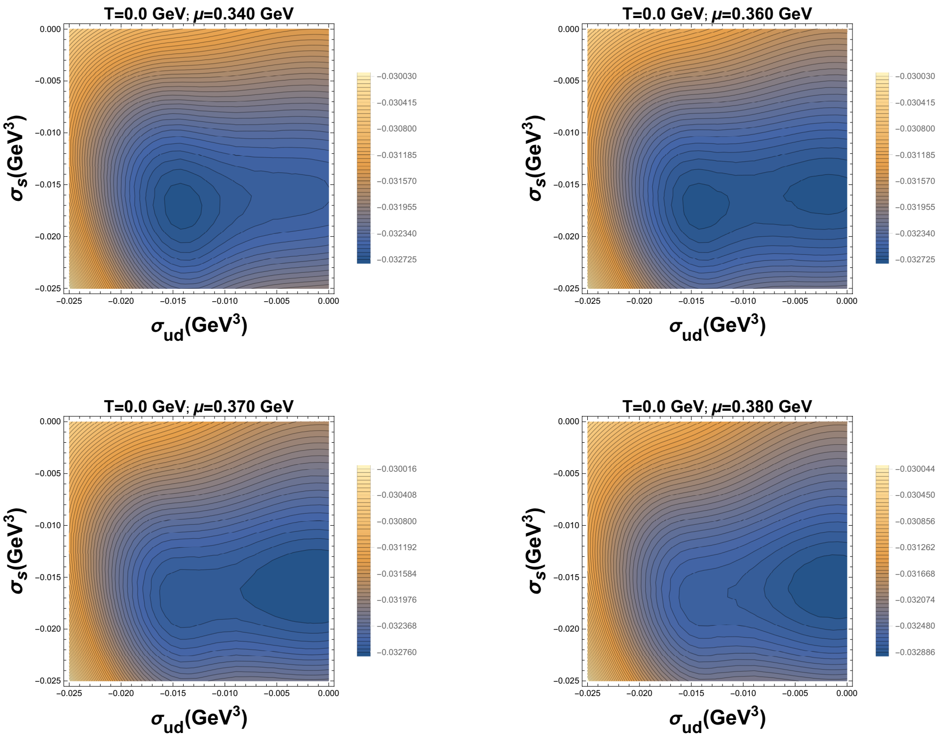

Figure 5.2: The figure shows the contour maps of the thermodynamics potential with the set of parameters in table(5.1) and $G_T = 2g$ at $T = 0.0$ GeV for different values of μ. The darker region in the plots show the lower value of the thermodynamic potential. The horizontal and vertical axes represents the non strange quark condensate σ_{ud} and strange quark condensate σ_s respectively. Existence of almost degenerate vacuum is clear from the figure near $\mu = 0.360$ GeV. Hence the chiral phase transition near $\mu = 0.360$ is a first order phase transition. Spin polarization condensation F_3 has no effect on the chiral phase transition. As we have shown in Fig.(5.3) non zero value of F_3 occurs near $\mu = 0.480$ GeV at $T = 0.0$GeV for $G_T = 2g$, which is far away from the critical quark chemical potential for the chiral phase transition.

In the study of spin polarization in NJL model, the parameter which plays the crucial role is the tensor channel interaction G_T. If one considers only vector current interaction, e.g. one gluon exchange interaction in perturbative QCD processes, then such a tensor interaction can not be generated by Fierz transformation. However, such a tensor interaction can be generated from two gluon exchange diagrams [194]. It is relevant to point out that one can also get tensor channel interaction by Fierz transformation from scalar and pseudo scalar interaction [40],

$$g\left[(\bar{\psi}\psi)^2 + (\bar{\psi}i\gamma_5\lambda_a\psi)^2\right] = \frac{g}{4}\left[(\bar{\psi}\psi)^2 - \frac{1}{2}(\bar{\psi}\gamma^\mu\gamma^\nu\lambda_a\psi)^2 + ...\right], \tag{5.7}$$

which gives $|g/G_T| = 2$. In the present investigation we can take G_T as a free parameter to study the inter relationship between scalar and tensor condensates. It may also be noted that the parameters g and G_T may be considered independently to derive mesonic properties [204, 205, 206]. It has been shown that $SU(2)$ NJL model with both positive and negative tensor couplings can describe the phenomenology of mesons. Indeed $SU(2)$ Lagrangian has been considered with vector, axial vector and tensor interaction in Ref. [206] where, the gap equations are solved in the usual Hartree approximation while mesons are described in the random phase approximation [206]. In this work we have only considered G_T as a free parameter with positive values only i.e. G_T and g are of same sign. In the literature various values have been considered e.g. $G_T = 2g, 1.5g$ [194] as well as $G_T = 4.0g$ [206]. We have also obtained our results taking different values of G_T. Results with some specific parameter sets have been mentioned in the result and discussion section.

5.3 Results and Discussions

We begin the discussion with the parameterization of the model. The parameters to be fixed are the three current quark masses (m_u, m_d, m_s), the scalar coupling (g), the determinant coupling K, the tensor coupling(G_T) and the three momentum cut-off Λ to regularize divergent integrals. Except for the tensor coupling G_T, there are several parameter sets available for NJL model [49]. These fits are obtained using low energy hadronic properties such as pion decay constant and masses of pion, kaon and η' [56, 57, 58]. The determinant interaction is important as it breaks $U(1)_A$ symmetry and gives correct η mass. One may note that there is discrepancy in determination of the determinant coupling K. For example in Ref. [56] the value of the coupling differs by as much as 30 percent compared to value used in present work. This discrepancy arises due to difference in treatment of η' mesons with a high mass [49]. In fact, this leads to a nonphysical imaginary part for the corresponding polarization diagram in the η' meson channel. This is unavoidable because NJL is not confining and is unrealistic in this context. Within the above mentioned limitations of the model and the uncertainty in the value of the determinant coupling, we proceed with the present parameter set as given in Table (5.1) [49].

Parameters and couplings	**Value**
Three momentum cutoff (Λ)	$\Lambda = 602.3 \times 10^{-3}$ (GeV)
u quark mass (m_u)	$m_u = 5.5 \times 10^{-3}$ (GeV)
d quark mass (m_d)	$m_d = 5.5\times 10^{-3}$ (GeV)
s quark mass (m_s)	$m_s = 140.7 \times 10^{-3}$ (GeV)
Scalar coupling (g)	$g = 1.835/\Lambda^2$
Determinant interaction (K)	$K = 12.36/\Lambda^5$

Table 5.1: Parameter set considered in this work for 2+1 NJL model apart from the tensor coupling G_T.

Let us first note that there are four condensates, σ_{ud}, σ_s, $F_3 \equiv \langle \bar{u}\Sigma_z u\rangle - \langle \bar{d}\Sigma_z d\rangle$ and $F_8 \equiv \frac{1}{\sqrt{3}}\left(\langle \bar{u}\Sigma_z u\rangle + \langle \bar{d}\Sigma_z d\rangle - 2\langle \bar{s}\Sigma_z s\rangle\right)$, to be determined from the solution of the gap Eq.(5.6). However for simplicity we shall first consider $F_8 = \frac{F_3}{\sqrt{3}}$, so that the spin polarization condensate for d quarks and s quarks are treated at the same footing i.e. $\langle \bar{d}\Sigma_z d\rangle \equiv \langle \bar{s}\Sigma_z s\rangle$ [198]. The results in such a scenario is determined below.

5.3.1 Results with $F_8 = \frac{F_3}{\sqrt{3}}$

Chiral phase transition and the behavior of quark masses for $G_T = 2g$ at zero temperature

Let us consider the thermodynamic potential at zero temperature as a function of quark chemical potential (μ) along with the condition $F_8 = F_3/\sqrt{3}$ [198]. For quantitative analysis we consider the tensor coupling $G_T = 2g$. Fig.(5.1) shows the behavior of the constituent quark masses as a function of quark chemical potential at zero temperature in the presence as well as in the absence of spin polarization condensate F_3.

From Fig.(5.1) it is clear that the vacuum masses ($T = 0, \mu = 0$), for the non strange quarks are 0.368 GeV and the strange quark mass is 0.549 GeV. The vacuum masses for the constituent quarks remain the same as the case with $G_T = 0$, as the tensor condensates appear only at large chemical potential. This is chiral symmetry broken phase where constituent quark masses are generated dynamically. Close to $\mu = \mu_c = 0.360$ GeV there is sudden drop in the masses of u, d quarks $M_u = M_d$. Because of the flavour mixing due to the determinant interaction the strange quark mass also changes at $\mu = \mu_c$. This sudden change in the constituent mass indicates a first-order phase transitions. It is also expected that chiral phase transition should occur in the 2+1 flavor NJL model near $\mu = 0.360$ GeV at zero temperature in the absence of spin polarization. Using the gap equations it can be shown that at zero temperature and zero chemical potential $F_3 = 0$ is a solution. It turns out that at zero temperature and zero chemical potential $F_3 = 0$ is also a stable solution, hence F_3 does not affect the constituent quark masses at low chemical potential at zero temperature. As the chemical potential is increased beyond the chiral restoration for the light quarks, it is observed that the spin polarized condensate develops for a range of chemical potential. In particular, as shown in Fig. (5.3) for zero temperature, a non zero F_3 starts to develop at $\mu \simeq 0.480$ GeV and increases slightly with μ, becoming a maximum around $\mu \simeq 0.510$ GeV, beyond which it decreases and eventually vanishes at $\mu \simeq 0.600$ GeV. Therefore we observe here in Fig.(5.1) that the chiral transition for the light quarks is not affected by the spin polarization condensates as the latter exist at μ larger than μ_c for $G_T = 2g$. It is important to mention that both $\bar{\psi}\psi$ and $\bar{\psi}\gamma^\mu\gamma^\nu\psi$ break the chiral symmetry, but their thermodynamic behavior is quite opposite. At zero temperature and zero chemical potential non zero value of scalar condensation is thermodynamically stable, while the tensor condensate vanishes. However at high chemical potential when the tensor condensate takes non zero value the chiral condensate vanishes but for small current quark mass. The non invariance of the tensor interaction under chiral symmetry can be manifested in the change of quark masses even if the scalar condensate vanishes for the light quarks.

We can also understand the behavior of the constituent quark masses $M_u = M_d$ and M_s in the presence and absence of the spin polarization condensation by looking into the behaviour of thermodynamic potential as a function of quark-antiquark condensates σ_{ud}, σ_s and spin polarization condensate F_3 for different values of temperature (T) and chemical potential μ. Contour plots of thermodynamic potential in the $\sigma_{ud} - \sigma_s$ plane for different value of chemical potential (μ) at zero temperature have been shown in Fig.(5.2) with the set of parameters given in table(5.1) and $G_T = 2g$. The darker regions in the plots show the lower value of the thermodynamic potential. The horizontal and vertical axes represent the nonstrange quark-antiquark condensate σ_{ud} and strange quark-antiquark condensate σ_s. As may be observed in Fig.(5.2), for zero temperature and $\mu < \mu_c \sim 0.360$ GeV minimization of the thermodynamic potential gives us a unique nonzero value of the quark-antiquark condensate. This nonzero value of both σ_{ud} and σ_s indicates chiral symmetry broken phase at zero temperature and $\mu \leq 0.360$ GeV. At $\mu = 0.360$ GeV one can see the existence of almost degenerate vacua in the thermodynamic potential one for $\sigma_{ud} \sim -0.015$ GeV^3 and the other at $\sigma_{ud} \sim 0.0$ GeV^3. As the chemical potential is increased this degeneracy is lifted and the vacuum with σ_{ud} is close to zero has the minimum value for the thermodynamic potential. At $\mu = 0.4$ GeV the value of σ_{ud} as well as M_u is very small and is close to the current quark mass value. This indicates that at chemical potential larger than $\mu_c = 0.360$GeV chiral symmetry is restored. This chiral symmetry restoration is partial in nature in the sense that while the scalar condensate $\sigma_{ud} \simeq 0$, but for the current quark masses ($m_u, m_d \neq 0$), the strange condensate σ_s is rather large as can be seen in Fig.(5.1) and Fig.(5.2) . As μ is further increased beyond μ_c, σ_s also approaches its (approximate) chiral limit continuously. Degeneracy in the thermodynamic potential and a sharp jump in the order parameter (σ_{ud}) indicates first order phase transition. Hence the chiral transition at zero temperature is of first order in nature. This first order nature of the chiral phase transition can also be seen at finite temperature, however, at relatively larger temperature chiral phase transition does not remain as a first order phase transition. In fact, the end of the first order transition to the crossover defines the critical end point. At higher temperatures, beyond the critical temperature quark-antiquark condensate changes smoothly across the critical chemical potential.

When we take $G_T = 2g$, the value of F_3 is not large enough near $\mu = 0.360$ GeV and the chiral phase transition is unaffected by the spin polarization. Since quark-antiquark condensates σ_{ud} and σ_s are intimately connected with the F_3, non zero value of F_3 can change the quark dynamical mass (see Fig.(5.1)). Strange quark mass is more affected by the presence of the spin polarization condensate (F_3), because dynamical mass of u quark becomes very small just after the chiral phase transition, however, strange quark has a substantial mass even after the chiral phase transition. Similar to the result at zero temperature, for $G_T = 2g$ chiral phase transition is almost unaffected in the presence of spin polarization at finite temperature also.

Behavior of F_3 for $G_T = 2g$

Next let us focus our attention to the thermodynamic behavior of F_3. Fig.(5.3) shows the contour plots of the thermodynamic potential in $\sigma_s - F_3$ plane at zero temperature with increasing value of the chemical potential (μ) for $G_T = 2g$. As before the darkest regions in the contour plots show the global minimum of the thermodynamic potential and the corresponding values of σ_s and F_3 are correct condensation value. It is clear from the Fig.(5.3) that spin polarization is possible within the small range of chemical potential $\mu \simeq 0.480 - 0.570$ GeV at zero temperature. From this figure it is clear that with increase in chemical potential σ_s decreases. In this work, we have kept the value of $\mu \leq \Lambda$, because Λ is the cut-off of the theory. When the chemical potential is close to 0.6 GeV both σ_s and F_3 becomes zero. For large chemical potentials($\mu > 570$ MeV), spin polarization condensate completely melts along with the other condensates. Presence of spin polarization condensation can affect the QCD phase diagram in many different ways. As we have already mentioned that the spin polarization condensate coming from the tensor interaction also breaks the chiral symmetry, an obvious effect of a large value of spin polarization condensate should be seen in the chiral phase transition. We have also observed that F_3 decreases with increasing temperature and vanishes at few tens of MeV. Therefore such condensates do not affect the critical end point.

Quark masses and ferromagnetic condensate for larger tensor coupling

The left plot and the right plot in Fig.(5.4) are for quark masses and ferromagnetic condensate respectively, for the tensor coupling $G_T = 2.5g$ and $G_T = 2.8g$. One may note that for larger tensor coupling the u and d quark masses are not affected but the strange quark mass is significantly affected. Ferromagnetic condensate is stronger for larger value of tensor coupling and survives for a longer range of quark chemical potential. It is important to mention that for tensor couplings greater than $G_T = 3g$ the chiral transition itself is affected. However the requirement of baryon matter stability places a upper bound on the value of tensor coupling.

Finite temperature effect on the spin polarization condensate F_3 for $G_T = 2g$

After demonstrating the behavior of the spin polarization condensate as a function of chemical potential at zero temperature for different values of the tensor coupling, let us look into the temperature behavior of F_3 for a fixed value of $G_T = 2g$. Temperature behavior of spin polarization condensate as well as σ_s is shown in Fig.(5.5). Fig.(5.5) shows the contour plots of thermodynamic potential in the plane of $\sigma_s - F_3$ for different values of temperature and chemical potential. Each row shows the behavior of thermodynamic potential as a function of increasing chemical potential for a fixed temperature. On the other hand, each column shows the behavior of the thermodynamic potential as a function of temperature for a fixed value of chemical potential. From the first two row in Fig.(5.5), for temperature $T = 0.02$ GeV and 0.04 GeV, it is clear that as the chemical potential increases non zero value of spin polarization develops. It attains a maximum value at an intermediate value of the chemical potential and as the chemical potential becomes very high F_3 becomes zero. However, each column shows that with increasing temperature the formation of the spin polarization becomes difficult and the maximum value of F_3 also decreases with temperature. The third row in Fig.(5.5) shows that when the temperature is $T = 0.06$ GeV, value of the spin polarization condensate F_3 is almost zero. Hence one can conclude that as the temperature increases the range of chemical potential within which spin polarization can exist decreases. Further there exists a temperature beyond which spin polarization cannot occur irrespective of the value of chemical potential for a given value of G_T. Also note that with increase in temperature and chemical potential strange quark condensate (σ_s) decreases.

Threshold coupling for existence of F_3

The existence of spin polarization inevitably depends on the value of G_T. G_T determines the strength of the spin polarization condensation. The dependence of F_3 on the tensor coupling has been shown in the Fig(5.6). Fig.(5.6) shows the thermodynamic potential in $\sigma_s - F_3$ plane as a function of chemical potential for three different values of tensor couplings $G_T = 2g, 1.8g$ and $1.5g$ at zero temperature. Along each row in Fig.(5.6) the contours of thermodynamic potential have been shown for different values of the chemical potential but keeping G_T fixed. On the other hand in each column of Fig.(5.6) contours of thermodynamic potential have been shown for various values the tensor coupling constant G_T for a given chemical potential. Value of the spin polarization condensate decreases with decreasing value of G_T. When $G_T = 2g$, F_3 has a substantial non zero value at zero temperature and $\mu = 0.510$ GeV, however for $G_T = 1.8g$ this value starts to decrease and for $G_T = 1.5g$ spin polarization condensate F_3 almost vanishes. This result for zero temperature can be easily extended to a non zero temperature. For finite temperature one requires a larger value of G_T, for the spin polarization to exist. As G_T increases, the threshold μ above which F_3 starts becoming nonvanishing decreases, and the critical μ above which F_3 vanishes increases. Both these behavior lead to a larger range of μ that supports a non vanishing F_3 as G_T increases. Further the magnitude of F_3 increases with G_T.

5.3.2 Results for independent F_3, F_8

We have already discussed the variation of F_3 and F_8 with chemical potential where we have considered $F_8 = F_3/\sqrt{3}$ in the thermodynamic potential. However for more general situation we have to consider F_3 and F_8 simultaneously. In Fig.(5.7)(a), Fig.(5.7)(b), Fig.(5.7)(c) we have shown the variation of F_3 and F_8 with chemical potential at zero temperature for $G_T = 2g, 2.5g, 2.8g$ respectively. It is clear from the Fig.(5.7) that non zero F_3 appears at relatively smaller μ than F_8. Since F_8 is associated with strange quark-antiquark condensate it survives even at larger chemical potential relative to the F_3 condensate. It is also important to notice that with larger tensor coupling spin condensates appear at relatively smaller quark chemical potential.

5.3.3 Magnetic field due to spin polarization

The spin polarization condensate implies a alignment of spin of quarks. This will lead to a magnetic field due to quark magnetic moment. We estimate the strength of the effective magnetic field (B_{eff}) due to spin polarization condensate as [40]:

$$\bar{\mu}_q B_{eff} = G_T F, \quad \bar{\mu}_q = \frac{\mu_u + \mu_d}{2}, \quad \bar{\mu}_u = \frac{(\frac{2}{3}e)}{2m_q}, \quad \bar{\mu}_d = \frac{(-\frac{1}{3}e)}{2m_q} \tag{5.8}$$

Here F denotes the spin polarization condensate and $\bar{\mu}_q$ is the average magnetic moment of the light quarks. For an estimation of B_{eff} we take $F \sim 0.018$ GeV^3 (at quark chemical potential ~ 510 MeV) and $G_T = 2g$. Using these value we get $eB_{eff} \sim \mathrm{m}_\pi^2$ or 10^{18} Gauss. The value of the magnetic field on the surface of the magnetars is of the order of 10^{15} Gauss, but in the center the strength of the magnetic field can be higher. It is interesting to note that even this crude estimation of the magnetic field due to the spin polarized phase of the deconfined quark matter leads to a correct order of magnitude estimation of the magnetic field in the core of the magnetars.

5.4 Summary

In this chapter, we have considered the 2+1 flavor NJL model in the presence of tensor interaction with non zero current quark masses. The original idea of the presence of spin polarization in quark liquid was motivated considering one gluon exchange interactions in perturbative QCD processes [37]. Ferromagnetic quark matter can arise due to both axial vector and tensor type interaction. Although the axial vector type interaction can be generated from the one gluon exchange QCD interaction by Fierz transformation, the tensor type interactions cannot be generated using Fierz transformation. Thus at very high densities where perturbative QCD processes are relevant, tensor type of interaction will not be suitable to study spin polarization in quark matter. More importantly at moderate densities close to the chiral phase transition one expects nonperturbative effects to play an important role. In the present investigation within the ambit of NJL model applied to moderate densities, we have considered only the tensor type four point interaction. We might note here that the coupling constant of the tensor interaction is related to the scalar and pseudo scalar channel. However in general, this tensor coupling constant can be independent. We take the coupling constant of the tensor interaction G_T as a parameter of the model. We have taken various values of the tensor couplings G_T, e.g. $G_T = 2.0g$ and lower as well as relatively larger values of G_T, e.g. $G_T = 2.5g, 2.8g$ etc.

For 2+1 flavor NJL model, tensor type interaction at the mean field level leads to two types of spin polarization condensates, $F_3 = \langle\bar{\psi}\Sigma_z\lambda_3\psi\rangle$ and $F_8 = \langle\bar{\psi}\Sigma_z\lambda_8\psi\rangle$. Since we have various condensates in 2+1 flavor NJL model in the presence of tensor interaction we take a rather simplified approximation, where F_3 and F_8 are not independent rather $F_8 = F_3/\sqrt{3}$. One may note that in general F_3 and F_8 are independent due to the fact that F_8 is associated with the strange quark spin polarization condensate, on the other hand F_3 contains only u, d quark spin polarization condensates. Therefore we have also considered the case where F_3 and F_8 are treated independently. Generically spin polarization for moderate tensor coupling (e.g. $G_T = 2g$) does not appear at zero temperature and zero chemical potential, rather it appears at high μ in the chiral restored phase. At large chemical potential and small temperature the generic feature of such spin polarized condensate lies in affecting the strange quark mass rather than the non-strange quark masses for moderate tensor coupling. Such spin polarized condensate vanishes for temperatures of the order of few tens of MeV and thus can be relevant for neutron stars and proto neutron stars. We also find that there is a threshold tensor coupling, below which the spin polarization condensates do not develop.

Unlike superconducting diquark condensate, the spin polarization condensate is not a monotonic function of chemical potential and as the chemical potential is increased the magnitude becomes a maximum beyond which it vanishes when μ is increased further. The range of chemical potential for which such condensate exists as well as the magnitude of the condensate, increases with the strength of the tensor coupling. We estimate the magnitude of the magnetic field corresponding to the ferromagnetic condensate in high density quark matter to be of the order of $\sim m_\pi^2 \sim 10^{18}$ Gauss. It is important to mention that although spin polarization condensate was thought as a source of magnetic field in magnetars, magnetic field can also be present in the neutron stars originated from the progenitor star. External magnetic field can affect the formation of spin condensates. In this context it has been shown recently that one can have non vanishing spin polarization condensate for quark matter in the presence of magnetic field [207].

This concludes the discussion on spontaneous spin polarization. In the next section we give a summary of this thesis and give some future directions.

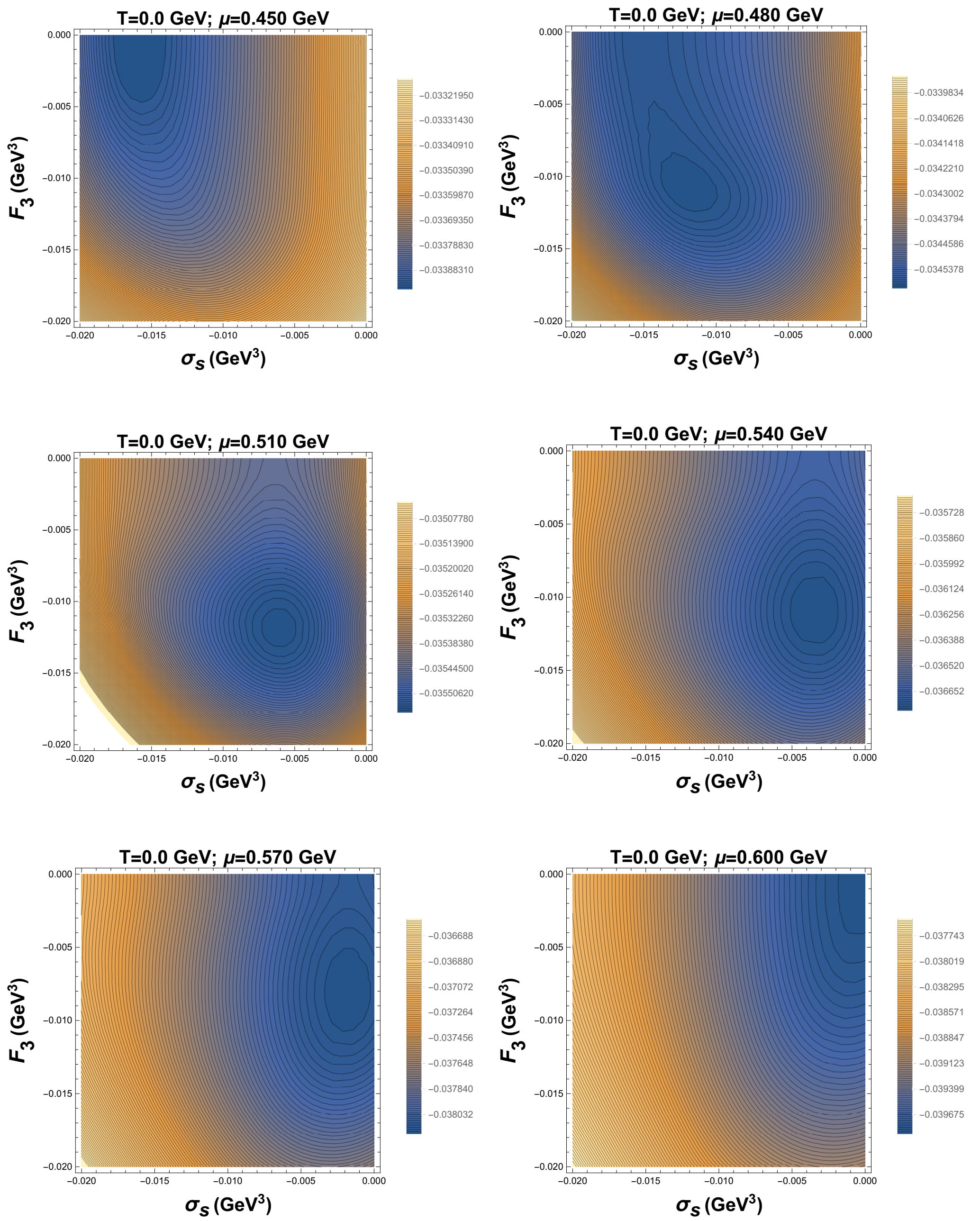

Figure 5.3: This figure shows the contour plots of the thermodynamic potential in $\sigma_s - F_3$ plane at zero temperature with different values of quark chemical potentials (μ) for the case of $G_T = 2g$ and $F_8 = F_3/\sqrt{3}$. It is clear from the plots that non zero spin polarization appears at $\mu = 0.480$ GeV, reaches its maximum value near $\mu = 0.510$ GeV and it completely melts near $\mu = 0.600$ GeV.

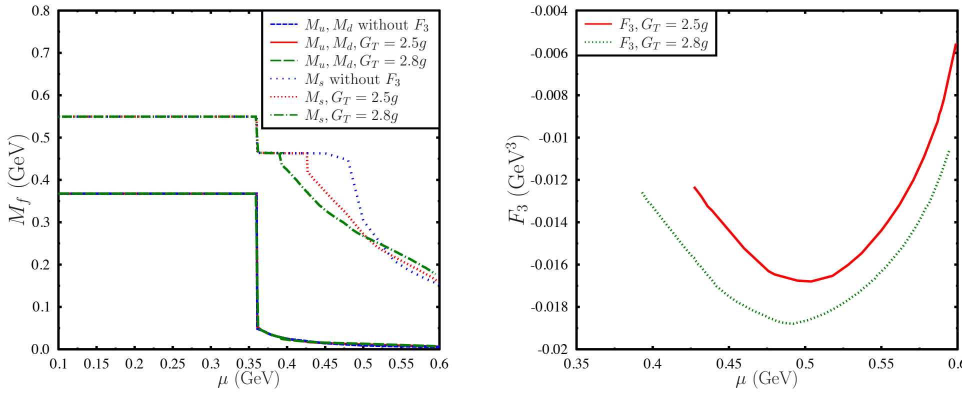

Figure 5.4: Left Plot: Dependence of constituent quark mass on the quark chemical potential at zero temperature in the presence as well as in the absence of spin polarization condensation for different values of tensor couplings for $F_8 = F_3/\sqrt{3}$. Sharp jump in the value of M_u and M_s near $\mu = 0.360$ GeV in both plots indicates the first order chiral phase transition which is expected for standard 2+1 flavour NJL model. Right plot: Variation of spin polarization condensate with quark chemical potential at zero temperature with different values of tensor couplings $G_T = 2.5g$ and $G_T = 2.8g$. For larger tensor coupling tensor condensate form at relatively smaller chemical potential and it remains non zero for a wide range of chemical potential.

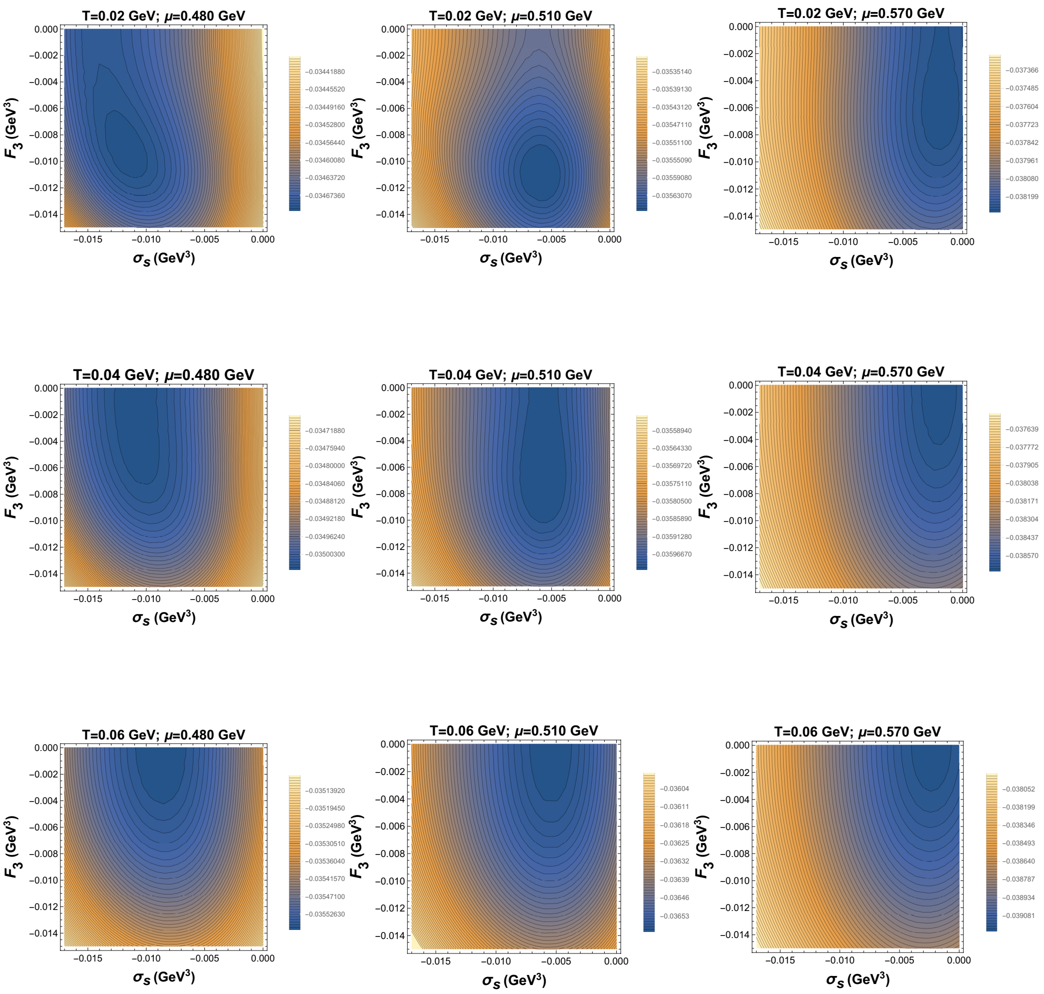

Figure 5.5: This figure shows the contour plots of the thermodynamic potential in $\sigma_s - F_3$ plane for finite temperature (T) and finite chemical potential (μ) with $G_T = 2g$ and $F_8 = F_3/\sqrt{3}$. Along each row as we move from left to the right, temperature has been kept fixed but μ is increasing, similarly along each column μ has been kept fixed with T increasing. Darker regions in these contour plots show the global minimum of the thermodynamic potential. It is clear from the plots that at small temperature non zero value of the spin polarization starts to appear at smaller value of the chemical potential and it also melts at higher chemical potential. Thus for smaller temperature the domain of μ where one can get non zero spin polarization is larger. This domain of existence for the spin polarization condensate becomes smaller with increasing temperature T for a given value of G_T. In fact when the temperature is $T = 0.06$ GeV we cannot get spin polarization for any value of μ.

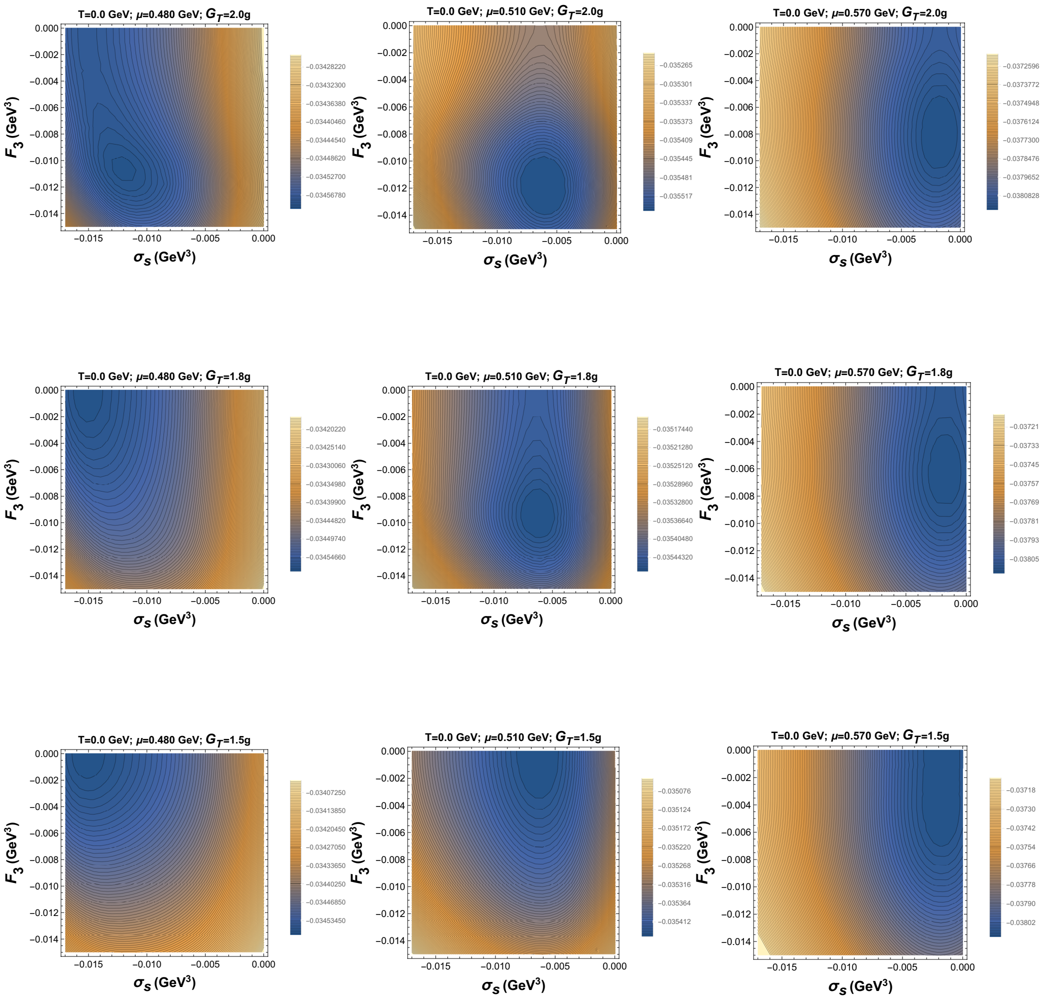

Figure 5.6: This figure shows the contour plots of the thermodynamic potential in $\sigma_s - F_3$ plane for zero temperature (T) and finite chemical potential (μ) with different values of tensor coupling G_T and $F_8 = F_3/\sqrt{3}$. In the first, second and the third row the tensor couplings are taken as $G_T = 2g, 1.8g$ and $1.5g$ respectively. Along each row temperature and G_T has been kept fixed but μ is increasing, similarly along each column μ and T has been kept fixed with G_T decreasing. Darker regions in these contour plots shows the global minimum of the thermodynamic potential. It is clear from the plots that at zero temperature, for larger value of tensor coupling spin polarization can exist for a relatively wide range of chemical potential. With the decreasing value of tensor coupling e.g. for $G_T = 1.5g$ spin polarization almost vanishes. This result can be easily extended to finite temperature. For non zero temperature existence of spin polarization requires lager value of G_T.

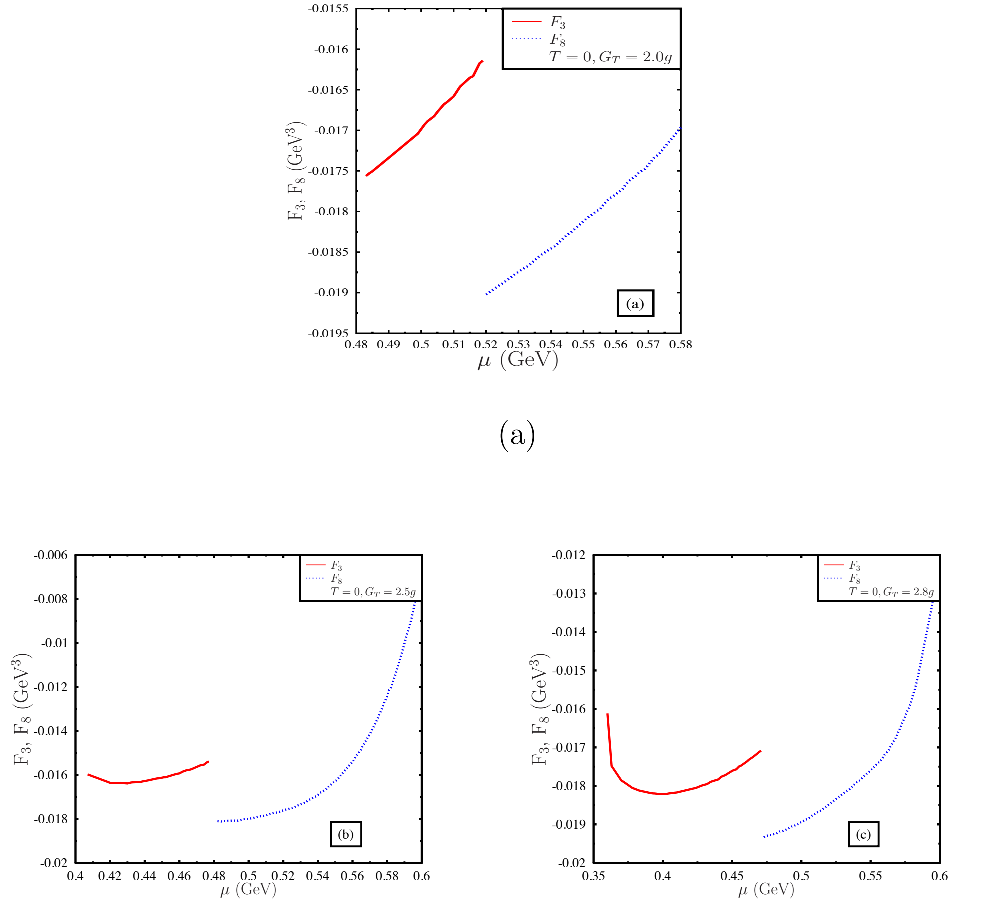

(a)

(b) (c)

Figure 5.7: Plot (a), (b) and (c) show the variation of F_3 (red solid line) and F_8 (blue dotted line) with chemical potential where F_3 and F_8 considered simultaneously in the thermodynamic potential at zero temperature for $G_T = 2g, 2.5g, 2.8g$ respectively. It is clear from the Fig.(5.7) that non zero F_3 appears at relatively smaller μ than F_8. Since F_8 is associated with strange quark-antiquark condensate it survives even at larger chemical potential relative to the F_3 condensate. It is also important to notice that with larger tensor coupling spin condensates appear at relatively smaller quark chemical potential.

Chapter 6

Summary and Conclusions

Quantum Chromodynamics has been successfully applied in explaining high energy collisions involving hadrons. This is possible because at high energies the QCD coupling is weak and perturbative methods of quantum field theory can be used. However at lower energies the physics is more complicated. Non-pertubative effects play important role resulting in spontaneous breaking of chiral symmetry and confinement. Spontaneous breaking of chiral symmetry results in generation of large masses of hadrons and hence most of the mass of the observable universe. Confinement binds the quarks and gluons into colorless hadronics states. However under extreme conditions of temperature and density, i.e. trillion degree kelvin and densities approaching nuclear matter density, the strength of interaction is weak enough, owing to asymptotic freedom, that quarks and gluons can become free and non longer exist in colorless bound states. This state is known as quark gluon plasma. Quark gluon plasma formed in heavy ion collisions or as it may possibly exist in neutron stars is expected to be strongly coupled. Results in heavy ion collision are in disagreement with perturbative results and densities reached in neutron stars are not expected to be high enough for perturbative results to hold. Thus despite the success of QCD the phase diagram of strongly interacting matter is still not fully understood.

In light of lack of first principle methods we use phenomenological models. Two such models are NJL model and PQM model. NJL model is a model of quarks based on four fermi interaction. It exhibits spontaneous chiral symmetry breaking and the parameters are fit to reproduce low energy hadronic spectrum. It has been successfully applied in low energy hadronic physics. Quark meson model is an extension of NJL model. Whereas in NJL model degrees of freedom are quarks, in QM model degrees of freedom are quarks and mesons. Quarks are coupled to mesons and mesons self-interact. This model is further extended by coupling the quarks to polyakov loop. By doing so one includes the effect of gluons which are otherwise absent in the model. Polyakov loop is calculated in Lattice QCD, which is a first principle caculation. Doing so does not lead to confinement since there are no dynamical gluons in the model, however it improves the equation of state by statistically suppressing quark contribution to thermodynamics quantities around and below chiral transition temperature. We have discussed both the NJL and PQM model in detail in Chapter 2. PQM model is also discussed in Chapter 3. We have also discussed the derivation of transport coefficients from Boltzmann equation for quasiparticles and solution for Dirac equation with background magnetic field in Chapter 2.

Having discussed the mathematical framework of phenomenological models and theory of transport coefficients we discuss in detail the calculation of these coefficients in Chapter 3. The scattering amplitudes for meson-meson, meson-quark and quark-quark are calculated from which the relaxation times are obtained. We have kept the energy dependence of relaxation time in our calculation of transport coefficients without approximating by averaging relaxation time over energy. Do so we obtain a value of $\eta/s \sim 0.23$ which is close to KSS bound and also in accordance with data on heavy ion collision which indicate a small value for this ratio. We also find a peak in ζ/s near the chiral transition which is also indicated in Lattice QCD results. Thermal conductivity has also been calculated at finite density. At large temperatures conductivity shows the expected T^2 behavior. Below the chiral transition thermal conductivity is suppressed as quark contribution is suppressed due to polyakov loop.

Having calculated transport properties of quark matter at high temperatures, we turn to quark matter at high densities in Chapter 4. At high densities quark matter is expected to be in color superconducting phase. We use a three flavor NJL model with determinant interaction as at such high densities strange quark could play an important role and its presence affects charge neutrality. We also include a background magnetic field since neutron stars where such high densities could be reached are known to have large magnetic fields which could affect properties of hadronic matter. Color superconductivity is studied using method of Bogoliubov transformation. Thermodynamic potential is calculated using train ground state and masses and superconducting gap is obtained by minimizing thermodynamic potential. Gaps are calculated as a function of varying quark chemical potential and magnetic field. Charge neutrality conditions are imposed and resulting gapless modes are studied.

After studying the interplay of color superconductivity and magnetic field we focus on origin of large magnetic fields in neutron stars. Spontaneous spin polarization of quark matter has been suggested as a possible mechanism for the large magnetic fields of neutron stars. We use a three flavor NJL model with determinant interaction and tensor interaction to study the spin polarization condensates. In three flavor case this leads to two spin polarization condensates, F_3 and F_8. We also consider non-zero current quark masses for the two light flavors. This combined with determinant interaction affects the strange mass significantly which has implications for charge neutrality. We find the two condensates to be non-zero in two distinct intervals of quark chemical potential beyond the chiral transition. In the chiral symmetry broken phase the two condensates are zero. This behavior is complimentary to the case where axial vector interactions are used to study spin polarization. In that case spin condensates are non-zero in the symmetry broken phase and go to zero as symmetry is restored.

We have discussed in the thesis the transport coefficients like viscosity and thermal conductivity of quark matter within NJL and PQM models. There are other interesting transport coefficients of heavy quarks like drag and diffusion coefficients. Incidentally, the related experimental data on nuclear modification factor $\mathrm{R}_A A$, the elliptic flow data v_2 remain a challenge to almost all the models of heavy quark dynamics. It will be interesting to see how the non-perturbative features of chiral symmetry breaking and polyakov loop expectation value, which are quite different from the asymptotic values, near the transition temperature, affect the heavy quark transport coefficients.

Apart from QGP being the most perfect fluid, with the least value for the viscosity to entropy ratio, it has also been the most vortical fluid. It will be interesting to see the thermodynamic properties of the quark gluon matter in presence of vorticity and their phenomenological implications in such effective models.

The situation at high density phase is even more interesting. What we have discussed here is the homogenous phases of condensates, both in quark-anti quark as well as diquark channels. However there are indications that in the presence of difference in chemical potential of different flavors, inhomogenous phases may be important regarding stability of the corresponding condensate phase. It is even expected that the critical point in the QCD phase diagram could be replaced by an elipses point at which the inhomgenous phase and two homogenous phases with broken and restored symmetry meet. Clearly much more work is needed to have an understanding on matter under extreme conditions.

Chapter 7

Appendix

7.1 Appendix A

7.1.1 A. Evaluation of operator expectation values of some operators

We give here some details of the evaluation of some operators at finite T,μ and B in the state given in Eq.(4.17). As the state is obtained from $|0\rangle$, one can calculate the expectation values of different operators. e.g.

$$\langle q_r^{ia\dagger}(n,k_{\not x}), q_{r'}^{jb}(n',k'_{\not x})\rangle = \delta^{ij}\delta^{ab}\delta_{rr'}\delta_{nn'}\delta(\mathbf{k}_{\not x}-\mathbf{k}'_{\not x})F^{ia}(\mathbf{k}_{\not x}). \tag{7.1}$$

where,

$$F^{ia}(\mathbf{k}_{\not x}) = \sin^2\theta_-^{ia} + \sin^2 f\left(1-\sin^2\theta_-^{ia} - |\epsilon^{ij}\epsilon^{ab}\sin^2\theta_-^{jb}\right)(1-\delta^{a3})(1-\delta^{i3}). \tag{7.2}$$

Similarly for the expectation values for the operators involving anti-quarks, we have

$$\langle \tilde{q}_r^{ia\dagger}(n,k_{\not x}), \tilde{q}_{r'}^{jb}(n',k'_{\not x})\rangle = \delta^{ij}\delta^{ab}\delta_{rr'}\delta_{nn'}\delta(\mathbf{k}_{\not x}-\mathbf{k}'_{\not x})(1-F_1^{ia}(\mathbf{k}_{\not x}). \tag{7.3}$$

where,

$$F_1^{ia}(\mathbf{k}_{\not x}) = \sin^2\theta_+^{ia} + \sin^2 f_1\left(1-\sin^2\theta_+^{ia} - |\epsilon^{ij}\epsilon^{ab}|\sin^2\theta_+^{jb}\right)(1-\delta^{a3})(1-\delta^{i3}). \tag{7.4}$$

Using the field operator expansion of Eq.(4.10) and Eq.s (7.1) and (7.3), one can evaluate

$$\langle \psi_\alpha^{ia\dagger}(\mathbf{x})\psi_\beta^{jb}(\mathbf{y})\rangle = \sum_n \frac{|q_iB|}{(2\pi)^2}\int dk_{\not x}e^{ik_{\not x}\cdot(\mathbf{x}-\mathbf{y})}\Lambda_-^{ia,jb}{}_{\beta\alpha}(n,k_{\not x}) \tag{7.5}$$

with

$$\Lambda_{-}^{ia,jb} = \delta^{ij}\delta^{ab}\left[F^{ia}(n,k_z)U_{\beta r}(n,k_{\not x})U_{r\alpha}(n,k_{\not x})^{\dagger} + F_1^{ia}(n,k_z)V_{\beta r}(n,-k_{\not x})V_{r\alpha}(n,-k_{\not x})^{\dagger}\right] \tag{7.6}$$

Explicitly,

$$\begin{aligned}
U_r(n,\boldsymbol{p}_{\not x})U_r^{\dagger}(n,\boldsymbol{p}_{\not x}) &= \frac{1}{2}\begin{pmatrix} (1+\cos\phi)I_n^2 & 0 & \hat{p}_z\sin\phi I_n^2 & i\hat{p}_\perp \sin\phi I_n I_{n-1} \\ 0 & (1+\cos\phi)I_{n-1}^2 & -i\hat{p}_\perp\sin\phi I_n I_{n-1} & -\hat{p}_z\sin\phi I_{n-1}^2 \\ \hat{p}_z\sin\phi I_n^2 & i\hat{p}_\perp\sin\phi I_n I_{n-1} & (1-\cos\phi)I_n^2 & 0 \\ -i\hat{p}_\perp\sin\phi I_n I_{n-1} & -\hat{p}_z\sin\phi I_{n-1}^2 & 0 & (1-\cos\phi)I_{n-1}^2 \end{pmatrix}. \\
&= \frac{1}{2}\Big[I_n^2(1+\gamma^0\cos\phi)\Pi^+ + I_{n-1}^2(1+\gamma^0\cos\phi)\Pi^- \\
&+ \frac{\hat{p}_z}{2}\sin\phi\left(\gamma_0\gamma^3(I_n^2+I_{n-1}^2)+\gamma^5(I_n^2-I_{n-1}^2)\right) - \hat{p}_\perp\sin\phi\gamma^2\gamma^0\Big]
\end{aligned} \tag{7.7}$$

where, we have defined $\Pi^{\pm} = (1 \pm i\gamma^1\gamma^2)/2$.

Similarly for the anti-quark spinors

$$\begin{aligned}
V_r(n,-\boldsymbol{p}_{\not x})V_r^{\dagger}(n,-\boldsymbol{p}_{\not x}) &= \frac{1}{2}\begin{pmatrix} (1-\cos\phi)I_n^2 & 0 & -\hat{p}_z\sin\phi I_n^2 & -i\hat{p}_\perp \sin\phi I_n I_{n-1} \\ 0 & (1-\cos\phi)I_{n-1}^2 & i\hat{p}_\perp\sin\phi I_n I_{n-1} & \hat{p}_z\sin\phi I_{n-1}^2 \\ -\hat{p}_z\sin\phi I_n^2 & -i\hat{p}_\perp\sin\phi I_n I_{n-1} & (1+\cos\phi)I_n^2 & 0 \\ i\hat{p}_\perp\sin\phi I_n I_{n-1} & \hat{p}_z\sin\phi I_{n-1}^2 & 0 & (1+\cos\phi)I_{n-1}^2 \end{pmatrix}. \\
&= \frac{1}{2}\Big[I_n^2(1-\gamma^0\cos\phi)\Pi^+ + I_{n-1}^2(1-\gamma^0\cos\phi)\Pi^- \\
&- \frac{\hat{p}_z}{2}\sin\phi\left(\gamma_0\gamma^3(I_n^2+I_{n-1}^2)+\gamma^5(I_n^2-I_{n-1}^2)\right) + \hat{p}_\perp\sin\phi\gamma^2\gamma^0\Big]
\end{aligned} \tag{7.8}$$

This leads to, e.g. for the expectation value of chiral condensate for a given flavor as

$$I_s^i = \langle\bar{\psi}^i\psi^i\rangle = -\frac{1}{(2\pi)^2}\sum_n\sum_a\int dp_y dp_z\left(1-F^{ia}-F_1^{ia}\right)\cos\phi_n^i(I_n^2+I_{n-1}^2) \tag{7.9}$$

One can integrate over dp_y to obtain the contribution for the quarks that are charged as

$$I_s^i = \sum_a\sum_n\frac{\alpha_n}{(2\pi)^2}|q_iB|\int dp_z\left(1-F^{ia}-F_1^{ia}\right)\cos\phi_n^i \tag{7.10}$$

while, the contribution from the quarks that are neutral (down blue strange blue) is given as

$$I_s^i = \frac{2}{(2\pi)^3}\int d\mathbf{p}\cos\phi^i(1-\sin^2\theta_-^{i3}-\sin^2\theta_+^{i3}) \quad (i=2,3) \tag{7.11}$$

Next, we discuss about the contributions to diquark condensates.Similar to Eq.(7.12), we have

$$\begin{aligned}
\langle q_r^{ia}(n,k_{\not x}), q_{r'}^{jb}(n',k'_{\not x})\rangle &= r\delta_{r,-r'}\epsilon^{ij}\epsilon^{3ab}\delta_{nn'}\delta(\mathbf{k}_{\not x}+\mathbf{k}'_{\not x})\sin 2f(n,k_z)\left(1-\sin^2\theta_-^{ia}-\sin^2\theta_-^{jb}\right) \\
&\equiv r\delta_{r,-r'}\epsilon^{ij}\epsilon^{3ab}\delta_{nn'}\delta(\mathbf{k}_{\not x}+\mathbf{k}'_{\not x})G(k_z,n)
\end{aligned} \tag{7.12}$$

and, for anti-quark operators

$$\begin{aligned}\langle \tilde{q}_r^{ia}(n,k_{\not z}), \tilde{q}_{r'}^{jb}(n',k'_{\not z})\rangle &= r\delta_{r,-r'}\epsilon^{ij}\epsilon^{3ab}\delta_{nn'}\delta(\mathbf{k}_{\not z}+\mathbf{k}'_{\not z})\sin 2f(n,k_z)\left(1-\sin^2\theta_-^{ia}-\sin^2\theta_-^{jb}\right) \\ &\equiv r\delta_{r,-r'}\epsilon^{ij}\epsilon^{3ab}\delta_{nn'}\delta(\mathbf{k}_{\not z}+\mathbf{k}'_{\not z})G_1(k_z,n) \qquad (7.13)\end{aligned}$$

For the diquark condensates we have

$$\langle\psi_\alpha^{ia}(\mathbf{x})\psi_\beta^{jb}(\mathbf{y})\rangle = \epsilon^{ij}\epsilon^{3ab}\sum_n \frac{|q_iB|}{(2\pi)^2}\int dk_{\not z}\, e^{ik_{\not z}\cdot(\mathbf{x}-\mathbf{y})}\left[P_uC\gamma^5G(k_z,n)+P_vC\gamma^5G_1(k_z,n)\right]_{\beta\alpha} \qquad (7.14)$$

where $P_uC\gamma^5=\sum_r rU_{\alpha r}U'_{-r\beta}$ and $P_vC\gamma^5=\sum_r rV_{\alpha r}V'_{-r\beta}$ and the prime on the spinors denotes a spinor with opposite charge and momentum corresponding to the unprimed spinors. Explicitly,

$$P_u = \frac{1}{2}\begin{pmatrix} \cos\frac{\phi}{2}\cos\frac{\phi'}{2}I_n^2 & 0 & \hat{p}_z\cos\frac{\phi}{2}\sin\frac{\phi'}{2}I_n^2 & i\hat{p}_\perp\cos\frac{\phi}{2}\sin\frac{\phi'}{2}I_nI_{n-1} \\ 0 & \cos\frac{\phi}{2}\cos\frac{\phi'}{2}I_{n-1}^2 & -i\hat{p}_\perp\cos\frac{\phi}{2}\sin\frac{\phi'}{2}I_nI_{n-1} & -\hat{p}_z\cos\frac{\phi}{2}\sin\frac{\phi'}{2}I_{n-1}^2 \\ \hat{p}_z\cos\frac{\phi'}{2}\sin\frac{\phi}{2}I_n^2 & i\hat{p}_\perp\cos\frac{\phi'}{2}\sin\frac{\phi}{2}I_nI_{n-1} & \sin\frac{\phi}{2}\sin\frac{\phi'}{2}I_n^2 & 0 \\ -i\hat{p}_\perp\sin\frac{\phi}{2}\cos\frac{\phi'}{2}I_nI_{n-1} & -\hat{p}_z\sin\frac{\phi}{2}\cos\frac{\phi'}{2}I_{n-1}^2 & 0 & \sin\frac{\phi}{2}\sin\frac{\phi'}{2}I_{n-1}^2 \end{pmatrix} \qquad (7.15)$$

and,

$$P_v = \frac{1}{2}\begin{pmatrix} -\sin\frac{\phi}{2}\sin\frac{\phi'}{2}I_n^2 & 0 & \hat{p}_z\sin\frac{\phi}{2}\cos\frac{\phi'}{2}I_n^2 & i\hat{p}_\perp\sin\frac{\phi}{2}\cos\frac{\phi'}{2}I_nI_{n-1} \\ 0 & -\sin\frac{\phi}{2}\sin\frac{\phi'}{2}I_{n-1}^2 & -i\hat{p}_\perp\sin\frac{\phi}{2}\cos\frac{\phi'}{2}I_nI_{n-1} & -\hat{p}_z\sin\frac{\phi}{2}\cos\frac{\phi'}{2}I_{n-1}^2 \\ \hat{p}_z\cos\frac{\phi}{2}\sin\frac{\phi'}{2}I_n^2 & i\hat{p}_\perp\cos\frac{\phi}{2}\sin\frac{\phi'}{2}I_nI_{n-1} & -\cos\frac{\phi}{2}\cos\frac{\phi'}{2}I_n^2 & 0 \\ -i\hat{p}_\perp\cos\frac{\phi}{2}\sin\frac{\phi'}{2}I_nI_{n-1} & -\hat{p}_z\cos\frac{\phi}{2}\sin\frac{\phi'}{2}I_{n-1}^2 & 0 & -\cos\frac{\phi}{2}\cos\frac{\phi'}{2}I_{n-1}^2 \end{pmatrix} \qquad (7.16)$$

This leads to e.g. for expectation value of the diquark condensate as,

$$\begin{aligned} I_D &= \langle\bar{\psi}_c^{ia}\gamma^5\psi^{jb}\rangle\epsilon^{ij}\epsilon^{3ab} \\ &= \frac{2}{(2\pi)^2}\sum_n \alpha_n|q_iB|\int dp_z\cos\left(\frac{\phi_1-\phi_2}{2}\right)\Big[\sin 2f\left(1-\sin^2\theta_-^1-\sin^2\theta_-^2\right) \\ &+ \sin 2f_1\left(1-\sin^2\theta_+^1-\sin^2\theta_+^2\right)\Big] \qquad (7.17)\end{aligned}$$

7.2 Spontaneous Spin Polarization

7.2.1 Gap Equations

The gap equations for four independent condensates, two chiral condensates σ_{ud}, σ_s and two spin polarization condensates F_3, F_8 are as follow,

$$
\begin{aligned}
\frac{\partial\Omega}{\partial\sigma_{ud}} = & -N_c \int \frac{d^3p}{(2\pi)^3} \\
& \Bigg[\frac{M_u}{E_{u_+}} \left(1 + \frac{G_T(F_3 + F_8/\sqrt{3})}{\sqrt{p_T^2 + M_u^2}}\right)(-4g + 2K\sigma_s)\left\{1 - \frac{1}{1+e^{\beta(E_{u_+}-\mu)}} - \frac{1}{1+e^{\beta(E_{u_+}+\mu)}}\right\} \\
& + \frac{M_u}{E_{u_-}} \left(1 - \frac{G_T(F_3 + F_8/\sqrt{3})}{\sqrt{p_T^2 + M_u^2}}\right)(-4g + 2K\sigma_s)\left\{1 - \frac{1}{1+e^{\beta(E_{u_-}-\mu)}} - \frac{1}{1+e^{\beta(E_{u_-}+\mu)}}\right\} \\
& + \frac{M_d}{E_{d_+}} \left(1 + \frac{G_T(F_3 - F_8/\sqrt{3})}{\sqrt{p_T^2 + M_d^2}}\right)(-4g + 2K\sigma_s)\left\{1 - \frac{1}{1+e^{\beta(E_{d_+}-\mu)}} - \frac{1}{1+e^{\beta(E_{d_+}+\mu)}}\right\} \\
& + \frac{M_d}{E_{d_-}} \left(1 - \frac{G_T(F_3 - F_8/\sqrt{3})}{\sqrt{p_T^2 + M_d^2}}\right)(-4g + 2K\sigma_s)\left\{1 - \frac{1}{1+e^{\beta(E_{d_-}-\mu)}} - \frac{1}{1+e^{\beta(E_{d_-}+\mu)}}\right\} \\
& + \frac{M_s}{E_{s_+}} \left(1 + \frac{2G_T F_8/\sqrt{3}}{\sqrt{p_T^2 + M_s^2}}\right)(4K\sigma_{ud})\left\{1 - \frac{1}{1+e^{\beta(E_{s_+}-\mu)}} - \frac{1}{1+e^{\beta(E_{s_+}+\mu)}}\right\} \\
& + \frac{M_s}{E_{s_-}} \left(1 - \frac{2G_T F_8/\sqrt{3}}{\sqrt{p_T^2 + M_s^2}}\right)(4K\sigma_{ud})\left\{1 - \frac{1}{1+e^{\beta(E_{s_-}-\mu)}} - \frac{1}{1+e^{\beta(E_{s_-}+\mu)}}\right\}\Bigg] \\
& + 8g\sigma_{ud} - 8K\sigma_{ud}\sigma_s = 0
\end{aligned}
$$

$$
\begin{aligned}
\frac{\partial\Omega}{\partial\sigma_s} = & -N_c \int \frac{d^3p}{(2\pi)^3} \Bigg[\frac{M_u}{E_{u_+}} \left(1 + \frac{G_T(F_3 + F_8/\sqrt{3})}{\sqrt{p_T^2 + M_u^2}}\right)(2K\sigma_{ud})\left\{1 - \frac{1}{1+e^{\beta(E_{u_+}-\mu)}} - \frac{1}{1+e^{\beta(E_{u_+}+\mu)}}\right\} \\
& + \frac{M_u}{E_{u_-}} \left(1 - \frac{G_T(F_3 + F_8/\sqrt{3})}{\sqrt{p_T^2 + M_u^2}}\right)(2K\sigma_{ud})\left\{1 - \frac{1}{1+e^{\beta(E_{u_-}-\mu)}} - \frac{1}{1+e^{\beta(E_{u_-}+\mu)}}\right\} \\
& + \frac{M_d}{E_{d_+}} \left(1 + \frac{G_T(F_3 - F_8/\sqrt{3})}{\sqrt{p_T^2 + M_d^2}}\right)(2K\sigma_{ud})\left\{1 - \frac{1}{1+e^{\beta(E_{d_+}-\mu)}} - \frac{1}{1+e^{\beta(E_{d_+}+\mu)}}\right\} \\
& + \frac{M_d}{E_{d_-}} \left(1 - \frac{G_T(F_3 - F_8/\sqrt{3})}{\sqrt{p_T^2 + M_d^2}}\right)(2K\sigma_{ud})\left\{1 - \frac{1}{1+e^{\beta(E_{d_-}-\mu)}} - \frac{1}{1+e^{\beta(E_{d_-}+\mu)}}\right\} \\
& + \frac{M_s}{E_{s_+}} \left(1 + \frac{2G_T F_8/\sqrt{3}}{\sqrt{p_T^2 + M_s^2}}\right)(-4g)\left\{1 - \frac{1}{1+e^{\beta(E_{s_+}-\mu)}} - \frac{1}{1+e^{\beta(E_{s_+}+\mu)}}\right\} \\
& + \frac{M_s}{E_{s_-}} \left(1 - \frac{2G_T F_8/\sqrt{3}}{\sqrt{p_T^2 + M_s^2}}\right)(-4g)\left\{1 - \frac{1}{1+e^{\beta(E_{s_-}-\mu)}} - \frac{1}{1+e^{\beta(E_{s_-}+\mu)}}\right\}\Bigg] + 4g\sigma_s - 4K\sigma_{ud}^2 =
\end{aligned}
$$

$$
\begin{aligned}
\frac{\partial\Omega}{\partial F_3} =& -N_c\int\frac{d^3p}{(2\pi)^3} \\
&\Bigg[G_T\frac{\sqrt{p_T^2+M_u^2}+G_T(F_3+F_8/\sqrt{3})}{E_{u_+}}\left\{1-\frac{1}{1+e^{\beta(E_{u_+}-\mu)}}-\frac{1}{1+e^{\beta(E_{u_+}+\mu)}}\right\} \\
&-G_T\frac{\sqrt{p_T^2+M_u^2}-G_T(F_3+F_8/\sqrt{3})}{E_{u_-}}\left\{1-\frac{1}{1+e^{\beta(E_{u_-}-\mu)}}-\frac{1}{1+e^{\beta(E_{u_-}+\mu)}}\right\} \\
&+G_T\frac{\sqrt{p_T^2+M_d^2}+G_T(F_3-F_8/\sqrt{3})}{E_{d_+}}\left\{1-\frac{1}{1+e^{\beta(E_{d_+}-\mu)}}-\frac{1}{1+e^{\beta(E_{d_+}+\mu)}}\right\} \\
&-G_T\frac{\sqrt{p_T^2+M_d^2}-G_T(F_3-F_8/\sqrt{3})}{E_{d_-}}\left\{1-\frac{1}{1+e^{\beta(E_{d_-}-\mu)}}-\frac{1}{1+e^{\beta(E_{d_-}+\mu)}}\right\}\Bigg] \\
&+G_TF_3 = 0
\end{aligned}
$$

$$
\begin{aligned}
\frac{\partial\Omega}{\partial F_8} =& -N_c\int\frac{d^3p}{(2\pi)^3} \\
&\Bigg[\frac{G_T}{\sqrt{3}}\frac{\sqrt{p^2+M_u^2}+G_T(F_3+F_8/\sqrt{3})}{E_{u_+}}\left\{1-\frac{1}{1+e^{\beta(E_{u_+}-\mu)}}-\frac{1}{1+e^{\beta(E_{u_+}+\mu)}}\right\} \\
&-\frac{G_T}{\sqrt{3}}\frac{\sqrt{p^2+M_u^2}-G_T(F_3+F_8/\sqrt{3})}{E_{u_-}}\left\{1-\frac{1}{1+e^{\beta(E_{u_-}-\mu)}}-\frac{1}{1+e^{\beta(E_{u_-}+\mu)}}\right\} \\
&-\frac{G_T}{\sqrt{3}}\frac{\sqrt{p^2+M_d^2}+G_T(F_3-F_8/\sqrt{3})}{E_{d_+}}\left\{1-\frac{1}{1+e^{\beta(E_{d_+}-\mu)}}-\frac{1}{1+e^{\beta(E_{d_+}+\mu)}}\right\} \\
&+\frac{G_T}{\sqrt{3}}\frac{\sqrt{p^2+M_d^2}-G_T(F_3-F_8/\sqrt{3})}{E_{d_-}}\left\{1-\frac{1}{1+e^{\beta(E_{d_-}-\mu)}}-\frac{1}{1+e^{\beta(E_{d_-}+\mu)}}\right\} \\
&+2\frac{G_T}{\sqrt{3}}\frac{\sqrt{p^2+M_s^2}+2G_TF_8/\sqrt{3}}{E_{s_+}}\left\{1-\frac{1}{1+e^{\beta(E_{s_+}-\mu)}}-\frac{1}{1+e^{\beta(E_{s_+}+\mu)}}\right\} \\
&-2\frac{G_T}{\sqrt{3}}\frac{\sqrt{p^2+M_s^2}-2G_TF_8/\sqrt{3}}{E_{s_-}}\left\{1-\frac{1}{1+e^{\beta(E_{s_-}-\mu)}}-\frac{1}{1+e^{\beta(E_{s_-}+\mu)}}\right\}\Bigg]+G_TF_8 = 0
\end{aligned}
$$

Bibliography

[1] Chihiro Sasaki and Krzysztof Redlich. Transport coefficients near chiral phase transition. *Nucl. Phys.*, A832:62–75, 2010.

[2] M. Herrero. The Standard model. *NATO Sci. Ser. C*, 534:1–59, 1999.

[3] Charles W. Misner, K. S. Thorne, and J. A. Wheeler. *Gravitation*. W. H. Freeman, San Francisco, 1973.

[4] Michael E. Peskin and Daniel V. Schroeder. *An Introduction to quantum field theory*. Addison-Wesley, Reading, USA, 1995.

[5] M. A. Stephanov. QCD phase diagram: An Overview. *PoS*, LAT2006:024, 2006.

[6] I. Arsene et al. Quark gluon plasma and color glass condensate at RHIC? The Perspective from the BRAHMS experiment. *Nucl. Phys.*, A757:1–27, 2005.

[7] Gergely Endrdi. QCD phase diagram: overview of recent lattice results. *J. Phys. Conf. Ser.*, 503:012009, 2014.

[8] Peter Brockway Arnold, Guy D. Moore, and Laurence G. Yaffe. Transport coefficients in high temperature gauge theories. 1. Leading log results. *JHEP*, 11:001, 2000.

[9] Peter Brockway Arnold, Guy D Moore, and Laurence G. Yaffe. Transport coefficients in high temperature gauge theories. 2. Beyond leading log. *JHEP*, 05:051, 2003.

[10] Peter Brockway Arnold, Caglar Dogan, and Guy D. Moore. The Bulk Viscosity of High-Temperature QCD. *Phys. Rev.*, D74:085021, 2006.

[11] P. Kovtun, Dan T. Son, and Andrei O. Starinets. Viscosity in strongly interacting quantum field theories from black hole physics. *Phys. Rev. Lett.*, 94:111601, 2005.

[12] Atsushi Nakamura and Sunao Sakai. Transport coefficients of gluon plasma. *Phys. Rev. Lett.*, 94:072305, 2005.

[13] Harvey B. Meyer. A Calculation of the shear viscosity in SU(3) gluodynamics. *Phys. Rev.*, D76:101701, 2007.

[14] Harvey B. Meyer. A Calculation of the bulk viscosity in SU(3) gluodynamics. *Phys. Rev. Lett.*, 100:162001, 2008.

[15] P. Chakraborty and J. I. Kapusta. Quasi-Particle Theory of Shear and Bulk Viscosities of Hadronic Matter. *Phys. Rev.*, C83:014906, 2011.

[16] John C. Collins and M. J. Perry. Superdense Matter: Neutrons Or Asymptotically Free Quarks? *Phys. Rev. Lett.*, 34:1353, 1975.

[17] Bertrand C. Barrois. Superconducting Quark Matter. *Nucl. Phys.*, B129:390–396, 1977.

[18] D. Bailin and A. Love. Superfluidity and Superconductivity in Relativistic Fermion Systems. *Phys. Rept.*, 107:325, 1984.

[19] Mark G. Alford, Krishna Rajagopal, and Frank Wilczek. QCD at finite baryon density: Nucleon droplets and color superconductivity. *Phys. Lett.*, B422:247–256, 1998.

[20] R. Rapp, Thomas Schfer, Edward V. Shuryak, and M. Velkovsky. Diquark Bose condensates in high density matter and instantons. *Phys. Rev. Lett.*, 81:53–56, 1998.

[21] Robert D. Pisarski and Dirk H. Rischke. Superfluidity in a model of massless fermions coupled to scalar bosons. *Phys. Rev.*, D60:094013, 1999.

[22] Fridolin Weber. From boson condensation to quark deconfinement: The Many faces of neutron star interiors. *Acta Phys. Polon.*, B30:3149–3169, 1999.

[23] Robert D. Pisarski and Dirk H. Rischke. Gaps and critical temperature for color superconductivity. *Phys. Rev.*, D61:051501, 2000.

[24] G. W. Carter and Dmitri Diakonov. Light quarks in the instanton vacuum at finite baryon density. *Phys. Rev.*, D60:016004, 1999.

[25] R. Rapp, Thomas Schfer, Edward V. Shuryak, and M. Velkovsky. High density QCD and instantons. *Annals Phys.*, 280:35–99, 2000.

[26] Paolo Amore, Michael C. Birse, Judith A. McGovern, and Niels R. Walet. Color superconductivity in finite systems. *Phys. Rev.*, D65:074005, 2002.

[27] Mark Alford and Krishna Rajagopal. Absence of two flavor color superconductivity in compact stars. *JHEP*, 06:031, 2002.

[28] Andrew W. Steiner, Sanjay Reddy, and Madappa Prakash. Color neutral superconducting quark matter. *Phys. Rev.*, D66:094007, 2002.

[29] F. Neumann, M. Buballa, and M. Oertel. Mixed phases of color superconducting quark matter. *Nucl. Phys.*, A714:481–501, 2003.

[30] Efrain J. Ferrer, Vivian de la Incera, and Cristina Manuel. Magnetic color flavor locking phase in high density QCD. *Phys. Rev. Lett.*, 95:152002, 2005.

[31] Efrain J. Ferrer, Vivian de la Incera, and Cristina Manuel. Color-superconducting gap in the presence of a magnetic field. *Nucl. Phys.*, B747:88–112, 2006.

[32] Efrain J. Ferrer and Vivian de la Incera. Magnetic Phases in Three-Flavor Color Superconductivity. *Phys. Rev.*, D76:045011, 2007.

[33] Jorge L. Noronha and Igor A. Shovkovy. Color-flavor locked superconductor in a magnetic field. *Phys. Rev.*, D76:105030, 2007. [Erratum: Phys. Rev.D86,049901(2012)].

[34] Kenji Fukushima and Harmen J. Warringa. Color superconducting matter in a magnetic field. *Phys. Rev. Lett.*, 100:032007, 2008.

[35] Sh. Fayazbakhsh and N. Sadooghi. Color neutral 2SC phase of cold and dense quark matter in the presence of constant magnetic fields. *Phys. Rev.*, D82:045010, 2010.

[36] Sh. Fayazbakhsh and N. Sadooghi. Phase diagram of hot magnetized two-flavor color superconducting quark matter. *Phys. Rev.*, D83:025026, 2011.

[37] Toshitaka Tatsumi. Ferromagnetism of quark liquid. *Phys. Lett.*, B489:280–286, 2000.

[38] E. Nakano, T. Maruyama, and T. Tatsumi. Spin polarization and color superconductivity in quark matter. *Phys. Rev.*, D68:105001, 2003.

[39] Shinji Maedan. Spin polarization and chiral symmetry breaking at finite density. *Prog. Theor. Phys.*, 118:729–748, 2007.

[40] Yasuhiko Tsue, Joao da Providencia, Constanca Providencia, and Masatoshi Yamamura. Effective Potential Approach to Quark Ferromagnetization in High Density Quark Matter. *Prog. Theor. Phys.*, 128:507–522, 2012.

[41] H. BOHR, P.K. PANDA, C. PROVIDNCIA, and J.D. PROVIDNCIA. Spin polarization in high density quark matter. 2013.

[42] Edwin Laermann and Owe Philipsen. The Status of lattice QCD at finite temperature. *Ann. Rev. Nucl. Part. Sci.*, 53:163–198, 2003.

[43] F. Karsch and E. Laermann. Thermodynamics and in medium hadron properties from lattice QCD. pages 1–59, 2003.

[44] C. R. Allton, S. Ejiri, S. J. Hands, O. Kaczmarek, F. Karsch, E. Laermann, and C. Schmidt. The Equation of state for two flavor QCD at nonzero chemical potential. *Phys. Rev.*, D68:014507, 2003.

[45] Shinji Ejiri, Chris R. Allton, Simon J. Hands, Olaf Kaczmarek, Frithjof Karsch, Edwin Laermann, and Christian Schmidt. Study of QCD thermodynamics at finite density by Taylor expansion. *Prog. Theor. Phys. Suppl.*, 153:118–126, 2004.

[46] Yoichiro Nambu and G. Jona-Lasinio. Dynamical Model of Elementary Particles Based on an Analogy with Superconductivity. 1. *Phys. Rev.*, 122:345–358, 1961. [,127(1961)].

[47] Yoichiro Nambu and G. Jona-Lasinio. DYNAMICAL MODEL OF ELEMENTARY PARTICLES BASED ON AN ANALOGY WITH SUPERCONDUCTIVITY. II. *Phys. Rev.*, 124:246–254, 1961. [,141(1961)].

[48] Juergen Berges and Krishna Rajagopal. Color superconductivity and chiral symmetry restoration at nonzero baryon density and temperature. *Nucl. Phys.*, B538:215–232, 1999.

[49] Michael Buballa. NJL model analysis of quark matter at large density. *Phys. Rept.*, 407:205–376, 2005.

[50] P. Zhuang, J. Hufner, S. P. Klevansky, and L. Neise. Transport properties of a quark plasma and critical scattering at the chiral phase transition. *Phys. Rev.*, D51:3728–3738, 1995.

[51] M. L. Goldberger and S. B. Treiman. Decay of the pi meson. *Phys. Rev.*, 110:1178–1184, 1958.

[52] Murray Gell-Mann, R. J. Oakes, and B. Renner. Behavior of current divergences under SU(3) x SU(3). *Phys. Rev.*, 175:2195–2199, 1968.

[53] Kaoru Hagiwara et al. Review of particle physics. Particle Data Group. *Phys. Rev.*, D66:010001, 2002.

[54] Barry R. Holstein. How large is f(pi)? *Phys. Lett.*, B244:83–87, 1990.

[55] Leonardo Giusti, F. Rapuano, M. Talevi, and A. Vladikas. The QCD chiral condensate from the lattice. *Nucl. Phys.*, B538:249–277, 1999.

[56] Tetsuo Hatsuda and Teiji Kunihiro. QCD phenomenology based on a chiral effective Lagrangian. *Phys. Rept.*, 247:221–367, 1994.

[57] Matthias F. M. Lutz, S. Klimt, and W. Weise. Meson properties at finite temperature and baryon density. *Nucl. Phys.*, A542:521–558, 1992.

[58] P. Rehberg, S. P. Klevansky, and J. Hufner. Hadronization in the SU(3) Nambu-Jona-Lasinio model. *Phys. Rev.*, C53:410–429, 1996.

[59] Paramita Deb, Guru Prakash Kadam, and Hiranmaya Mishra. Estimating transport coefficients in hot and dense quark matter. *Phys. Rev.*, D94(9):094002, 2016.

[60] C. Sasaki and K. Redlich. Bulk viscosity in quasi particle models. *Phys. Rev.*, C79:055207, 2009.

[61] M. Bluhm, B. Kampfer, and K. Redlich. Bulk and shear viscosities of the gluon plasma in a quasiparticle description. *Phys. Rev.*, C84:025201, 2011.

[62] A. S. Khvorostukhin, V. D. Toneev, and D. N. Voskresensky. Viscosity Coefficients for Hadron and Quark-Gluon Phases. *Nucl. Phys.*, A845:106–146, 2010.

[63] M. Albright and J. I. Kapusta. Quasiparticle Theory of Transport Coefficients for Hadronic Matter at Finite Temperature and Baryon Density. *Phys. Rev.*, C93(1):014903, 2016.

[64] Ulrich Heinz and Raimond Snellings. Collective flow and viscosity in relativistic heavy-ion collisions. *Ann. Rev. Nucl. Part. Sci.*, 63:123–151, 2013.

[65] Miklos Gyulassy and Larry McLerran. New forms of QCD matter discovered at RHIC. *Nucl. Phys.*, A750:30–63, 2005.

[66] Harri Niemi, Gabriel S. Denicol, Pasi Huovinen, Etele Molnar, and Dirk H. Rischke. Influence of the shear viscosity of the quark-gluon plasma on elliptic flow in ultrarelativistic heavy-ion collisions. *Phys. Rev. Lett.*, 106:212302, 2011.

[67] Laszlo P. Csernai, Joseph.I. Kapusta, and Larry D. McLerran. On the Strongly-Interacting Low-Viscosity Matter Created in Relativistic Nuclear Collisions. *Phys. Rev. Lett.*, 97:152303, 2006.

[68] Matthew Luzum and Paul Romatschke. Viscous Hydrodynamic Predictions for Nuclear Collisions at the LHC. *Phys. Rev. Lett.*, 103:262302, 2009.

[69] Paul Romatschke and Ulrike Romatschke. Viscosity Information from Relativistic Nuclear Collisions: How Perfect is the Fluid Observed at RHIC? *Phys. Rev. Lett.*, 99:172301, 2007.

[70] Tetsufumi Hirano and Miklos Gyulassy. Perfect fluidity of the quark gluon plasma core as seen through its dissipative hadronic corona. *Nucl. Phys.*, A769:71–94, 2006.

[71] Charles Gale, Sangyong Jeon, and Bjoern Schenke. Hydrodynamic Modeling of Heavy-Ion Collisions. *Int. J. Mod. Phys.*, A28:1340011, 2013.

[72] Sreemoyee Sarkar and Rishi Sharma. The shear viscosity of two-flavor crystalline color superconducting quark matter. *Phys. Rev.*, D96:094025, 2017.

[73] H. Heiselberg and C. J. Pethick. Transport and relaxation in degenerate quark plasmas. *Phys. Rev.*, D48:2916–2928, 1993.

[74] N. Chamel and P. Haensel. Physics of Neutron Star Crusts. *Living Rev. Rel.*, 11:10, 2008.

[75] D. G. Yakovlev, A. D. Kaminker, Oleg Y. Gnedin, and P. Haensel. Neutrino emission from neutron stars. *Phys. Rept.*, 354:1, 2001.

[76] D. G. Yakovlev, Oleg Y. Gnedin, A. D. Kaminker, K. P. Levenfish, and Alexander Y. Potekhin. Neutron star cooling: Theoretical aspects and observational constraints. *Adv. Space Res.*, 33(4):523–530, 2004.

[77] Nils Andersson. A New class of unstable modes of rotating relativistic stars. *Astrophys. J.*, 502:708–713, 1998.

[78] Nils Andersson and Kostas D. Kokkotas. Towards gravitational wave asteroseismology. *Mon. Not. Roy. Astron. Soc.*, 299:1059–1068, 1998.

[79] T. K. Jha, H. Mishra, and V. Sreekanth. Bulk viscosity in hyperonic star and r-mode instability. *Phys. Rev.*, C82:025803, 2010.

[80] Ryogo Kubo. Statistical mechanical theory of irreversible processes. 1. General theory and simple applications in magnetic and conduction problems. *J. Phys. Soc. Jap.*, 12:570–586, 1957.

[81] Nasser Demir and Steffen A. Bass. Shear-Viscosity to Entropy-Density Ratio of a Relativistic Hadron Gas. *Phys. Rev. Lett.*, 102:172302, 2009.

[82] V. Ozvenchuk, O. Linnyk, M. I. Gorenstein, E. L. Bratkovskaya, and W. Cassing. Shear and bulk viscosities of strongly interacting infinite parton-hadron matter within the parton-hadron-string dynamics transport approach. *Phys. Rev.*, C87(6):064903, 2013.

[83] A. S. Khvorostukhin, V. D. Toneev, and D. N. Voskresensky. Remarks concerning bulk viscosity of hadron matter in relaxation time ansatz. *Nucl. Phys.*, A915:158–169, 2013.

[84] Kazunori Itakura, Osamu Morimatsu, and Hiroshi Otomo. Shear viscosity of a hadronic gas mixture. *Phys. Rev.*, D77:014014, 2008.

[85] Robert Lang, Norbert Kaiser, and Wolfram Weise. Shear Viscosity of a Hot Pion Gas. *Eur. Phys. J.*, A48:109, 2012.

[86] D. Fernandez-Fraile and A. Gomez Nicola. Transport coefficients and resonances for a meson gas in Chiral Perturbation Theory. *Eur. Phys. J.*, C62:37–54, 2009.

[87] Sukanya Mitra, Sabyasachi Ghosh, and Sourav Sarkar. Effect of spectral modification of ρ on shear viscosity of a pion gas. *Phys. Rev.*, C85:064917, 2012.

[88] Madappa Prakash, Manju Prakash, R. Venugopalan, and G. Welke. Nonequilibrium properties of hadronic mixtures. *Phys. Rept.*, 227:321–366, 1993.

[89] Antonio Dobado and Silvia N. Santalla. Pion gas viscosity at low temperature and density. *Phys. Rev.*, D65:096011, 2002.

[90] Rudy Marty, Elena Bratkovskaya, Wolfgang Cassing, Jrg Aichelin, and Hamza Berrehrah. Transport coefficients from the Nambu-Jona-Lasinio model for $SU(3)_f$. *Phys. Rev.*, C88:045204, 2013.

[91] Antonio Dobado, Felipe J. Llanes-Estrada, and Juan M. Torres-Rincon. Bulk viscosity of low-temperature strongly interacting matter. *Phys. Lett.*, B702:43–48, 2011.

[92] Krishna Rajagopal and Nilesh Tripuraneni. Bulk Viscosity and Cavitation in Boost-Invariant Hydrodynamic Expansion. *JHEP*, 03:018, 2010.

[93] Jitesh R. Bhatt, Hiranmaya Mishra, and V. Sreekanth. Thermal photons in QGP and non-ideal effects. *JHEP*, 11:106, 2010.

[94] Jitesh R. Bhatt, Hiranmaya Mishra, and V. Sreekanth. Shear viscosity, cavitation and hydrodynamics at LHC. *Phys. Lett.*, B704:486–489, 2011.

[95] Jitesh R. Bhatt, Hiranmaya Mishra, and V. Sreekanth. Cavitation and thermal dilepton production in QGP. *Nucl. Phys.*, A875:181–196, 2012.

[96] Sukanya Mitra and Sourav Sarkar. Medium effects on the viscosities of a pion gas. *Phys. Rev.*, D87(9):094026, 2013.

[97] Sukanya Mitra, Utsab Gangopadhyaya, and Sourav Sarkar. Medium effects on the relaxation of dissipative flows in a hot pion gas. *Phys. Rev.*, D91(9):094012, 2015.

[98] G. S. Denicol, H. Niemi, E. Molnar, and D. H. Rischke. Derivation of transient relativistic fluid dynamics from the Boltzmann equation. *Phys. Rev.*, D85:114047, 2012. [Erratum: Phys. Rev.D91,no.3,039902(2015)].

[99] M. Greif, F. Reining, I. Bouras, G. S. Denicol, Z. Xu, and C. Greiner. Heat conductivity in relativistic systems investigated using a partonic cascade. *Phys. Rev.*, E87:033019, 2013.

[100] G. S. Denicol, H. Niemi, I. Bouras, E. Molnar, Z. Xu, D. H. Rischke, and C. Greiner. Solving the heat-flow problem with transient relativistic fluid dynamics. *Phys. Rev.*, D89(7):074005, 2014.

[101] Joseph I. Kapusta and Juan M. Torres-Rincon. Thermal Conductivity and Chiral Critical Point in Heavy Ion Collisions. *Phys. Rev.*, C86:054911, 2012.

[102] M. Iwasaki and T. Fukutome. J. phys. g36, 115012, 2009. 2009.

[103] Seung-il Nam. Thermal conductivity of the quark matter for the SU(2) light-flavor sector. *Mod. Phys. Lett.*, A30(10):1550054, 2015.

[104] Sabyasachi Ghosh. Thermal conductivity of hot pionic medium due to pion self-energy for $\pi\sigma$ and $\pi\rho$ loops. *Int. J. Mod. Phys.*, E24(07):1550058, 2015.

[105] Pracheta Singha, Aman Abhishek, Guruprasad Kadam, Sabyasachi Ghosh, and Hiranmaya Mishra. Calculations of shear, bulk viscosities and electrical conductivity in the Polyakov-quarkmeson model. *J. Phys.*, G46(1):015201, 2019.

[106] Frithjof Karsch, Dmitri Kharzeev, and Kirill Tuchin. Universal properties of bulk viscosity near the QCD phase transition. *Phys. Lett.*, B663:217–221, 2008.

[107] S. Gavin. TRANSPORT COEFFICIENTS IN ULTRARELATIVISTIC HEAVY ION COLLISIONS. *Nucl. Phys.*, A435:826–843, 1985.

[108] A. Hosoya and K. Kajantie. Transport Coefficients of QCD Matter. *Nucl. Phys.*, B250:666–688, 1985.

[109] P. Danielewicz and M. Gyulassy. Dissipative Phenomena in Quark Gluon Plasmas. *Phys. Rev.*, D31:53–62, 1985.

[110] O. Scavenius, A. Mocsy, I. N. Mishustin, and D. H. Rischke. Chiral phase transition within effective models with constituent quarks. *Phys. Rev.*, C64:045202, 2001.

[111] D. T. Son and Misha A. Stephanov. Real time pion propagation in finite temperature QCD. *Phys. Rev.*, D66:076011, 2002.

[112] Bastian B. Brandt, Anthony Francis, Harvey B. Meyer, and Daniel Robaina. Pion quasiparticle in the low-temperature phase of QCD. *Phys. Rev.*, D92(9):094510, 2015.

[113] Sourendu Gupta and Rishi Sharma. Effective field theory for warm QCD. *Phys. Rev.*, D97(3):036025, 2018.

[114] Dmitri E. Kharzeev, Larry D. McLerran, and Harmen J. Warringa. The Effects of topological charge change in heavy ion collisions: 'Event by event P and CP violation'. *Nucl. Phys.*, A803:227–253, 2008.

[115] V. Skokov, A. Yu. Illarionov, and V. Toneev. Estimate of the magnetic field strength in heavy-ion collisions. *Int. J. Mod. Phys.*, A24:5925–5932, 2009.

[116] Dmitri E. Kharzeev. Topologically induced local P and CP violation in QCD x QED. *Annals Phys.*, 325:205–218, 2010.

[117] Kenji Fukushima, Marco Ruggieri, and Raoul Gatto. Chiral magnetic effect in the PNJL model. *Phys. Rev.*, D81:114031, 2010.

[118] Massimo D'Elia, Swagato Mukherjee, and Francesco Sanfilippo. QCD Phase Transition in a Strong Magnetic Background. *Phys. Rev.*, D82:051501, 2010.

[119] Ana Julia Mizher, M. N. Chernodub, and Eduardo S. Fraga. Phase diagram of hot QCD in an external magnetic field: possible splitting of deconfinement and chiral transitions. *Phys. Rev.*, D82:105016, 2010.

[120] Sutapa Ghosh, Soma Mandal, and Somenath Chakrabarty. Chiral properties of QCD vacuum in magnetars- A Nambu-Jona-Lasinio model with semi-classical approximation. *Phys. Rev.*, C75:015805, 2007.

[121] Robert C. Duncan and Christopher Thompson. Formation of very strongly magnetized neutron stars - implications for gamma-ray bursts. *Astrophys. J.*, 392:L9, 1992.

[122] Christopher Thompson and Robert C. Duncan. Neutron star dynamos and the origins of pulsar magnetism. *Astrophys. J.*, 408:194, 1993.

[123] Christopher Thompson and Robert C. Duncan. The Soft gamma repeaters as very strongly magnetized neutron stars - 1. Radiative mechanism for outbursts. *Mon. Not. Roy. Astron. Soc.*, 275:255–300, 1995.

[124] Christopher Thompson and Robert C. Duncan. The Soft gamma repeaters as very strongly magnetized neutron stars. 2. Quiescent neutrino, x-ray, and Alfven wave emission. *Astrophys. J.*, 473:322, 1996.

[125] Christian Y. Cardall, Madappa Prakash, and James M. Lattimer. Effects of strong magnetic fields on neutron star structure. *Astrophys. J.*, 554:322–339, 2001.

[126] A. E. Broderick, M. Prakash, and J. M. Lattimer. Effects of strong magnetic fields in strange baryonic matter. *Phys. Lett.*, B531:167–174, 2002.

[127] D. Lai and S. L. Shapiro. Astrophys. j.383, 745 (1991). 1991.

[128] D. Bandyopadhyaya, S. Chakrabarty, and S. Pal. Phys. rev.lett.79, 2176 (1997). 1997.

[129] E. J. Ferrer, V. Incera, J. P. Keith, and P. Springsteen. Phys.rev. c82, 065802 (2010). 2010.

[130] Xu-Guang Huang, Mei Huang, Dirk H. Rischke, and Armen Sedrakian. Anisotropic Hydrodynamics, Bulk Viscosities and R-Modes of Strange Quark Stars with Strong Magnetic Fields. *Phys. Rev.*, D81:045015, 2010.

[131] E. V. Gorbar, V. A. Miransky, and I. A. Shovkovy. Chiral asymmetry of the Fermi surface in dense relativistic matter in a magnetic field. *Phys. Rev.*, C80:032801, 2009.

[132] E. V. Gorbar, V. A. Miransky, and I. A. Shovkovy. Chiral asymmetry and axial anomaly in magnetized relativistic matter. *Phys. Lett.*, B695:354–358, 2011.

[133] V. P. Gusynin, V. A. Miransky, and I. A. Shovkovy. Catalysis of dynamical flavor symmetry breaking by a magnetic field in (2+1)-dimensions. *Phys. Rev. Lett.*, 73:3499–3502, 1994. [Erratum: Phys. Rev. Lett.76,1005(1996)].

[134] V. P. Gusynin, V. A. Miransky, and I. A. Shovkovy. Dimensional reduction and dynamical chiral symmetry breaking by a magnetic field in (3+1)-dimensions. *Phys. Lett.*, B349:477–483, 1995.

[135] V. P. Gusynin, V. A. Miransky, and I. A. Shovkovy. Dimensional reduction and catalysis of dynamical symmetry breaking by a magnetic field. *Nucl. Phys.*, B462:249–290, 1996.

[136] Efrain J. Ferrer and Vivian de la Incera. Dynamically Induced Zeeman Effect in Massless QED. *Phys. Rev. Lett.*, 102:050402, 2009.

[137] Efrain J. Ferrer and Vivian de la Incera. Dynamically Generated Anomalous Magnetic Moment in Massless QED. *Nucl. Phys.*, B824:217–238, 2010.

[138] D. Ebert and K. G. Klimenko. Quark droplets stability induced by external magnetic field. *Nucl. Phys.*, A728:203–225, 2003.

[139] Jorn K. Boomsma and Daniel Boer. The Influence of strong magnetic fields and instantons on the phase structure of the two-flavor NJL model. *Phys. Rev.*, D81:074005, 2010.

[140] D. P. Menezes, M. Benghi Pinto, S. S. Avancini, and C. Providencia. Quark matter under strong magnetic fields in the su(3) Nambu-Jona-Lasinio Model. *Phys. Rev.*, C80:065805, 2009.

[141] D. P. Menezes, M. Benghi Pinto, S. S. Avancini, A. Perez Martinez, and C. Providencia. Quark matter under strong magnetic fields in the Nambu-Jona-Lasinio Model. *Phys. Rev.*, C79:035807, 2009.

[142] Bhaswar Chatterjee, Hiranmaya Mishra, and Amruta Mishra. Vacuum structure and chiral symmetry breaking in strong magnetic fields for hot and dense quark matter. *Phys. Rev.*, D84:014016, 2011.

[143] Mark G. Alford, Krishna Rajagopal, and Frank Wilczek. Color flavor locking and chiral symmetry breaking in high density QCD. *Nucl. Phys.*, B537:443–458, 1999.

[144] Mark Alford, Chris Kouvaris, and Krishna Rajagopal. Gapless color flavor locked quark matter. *Phys. Rev. Lett.*, 92:222001, 2004.

[145] Krishna Rajagopal and Andreas Schmitt. Stressed pairing in conventional color superconductors is unavoidable. *Phys. Rev.*, D73:045003, 2006.

[146] Efrain J. Ferrer and Vivian de la Incera. Magnetic fields boosted by gluon vortices in color superconductivity. *Phys. Rev. Lett.*, 97:122301, 2006.

[147] Efrain J. Ferrer and Vivian de la Incera. Chromomagnetic Instability and Induced Magnetic Field in Neutral Two-Flavor Color Superconductivity. *Phys. Rev.*, D76:114012, 2007.

[148] E. V. Gorbar. On color superconductivity in external magnetic field. *Phys. Rev.*, D62:014007, 2000.

[149] Mark G. Alford, Juergen Berges, and Krishna Rajagopal. Magnetic fields within color superconducting neutron star cores. *Nucl. Phys.*, B571:269–284, 2000.

[150] Mei Huang and Igor Shovkovy. Gapless color superconductivity at zero and at finite temperature. *Nucl. Phys.*, A729:835–863, 2003.

[151] Amruta Mishra and Hiranmaya Mishra. Color superconducting 2SC+s quark matter and gapless modes at finite temperatures. *Phys. Rev.*, D71:074023, 2005.

[152] Tanumoy Mandal, Prashanth Jaikumar, and Sanatan Digal. Chiral and Diquark condensates at large magnetic field in two-flavor superconducting quark matter. 2009.

[153] Tanumoy Mandal and Prashanth Jaikumar. Neutrality of a magnetized two-flavor quark superconductor. *Phys. Rev.*, C87:045208, 2013.

[154] Tanumoy Mandal and Prashanth Jaikumar. Effect of temperature and magnetic field on two-flavor superconducting quark matter. *Phys. Rev.*, D94(7):074016, 2016.

[155] M. Coppola, P. Allen, A. G. Grunfeld, and N. N. Scoccola. Magnetized color superconducting quark matter under compact star conditions: Phase structure within the SU(2)f NJL model. *Phys. Rev.*, D96(5):056013, 2017.

[156] M. de J. Anguiano-Galicia, A. Bashir, and A. Raya. Anti-psi psi-condensate in constant magnetic fields. *Phys. Rev.*, D76:127702, 2007.

[157] Amruta Mishra and Hiranmaya Mishra. Chiral symmetry breaking, color superconductivity and color neutral quark matter: A Variational approach. *Phys. Rev.*, D69:014014, 2004.

[158] Hiranmaya Mishra and Jitendra C. Parikh. Chiral symmetry breaking, color superconductivity and equation of state at high density: A Variational approach. *Nucl. Phys.*, A679:597–615, 2001.

[159] A. Mishra and S. P. Misra. Gluon condensates, chiral symmetry breaking and pion wave function. *Z. Phys.*, C58:325–332, 1993.

[160] S. P. Misra. Indian j. phys. 70a, 355 (1996). 1996.

[161] H. Mishra and S. P. Misra. Chiral symmetry breaking and pion wave function. *Phys. Rev.*, D48:5376–5381, 1993.

[162] H. Umezawa, H. Matsumoto, and M. Tachiki. *THERMO FIELD DYNAMICS AND CONDENSED STATES.* 1982.

[163] P. A. Henning. Thermo field dynamics for quantum fields with continuous mass spectrum. *Phys. Rept.*, 253:235–380, 1995.

[164] Amruta Mishra and Hiranmaya Mishra. Vacuum structure and effective potential at finite temperature: A Variational approach. *J. Phys.*, G23:143–150, 1997.

[165] Max A. Metlitski and Ariel R. Zhitnitsky. Anomalous axion interactions and topological currents in dense matter. *Phys. Rev.*, D72:045011, 2005.

[166] Amruta Mishra and Hiranmaya Mishra. Color superconductivity with determinant interaction in strange quark matter. *Phys. Rev.*, D74:054024, 2006.

[167] Mark G. Alford and Armen Sedrakian. Color-magnetic flux tubes in quark matter cores of neutron stars. *J. Phys.*, G37:075202, 2010.

[168] Andrew W. Steiner. The Color-superconducting 't Hooft interaction. *Phys. Rev.*, D72:054024, 2005.

[169] F. Gastineau, R. Nebauer, and J. Aichelin. Thermodynamics of the three flavor NJL model: Chiral symmetry breaking and color superconductivity. *Phys. Rev.*, C65:045204, 2002.

[170] L.P. Gorkov A.A. Abrikosov. Zh. eskp. teor.39, 1781,1960. 1960.

[171] Mark G. Alford, Juergen Berges, and Krishna Rajagopal. Gapless color superconductivity. *Phys. Rev. Lett.*, 84:598–601, 2000.

[172] E. Elizalde. , j. phys. math. gen. 18,1637 (1985). 1985.

[173] Stefan B. Rster, Verena Werth, Michael Buballa, Igor A. Shovkovy, and Dirk H. Rischke. Phase diagram of neutral quark matter at moderate densities. *Ser. Adv. Quant. Many Body Theor.*, 8:63–89, 2006.

[174] Stefan B. Ruester, Igor A. Shovkovy, and Dirk H. Rischke. Phase diagram of dense neutral three-flavor quark matter. *Nucl. Phys.*, A743:127–146, 2004.

[175] Klaus Schertler, Stefan Leupold, and Jurgen Schaffner-Bielich. Neutron stars and quark phases in the NJL model. *Phys. Rev.*, C60:025801, 1999.

[176] Florian Preis, Anton Rebhan, and Andreas Schmitt. Inverse magnetic catalysis in dense holographic matter. *JHEP*, 03:033, 2011.

[177] Ioannis Giannakis and Hai-Cang Ren. Chromomagnetic instability and the LOFF state in a two flavor color superconductor. *Phys. Lett.*, B611:137–146, 2005.

[178] Mei Huang and Igor A. Shovkovy. Screening masses in neutral two-flavor color superconductor. *Phys. Rev.*, D70:094030, 2004.

[179] Kenji Fukushima. Analytical and numerical evaluation of the Debye and Meissner masses in dense neutral three-flavor quark matter. *Phys. Rev.*, D72:074002, 2005.

[180] Krishna Rajagopal and Rishi Sharma. The Crystallography of Three-Flavor Quark Matter. *Phys. Rev.*, D74:094019, 2006.

[181] Jeffrey A. Bowers and Krishna Rajagopal. The Crystallography of color superconductivity. *Phys. Rev.*, D66:065002, 2002.

[182] Gordon Baym, Tetsuo Hatsuda, Toru Kojo, Philip D. Powell, Yifan Song, and Tatsuyuki Takatsuka. From hadrons to quarks in neutron stars: a review. *Rept. Prog. Phys.*, 81(5):056902, 2018.

[183] N. Itoh. Hydrostatic Equilibrium of Hypothetical Quark Stars. *Prog. Theor. Phys.*, 44:291, 1970.

[184] Takumi Muto, Ryozo Tamagaki, and Toshitaka Tatsumi. A Chiral symmetry approach to meson condensations. *Prog. Theor. Phys. Suppl.*, 112:159–196, 1993.

[185] Mark G. Alford, Andreas Schmitt, Krishna Rajagopal, and Thomas Schfer. Color superconductivity in dense quark matter. *Rev. Mod. Phys.*, 80:1455–1515, 2008.

[186] Kei Iida and Gordon Baym. The Superfluid phases of quark matter: Ginzburg-Landau theory and color neutrality. *Phys. Rev.*, D63:074018, 2001. [Erratum: Phys. Rev.D66,059903(2002)].

[187] Debades Bandyopadhyay, Somenath Chakrabarty, and Subrata Pal. The Quantizing magnetic field and quark - hadron phase transition in a neutron star. *Phys. Rev. Lett.*, 79:2176–2179, 1997.

[188] G. Chanmugam. Magnetic fields of degenerate stars. *Ann. Rev. Astron. Astrophys.*, 30:143–184, 1992.

[189] Tomoyuki Maruyama and Toshitaka Tatsumi. Ferromagnetism of nuclear matter in the relativistic approach. *Nucl. Phys.*, A693:710–730, 2001.

[190] V. R. Pandharipande, V. K. Garde, and J. K. Srivastava. The magnetic susceptibility of dense neutron matter. *Phys. Lett.*, 38B:485–486, 1972.

[191] R. Niembro, S. Marcos, M. L. Quelle, and J. Navarro. Magnetic susceptibility of neutron matter in a relativistic approach. *Phys. Lett.*, B249:373–376, 1990.

[192] S. Marcos, R. Niembro, M. L. Quelle, and J. Navarro. Magnetic susceptibility of neutron matter in a relativistic sigma + omega + pi + rho Hartree-Fock approach. *Phys. Lett.*, B271:277–280, 1991.

[193] T. Maruyama, E. Nakano, and T. Tatsumi. Horizons inworld physics (nova science, ny, 2011),vol.276, chap.7. 2011.

[194] Hiroaki Matsuoka, Yasuhiko Tsue, Joao da Providencia, Constancia Providencia, and Masatoshi Yamamura. Spin polarization and color superconductivity in the NambuJona-Lasinio model at finite temperature. *Phys. Rev.*, D95(5):054025, 2017.

[195] Hiroaki Matsuoka, Yasuhiko Tsue, Joo da Providncia, Constana Providncia, Masatoshi Yamamura, and Henrik Bohr. Spin-polarized versus chiral condensate in quark matter at finite temperature and density. *PTEP*, 2016(5):053D02, 2016.

[196] Masatoshi Morimoto, Yasuhiko Tsue, J. da Providencia, C. Providencia, and Masatoshi Yamamura. Spontaneous magnetization under a pseudovector interaction between quarks in high density quark matter. *Int. J. Mod. Phys.*, E27(04):1850028, 2018.

[197] E. Nakano and T. Tatsumi. Chiral symmetry and density wave in quark matter. *Phys. Rev.*, D71:114006, 2005.

[198] H. Bohr, P. K. Panda, C. Providencia, and J. D. Providencia. Int. j. mod. phys. e 22, no.4, 1350019 (2013). 2013.

[199] U. Vogl and W. Weise. The Nambu and Jona Lasinio model: Its implications for hadrons and nuclei. *Prog. Part. Nucl. Phys.*, 27:195–272, 1991.

[200] J. Mueller and S. P. Klevansky. Chiral perturbation theory and the SU(2) Nambu-Jona-Lasinio model: A Comparison. *Phys. Rev.*, C50:410–422, 1994.

[201] S. P. Klevansky. The Nambu-Jona-Lasinio model of quantum chromodynamics. *Rev. Mod. Phys.*, 64:649–708, 1992.

[202] Hiroaki Kohyama, Diji Kimura, and Tomohiro Inagaki. Parameter fitting in three-flavor NambuJona-Lasinio model with various regularizations. *Nucl. Phys.*, B906:524–548, 2016.

[203] H. Kohyama, D. Kimura, and T. Inagaki. Regularization dependence on phase diagram in NambuJona-Lasinio model. *Nucl. Phys.*, B896:682–715, 2015.

[204] M. Jaminon and E. Ruiz Arriola. Vector mesons from tensor couplings in the NJL model. *Phys. Lett.*, B443:33–39, 1998.

[205] M. Jaminon, M. C. Ruivo, and C. A. de Sousa. Pion and rho meson observables in a Nambu-Jona-Lasinio model including a tensor interaction. *Int. J. Mod. Phys.*, A17:4903–4925, 2002.

[206] O. A. Battistel, T. H. Pimenta, and G. Dallabona. Phenomenological implications of a predictive formulation of the NambuJona-Lasinio model having tensor couplings and isospin symmetry breaking terms. *Phys. Rev.*, D94(8):085011, 2016.

[207] Shijun Mao and Dirk H. Rischke. Dynamically generated magnetic moment in the Wigner-function formalism. *Phys. Lett.*, B792:149–155, 2019.

List of Publications

Thesis Related Publications

- **Aman Abhishek**, Hiranmaya Mishra, "Chiral symmetry breaking, color superconductivity, and equation of state for magnetized strange quark matter", Phys. Rev. D 99,054016(2019), DOI:10.1103/PhysRevD.99.054016, arXiv:1810.09276 [hep-ph]

- **Aman Abhishek**, Hiranmaya Mishra, Sabyasachi Ghosh, "Transport Coefficients in Polyakov Quark Meson coupling model: a relaxation time approximation", PRD97,014005(2018), DOI: 10.1103/PhysRevD.97.014005, arXiv:1709.08013 [hep-ph]

- **Aman Abhishek**, Arpan Das, Hiranmaya Mishra, Ranjita K. Mohapatra, "Spin Polarization and Chiral Condensation in 2+1 flavor Nambu-Jona-Lasinio model at finite temperature and baryon chemical potential", arXiv: 1812:10238

Attached with thesis

- Pracheta Singha, Aman Abhishek, Guru Kadam, Sabyasachi Ghosh, Hiranmaya Mishra, "Calculations of Shear, Bulk viscosities and Electrical Conductivity in Polyakov-Quark-Meson model", J.Phys. G46(2019), 015201. DOI:10.1088/1361-6471/aaf256, arXiv:1705.03084 [nucl-th]
- Sabyasachi Ghosh, Fernando E. Serna, Aman Abhishek, Gastao Krein, Hiranmaya Mishra, "Transport responses from rate of decay and scattering processes in the NambuJona-Lasinio model" , Phys. Rev. D 99, 014004(2019). DOI: 10.1103/PhysRevD.99.014004, arXiv:1809.07594 [nucl-th]
- Aman Abhishek, Hiranmaya Mishra, Sabyasachi Ghosh, "Transport coefficients in Polyakov loop quark meson coupling model: a quasiparticle approach", Published in Proceeding of Science(PoS) Critical Point and Onset of Deconfinement(CPOD) 2017 (2018) 080, DOI:10.22323/1.311.0080
- Balbeer Singh, Aman Abhishek, Santosh K. Das, Hiranmaya Mishra, "Heavy Quark Diffusion in a Polyakov loop plasma", arXiv: 1812.05263

Transport coefficients in the Polyakov quark meson coupling model: A relaxation time approximation

Aman Abhishek[1,2,*] and Hiranmaya Mishra[1,†]

[1]*Theory Division, Physical Research Laboratory, Navrangpura, Ahmedabad 380 009, India*
[2]*Indian Institute of Technology Gandhinagar, Gandhinagar 382355, Gujarat, India*

Sabyasachi Ghosh[3]

[3]*Department of Physics, University of Calcutta, 92, A.P.C. Road, Kolkata 700009, India*

(Received 4 October 2017; published 12 January 2018)

We compute the transport coefficients, namely, the coefficients of shear and bulk viscosities, as well as thermal conductivity for hot and dense matter. The calculations are performed within the Polyakov quark meson model. The estimation of the transport coefficients is made using the Boltzmann kinetic equation within the relaxation time approximation. The energy-dependent relaxation time is estimated from meson-meson scattering, quark-meson scattering, and quark-quark scattering within the model. In our calculations, the shear viscosity to entropy ratio and the coefficient of thermal conductivity show a minimum at the critical temperature, while the ratio of bulk viscosity to entropy density exhibits a peak at this transition point. The effect of confinement modeled through a Polyakov loop potential plays an important role both below and above the critical temperature.

DOI: 10.1103/PhysRevD.97.014005

I. INTRODUCTION

Transport coefficients of matter under extreme conditions of temperature, density, or external fields are interesting for several reasons. In the context of relativistic heavy ion collisions, these properties enter as dissipative coefficients in the hydrodynamic evolution of the quark gluon plasma that is produced following the collision [1–5]. Indeed, an extremely low value of the shear viscosity-to-entropy ratio (η/s) is needed to successfully describe the collective dynamics of the quark gluon matter at high temperature and vanishing chemical potential to explain the elliptic flow data [6,7]. At intermediate densities, near the chiral phase transition, which is being probed at the Facility for antiproton and Ion Research (FAIR) program at Geselleschaft fuer Schwerionenforschung (GSI)–[8] and the Nuclotron-based Ion Collider fAcility (NICA) program at Joint Institute for Nuclear Research(JINR)–[9] motivates us to understand the behavior of transport coefficients at finite chemical potential and temperature. Further, in the low-temperature and high-density regime, the matter could be in one of the possible types of color superconducting phases of which the transport properties also need to be understood [10,11]. The cooling of neutron stars at short time scales constrains the thermal conductivity [12,13], while the cooling through neutrino emission on much larger time scales constrains the phase of the matter in the interior of the compact star [14,15]. Further, the observable regarding the viscosity of the such matter is the r-mode instability. In the absence of viscous damping, the fluid in the rotating star becomes unstable to a mode that is coupled to gravity and radiates away the angular momentum of the star [16,17]. Apart from the wide variety of applications of the transport coefficients of strongly interacting matter, their temperature and chemical potential dependence may also be indicative of a phase transition [18].

Transport coefficients for QCD matter in principle can be calculated using Kubo formulation [19]. However, QCD is strongly interacting for both at energies accessible in heavy ion collision experiments as well as for the densities expected to be there in the core of the neutron stars making the perturbative estimations unreliable. Calculations using lattice QCD simulations at finite chemical potential are also challenging and are limited only to the equilibrium thermodynamic properties at small chemical potentials.

The understanding of the elliptic flow in relativistic heavy ion collisions using hydrodynamics with a low (η/s) and its connection to the conjectured lower bound ($\eta/s > 1/4\pi$) using ADS/CFT correspondence [20] stimulated extensive investigation of this ratio for QCD matter. These have been studied using perturbative QCD [21],

*aman@prl.res.in
†hm@prl.res.in

transport simulations of the Boltzmann equation [22,23], relaxation time approximation for solving the Boltzmann equations [24–27], and lattice simulation of QCD [28]. Most of these calculations have been performed at vanishing baryon density. The general variation of this ratio with temperature in most of these studies shows a minimum at the transition temperature. The numerical value of η at the minimum, however, differs by an order of magnitude. For example, near transition temperature, Refs. [29–33] have predicted η of order 0.001 GeV^3, $\eta = 0.002$–$0.003\ \mathrm{GeV}^3$, while Ref. [34] predicts a value of $\eta \simeq 0.4\ \mathrm{GeV}^3$. Further, the behavior of η/s shows a monotonic decrease in the Nambu–Jona-Lasinio (NJL) model in Ref. [35].

The bulk viscosity coefficient ζ has also been estimated in various effective models as well as in lattice QCD. The rise of the bulk viscosity coefficient near the transition temperature has been observed in these effective models such as chiral perturbation theory [36], quasiparticle models [37], the linear sigma model [38], and the Nambu–Jona-Lasinio model [24,25]. Large bulk viscosity of matter produced in relativistic heavy ion collisions can give rise to different interesting phenomenon such as cavitation where pressure vanishes and hydrodynamic description of evolution becomes invalid [39]. Here, again, the numerical values of the bulk viscosity coefficients vary widely from 10^{-5} [40] to $10^{-2}\ \mathrm{GeV}^3$ [24].

The other transport coefficient that is important at finite baryon density is the coefficient of thermal conductivity λ [41–43]. The effects of thermal conductivity in relativistic hydrodynamics have been discussed recently in Refs. [43,44]. This coefficient has been evaluated in various effective models like the Nambu–Jona-Lasinio model using the Green-Kubo approach [45], relaxation time approximation [25], and the instanton liquid model [46]. The results, however, vary over a wide range of values, with $\lambda = 0.008\ \mathrm{GeV}^{-2}$ as in Ref. [31] to $\lambda \sim 10\ \mathrm{GeV}^{-2}$ as in Ref. [35] for a range of temperatures ($0.12\ \mathrm{GeV} < T < 0.17\ \mathrm{GeV}$), which has been nicely tabulated in Ref. [47].

We shall attempt here to estimate these transport coefficients within an effective model of strong interaction, the Polyakov loop extended quark meson (PQM) model. It has become quite popular during last few years due to its close relationship with the linear sigma model that captures the chiral symmetry breaking aspect while being in agreement with the lattice QCD results for thermodynamics at vanishing baryon density. The physics of confinement is taken care of at least partially by coupling the quark field to the Polyakov loops so that quark excitations are suppressed below the transition temperature. Let us note that the transport coefficients like bulk viscosity apart from the distribution functions also depend upon the bulk thermodynamic quantities like the velocity of sound. We wish to explore the effects of such nonperturbative properties on the transport coefficients.

The transport coefficients are evaluated within the relaxation time approximation of the Boltzmann equation. The relaxation time is calculated by evaluating the scattering rates of the particles in the model, namely, the quarks and pion and sigma mesons, with their respective medium-dependent masses. The scattering processes considered here are meson scatterings as considered in Ref. [38], quark scattering through meson exchanges as in Refs. [24,25,35] and quark-meson scattering. As we shall see in the following, each of these processes brings out distinct features for the transport coefficients. We would like to mention here that these coefficients have also been estimated using Kubo formulation through one-loop self-energies for quarks and mesons in a separate work [48].

We organize the present investigation as follows. In the following section, we discuss the two-flavor PQM model thermodynamics. The reason is that the expressions for transport coefficients involve meson masses which are medium dependent. Further, some transport coefficients like the bulk viscosity involves bulk thermodynamical properties such as energy density, pressure and the velocity of sound. As the order parameters for chiral and confinement-deconfinement transitions are coupled, this leads to nontrivial relations for derivatives of the thermodynamic potential with respect to external parameters like chemical potential or temperature as the mean fields themselves are also medium dependent. Furthermore, the implicit dependence of these mean fields/order parameters are calculated here analytically to avoid possible numerical errors. In Sec. III, we give the expressions for the transport coefficients in terms of relaxation time and estimate them to finally give the results for these coefficients. We also compare them with the same obtained with alternate approaches like the NJL model so that the effects of the confinement-deconfinement transition modeled through the Polyakov loop potential are explicitly seen. Finally, we summarize and draw the conclusions of the present investigation in Sec. IV.

II. THERMODYNAMICS OF PQM MODEL

We shall adopt here an effective model that captures two important features of QCD, namely, chiral symmetry breaking and its restoration at high temperature and/densities as well as the confinement-deconfinement transitions. Two such effective models have become popular recently—the Polyakov loop extended Nambu–Jona-Lasinio model and the PQM. These models are extensions, respectively, of the NJL model and linear sigma model that captures various aspects of chiral symmetry breaking pattern of strong interaction physics. Explicitly, the Lagrangian of the PQM model is given by [49–53]

$$\mathcal{L} = \bar{\psi}(i\gamma^\mu D_\mu - m - g_\sigma(\sigma + i\gamma_5 \boldsymbol{\tau}\cdot\boldsymbol{\pi}))\psi + \frac{1}{2}[\partial_\mu\sigma\partial^\mu\sigma + \partial_\mu\boldsymbol{\pi}\partial^\mu\boldsymbol{\pi}] - U_\chi(\sigma,\boldsymbol{\pi}) - U_P(\phi,\bar{\phi}). \quad (1)$$

In the above, the first term is the kinetic and interaction term for the quark doublet $\psi = (u, d)$ interacting with the scalar (σ) and the isovector pseudoscalar pion ($\boldsymbol{\pi}$) field. The scalar field σ and the pion field $\boldsymbol{\pi}$ together form an SU(2) isovector field. The quark field is also coupled to a spatially constant temporal gauge field A_0 through the covariant derivative $D_\mu = \partial_\mu - ieA_\mu$; $A_\mu = \delta_{\mu 0}A_\mu$.

The mesonic potential $U_\chi(\sigma, \pi)$ essentially describes the chiral symmetry breaking pattern in strong interaction and is given by

$$U_\chi(\sigma, \boldsymbol{\pi}) = \frac{\lambda}{4}(\sigma^2 + \boldsymbol{\pi}^2 - v^2)^2 - c\sigma. \tag{2}$$

The last term in the Lagrangian in Eq. (1) is responsible for including the physics of color confinement in terms of a potential energy for the expectation value of the Polyakov loop ϕ and $\bar{\phi}$, which are defined in terms of the Polyakov loop operator, which is a Wilson loop in the temporal direction,

$$\mathcal{P} = P\exp\left(i\int_0^\beta dx_0 A_0(x_0, \mathbf{x})\right). \tag{3}$$

In the Polyakov gauge, A_0 is time independent and is in the Cartan subalgebra, i.e., $A_0^a = A_0^3\lambda_3 + A_0^8\lambda_8$. One can perform the integration over the time variable trivially as path ordering becomes irrelevant so that $\mathcal{P}(\mathbf{x}) = \exp(\beta A_0)$. The Polyakov loop variable ϕ and its Hermitian conjugate $\bar{\phi}$ are defined as

$$\phi(\mathbf{x}) = \frac{1}{N_c}\mathrm{Tr}\mathcal{P}(\mathbf{x}) \quad \bar{\phi}(\mathbf{x}) = \frac{1}{N_c}\mathcal{P}^\dagger(\mathbf{x}). \tag{4}$$

In the limit of heavy quark mass, the confining phase is center symmetric, and therefore $\langle\phi\rangle = 0$, while for the deconfined phase, $\langle\phi\rangle \neq 0$. Finite quark masses break this symmetry explicitly. The explicit form of the potential $U_p(\phi, \bar{\phi})$ is not known from first principle calculations. The common strategy is to choose a functional form of the potential that reproduces the pure gauge lattice simulation thermodynamic results. Several forms of this potential have been suggested in the literature. We shall use here the polynomial parametrization [49]

$$U_P(\phi, \bar{\phi}) = T^4\left[-\frac{b_2(T)}{2}\bar{\phi}\phi - \frac{b_3}{2}(\phi^3 + \bar{\phi}^3) + \frac{b_4}{4}(\bar{\phi}\phi)^2\right] \tag{5}$$

with the temperature-dependent coefficient b_2 given as

$$b_2(T) = a_0 + a_1\left(\frac{T_0}{T}\right) + a_2\left(\frac{T_0}{T}\right)^2 + a_3\left(\frac{T_0}{T}\right)^3. \tag{6}$$

The numerical values of the parameters are

$$\begin{aligned} a_0 &= 6.75, \quad a_1 = -1.95, \\ a_2 &= 2.625, \quad a_3 = -7.44 \end{aligned} \tag{7}$$

$$b_3 = 0.75, \qquad b_4 = 7.5. \tag{8}$$

The parameter T_0 corresponds to the transition temperature of Yang-Mills theory. However, for the full dynamical QCD, there is a flavor dependence on $T_0(N_f)$. For two flavors, we take it to be $T_0(2) = 192$ MeV as in Ref. [49].

The Lagrangian in Eq. (1) is invariant under $SU(2)_L \times SU(2)_R$ transformation when the explicit symmetry breaking term $c\sigma$ vanishes in the potential U_χ in Eq. (2). The parameters of the potential U_χ are chosen such that the chiral symmetry is spontaneously broken in the vacuum. The expectation values of the meson fields in vacuum are $\langle\sigma\rangle = f_\pi$ and $\langle\boldsymbol{\pi}\rangle = 0$. Here, $f_\pi = 93$ MeV is the pion decay constant. The coefficient of the symmetry breaking linear term is decided from the partial conservation of the axial vector current as $c = f_\pi m_\pi^2$, $m_\pi = 138$ MeV, being the pion mass. Then, minimizing the potential, one has $v^2 = f_\pi^2 - m_\pi^2/\lambda$. The quartic coupling for the meson λ is determined from the mass of the sigma meson given as $m_\sigma^2 = m_\pi^2 + 2\lambda f_\pi^2$. In the present work, we take $m_\sigma = 600$ MeV, which gives $\lambda = 19.7$. The coupling g_σ is fixed here from the constituent quark mass in vacuum $M_q = g_q f_\pi$, which has to be about one-third of nucleon mass that leads to $g_\sigma = 3.3$ [54].

To calculate the bulk thermodynamical properties of the system, we use a mean field approximation for the meson and the Polyakov fields while retaining the quantum and thermal fluctuations of the quark fields. The thermodynamic potential can then be written as

$$\Omega(T, \mu) = \Omega_{\bar{q}q} + U_\chi + U_P(\phi, \bar{\phi}). \tag{9}$$

The fermionic part of the thermodynamic potential is given as

$$\Omega_{\bar{q}q} = -2N_f T\int\frac{d^3p}{(2\pi)^3}[\ln(1 + 3(\phi + \bar{\phi}e^{-\beta\omega_-})e^{-\beta\omega_-} + e^{-3\beta\omega_-}) + \ln(1 + 3(\phi + \bar{\phi}e^{-\beta\omega_+})e^{-\beta\omega_+} + e^{-3\beta\omega_+})] \tag{10}$$

modulo a divergent vacuum part. In the above, $\omega_\mp = E_p \mp \mu$, with the single particle quark/antiquark energy $E_p = \sqrt{\mathbf{p}^2 + M^2}$. The constituent quark/antiquark mass is defined to be

$$M^2 = g_\sigma^2(\sigma^2 + \pi^2). \tag{11}$$

The divergent vacuum part arises from the negative energy states of the Dirac sea. Using standard renormalization, it can be partly absorbed in the coupling λ and v^2.

However, a logarithmic correction from the renormalization scale remains, and we neglect it in the calculations that follow [54].

The mean fields are obtained by minimizing Ω with respect to σ, ϕ, $\bar{\phi}$, and π. Extremizing the effective potential with respect to the σ field leads to

$$\lambda(\sigma^2 + \pi^2 - v^2) - c + g_\sigma \rho_s = 0, \tag{12}$$

where the scalar density $\rho_s = -\langle \bar{\psi}\psi \rangle$ is given by

$$\rho_s = 6N_f g_\sigma \sigma \int \frac{d\mathbf{p}}{(2\pi)^3} \frac{1}{E_P}[f_-(\mathbf{p}) + f_+(\mathbf{p})]. \tag{13}$$

In the above, $f_\mp(\mathbf{p})$ are the distribution functions for the quarks and antiquarks given as

$$f_-(\mathbf{p}) = \frac{\phi e^{-\beta\omega_-} + 2\bar{\phi} e^{-2\beta\omega_-} + e^{-3\beta\omega_-}}{1 + 3\phi e^{-\beta\omega_-} + 3\bar{\phi} e^{-2\beta\omega_-} + e^{-3\beta\omega_-}} \tag{14}$$

and

$$f_+(\mathbf{p}) = \frac{\bar{\phi} e^{-\beta\omega_+} + 2\phi e^{-2\beta\omega_+} + e^{-3\beta\omega_+}}{1 + 3\bar{\phi} e^{-\beta\omega_+} + 3\phi e^{-2\beta\omega_+} + e^{-3\beta\omega_+}}. \tag{15}$$

The condition $\frac{\partial\Omega}{\partial\phi} = 0$ leads to

$$T^4\left[-\frac{b_2}{2}\bar{\phi} - \frac{b_3}{2}\phi^2 + \frac{b_4}{2}\bar{\phi}\phi\bar{\phi}\right] + I_\phi = 0, \tag{16}$$

where

$$I_\phi = \frac{\partial\Omega_{\bar{q}q}}{\partial\phi} = -6N_f T \int \frac{d\mathbf{p}}{(2\pi)^3} \times \left[\frac{e^{-\beta\omega_-}}{1 + 3\phi e^{-\beta\omega_-} + 3\bar{\phi} e^{-2\beta\omega_-} + e^{-3\beta\omega_-}} + \frac{e^{-2\beta\omega_+}}{1 + 3\bar{\phi} e^{-\beta\omega_+} + 3\phi e^{-2\beta\omega_+} + e^{-3\beta\omega_+}}\right]. \tag{17}$$

Similarly, $\frac{\partial\Omega}{\partial\bar{\phi}} = 0$ leads to

$$T^4\left[-\frac{b_2}{2}\phi - \frac{b_3}{2}\bar{\phi}^2 + \frac{b_4}{2}\bar{\phi}\phi^2\right] + I_{\bar{\phi}} = 0 \tag{18}$$

with

$$I_{\bar{\phi}} = \frac{\partial\Omega_{\bar{q}q}}{\partial\bar{\phi}} = -6N_f T \int \frac{d\mathbf{p}}{(2\pi)^3} \times \left[\frac{e^{-2\beta\omega_-}}{1 + 3\phi e^{-\beta\omega_-} + 3\bar{\phi} e^{-2\beta\omega_-} + e^{-3\beta\omega_-}} + \frac{e^{-\beta\omega_+}}{1 + 3\phi e^{-\beta\omega_+} + 3\bar{\phi} e^{-2\beta\omega_+} + e^{-3\beta\omega_+}}\right]. \tag{19}$$

Finally, minimization of the effective potential with respect to π fields leads to

$$\frac{\partial\Omega}{\partial\pi} = \lambda(\sigma^2 + \pi^2 - v^2)\pi + g\rho_{ps} = 0, \tag{20}$$

where the pseudoscalar density can be expressed as

$$\rho_{ps} = \langle \bar{q}\imath\gamma_5\tau q\rangle = 6N_f g_\sigma \pi \int \frac{d\mathbf{p}}{(2\pi)^3}\frac{1}{E_P}[f_-(\mathbf{p}) + f_+(\mathbf{p})]. \tag{21}$$

The σ and π masses are determined by the curvature of Ω at the global minimum

$$M_\sigma^2 = \frac{\partial^2\Omega}{\partial\sigma^2}, \qquad M_{\pi_i}^2 = \frac{\partial^2\Omega}{\partial\pi_i^2}. \tag{22}$$

These equations lead to the masses for the σ and pions given as

$$M_\sigma^2 = m_\pi^2 + \lambda(3\sigma^2 - f_\pi^2) + g_\sigma^2 \frac{\partial\rho_s}{\partial\sigma} \tag{23}$$

$$M_\pi^2 = m_\pi^2 + \lambda(\sigma^2 - f_\pi^2) + g_\sigma^2 \frac{\partial\rho_{ps}}{\partial\pi}. \tag{24}$$

Explicitly, using Eq. (13),

$$\frac{\partial\rho_s}{\partial\sigma} = \frac{6}{\pi^2}\int dp\, p^2 \times \left[\frac{g_\sigma p^2}{E(\mathbf{p})^3}(f_-(\mathbf{p}) + f_+(\mathbf{p})) + \frac{M}{E(\mathbf{p})}\left(\frac{\partial f_-}{\partial\sigma} + \frac{\partial f_+}{\partial\sigma}\right)\right]. \tag{25}$$

The derivatives of the distribution functions with respect to the scalar field σ are given as

$$\frac{\partial f_-(\mathbf{p})}{\partial\sigma} = \frac{\beta g_\sigma^2\sigma}{E(\mathbf{p})}\left[3f_-^2 - \frac{3e^{-3\beta\omega_-} + 4\bar{\phi} e^{-2\beta\omega_-} + \phi e^{-\beta\omega_-}}{1 + 3\phi e^{-\beta\omega_-} + 3\bar{\phi} e^{-2\beta\omega_-} + e^{-3\beta\omega_-}}\right] \tag{26}$$

and

$$\frac{\partial f_+}{\partial\sigma} = \frac{\beta g_\sigma^2\sigma}{E(\mathbf{p})}\left[3f_+^2 - \frac{3e^{-3\beta\omega_+} + 4\phi e^{-2\beta\omega_+} + \bar{\phi} e^{-\beta\omega_+}}{1 + 3\bar{\phi} e^{-\beta\omega_+} + 3\phi e^{-2\beta\omega_+} + e^{-3\beta\omega_+}}\right]. \tag{27}$$

Similarly, using Eq. (21),

$$\frac{\partial\rho_{ps}}{\partial\pi} = \frac{6}{\pi^2}\int dp \frac{p^2}{E(\mathbf{p})}[f_-(\mathbf{p}) + f_+(\mathbf{p})]. \tag{28}$$

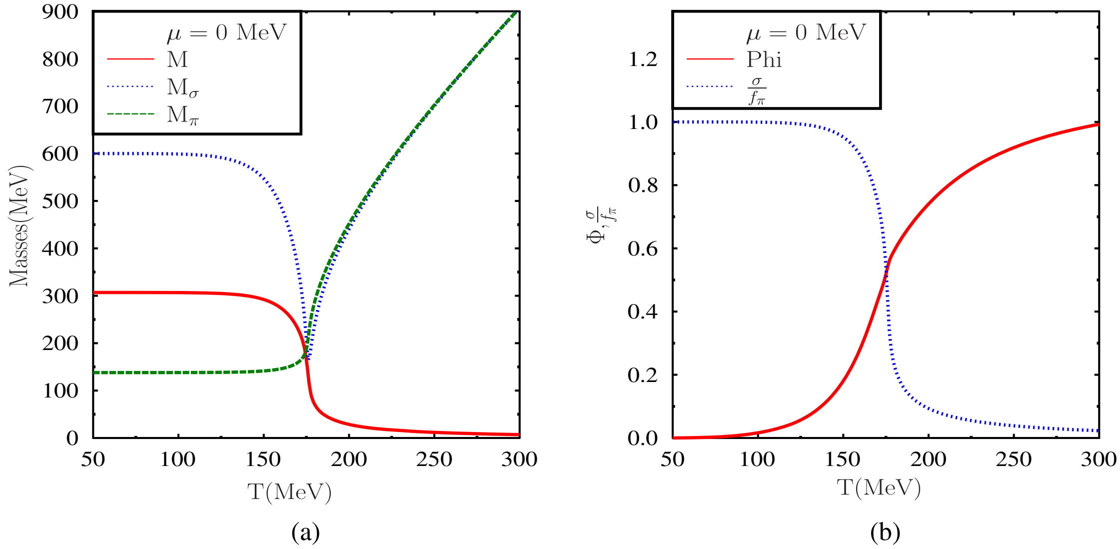

FIG. 1. (a) Temperature dependence of the masses of constituent quarks (M) and pions (M_π) and sigma mesons (M_σ) and (b) the order parameters σ and ϕ as a function of temperature for $\mu = 0$ MeV.

In the above, we have set the expectation value of the pion field to be zero, i.e., $\boldsymbol{\pi} = 0$, so that the constituent quark mass is $M^2 = g_\sigma^2 \sigma^2$.

The net quark density is given by

$$n = -\frac{\partial \Omega}{\partial \mu} = \frac{6}{\pi^2} \int p^2 dp [f_-(\mathbf{p}) - f_+(\mathbf{p})] \tag{29}$$

The energy density $\epsilon = \Omega - T \partial\Omega/\partial T + \mu \rho_q$ is given by

$$\epsilon = \frac{6}{\pi^2} \int p^2 dp E(\mathbf{p})(f_-(\mathbf{p}) + f_+(\mathbf{p})) + U_\chi - 3U_P(\phi, \bar{\phi}) + \frac{T^5}{2} \frac{db_2(T)}{dT} \bar{\phi}\phi. \tag{30}$$

In Fig. 1(a), we have plotted the constituent quark mass and the meson masses as given in Eqs. (23) and (24) as a function of temperature for vanishing baryon density. In the chirally broken phase, the pion mass, being the mass of an approximate Goldstone mode, is protected and varies weakly with temperature. On the other hand, the mass of σ, M_σ, which is approximately twice the constituent quark mass, M, drops significantly near the crossover temperature. At high temperature, being chiral partners, the masses of the σ and π mesons become degenerate and increase linearly with temperature. In Fig. 1(b), we have plotted the order parameters σ and ϕ as a function of temperature for the vanishing quark chemical potential. We also note that for $\mu = 0$ the order parameters ϕ and $\bar{\phi}$ are the same. Because of the approximate chiral symmetry, the chiral order parameter decreases with temperatures to small values but never vanishes. The Polyakov loop parameter, on the other hand, grows from $\phi = 0$ at zero temperature to about $\phi = 1$ at high temperatures. We might mention here that at very high temperature the value of the Polyakov loop parameter exceeds unity, the value in the infinite quark mass limit.

Next, in Fig. 2, we show the dependence of the trace anomaly $(\epsilon - 3p)/T^4$ on temperature. The conformal symmetry is broken maximally at the critical temperature. Further, finite chemical potential enhances this breaking as it breaks scale symmetry explicitly. As we shall see later, this will have its implication on the bulk viscosity coefficients.

Next, to discuss critical behavior as well as to calculate different thermodynamic quantities, one has to take derivatives of the thermodynamic potential with respect to the mean fields as well as the parameters like temperature and the chemical potential. Vanishing of the first-order

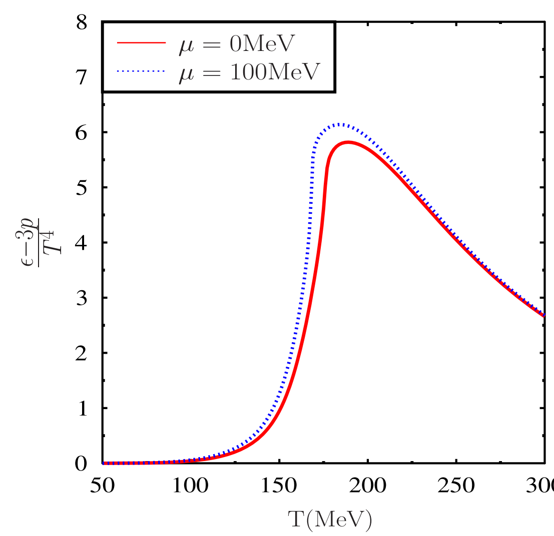

FIG. 2. Temperature dependence of the scaled trace anomaly $\frac{\epsilon - 3p}{T^4}$.

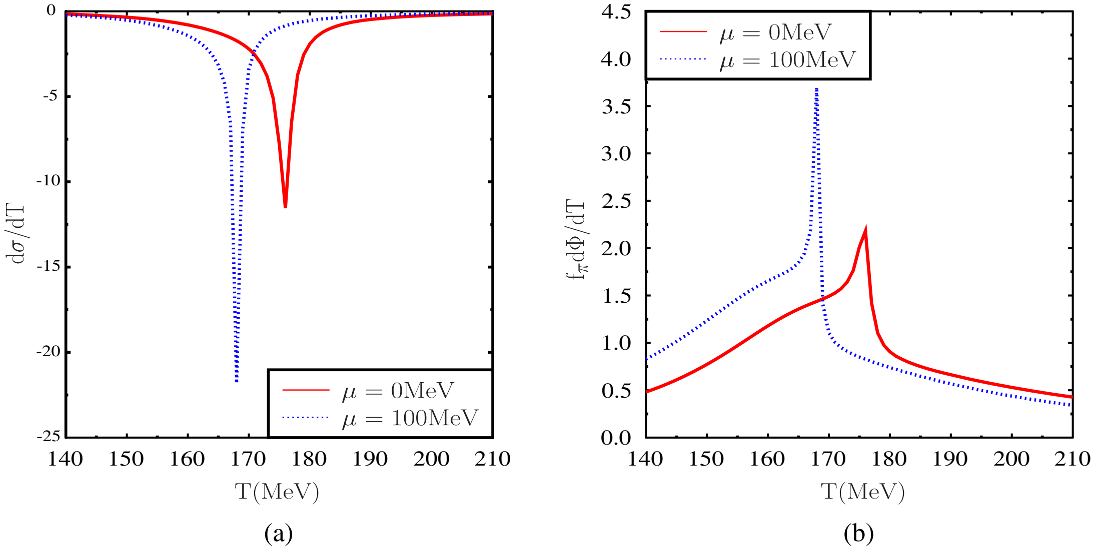

FIG. 3. (a) Temperature derivative of the chiral order parameter ($\frac{d\sigma}{dT}$) and (b) Polyakov loop parameter ($\frac{d\phi}{dT}$) as a function of temperature.

derivatives of the thermodynamic potential with respect to the order parameters leads to the values of the order parameters satisfying the coupled gap equations as shown. However, to calculate many different thermodynamic quantities, one also has to take into account the implicit dependence of the order parameters on temperature as well as chemical potential. One can do a numerical differentiation of the order parameters after solving for them from the gap equation. However, this can be numerically less accurate, particularly for the higher-order derivatives. We shall use here a semianalytic approach to calculate the implicit contributions to the extent of taking the differentiation of the expressions analytically [55]. Only the values of the final expressions so obtained are computed numerically. For example, to calculate the derivative of the order parameter X, $(X = \sigma, \phi, \bar{\phi})$ with respect to temperature is given by the equation

$$\frac{\partial}{\partial T}\left(\frac{\partial\Omega}{\partial X}\right) + \frac{\partial}{\partial\sigma}\left(\frac{\partial\Omega}{\partial X}\right)\frac{d\sigma}{dT} + \frac{\partial}{\partial\phi}\left(\frac{\partial\Omega}{\partial X}\right)\frac{d\phi}{dT} + \frac{\partial}{\partial\bar{\phi}}\left(\frac{\partial\Omega}{\partial X}\right)\frac{d\bar{\phi}}{dT} = 0. \tag{31}$$

Thus, we have a matrix equation of the type $\mathbf{A}\cdot\mathbf{Y} = \mathbf{B}$, where $\mathbf{A}$ is the coefficient matrix of the variables $\mathbf{Y} = (\frac{\mathbf{d}\sigma}{\mathbf{dT}}, \frac{\mathbf{d}\phi}{\mathbf{dT}}, \frac{\mathbf{d}\bar{\phi}}{\mathbf{dT}})^{\mathbf{T}}$, and $\mathbf{B}$ is the matrix of derivatives of the thermodynamic potential involving explicit dependence on temperature, i.e., $\mathbf{B} = (-\frac{\partial}{\partial \mathbf{T}}(-\frac{\partial\Omega}{\partial\sigma}, -\frac{\partial\Omega}{\partial\phi}, -\frac{\partial\Omega}{\partial\bar{\phi}})^{\mathbf{T}})$. These matrix equations can be solved using Cramer's rule. The coefficient matrix $\mathbf{A}$ is given by

$$\mathbf{A} = \begin{bmatrix} \Omega_{\sigma\sigma} & \Omega_{\sigma\phi} & \Omega_{\sigma\bar{\phi}} \\ \Omega_{\phi\sigma} & \Omega_{\phi\phi} & \Omega_{\phi\bar{\phi}} \\ \Omega_{\bar{\phi}\sigma} & \Omega_{\bar{\phi}\phi} & \Omega_{\bar{\phi}\bar{\phi}} \end{bmatrix} \tag{32}$$

with $\Omega_{ab} = \frac{\partial^2\Omega}{\partial a\partial b}$, where a, b stand for σ, ϕ and $\bar{\phi}$. Similarly, to calculate the derivatives with respect to chemical potential, the coefficient matrix $\mathbf{A}$ remains the same, while the matrix $\mathbf{B}$ will involve derivatives of the thermodynamic potential involving explicit dependence on the chemical potential.

Solving Eq. (31) this way, we have plotted the derivatives of the order parameters in Fig. 3. The critical temperature is defined by the position of the peaks of these derivatives of the order parameters. At zero chemical potential, this occurs at $T_C \simeq 176$ MeV. Let us note that at T_C the quark mass is $m_q = g_\sigma\sigma = 134$ MeV, while the Polyakov loop variable $\phi \sim = 0.5$. Thus, at the critical temperature, the effect of interaction is significant. As the chemical potential for the quarks increases, the critical temperature decreases. With finite chemical potential, the peaks also become sharper, and at higher chemical potential, the transition becomes a first-order one. The critical point within this model occurs at $(T_c, \mu_c) = (155, 163)$ MeV.

The other thermodynamic quantity that enters into the transport coefficient calculation is the velocity of sound. The same at constant density is defined as

$$c_s^2 = \left(-\frac{\partial P}{\partial\epsilon}\right)_n = \frac{s\chi_{\mu\mu} - \rho\chi_{\mu T}}{T(\chi_{TT}\chi_{\mu\mu} - \chi_{\mu T}^2)}, \tag{33}$$

where P, the pressure, is the negative of the thermodynamic potential given in Eq. (9). Further, $s = -\frac{\partial\Omega}{\partial T}$ is the entropy density, and the susceptibilities are defined as $\chi_{xy} = -\frac{\partial^2\Omega}{\partial x\partial y}$. The velocity of sound shows a minimum near the crossover temperature as may be seen in Fig. 4. Within the model, at low temperature when the constituent quarks start contributing to the pressure, their contribution to the energy

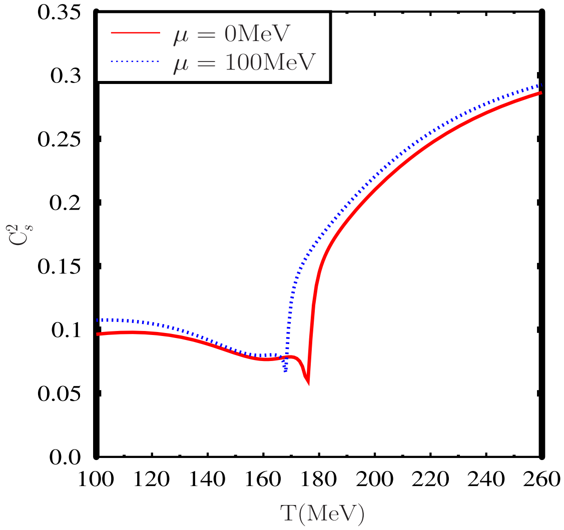

FIG. 4. Temperature dependence of the velocity of sound at constant density.

density is significant compared to their contribution to the pressure, leading to decreasing behavior of the velocity of sound until the crossover temperature, beyond which it increases as the quarks become light and approach the massless limit of $c_s^2 = \frac{1}{3}$. Such a dip in the velocity of sound is also observed in lattice simulation [56]. As we shall observe later, this behavior will have important consequences for the behavior of bulk viscosity as a function of temperature. We might mention here that such a dip for the sound velocity was not observed for two-flavor NJL [25]. For the linear sigma model calculations, such a dip was observed only for a large sigma meson mass [38].

III. TRANSPORT COEFFICIENTS IN RELAXATION TIME APPROXIMATION

We shall attempt here to estimate the transport coefficients in the relaxation time approximation where the particle masses are medium dependent. Such attempts were made earlier for the σ model [38] as well as in the NJL model to compute the shear and bulk viscosity coefficients. Such an approach was also made to estimate the viscosity coefficients of pure gluon matter [57]. In all these attempts, the expressions for the viscosity coefficients were derived for vanishing chemical potential. Several attempts were made to estimate these coefficients with finite chemical potential with different *Ansätze*. These expressions were put on firmer ground by deriving the expressions when there are mean fields and medium-dependent masses in a quasiparticle picture [58]. The resulting expressions for the transport coefficients were manifestly positive definite as they should be. These expressions were derived explicitly for the NJL model [25]. We use the same expressions here for the transport coefficients. The shear viscosity coefficient is given by

$$\eta = \frac{1}{15T}\sum_a \int \frac{d\mathbf{p}}{(2\pi)^3}\frac{p_a^4}{E_a^2}\tau(E_a) f_a^0(1 \pm f_a^0), \qquad (34)$$

where the sum is over all the different species contributing to the viscosity coefficients including the antiparticles and τ^a is the energy-dependent relaxation time that we define in the following subsection. The coefficient of bulk viscosity is given by

$$\zeta = \frac{1}{9T}\sum_a \int \frac{d\mathbf{p}}{(2\pi)^3}\frac{\tau^a}{E_a{}^2} f_a{}^0(1 \pm f_a{}^0)\Big[\mathbf{p}^2(1-3v_n{}^2) - 3v_n{}^2\left(M^2 - TM\frac{dM}{dT} - \mu M\frac{dM}{d\mu}\right) + 3\left(\frac{\partial P}{\partial n}\right)_\epsilon\left(M\frac{dM}{d\mu} - E_a t^a\right)\Big]^2. \qquad (35)$$

The thermal conductivity, on the other hand, is given by

$$\lambda = \left(\frac{w}{nT}\right)^2 \sum_a \int \frac{d\mathbf{p}}{(2\pi)^3}\frac{\mathbf{p}^2}{3E_a^2}\tau_a(E_a)\left(t_a - \frac{nE_a}{w}\right)^2 \times f_a^0(1 \pm f_a^0). \qquad (36)$$

In the above expressions, f_a^0 is the equilibrium fermion/boson distribution functions depending upon the statistics with $(1 \pm f_a^0)$ being the Bose enhancement/Fermi suppression factors and $t_a = +1, -1$, and 0 for the quark, antiquark, and meson, respectively. Further, $c_s^2 = (\frac{\partial p}{\partial \epsilon})_n$ is the velocity of sound at constant density, and $w = \epsilon + p$ is the enthalpy density.

A. Relaxation time estimation—Meson scatterings

As may be noted, the expressions for the transport coefficients as in Eqs. (34), (35), and (36) depend not only on bulk thermodynamic properties like energy density, pressure, and velocity of sound but also on the energy-dependent relaxation time $\tau(E)$. In the following, we shall first estimate the relaxation times involving meson exchanges similar to Ref. [38].

Using the Lagrangian Eq. (1), we calculate the relaxation time in the PQM model by taking into account the following scattering amplitudes with the corresponding matrix elements being given as

$$M_{\sigma+\sigma\to\sigma+\sigma} = -6\lambda - 36\lambda^2 f_\pi{}^2 \times \left(\frac{1}{s-m_\sigma{}^2} + \frac{1}{t-m_\pi{}^2} + \frac{1}{u-m_\pi{}^2}\right) \qquad (37)$$

$$M_{\pi+\sigma\to\pi+\sigma} = -2\lambda - 4\lambda^2 f_\pi{}^2 \times \left(\frac{3}{t-m_\sigma{}^2} + \frac{1}{u-m_\pi{}^2} + \frac{1}{s-m_\pi{}^2}\right) \qquad (38)$$

$$M_{\pi+\pi\to\pi+\pi} = -2\lambda\left(\frac{s-m_\pi{}^2}{s-m_\sigma{}^2}\delta_{\rm ab}\delta_{\rm cd} + \frac{t-m_\pi{}^2}{t-m_\sigma{}^2}\delta_{\rm ac}\delta_{\rm bd} + \frac{u-m_\pi{}^2}{u-m_\sigma{}^2}\delta_{\rm ad}\delta_{\rm bc}\right) \tag{39}$$

$$M_{\pi+\pi\to\sigma+\sigma} = -6\lambda - 4\lambda^2 f_\pi{}^2 \times\left(\frac{3}{s-m_\sigma{}^2} + \frac{1}{t-m_\pi{}^2} + \frac{1}{u-m_\pi{}^2}\right). \tag{40}$$

The terms involving the propagators yield divergent integrals due to the poles in the s and u channels, which is known in the literature [38]. To regulate these integrals, one can include a width for the mesons as evaluated in the next subsection [Eq. (54)]. However, such a substitution violates crossing symmetry. Further, these terms are generated from the three-point vertices, which are not taken into account in the mean field approximation used in solving the gap equations and the resulting equation of state. Hence, to be consistent with the equation of state while maintaining crossing symmetry for the scattering amplitudes, we approximate the above scattering amplitudes by their limits when s, t, and u are taken to be infinity and the scattering amplitudes reduce to constants [38]. Thus, the scattering amplitudes essentially reduce to constants. This allows us to compare our results with the earlier work of Ref. [38] and study the effect of the Polyakov loop and quarks within a similar approximation.

The energy-dependent interaction frequency $\omega_a(E_a)$ for the particle species a arising from a scattering process $a, b \to c, d$, which is also the inverse of the energy-dependent relaxation time $\tau(E_a)$, is given by, with $d\Gamma_i = \frac{d\mathbf{p}_i}{2E_i(\mathbf{p})(2\pi)^3}$ [25],

$$\omega(E_a) \equiv \tau(E_a)^{-1} = \sum_b \int d\Gamma_b f_b^0 W_{ab}(s). \tag{41}$$

In the above, the summation is over all the particles except the species a with a, b as the initial state.

The quantity W_{ab} is dimensionless and Lorentz invariant, and depends only on the Mandelstam variable s and is given by

$$W_{ab}(s) = \frac{1}{1+\delta_{ab}}\int d\Gamma_c d\Gamma_d (2\pi)^4\delta^4(p_a+p_b-p_c-p_d) \times |M|^2(1+f_c)(1+f_d). \tag{42}$$

In the above, we have included the Bose enhancement factors for the meson scattering. The quantity $W_{ab}(s)$ is related to the cross section by noting that, with t as the Mandelstam variable $t=(p_a-p_c)^2$,

$$\frac{d\sigma}{dt} = \frac{1}{64\pi s}\frac{1}{p_{ab}^2}|M|^2, \tag{43}$$

where $p_{ab}(s) = 1/(2\sqrt{s})\sqrt{\lambda(s, m_a^2, m_b^2)}$, and the kinematic function $\lambda(x,y,z) = x^2+y^2+z^2-2xy-2yz-2zx$ is the magnitude of the 3-momentum of the incoming particle in the c.m. frame. In the c.m. frame, using the energy momentum–conserving delta function and integrating over the final momenta, we have

$$W_{ab}(s) = \frac{4\sqrt{s}p_{ab}(s)}{1+\delta_{ab}}\int_{t_{\rm min}}^{t_{\rm max}} dt\left(\frac{d\sigma}{dt}\right) \times(1+f_c(E_c))(1+f_d(E_d)), \tag{44}$$

where

$$t_{\rm max,min} = m_a^2 + m_c^2 - \frac{1}{2s}(s+m_a^2-m_b^2)(s+m_c^2-m_d^2) \pm\frac{1}{2s}\sqrt{\lambda(s,m_a^2,m_b^2)\lambda(s,m_c^2,m_d^2)}.$$

In the limit of constant $|M|^2$, Eq. (44) reduces to

$$W_{ab}(s) = \frac{1}{1+\delta_{ab}}\frac{|M|^2}{16\pi\sqrt{s}p_{ab}}(t_{\rm max}-t_{\rm min})(1+f_c(E_c)) \times(1+f_d(E_d)), \tag{45}$$

and the transition frequency or the inverse relaxation time is given as

$$\omega(E_a) \equiv \tau(E_a)^{-1} = \frac{1}{256\pi^3 E_a}\int_{m_b}^\infty dE_b\sqrt{E_b^2-m_b^2}f(E_b)|M|^2 \times\int_{-1}^1 \frac{dx}{1+\delta_{ab}}\frac{1}{p_{ab}\sqrt{s}}(t_{\rm max}-t_{\rm min}). \tag{46}$$

In the above,

$$s = 2E_aE_b\left(1+\frac{m_a^2+m_b^2}{2E_aE_b} - \frac{p_ap_b}{E_aE_b}x\right).$$

To calculate, e.g., the π^+ relaxation time (τ_{π^+}), we consider the scattering processes $\pi^+ + \pi^i \to \pi^+ + \pi^i$ ($i = +, -, 0$) and $\pi^+ + \sigma \to \pi^+ + \sigma$.

To get an order of magnitude of the average relaxation time, one can also calculate an energy-averaged mean interaction frequency for a given species as $\bar{\omega}_a \equiv \bar{\tau}_a{}^{-1}$ as

$$\bar{\omega}_a = \frac{1}{n_a}\int\frac{d\mathbf{p}}{(2\pi)^3}\omega_a(E_a)f_a(E_a), \tag{47}$$

with

$$n_a = \int\frac{d\mathbf{p}}{(2\pi)^3}f_a(E_a). \tag{48}$$

B. Relaxation time estimation—Quark scatterings

We next consider the quark scattering within the model through the exchange of pion and sigma meson resonances. The approach is similar to Refs. [25,35,59] performed within the NJL model to estimate the corresponding relaxation time for the quarks and antiquarks. The transition frequency is again given by Eq. (41), with the corresponding W_{ab} given as

$$W^q_{ab}(s) = \frac{2\sqrt{s(s-4m^2)}}{1+\delta_{ab}}\int_{t_{\min}}^0 dt\left(\frac{d\sigma}{dt}\right)\left(1-f_c\left(\frac{\sqrt{s}}{2},\mu\right)\right) \times\left(1-f_d\left(\frac{\sqrt{s}}{2},\mu\right)\right), \tag{49}$$

where

$$\frac{d\sigma}{dt} = \frac{1}{16\pi s(s-4m^2)}\frac{1}{p^2_{ab}}|\bar{M}|^2, \tag{50}$$

with the corresponding suppression factors appropriate for fermions. For the quark scatterings, in the present case for two flavors, we consider the following scattering processes:

$$\begin{array}{lll} u\bar{u}\to u\bar{u}, & u\bar{d}\to u\bar{d}, & u\bar{u}\to d\bar{d}, \\ uu\to uu, & ud\to ud, & \bar{u}\bar{u}\to\bar{u}\bar{u}, \\ \bar{u}\bar{d}\to\bar{u}\bar{d}, & d\bar{d}\to d\bar{d}, & d\bar{d}\to u\bar{u}, \\ d\bar{u}\to d\bar{u}, & dd\to dd, & \bar{d}\bar{d}\to\bar{d}\bar{d}. \end{array}$$

One can use i-spin symmetry, charge conjugation symmetry, and crossing symmetry to relate the matrix element square for the above 12 processes to get them related to one another, and one has to evaluate only two independent matrix elements to evaluate all the 12 processes. We choose these, as in Ref. [59], to be the processes $u\bar{u}\to u\bar{u}$ and $u\bar{d}\to u\bar{d}$ and use the symmetry conditions to calculate the rest. We note, however, that, while the matrix elements are related, the thermal-averaged rates are not, as they involve also the thermal distribution functions for the initial states as well as the Pauli blocking factors for the final states. We also write down the square of the matrix elements for these two processes explicitly [25,59]:

$$\begin{aligned}|\bar{M}_{u\bar{u}\to u\bar{u}}|^2 = g^4_\sigma\Big[&s^2|D_\pi(\sqrt{s},0)|^2 + t^2|D_\pi(0,\sqrt{-t})|^2(s-4m^2)^2|D_\sigma(\sqrt{s},0)|^2 + (t-4m^2)^2|D_\sigma(0,\sqrt{-t})|^2 \\ &+\frac{1}{N_c}\mathrm{Re}(stD^*_\pi(\sqrt{s},0)D_\pi(0,\sqrt{-t}) + s(4m^2-t)D^*_\pi(\sqrt{s},0)D_\sigma(0,\sqrt{-t}) \\ &+t(4m^2-s)D_\pi(0,\sqrt{-t})D^*_\sigma(\sqrt{s},0) + (4m^2-s)(4m^2-t)D_\sigma(0,\sqrt{-t})D^*_\sigma(\sqrt{s},0))\Big].\end{aligned} \tag{51}$$

Similarly, the same for the process $u\bar{d}\to u\bar{d}$ is given as [59]

$$\begin{aligned}|\bar{M}_{u\bar{d}\to u\bar{d}}|^2 = g^4_\sigma\Big[&4s^2|D_\pi(\sqrt{s},0)|^2 + t^2|D_\pi(0,\sqrt{-t})|^2(s-4m^2)^2|D_\sigma(\sqrt{s},0)|^2 + (t-4m^2)^2|D_\sigma(0,\sqrt{-t})|^2 \\ &+\frac{1}{N_c}\mathrm{Re}(-2stD^*_\pi(\sqrt{s},0)D_\pi(0,\sqrt{-t}) + 2s(4m^2-t)D^*_\pi(\sqrt{s},0)D_\sigma(0,\sqrt{-t}))\Big].\end{aligned} \tag{52}$$

The meson propagators $D_a(\sqrt{s},0)$, $(a=\sigma,\pi)$ are given by

$$D_a(\sqrt{s},\mathbf{0}) = \frac{i}{s-M^2_a - iIm\Pi_{M_a}(\sqrt{s},\mathbf{0})}. \tag{53}$$

In the above, the masses of the mesons are given by Eqs. (23) and (24) determined by the curvature of the thermodynamic potential. Further, in Eq. (53), $Im\Pi(\sqrt{s},0)$, which is related to the width of the resonance as $\Gamma_a = Im\Pi_a/M_a$, is given as [59]

$$Im\Pi_a(\omega,\mathbf{0}) = \theta(\omega^2-4m^2)\frac{N_cN_f}{8\pi\omega}(\omega^2-\epsilon^2_a)\sqrt{\omega^2-4m^2} \times(1-f_-(\omega)-f_+(\omega)), \tag{54}$$

with $\epsilon_a = 0$ for pions and $\epsilon_a = 2m$ for sigma mesons.

With the squared matrix elements for the quark scatterings given as above, the transition frequency for the quark of a given species is

$$\omega_q(E_a) = \frac{1}{2E_a}\int d\pi_b f(E_b)W^q_{ab}. \tag{55}$$

C. Quark pion scattering and relaxation time

Next, we compute the contribution of quark meson scattering to the relaxation times for both mesons as well as quarks. One can argue that the dominant contribution comes from pions as their number is large compared to the sigma mesons both below and above T_c. Therefore, in the following, we consider the quark pion scattering only. The Lorentz-invariant scattering matrix element can be written as $\bar{U}(p_2)T_{ba}U(p_1)$, with $\bar{U}U = 2m_q$ and with p_1, p_2 denoting the initial and final the quark momenta, respectively, and q_1 and q_2, being the momenta of the pions,

$$T_{ba} = \delta_{ba}\frac{1}{2}(q_1+q_2)^\mu\gamma_\mu(\delta_{ab}B^{(+)} + i\epsilon_{abc}\tau_c B^{(-)}), \tag{56}$$

where

$$B^{(+)} = g_\sigma^2\left(\frac{1}{u-m_q^2} - \frac{1}{s-m_q^2}\right), \tag{57}$$

and

$$B^{(-)} = -g_\sigma^2\left(\frac{1}{u-m_q^2} + \frac{1}{s-m_q^2}\right). \tag{58}$$

Averaging over the spin and isospin factors, the matrix element square for the quark pion scattering is given by

$$|\bar{M}|^2 = \frac{g_\sigma^4}{6}((s-u)^2 - t(t-4m_\pi^2))(3B_+^2 + 2B_-^2). \tag{59}$$

The corresponding transition frequency is given by

$$\omega_{q\pi}(E_a) = \frac{1}{2E_a}\int d\pi_b f(E_b) W_{ab}^{(q-\pi)}, \tag{60}$$

where

$$W_{ab}^{(q-\pi)} = \frac{1}{8\pi}\times\frac{1}{2\sqrt{s}p_0}\int dt|\bar{M}_{q-\pi}|^2(1-f_q)(1+f_\pi). \tag{61}$$

In the above, $p_0^2 = (s+m_q^2-m_\pi^2)^2/(4s) - m_q^2$. The scattering will contribute to both the quark relaxation time as well as to the pion relaxation time using Eq. (60) with appropriate modification for the initial state.

Let us note that there are poles in the u channel in the quark pion scattering term beyond the critical temperature when the pion mass becomes larger than the quark mass. However, this is taken care of once we include the imaginary part of the quark self-energy in the propagators for the quarks in the calculation of the amplitude in Eqs. (57) and (58). The quark self-energy due to scattering with mesons can be written as [30]

$$\Sigma(p_0,\mathbf{p}) = m\Sigma_0 + \gamma\cdot\mathbf{p}\Sigma_3 - \gamma_0 p_0\Sigma_4 \tag{62}$$

so that the quark propagators get modified as

$$\begin{aligned} S(p_0,\mathbf{p}) &= \frac{1}{\not{p} - m - \Sigma} \\ &= \frac{m(1+\Sigma_0) + \gamma_0 p_0(1+\Sigma_4) - \gamma\cdot\mathbf{p}(1+\Sigma_3)}{p_0^2(1+\Sigma_4)^2 - \mathbf{p}^2(1+\Sigma_3)^2 - m^2(1+\Sigma_0)^2}. \end{aligned} \tag{63}$$

The imaginary part of the dimensionless Σ_j, $(j = 0,3,4)$, is given as

$$\begin{aligned} \mathrm{Im}\Sigma_j(p_0,\mathbf{p}) = \frac{g^2}{32\pi p}d_j\int_{E_{\min}}^{E_{\max}} dE_f C_j[f_b(E_b) \\ + f_-(E_f) + f_+(E_f)]. \end{aligned} \tag{64}$$

In the above, $E_b = E_f + p_0$, $p_0 = \sqrt{\mathbf{p}^2 + m^2}$ and $f_\pm$ are the distribution functions for the quarks/antiquarks, f_b is the meson distribution function, and, C_j's are weight factors given as

$$C_0 = 1, \qquad C_3 = \frac{m_M^2 - 2m^2 - 2E_f p_0}{2\mathbf{p}^2}, \qquad C_4 = -\frac{E_f}{p_0}. \tag{65}$$

The integration limits are given by

$$E_{\max,\min} = \frac{1}{2m^2}\left[(m_M^2 - 2m^2)p_0 \pm |\mathbf{p}|m_M\sqrt{m_M^2 - 4m^2}\right]. \tag{66}$$

Further, the degeneracy factors $d_{3,4}$ are 3 for pions and 1 for sigma, while d_0 is -3 for pions and 1 for the sigma meson. To calculate the total relaxation time for a quark of species a, we compute the total interaction frequency as $\omega_q^{\mathrm{total}}(E_a) = \omega(E_a) + \omega_{q\pi}(E_a)$. One can define an average relaxation time for the quarks similar to Eq. (47) as $\bar{\tau}_q^{\mathrm{total}} = \frac{1}{\bar{\omega}_q^{\mathrm{total}}}$,

$$\bar{\omega}_q^{\mathrm{total}} = \frac{1}{n_q}\int\frac{d\mathbf{p}}{(2\pi)^3}f_q(E)\omega_q^{\mathrm{total}}(E). \tag{67}$$

IV. RESULTS

A. Meson scatterings

Let us first discuss the results arising from meson scattering alone. Using Eqs. (46), with constant $|M|^2$ as discussed, we have plotted the average relaxation times for the σ meson and $\boldsymbol{\pi}$ mesons in Fig. 5. The relaxation times are minimum at the transition temperature. Because of larger mass of σ mesons below the transition temperature, $\bar{\tau}_\sigma$ is much larger as compared to $\bar{\tau}_{\boldsymbol{\pi}}$. They become almost degenerate after the chiral transition, as may be expected from the behavior of their masses beyond the transition

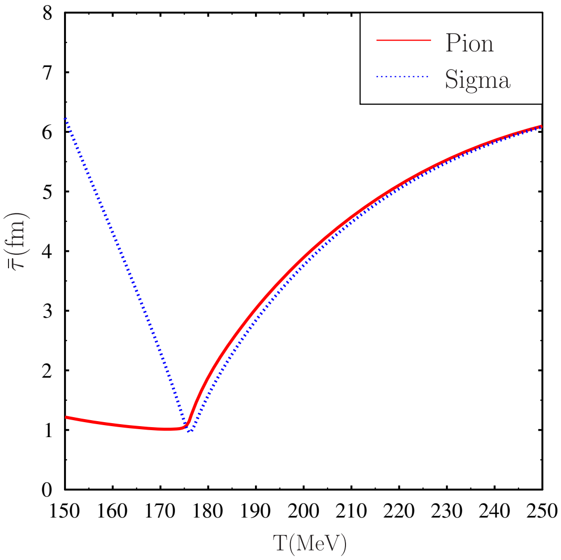

FIG. 5. Average relaxation time for pions (solid line) and sigma meson (dotted line). Only meson-meson scatterings are considered here.

temperature. We may comment here that the particle with larger relaxation time dominates the viscosities as it can transport energy and momentum to larger distances before interacting. In Fig. 6, we have shown the behavior of the specific viscosities (normalized to entropy density) as a function of temperature. In Fig. 6(a), we have plotted the temperature dependence of the ratio η/s for $\mu = 0$. The behavior of this ratio is essentially determined by the behavior of the relaxation time. Similar to Fig. 5, η/s shows a minimum at the crossover temperature, and the value at the minimum is about $\eta/s \sim 0.053$, which is slightly lower than the KSS bound of $1/4\pi$. We note that we have considered here only the contributions from meson scatterings. As we shall see later, inclusion of quark degrees of freedom increases the ratio. We have also compared with linear sigma model calculations [38] in which the quark as well as Polyakov loop contributions are not taken into account. The general behavior of the present calculations is similar to earlier calculations in the sense of having a minimum at the chiral crossover temperature. However, the magnitude of the ratio at the critical temperature is smaller compared to Ref. [38]. This is probably due to the fact that the entropy density in the present calculations has contributions including those of the gluon included through the Polyakov loop potential. The large entropy density, we believe, decreases the magnitude of the ratio.

In Fig. 6(b), the ratio of bulk viscosity to entropy is plotted, which shows a maximum at the transition temperature. We have also plotted in the same figure the results without quarks and the Polyakov loop potential. The present results show a distinct peak structure in the ζ/s ratio at the crossover temperature. Let us note that such a peak is expected as an effect of large conformality violation at the transition temperature as indicated in lattice simulations [28,60]. In Ref. [38], a peak structure is seen for a heavier sigma meson ($m_\sigma = 900$ MeV), which was interpreted as an effect of stronger self-coupling λ for higher M_σ. However, in the present case, this arises with quark and Polyakov loop degrees of freedom even with a lighter $M_\sigma = 600$ MeV. The other characteristic feature of the

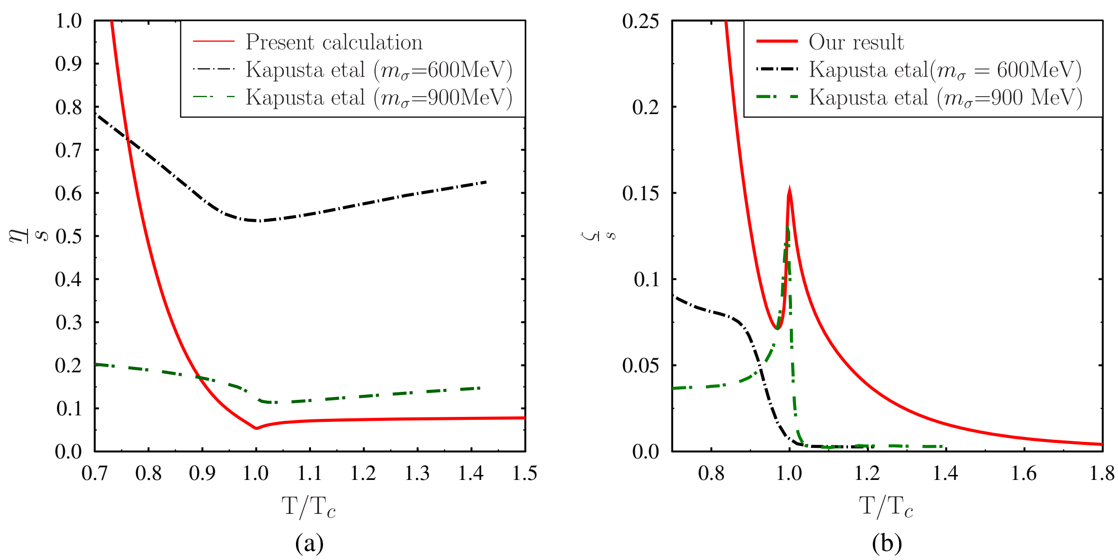

FIG. 6. Computations show mesonic contribution calculated using only meson-meson interactions. (a) Shear viscosity–to-entropy ratio for $\mu = 0$. Present results are shown by solid lines. The two dot dashed curves correspond to results of the linear sigma model of Ref. [38] corresponding two different masses for sigma mesons. (b) Bulk viscosity–to-entropy ratio for $\mu = 0$. Results for current calculations are shown by the solid line. The other results correspond to the work by Kapusta *et al.* (short dashed line) of the linear sigma model with ($m_\sigma = 600$ MeV) and Kapusta *et al.* (dash dot curve) for the linear sigma model with $m_\sigma = 900$ MeV [38].

present calculation is that, beyond the critical temperature, the ratio ζ/s falls at a slower rate as compared to results of previous calculations. This has to do with the fact that the velocity of sound approaches the ideal gas limit slowly as the effect of Polyakov loops on the quark distribution function remains significant beyond the critical temperature. In fact, at the transition temperature, the value of the Polyakov loop remains about half its value of the ideal limit. Apart from this, the masses of mesons also get affected by the quark distribution functions significantly beyond the critical temperature. These nonideal effects lead to a slower decrease of the ratio beyond the critical temperature.

B. Quark scatterings

Next, we discuss quark scattering. In Fig. 7, we show the behavior of average relaxation time for quark scattering. The quark scattering through the exchange of mesons is shown by the solid line in the figure. Let us recall that the average relaxation time is inversely proportional to the transition rate, which is related to the cross section. The dominant contribution here comes from the quark-antiquark scattering from the s channels through propagation of the resonance states, the pions, and the sigma mesons. The masses of the sigma meson decrease with temperature, becoming a minimum at the transition temperature, leading to an enhancement of the cross section. Beyond this, the cross section decreases due to the increase in the masses of the mesons. This, in turn, leads to a minimum in the relaxation time.

The average relaxation time for quarks including the quark meson scattering along with the quark scattering is shown as the dashed curve in Fig. 7. This curve lies below the quark-quark scattering curve as there is an additional contribution to the transition rate from the quark meson scattering. Below the critical temperature, the quark meson scattering dominates over the quark-quark scattering due to the smaller mass of the pions as compared to the massive constituent quarks. Beyond the critical temperature, one would have expected the quark meson scattering contribution to be negligible because of the suppression due to the large meson masses. However, as was noted earlier, beyond the critical temperature, there are poles in the scattering amplitude in the u channel for quark-pion scattering as the pion mass becomes larger than the quark masses. This is, however, regulated by the finite width of the quarks as calculated in Eq. (62). Nonetheless, the contribution of the quark-pion scattering to the total quark interaction frequency $\omega_{q\pi}(\mathrm{E})$ is non-negligible beyond the critical temperature.

We next discuss the contribution of different scatterings to the specific shear viscosity η/s. The same is shown in Fig. 8(a) for vanishing chemical potential. The contribution from the mesons to the shear viscosity arising from the meson scatterings only is shown by the green dashed curve,

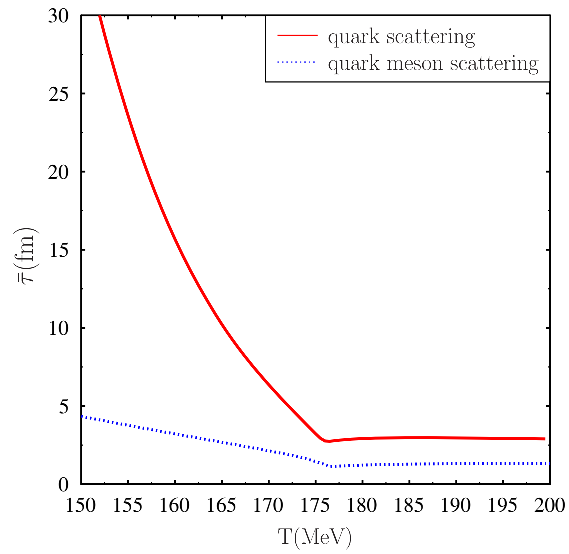

FIG. 7. Average relaxation time for quarks arising from quark scattering. The solid curve corresponds to quark quark-quark and quark-antiquark scattering with meson exchange. The dashed curve corresponds to including the effect of quark meson scatterings. Both the curves correspond to the $\mu = 0$ case.

while the effect of including the meson-quark scattering is shown by the maroon dotted curve. Similarly, the quark contribution to this ratio η/s arising from quark-quark scattering only is shown by the red solid line, while the total contributions including the quark-pion scattering is shown by the blue dotted line. This also demonstrates the importance of the scattering of quarks and mesons to the total viscosity coefficient. The total contributions from both the quarks and mesons is shown as the black dashed curve in Fig. 8.

In a similar manner, various contributions to the specific bulk viscosity (ζ/s) coefficient are shown in Fig. 8(b). As may be observed, while no peak structure is seen for this coefficient from the contributions arising from quarks scatterings only, such a structure is seen only when one includes the quark meson scattering. The total effect is shown as a black dashed curve in Fig. 8(b).

In Fig. 9, we compare the present results with earlier works on the NJL model. As may be noted, in general, the behavior is similar regarding the shear viscosity–to-entropy ratio. Both NJL as well as the present calculations of the PQM model show the similar behavior of having a minimum at the transition temperature as in Refs. [24,25]. The results of Ref. [35], on the other hand, show a monotonic decrease with temperature. The bulk viscosity–to-entropy ratio here, however, shows a much faster rise as the temperature is lowered below the critical temperature. In fact, both the specific viscosities rise much faster compared to NJL models below the critical temperature in the PQM model considered here. The reason could be due to the fact that the entropy density for the PQM model is smaller compared to NJL models. The Polyakov loop

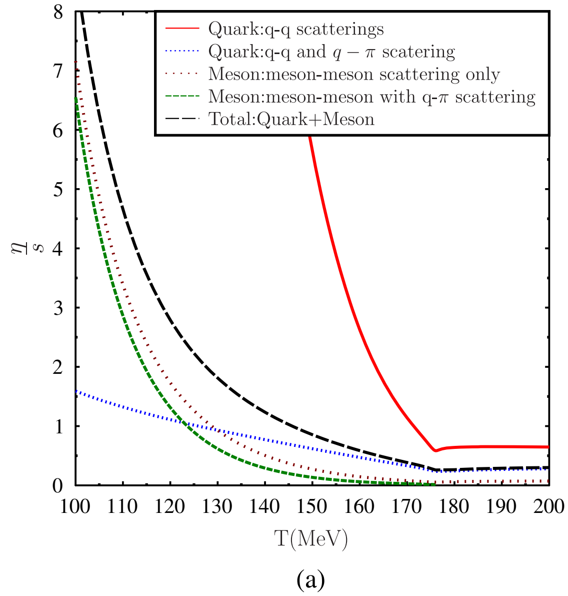

FIG. 8. Different contributions for specific viscosity coefficients. η/s is shown in the left, while ζ/s is shown on the right. In both the figures, contributions from the quarks with relaxation time computed using only quark-quark scattering(red solid line) and also including quark-meson scattering(blue dotted line) are shown as a function of temperature. The contribution of the mesons due to meson-meson scattering (green dashed curve) and including meson-quark scattering (maroon short dashed curve) is also shown. The total contribution from the quarks and mesons is shown by the black long dashed curve. All the curves correspond to the $\mu = 0$ case.

decreases as the temperature is lowered, which leads to a suppression of quark distribution functions, leading to decrease of entropy density at a faster rate as compared to the NJL model. Moreover, within the present approximation, pions do not contribute to the thermodynamics here. Further, for temperature larger than the critical temperature, the bulk viscosity vanishes slowly with an increase in temperature as compared to the NJL model. This is due to the fact that the Polyakov loop variable takes its asymptotic values only at very high temperatures.

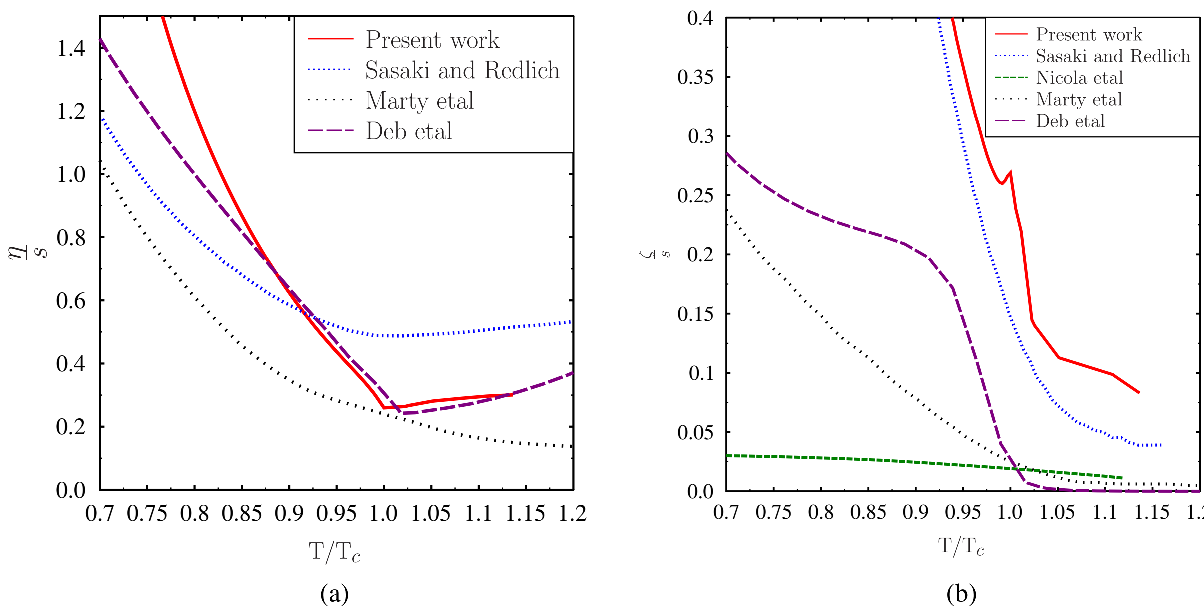

FIG. 9. (a) Shear viscosity–to-entropy ratio for $\mu = 0$. Present results are shown by solid lines. The dotted line corresponds to results of the NJL model of Ref. [24], the short dashed curve corresponds to results of Marty *et al.* Ref. [35], and the long dashed curves correspond to the results of Deb *et al.* of Ref. [25]. (b) The results of the bulk viscosity–to-entropy ratio compared with other results in NJL models. The notation is similar to that of (a).

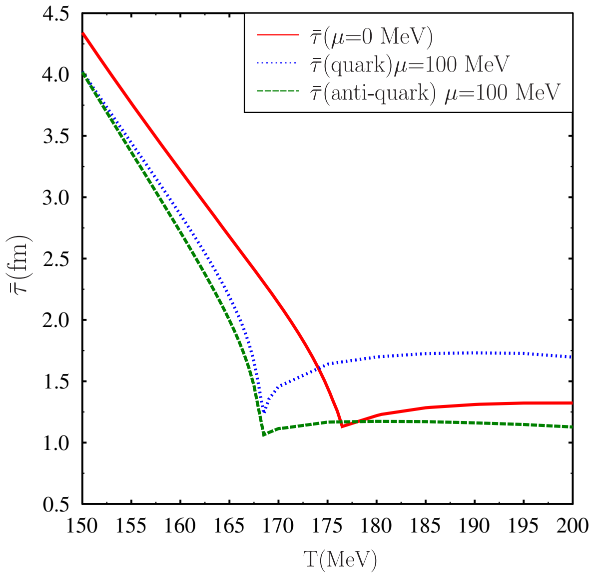

FIG. 10. Average relaxation time of quarks and antiquarks for $\mu = 100$ MeV. The solid line corresponds to the case of $\mu = 0$ MeV.

Next, we discuss the effect of finite chemical potential on the transport coefficients. To begin with, let us note that the average relaxation time $\bar{\tau}_a$ as in Eq. (67) depends both on the transition rate and the density of the particles in the initial state. To this end, let us discuss the case of $T > T_c$. Here, the quark densities are larger than those of antiquarks. Further, the dominant contribution in this range of temperatures arises from $u\bar{d} \to u\bar{d}$ scatterings. As there are fewer antiquarks to scatter off, the average transition frequency of quark-antiquark scattering decreases. This leads to $\bar{\tau}_q(\mu) > \bar{\tau}_q(\mu = 0)$. On the other hand, for the antiquarks, there are more quarks to scatter off than compared to the case of $\mu = 0$. Hence, this leads to $\bar{\tau}_{\bar{q}}(\mu) < \bar{\tau}_{\bar{q}}(\mu = 0)$. This expected behavior is seen in Fig. 10. Next, let us consider the case $T < T_c$. In this case, the antiquark density is heavily suppressed due to constituent quark mass, and the chemical potential and dominant contribution for quark relaxation time therefore arises from quark-quark scatterings. This leads to $\bar{\tau}_q(\mu) < \bar{\tau}_q(\mu = 0)$. On the other hand, for the antiquarks, though their number density is smaller, their interaction frequency is enhanced both by the larger amplitude for $M_{u\bar{d}\to u\bar{d}}$ scattering and the larger number of quarks as compared to case at $\mu = 0$. This leads to $\bar{\tau}_{\bar{q}}(\mu) < \bar{\tau}_q(\mu = 0) < \bar{\tau}_{\bar{q}}(\mu = 0)$. This general behavior is reflected in the average relaxation time dependence on T in Fig. 10 below the critical temperature.

In Fig. 11, we have shown the results for the viscosities at $\mu = 100$ MeV. Figure 11(a) shows the variation of the specific shear viscosity (η/s) as a function of temperature for zero and finite chemical potential. The behavior of shear viscosity essentially follows that of the behavior of the relaxation time. η/s has a minimum at the critical temperature with $\eta/s|_{\min} \sim 0.23$ $(\mu = 0)$ due to suppression of the scattering cross section at higher temperature. At finite μ, the ratio is a little higher as compared to the value at vanishing μ. This is due to two reasons. First, the relaxation time at nonzero chemical potential is larger, and, moreover, the quark density also becomes larger at finite chemical potential. At temperatures below the critical temperature and near the critical temperature, $\eta/s(\mu) < \eta/s(\mu = 0)$ as the relaxation time is lower. However, at lower

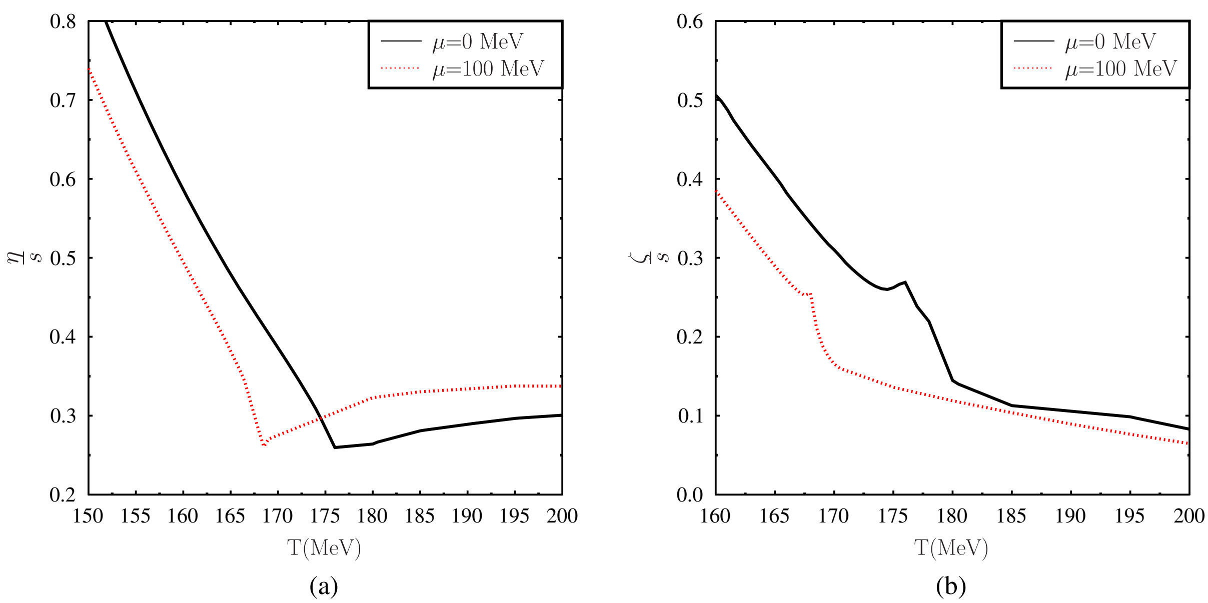

FIG. 11. Viscosities for $\mu = 100$ MeV. The left figure shows η/s as a function of temperature for $\mu = 0$ MeV (solid line) and $\mu = 100$ MeV (dotted line). The right figure shows the ratio ζ/s as a function of temperature.

temperatures, the meson scattering becomes significant, and η/s for finite chemical potential becomes similar to that at vanishing chemical potential as is observed in the figure.

In Fig. 11(b), we have plotted the bulk viscosity–to-entropy ratio for $\mu = 0$ MeV and $\mu = 100$ MeV. It turns out that at finite μ the specific bulk viscosity is smaller than the value at $\mu = 0$ MeV. The reason for it is the fact that the dominating contribution to the finite μ arises from the term $M^2 - TM\frac{dM}{dT} - \mu M\frac{dM}{d\mu}$ in the expression for ζ/s in Eq. (35). This is due to the sharp variations of the order parameters at finite chemical potential as may be observed in Fig. 3. As this term contributes negatively to the expression for ζ, the specific bulk viscosity at finite μ is lower than that at $\mu = 0$ MeV.

In Fig. 12, we have shown the results for thermal conductivity. We have plotted here the dimensionless quantity λ/T^2 as a function of temperature. We have plotted the results for $\mu = 100$ MeV. As is well known, thermal conduction, which involves the relative flow of energy and baryon number, vanishes at zero baryon density. In fact, λ diverges as $1/n^2$, as may be expected from the expression given in Eq. (36). However, in the dissipative current, the conductivity occurs as λn^2 [61,62], and the heat conduction vanishes for $\mu = 0$ [63]. On the other hand, in some cases, such as when the pion number is conserved, heat conduction can be sustained by pions. In the presence of a pionic chemical potential corresponding to a conserved pion number, thermal conductivity can be nonzero at vanishing baryonic chemical potential. This has been the basis for the estimation of thermal conductivity at zero baryon density but finite pion density [31,40,47]. However, in the present case, we consider the case of vanishing pion chemical potential and show only the contribution of quarks to thermal conductivity.

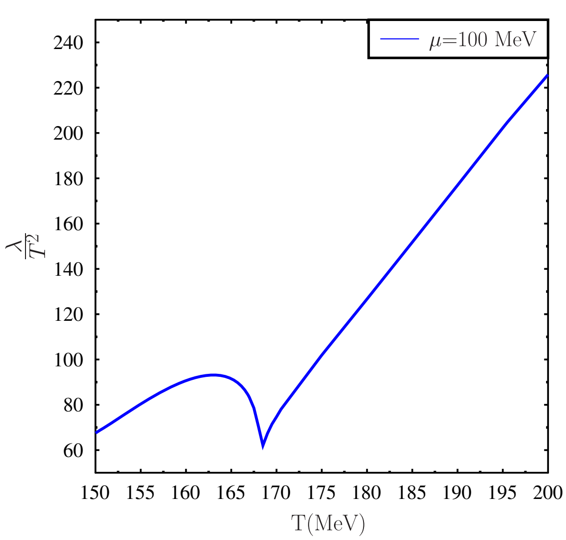

FIG. 12. Thermal conductivity in units of T^2 as a function of temperature for $\mu = 100$ MeV.

As expected from the behavior of the relaxation time, the specific thermal conductivity has a minimum at the critical temperature similar to Ref. [25] for the NJL model. The sharp rise of λ/T^2 can be understood by performing a dimensional argument to show that at very high temperature when chiral symmetry is restored the integral increases as T^3 while the prefactor $w/(nT)$ grows as T^2 for small chemical potentials. Apart from this kinematic consideration, the integrand further is multiplied by $\tau(E)$, which itself is an increasing function of temperature beyond T_c. This leads to the sharp rise of the ratio λ/T^2 beyond the critical temperature. Below the critical temperature, however, the ratio decreases, which is in contrast to the NJL results of Ref. [25]. The reason is twofold. First, the magnitude of the relaxation time decreases when quark meson scattering is included as compared to quark-quark scattering as shown in Fig. 7. Apart from this, in the integrand, the distribution functions are suppressed by Polyakov loops as compared to the NJL model. As the antiquark densities are suppressed compared to quark densities at finite chemical potential, the high-temperature behavior is decided by the quark-quark scattering.

V. SUMMARY

Transport coefficients of hot and dense matter are important inputs for the hydrodynamic evolution of the plasma that is produced following a heavy ion collision. In the present study, we have investigated these coefficients, taking into account the nonperturbative effects related to chiral symmetry breaking as well as confinement properties of strong interaction physics within an effective model, the Polyakov loop extended quark meson coupling model. These coefficients are estimated using the relaxation time approximation for the solutions of the Boltzman kinetic equation.

We first calculated the medium-dependent masses of the mesons and quarks within a mean field approximation. The contribution of the mesons to the transport coefficients has been calculated through estimating the relaxation time for the mesons arising both from meson-meson scattering and meson-quark scattering. The contribution to the transport coefficients arises mostly from the meson scatterings at temperatures below the critical temperature, while above the critical temperature, the contributions arising from the quark scatterings become dominant. In particular, quark meson scattering contributes significantly to the relaxation time for the quarks both below and above the critical temperature. The quark-pion scattering above the critical temperature gives significant contribution due to the pole structure of the corresponding scattering amplitude.

One important approximation in the present analysis is that the kinetic terms for the mesons are not modified at finite temperature and meson dispersion relation remains similar to those at the zero-temperature relativistic dispersion relation. The only temperature effect that remains in the meson dispersion lies in the temperature-dependent meson masses obtained through the curvature of the effective potential [54]. A more realistic approach would be to use effective field theory to have different dispersion relations for the mesons [64] depending upon their velocities and calculate the scattering processes to estimate the viscosities. However, such an approach is beyond the scope of present work in which we have restricted ourselves to thermal and density effects included in the masses and widths for the mesons.

In general, the effect of Polyakov loops lies in suppressing the quark contribution below the critical temperature. This leads to, in particular, the suppression of thermal conductivity at lower temperature arising from quark scattering. The effect of Polyakov loop also is significant near and above the critical temperature. Indeed, both the quark masses as well as Polyakov loop order parameter remain significantly different from their asymptotic values near the critical temperature. It will be interesting to examine the consequences of such nonperturbative features on the transport coefficients of heavy quarks as well as on the collective modes of QGP above and near the critical temperature. Some of these works are in progress and will be reported elsewhere.

ACKNOWLEDGMENTS

The authors would like to acknowledge many discussions with Guru Prasad Kadam and Pracheta Singha. S. G. is financially supported by University Grants Commission Dr. D. S. Kothari Post Doctoral Fellowship (India), under Grant No. F4-2/2006 (BSR)/PH/15-16/0060.

[1] U. Heinz and R. Snellings, Annu. Rev. Nucl. Part. Sci. **63**, 123 (2013).
[2] M. Gyulassy and L. McLerran, Nucl. Phys. **A750**, 30 (2005).
[3] H. Niemi, G. S. Denicol, P. Huovienen, E. Molnar, and D. H. Rischke, Phys. Rev. Lett. **106**, 212302 (2011).
[4] L. P. Csernai, J. I. Kapusta, and L. D. McLerran, Phys. Rev. Lett. **97**, 152303 (2006).
[5] M. Luzum and P. Romatschke, Phys. Rev. Lett. **103**, 262302 (2009).
[6] P. Romatschke and U. Romatschke, Phys. Rev. Lett. **99**, 172301 (2007); T. Hirano and M. Gyulassy, Nucl. Phys. **A769**, 71 (2006).
[7] C. Gale, S. Jeon, and B. Schenke, Int. J. Mod. Phys. A **28**, 1340011 (2013).
[8] B. Friman *et al.*, *The CBM Physics Book: Compressed Baryonic Matter in Laboratory Experiments*, Lecture Notes in Physics (Springer, Berlin, 2011).
[9] D. Blaschke, J. Aichelin, E. Bratkovskaya, V. Friese, M. Gazdzicki, J. Randrup, O. Rogachevsky, O. Teryaev, and V. Toneev, Eur. Phys. J. A **52**, 267 (2016).
[10] S. Sarkar and R. Sharma, Phys. Rev. D **96**, 094025 (2017).
[11] H. Heiselberg and C. Pethick, Phys. Rev. D **48**, 2916 (1993).
[12] N. Chamel and P. Hansel, Living Rev. Relativity **11**, 10 (2008).
[13] D. Page and S. Reddy, Annu. Rev. Nucl. Part. Sci. **56**, 327 (2006).
[14] D. G. Yakovlev, A. D. Kaminker, O. Y. Gnedin, and P. Haensel, Phys. Rep. **354**, 1 (2001).
[15] D. G. Yakovlev, O. Y. Gnedin, A. D. Kaminker, K. P. Levenfish, and A. Y. Potekhin, Adv. Space Res. **33**, 523 (2004).
[16] N. Andersson, Astrophys. J. **502**, 708 (1998); N. Andersson and K. D. Kokkotas, Mon. Not. R. Astron. Soc. **299**, 1059 (1998).
[17] T. K. Jha, H. Mishra, and V. Sreekanth, Phys. Rev. C **82**, 025803 (2010).
[18] J. I. Kapusta, *Relativistic Nuclear Collisions*, Landolt-Bornstein New Series, edited by R. Stock (Springer-Verlag, Berlin, 2010), Vol. I/23.
[19] R. Kubo, J. Phys. Soc. Jpn. **12**, 570 (1957).
[20] P. Kovtun, D. T. Son, and A. O. Starinets, Phys. Rev. Lett. **94**, 111601 (2005).
[21] P. Arnold, G. D. Moore, and L. G. Yaffe, J. High Energy Phys. 11 (2000) 001; 01 (2003) 030; 05 (2003) 051.
[22] N. Demir and S. A. Bass, Phys. Rev. Lett. **102**, 172302 (2009).
[23] V. Ozvenchuk, O. Linnyk, M. I. Gorenstein, E. L. Bratkovskaya, and W. Cassing, Phys. Rev. C **87**, 064903 (2013).
[24] C. Sasaki and K.Redlich, Nucl. Phys. **A832**, 62 (2010).
[25] P. Deb, G. P. Kadam, and H. Mishra, Phys. Rev. D **94**, 094002 (2016).
[26] A. S. Khvorostukhin, V. D. Toneev, and D. N. Voskresensky, Nucl. Phys. **A915**, 158 (2013).
[27] A. S. Khvorostukhin, V. D. Toneev, and D. N. Voskresensky, Nucl. Phys. **A845**, 106 (2010).
[28] H. B. Meyer, Phys. Rev. Lett. **100**, 162001 (2008).
[29] K. Itakura, O. Morimatsu, and H. Otomo, Phys. Rev. D **77**, 014014 (2008).
[30] R. Lang, N. Kaiser, and W. Weise, Eur. Phys. J. A **48**, 109 (2012).
[31] D. Fernandiz-Fraile and A. Gomez Nicola, Eur. Phys. J. C **62**, 37 (2009).
[32] S. Mitra, S. Ghosh, and S. Sarkar, Phys. Rev. C **85**, 064917 (2012).
[33] M. Prakash, M. Prakash, R. Venugopalan, and G. Welke, Phys. Rep. **227**, 321 (1993).
[34] A. Dobado and S. N. Santalla, Phys. Rev. D **65**, 096011 (2002); A. Dobado and F. J. Llanes-Estrada, Phys. Rev. D **69**, 116004 (2004).
[35] R. Marty, E. Bratkovskaya, W. Cassing, J. Aichelin, and H. Berrehrah, Phys. Rev. C **88**, 045204 (2013).

[36] A. Dobado, F. J. Llane-Estrada, and J. T. Rincon, Phys. Lett. B **702**, 43 (2011).
[37] M. Bluhm, B. Kampfer, and K. Redlich, Phys. Rev. C **79**, 055207 (2009).
[38] P. Chakraborty and J. I. Kapusta, Phys. Rev. C **83**, 014906 (2011).
[39] K. Rajagopal and N. Trupuraneni, J. High Energy Phys. 03 (2010) 018; J. Bhatt, H. Mishra, and V. Sreekanth, J. High Energy Phys. 11 (2010) 106; Phys. Lett. B **704**, 486 (2011); Nucl. Phys. **A875**, 181 (2012).
[40] S. Mitra and S. Sarkar, Phys. Rev. D **87**, 094026 (2013); S. Mitra, S. Gangopadhyaya, and S. Sarkar, Phys. Rev. D **91**, 094012 (2015).
[41] G. S. Denicol, H. Niemi, E. Molnar, and D. H. Rischke, Phys. Rev. D **85**, 114047 (2012).
[42] M. Greif, F. Reining, I. Bouras, G. S. Denicol, Z. Xu, and C. Greiner, Phys. Rev. E **87**, 033019 (2013).
[43] G. S. Denicol, H. Niemi, I. Bouras E. Molnar, Z. Xu, D. H. Rischke, and C. Greiner, Phys. Rev. D **89**, 074005 (2014).
[44] J. I. Kapusta and J. M. Torres-Rincon, Phys. Rev. C **86**, 054911 (2012).
[45] M. Iwasaki and T. Fukutome, J. Phys. G **36**, 115012 (2009).
[46] S. Nam, Mod. Phys. Lett. A **30**, 1550054 (2015).
[47] S. Ghosh, Int. J. Mod. Phys. E **24**, 1550058 (2015).
[48] P. Singha, A. Abhishek, G. Kadam, S. Ghosh, and H. Mishra, arXiv:1705.03084v2.
[49] B. J. Schaefer, J. M. Pawlowski, and J. Wambach, Phys. Rev. D **76**, 074023 (2007).
[50] U. S. Gupta and V. K. Tiwari, Phys. Rev. D **85**, 014010 (2012).
[51] B. W. Mintz, R. Stiele, R. O. Ramos, and J. S. Bielich, Phys. Rev. D **87**, 036004 (2013).
[52] S. Carignano, M. Buballa, and W. Elkamhawy, Phys. Rev. D **94**, 034023 (2016).
[53] H. Mishra and R. K. Mohapatra, Phys. Rev. D **95**, 094014 (2017).
[54] O. Scavenius, A. Mocsy, I. N. Mishustin, and D. H. Rischke, Phys. Rev. C **64**, 045202 (2001).
[55] S. K. Ghosh, A. Lahiri, S. Majumder, M. G. Mustafa, S. Raha, and R. Ray, Phys. Rev. D **90**, 054030 (2014).
[56] A. Bazavov *et al.*, Phys. Rev. D **90**,094503 (2014).
[57] M. Bluhm, B. Kampfer, and K. Redlich, Phys. Rev. C **84**, 025201 (2011).
[58] M. Albright and J. I. Kapusta, Phys. Rev. C **93**, 014903 (2016).
[59] P. Zhuang, J. Hufner, S. P. Klevansky, and L. Neise, Phys. Rev. D **51**, 3728 (1995).
[60] F. Karsch, D. Kharzeev, and K. Tuchin, Phys. Lett. B **663**, 217 (2008).
[61] S. Gavin, Nucl. Phys. **A435**, 826 (1985).
[62] A. Hosoya and K. Kajantie, Nucl. Phys. **B250**, 666 (1985).
[63] P. Danielewicz and M. Gyulassy, Phys. Rev. D **31**, 53 (1985).
[64] D. T. Son and M. A. Stephanov, Phys. Rev. D **66**, 076011 (2002); B. B. Brandt, A. Francis, H. B. Meyer, and D. Robaina, Phys. Rev. D **92**, 094510 (2015); S. Gupta and R. Sharma arXiv:1710.05345.

Chiral symmetry breaking, color superconductivity, and equation of state for magnetized strange quark matter

Aman Abhishek[1,2,*] and Hiranmaya Mishra[1,†]

[1]*Theory Division, Physical Research Laboratory, Navrangpura, Ahmedabad 380 009, India*
[2]*Indian Institute of Technology Gandhinagar, Gandhinagar, Gujarat 382 355, India*

(Received 25 October 2018; published 22 March 2019)

We investigate the vacuum structure of dense quark matter in strong magnetic fields in a three-flavor Nambu Jona Lasinio (NJL) model including the Kobayashi-Maskawa-t'Hooft (KMT) determinant term using a variational method. The method uses an explicit construct for the "ground" state in terms of quark-antiquark condensates as well as diquark condensates in the background of a constant magnetic field. The coupled mass gap equations and the superconducting gap equation are solved self-consistently and are used to compute the thermodynamic potential along with charge neutrality conditions imposed for bulk matter. Within the model, we observe inverse magnetic catalysis for chiral symmetry breaking for moderate magnetic fields. Further, we observe gapless modes in the presence of the magnetic field when charge neutrality conditions are imposed. The equation of state for charge neutral magnetized strange quark matter is derived, and found to be stiffer compared to the vanishing magnetic field counterpart. This could be relevant for gross structural properties of neutron stars.

DOI: 10.1103/PhysRevD.99.054016

I. INTRODUCTION

The structure of vacuum in quantum chromodynamics (QCD) and its modification under extreme environment has been a major theoretical and experimental challenge in current physics [1]. In particular, it is interesting to study the modification of the structure of ground state at high temperature and/or high baryon densities as related to the nonperturbative aspects of QCD. This is important not only from a theoretical point of view, but also for many applications to problems of quark-gluon plasma (QGP) that could be copiously produced in relativistic heavy ion collisions as well as for the ultradense cold nuclear/quark matter which could be present in the interior of compact stellar objects like neutron stars. In addition to hot and dense QCD, the effect of strong magnetic field on QCD vacuum structure has attracted recent attention. This is motivated by the possibility of creating ultrastrong magnetic fields in noncentral collisions at RHIC and LHC. The strengths of the magnetic fields are estimated to be of hadronic scale [2,3] of the order of $eB \sim 2\ m_\pi^2$ ($m_\pi^2 \simeq 10^{18}$ Gauss) at RHIC, to about $eB \sim 15\ m_\pi^2$ at LHC [3]. There have been recent calculations both analytic as well as with lattice simulations, which indicate that the QCD phase diagram is affected by strong magnetic fields [4–6].

In the context of cold dense matter, compact stars can be strongly magnetized. Neutron star observations indicate the magnetic field to be of the order of 10^{12}–10^{13} Gauss at the surface of ordinary pulsars [7]. Further, the magnetars which are strongly magnetized neutron stars, may have even stronger magnetic fields of the order of 10^{15}–10^{16} Gauss [8–14]. The physical upper limit on the magnetic field in a gravitationally bound star is 10^{18} Gauss which is obtained by comparing the magnetic and gravitational energies using virial theorem [7]. This limit could be higher for self-bound objects like quark stars [15]. Since the magnetic field strengths are of the order of QCD scale, this can affect both the thermodynamic as well as the hydrodynamics of such magnetized matter [16]. The phase structure of dense matter in the presence of the magnetic field along with a nonzero chiral density has been investigated for two-flavor Polyakov Loop extended Nambu-Jona Lasinio model (PNJL) model for high temperatures relevant for RHIC and LHC [17]. There have also been many investigations to look into the vacuum structure of QCD and it has been recognized that the strong magnetic field acts as a catalyzer of chiral symmetry breaking [18–22]. The effects of magnetic field on the equation of state have been recently studied in the Nambu Jona Lasinio model at zero temperature for three flavors and the equation of state has been computed for the cold quark matter [23,24] taking into account chiral condensate structure with the quark-antiquark pair for the ground state.

*aman@prl.res.in
†hm@prl.res.in

On the other hand, color superconductivity is now an accepted conjectured state of cold and dense quark matter describing Cooper pairing of quarks of different colors and different flavors [25,26]. One can have a rigorous treatment of the phenomenon of such pairing using asymptotic freedom of QCD at very high densities. In its simplest form, when masses of the three quarks can be neglected compared to the chemical potential one can have the color flavor locked (CFL) phase [25,26]. However, to apply it to neutron star matter, the situation is more complicated as for the densities expected in the interior of neutron star, the masses of strange quarks cannot be neglected. Further, many nontrivial complications arise when beta equilibrium and charge neutrality conditions are imposed in such systems [27]. Since the well known sign problem prevents the first principle lattice simulations at finite chemical potentials, one has to rely on effective models at this regime of moderate densities. One model that has been extensively studied in this context has been the Nambu Jona Lasinio (NJL) model with contact interactions [28,29].

Of late, there has been a lot of attention on the investigation of color superconductivity in the presence of the magnetic field [18,19,30–32]. Essentially, this is due to its possible application in the astrophysical situations as the densities in compact star cores are large enough to have a possible superconducting phase as well as such compact stars can have a strong magnetic field as mentioned above. Let us also mention here that although such systems can be color superconductors, these phases can be penetrated by a "rotated" long range magnetic field. The corresponding rotated gauge field is a linear combination of vacuum photon field and the eighth gluon field [33,34]. These rotated magnetic fields are not subjected to the Meissener effect. While the Cooper pair is neutral with respect to the magnetic field, the quark quasiparticles have well-defined charges. Therefore, the pairing phenomenon is affected by the presence of the magnetic field. Initially, the effect of the magnetic field on superconducting phase has been studied for the CFL phase [30] where all three quarks take part in the pairing dynamics. However, for realistic densities, such symmetric pairing is disfavored due to large strange quark mass that leads to large mismatch in the Fermi surface. The condition of charge neutrality further complicates the pairing mechanism leading to gapless modes for homogeneous diquark pairing [35,36]. Superconductivity for the two-flavor quark matter in the presence of the magnetic field has been studied in Refs. [19,37,38] within the NJL model. The effect of charge neutrality along with the interplay of chiral and superconducting condensates has been analyzed in Refs. [37,38] in this model. A complete three-flavor analysis of magnetized dense quark matter including superconductivity has not been attempted so far. In the present investigation we include the effects of strange quarks that take part in chiral condensation but not in the diquark channel in the magnetized quark matter. As we shall see, the strange quarks, similar to the vanishing magnetic field case, play an important role for charge neutral matter and the resulting equation of state. Moreover, with the inclusion of a flavor mixing interaction term, the strange quark scalar condensate not only affects the light quark condensates but also the diquark condensates.

We had earlier considered a variational approach to study chiral symmetry breaking as well as color superconductivity in hot and dense matter with an explicit structure for the "ground state" [36,39–41] with quark-antiquark condensate. The calculations were carried out within NJL model with minimization of free energy density to decide which condensate will exist at what density and/or temperature. A nice feature of the approach is that the four component quark field operator in the chiral symmetry broken phase gets determined from the vacuum structure. In the present work, we aim to investigate how the vacuum structure in the context of chiral symmetry breaking and color superconductivity gets modified in the presence of a magnetic field. In the context of chiral symmetry breaking, it was seen that, since the vacuum contains quark-antiquark pairs, the Dirac vacuum gets corrections due to the effective magnetic field apart from the modification of the medium or the Fermi sea of quarks. In our analysis we also keep these contributions to the equation of state.

We organize the paper as follows. In Sec. II, we discuss an ansatz state with quark-antiquark pairs related to chiral symmetry breaking, diquark and diantiquark pairs for the light flavors related to color superconductivity in the presence of a magnetic field. We then generalize such a state to include the effects of temperature and density. In Sec. III, we consider the three-flavor NJL model along with the so-called the Kobayashi-Maskawa-t'Hooft (KMT) term—the six fermion determinant interaction term which breaks U(1) axial symmetry as in QCD. We use this Hamiltonian and calculate its expectation value with respect to the ansatz state to compute the energy density as well the thermodynamic potential for this system. We minimize the thermodynamic potential to determine the ansatz functions and the resulting mass gap equations. These coupled mass and superconducting gap equations are solved and we discuss the results in Sec. IV. We discuss here the results with and without constraints of charge neutrality. Finally we summarize and conclude in Sec. V. In the Appendix we give some details of the derivation of the evaluation of expectation values of the order parameters.

II. THE ANSATZ FOR THE GROUND STATE

Let us first consider the ground state structure relevant for chiral symmetry breaking in the presence of a strong magnetic field [24]. We shall then modify the same relevant for color superconductivity. To make the notations clear, we first write down the field operator expansion for quarks with a current quark mass m and charge q in the momentum space in the presence of a constant magnetic field $\mathbf{B}$.

We take the field direction to be along the z axis. We choose the gauge such that the electromagnetic vector potential is given as $A_\mu(\boldsymbol{x}) = (0,0,Bx,0)$. The quark field operator expansion in the presence of a constant magnetic field is given as [24,42]

$$\psi(\mathbf{x}) = \sum_n \sum_r \int \frac{d\mathbf{p}_{\not{x}}}{2\pi}[q_r^0(n,\mathbf{p}_{\not{x}})U_r^0(x,\mathbf{p}_{\not{x}},n) + \tilde{q}_r^0(n,-\mathbf{p}_{\not{x}})V_r^0(x,-\mathbf{p}_{\not{x}},n)]e^{i\mathbf{p}_{\not{x}}\cdot\mathbf{x}_{\not{x}}}. \tag{1}$$

Here n is the Landau level and the sum over it runs from 0 to infinity. In the above, $\mathbf{p}_{\not{x}} \equiv (p_y, p_z)$, and $r = \pm 1$ denotes the up and down spins. We have suppressed the color and flavor indices of the quark field operators. The quark annihilation and antiquark creation operators, q_r^0 and $\tilde{q}_r^0$, respectively, satisfy the quantum algebra

$$\{q_r^0(n,\mathbf{p}_{\not{x}}), q_{r'}^{0\dagger}(n',\mathbf{p}'_{\not{x}})\} = \{\tilde{q}_r^0(n,\mathbf{p}_{\not{x}}), \tilde{q}_{r'}^{0\dagger}(n',\mathbf{p}'_{\not{x}})\} = \delta_{rr'}\delta_{nn'}\delta(\mathbf{p}_{\not{x}} - \mathbf{p}'_{\not{x}}). \tag{2}$$

In the above, U_r and V_r are the four component spinors for the quarks and antiquarks respectively. The explicit forms of the spinors for the fermions with mass m and electric charge q are given by

$$U_\uparrow^0(x,\boldsymbol{p}_{\not{x}},n) = \begin{pmatrix} \cos\frac{\phi_0}{2}(\theta(q)I_n + \theta(-q)I_{n-1}) \\ 0 \\ \hat{p}_z\sin\frac{\phi_0}{2}(\theta(q)I_n + \theta(-q)I_{n-1}) \\ -i\hat{p}_\perp\sin\frac{\phi_0}{2}(\theta(q)I_{n-1} - \theta(-q)I_n) \end{pmatrix} \tag{3a}$$

$$U_\downarrow^0(x,\boldsymbol{p}_{\not{x}},n) = \begin{pmatrix} 0 \\ \cos\frac{\phi_0}{2}(\theta(q)I_{n-1} + \theta(-q)I_n) \\ i\hat{p}_\perp\sin\frac{\phi_0}{2}(\theta(q)I_n - \theta(-q)I_{n-1}) \\ -\hat{p}_z\sin\frac{\phi_0}{2}(\theta(q)I_{n-1} + \theta(-q)I_n) \end{pmatrix} \tag{3b}$$

$$V_\uparrow^0(x,-\mathbf{p}_{\not{x}},n) = \begin{pmatrix} \hat{p}_\perp\sin\frac{\phi_0}{2}(\theta(q)I_n - \theta(-q)I_{n-1}) \\ i\hat{p}_z\sin\frac{\phi_0}{2}(\theta(q)I_{n-1} + \theta(-q)I_n) \\ 0 \\ i\cos\frac{\phi_0}{2}(\theta(q)I_{n-1} + \theta(-q)I_n) \end{pmatrix} \tag{3c}$$

$$V_\downarrow^0(x,-\boldsymbol{p}_{\not{x}},n) = \begin{pmatrix} i\hat{p}_z\sin\frac{\phi_0}{2}(\theta(q)I_n + \theta(-q)I_{n-1}) \\ \hat{p}_\perp\sin\frac{\phi_0}{2}(\theta(q)I_{n-1} - \theta(-q)I_n) \\ -i\cos\frac{\phi_0}{2}(\theta(q)I_n + \theta(-q)I_{n-1}) \\ 0 \end{pmatrix}. \tag{3d}$$

Here $\theta(x)$ is the Heaviside theta function. In the above, the energy of the nth Landau level is given as $\epsilon_n = \sqrt{m^2 + p_z^2 + 2n|q|B} \equiv \sqrt{m^2 + |p^2|}$ with $p^2 = p_z^2 + p_\perp^2$ so that $p_\perp^2 = 2n|q|B$, $\hat{p}_z = p_z/|p|$, $\hat{p}_\perp = \sqrt{2n|q|B}/|p|$. In Eqs. (3), $\cot\phi_0 = m/|p|$. Clearly, for vanishing masses $\phi_0 = \pi/2$. The functions I_n' s (with $n \geq 0$) are functions of $\xi = \sqrt{|qB|}(x - p_y/|qB|)$ and are given as

$$I_n(\xi) = c_n \exp\left(-\frac{\xi^2}{2}\right)H_n(\xi), \tag{4}$$

where $H_n(\xi)$ is the Hermite polynomial of the nth order and $I_{-1} = 0$. The normalization constant c_n is given by

$$c_n = \sqrt{\frac{\sqrt{|q|B}}{n!2^n\sqrt{\pi}}}.$$

The functions $I_n(\xi)$ satisfy the orthonormality condition

$$\int d\xi I_n(\xi)I_m(\xi) = \sqrt{|q|B}\delta_{n,m}, \tag{5}$$

so that the spinors are properly normalized. The detailed derivation of these spinors and some of their properties are presented in the Appendix of Ref. [24].

With the field operators now defined in terms of the annihilation and the creation operators in the presence of a constant magnetic field, one can write down an ansatz for the ground state as in Ref. [24]. The ground state is taken as a squeezed coherent state involving quark and antiquarks pairs. Explicitly [24,36,39,41],

$$|\Omega\rangle = \mathcal{U}_Q|0\rangle. \tag{6}$$

Here, $\mathcal{U}_Q$ is an unitary operator which creates quark-antiquark pairs from the vacuum $|0\rangle$ which in annihilated by the quark/antiquark annihilation operators given in Eq. (1). Explicitly, the operator $\mathcal{U}_Q$ is given as [24]

$$\mathcal{U}_Q = \exp\left(\sum_{n=0}^{\infty}\int d\boldsymbol{p}_{\not{x}} q_r^{0i\dagger}(n,\boldsymbol{p}_{\not{x}})a_{r,s}^i(n,p_z)h^i(n,\boldsymbol{p}_z) \times \tilde{q}_s^{0i}(n,-\boldsymbol{p}_{\not{x}}) - \text{H.c.}\right). \tag{7}$$

In the above ansatz for the ground state, the function $h^i(n,p_z)$ is a real function describing the quark-antiquark condensates related to the vacuum realignment for chiral symmetry breaking to be obtained from a minimization of the thermodynamic potential. In the above equation, the spin dependent structure $a_{r,s}^i$ is given by

$$a_{r,s}^i = \frac{1}{|\mathbf{p}_i|}[-\sqrt{2n|q_i|B}\delta_{r,s} - ip_z\delta_{r,-s}], \tag{8}$$

with $|\mathbf{p}_i| = \sqrt{p_z^2 + 2n|q_i|B}$ denoting the magnitude of the three momentum of the quark/antiquark of ith flavor (with electric charge q_i) in the presence of a magnetic field.

Summation over three colors and three flavors is understood in the exponent of $\mathcal{U}_Q$ in Eq. (7). Clearly, a nontrivial $h_i(n, p_z)$ breaks the chiral symmetry.

It is easy to show that the transformation of the ground state as in Eq. (6) is a Bogoliubov transformation. With the ground state transforming as Eq. (6), any operator O^0 in the $|0\rangle$ basis transforms as

$$O = \mathcal{U}_Q O^0 \mathcal{U}_Q^\dagger, \tag{9}$$

and, in particular, one can transform the creation and annihilation operators of Eq. (1) to define the transformed operators as above satisfying the same anticommutation relations as in Eq. (2):

$$\psi(\mathbf{x}) = \sum_n \sum_r \frac{1}{2\pi} \int d\mathbf{p}_{\chi}[q_r(n, \mathbf{p}_{\chi}) U_r(x, n, \mathbf{p}_{\chi}) + \tilde{q}_r(n, -\mathbf{p}_{\chi}) V_r(x, n, -\mathbf{p}_{\chi})] e^{i\mathbf{p}_{\chi}\cdot\mathbf{x}_{\chi}}, \tag{10}$$

with $q_r|\Omega\rangle = 0 = \tilde{q}_r^\dagger|\Omega\rangle$. In the above, we have suppressed the flavor and color indices. It is easy to see that the form of U, V spinors is exactly similar to the form of the spinors U_0, V_0 as in Eq. (3) but with the shift of the function $\phi_0 \to \phi = \phi_0 - 2h$ with the function $h(\mathbf{k})$ to be determined by a minimization of free energy. As we shall see later, it is more convenient to vary $\phi(\mathbf{k})$ rather than $h(\mathbf{k})$. Let us note that with Eq. (10), the four component quark field operator gets defined in terms of the vacuum structure for chiral symmetry breaking given through Eq. (6) and Eq. (7) in the presence of a magnetic field [43].

The chiral order parameter in the condensate vacuum $|\Omega\rangle$ can be evaluated explicitly using the field operator expansion given in Eq. (10) and is given by [24] (for ith flavor)

$$I_s^i = \langle\Omega|\bar{\psi}^i\psi^i|\Omega\rangle = -\sum_n N_c \alpha_n \frac{|q_i B|}{(2\pi)^2} \int dp_z \cos\phi^i. \tag{11}$$

This expression for the quark-antiquark condensate is exactly the same form as derived earlier in the absence of the magnetic field [39,40] once one realizes that in the presence of a quantizing magnetic field with discrete Landau levels, one has for the phase space integration [37]

$$\int \frac{d\mathbf{p}}{(2\pi)^3} \to \sum_{n=0}^{\infty} \alpha_n \frac{|qB|}{(2\pi)^2} \int dp_z.$$

Next, we would like to generalize the ansatz of Eq. (6) with quark-antiquark pairs in the presence of a magnetic field, to include quark-quark pairs for the description of the ground state as relevant for color superconductivity. However, few comments in this context are in order. It is known that in the presence of color superconductivity, the diquark is electromagnetically charged and the usual magnetic field will have a Meissner effect. However, a linear combination of the photon field and the gluon field given by $\tilde{A}_\mu = \cos\alpha A_\mu - \sin\alpha G_\mu^8$ still remains massless and is unscreened. For two-flavor color superconductivity, $\cos\alpha = g/\sqrt{g^2 + e^2/3} \sim 1/20$ [33]. The electron couples to this rotated gauge field by the coupling $\tilde{e} = e\cos(\alpha)$. The quark field couples to the rotated gauge field through its rotated charge $\tilde{Q}$. In units of $\tilde{e}$, the rotated charge matrix in the flavor-color space is given by

$$\tilde{Q} = Q_f \otimes \mathbf{1}_c - \mathbf{1}_f \otimes \frac{T_c^8}{2\sqrt{3}}. \tag{12}$$

Thus, the $\tilde{e}$ charges of red and green u quarks is $1/2$; red and green down and strange quarks is $-1/2$. The blue u quark has $\tilde{Q}$ charge as $+1$, while the blue d and s quarks are $\tilde{Q}$ chargeless. We shall take the rotated U(1) magnetic field along the z axis and spatially constant as before without the absence of superconductivity. The ansatz for the ground state with quark-antiquark condensate is now taken as, with i being the flavor index,

$$|\Omega\rangle_\chi = \exp\sum_{flav}(B_i^\dagger - B_i)|0\rangle. \tag{13}$$

The flavor dependent quark-antiquark pair creation operator for u quark ($i = 1$) is given as, with $a = 1, 2, 3$ being the color indices for red, blue and green respectively,

$$B_u^\dagger = \sum_{a=1}^{3}\sum_{n=0}^{\infty} \int d\boldsymbol{p}_{\chi} q_r^{1a}(n,\boldsymbol{p}_{\chi})^\dagger a_{r,s}^1(n,p_z) f^{1a}(n,\boldsymbol{p}_{\chi}) \tilde{q}_s^{1a}(n,-\boldsymbol{p}_{\chi}), \tag{14}$$

while, for the down and strange quarks ($i = 2, 3$) the same is given as

$$B_i^\dagger = \sum_{a=1}^{2}\sum_{n=0}^{\infty} \int d\boldsymbol{p}_{\chi} q_r^{ia}(n,\boldsymbol{p}_{\chi})^\dagger a_{r,s}^i(n,p_z) h^{ia}(n,\boldsymbol{p}_{\chi}) \tilde{q}_s^{1a}(n,-\boldsymbol{p}_{\chi}) + \int d\mathbf{p} q_r^{i3}(\mathbf{p})^\dagger (\sigma\cdot\hat{\mathbf{p}})_{rs} h^i(\mathbf{p}) \tilde{q}_s^{i3}(-\mathbf{p}). \tag{15}$$

The difference between the pair creation operator in Eqs. (14) and (15) lies on the contribution of the blue color. While the up blue quark has $\tilde{Q}$ charge, the blue quarks of down and strange quark are $\tilde{Q}$ neutral.

Next, we write down the ansatz state for having quark-quark condensates which is given by

$$|\Omega\rangle = U_d|\Omega\rangle_\chi \equiv \exp(B_d^\dagger - B_d)|\Omega\rangle_\chi. \tag{16}$$

In the above, $B_d^\dagger$ is the diquark (and di-antiquark) creation operator given as

$$B_d^\dagger = \sum_n \int dp_\chi [q_r^{ia}(n,p_\chi)^\dagger r f(n,p_z) q_{-r}^{jb}(n,-p_\chi,p_z) + i\tilde{q}_r^{ia}(n,p_\chi)^\dagger r f_1(n,p_z) \tilde{q}_{-r}^{jb}(n,p_\chi)^\dagger] \epsilon^{ij3}\epsilon^{3ab}. \quad (17)$$

In the above, i, j are the flavor indices, a, b are the color indices and $r = \pm 1/2$ are the spin indices. The Levi-Cività tensor ensures that the operator is antisymmetric in color and flavor space along with the fact that only u, d quarks with red and green colors take part in diquark condensation. The blue u, d quarks as well as the strange quarks (all three colors) do not take part in the diquark condensation. The functions $f(n,p_z)$ and $f_1(n,p_z)$ are condensate functions associated with quark-quark and antiquark-antiquark condensates respectively. These functions are assumed to be independent of color and flavor indices. We shall give a *post facto* justification for this that these functions depend upon the average energy and average chemical potentials of the quarks that condense.

To include the effects of temperature and density we next write down the state at finite temperature and density $|\Omega(\beta,\mu)\rangle$ through a thermal Bogoliubov transformation over the state $|\Omega\rangle$ using the thermofield dynamics (TFD) method as described in Refs. [24,44,45]. This is particularly useful while dealing with operators and expectation values. We write the thermal state as

$$|\Omega(\beta,\mu)\rangle = \mathcal{U}_{\beta,\mu}|\Omega\rangle = \mathcal{U}_{\beta,\mu}\mathcal{U}_Q|0\rangle, \quad (18)$$

where $\mathcal{U}_{\beta,\mu}$ is given as

$$\mathcal{U}_{\beta,\mu} = e^{\mathcal{B}^\dagger(\beta,\mu) - \mathcal{B}(\beta,\mu)},$$

with

$$\mathcal{B}^\dagger(\beta,\mu) = \sum_{n=0}^{\infty} \int [d\boldsymbol{k}_\chi q_r^{ia}(n,k_\chi)^\dagger \theta_-^{ia}(k_z,n,\beta,\mu) \underline{q}_r^{ia}(n,k_\chi)^\dagger + \tilde{q}_r^{ia}(n,k_\chi)\theta_+^{ia}(k_z,n,\beta,\mu)\underline{\tilde{q}}_r^{ia}(n,k_\chi)]. \quad (19)$$

In Eq. (19), the underlined operators are the operators in the extended Hilbert space associated with thermal doubling in the TFD method, and the color flavor dependent ansatz functions $\theta_\pm^{ia}(n,k_z,\beta,\mu)$ are related to quark and antiquark distributions as can be seen through the minimization of the thermodynamic potential.

All the functions in the ansatz in Eq. (18) are to be obtained by minimizing the thermodynamic potential. We shall carry out this minimization in the next section. However, before carrying out the minimization procedure, let us focus our attention to the expectation values of some known operators to show that with the above variational ansatz for the ground state given in Eq. (18) these reduce to the already known expressions in the appropriate limits.

Let us first consider the expectation value of the chiral order parameter. The expectation value for chiral order parameter for the ith flavor is given as

$$I_s^i = \langle\Omega(\beta,\mu)|\bar{\psi}_i\psi_i|\Omega(\beta,\mu)\rangle = \sum_{a=1}^{3} I_s^{ia}. \quad (20)$$

These expectation values can be evaluated easily once we realize that the state $|\Omega(\beta,\mu)\rangle$ as in Eq. (18) is obtained through successive Bogoliubov transformations on the state $|0\rangle$ as in Eqs. (13) and (16). The details of evaluation for the different order parameters is relegated to the Appendix. Explicitly, for the quarks that take part in superconductivity

$$I_s^{ia} = -\sum_n \alpha_n \frac{|q^{ia}B|}{(2\pi)^2} \times \int dp_z \cos\phi^{ia}(1 - F^{ia} - F_1^{ia}), \quad (i,a = 1,2), \quad (21)$$

where $\alpha_n = (2 - \delta_{n,0})$ is the degeneracy factor of the nth Landau level (all levels are doubly degenerate except the lowest Landau level). Further,

$$F^{ia} = \sin^2\theta_-^{ia} + \sin^2 f(1 - \sin^2\theta_-^{ia} - |\epsilon^{ij}|\epsilon^{ab}|\sin^2\theta_-^{jb}), \quad (22)$$

arising from the quarks which condense and

$$F_1^{ia} = \sin^2\theta_+^{ia} + \sin^2 f_1(1 - \sin^2\theta_+^{ia} - |\epsilon^{ij}|\epsilon^{ab}|\sin^2\theta_+^{jb}), \quad (23)$$

arising from antiquarks which condense. Thus, the scalar condensates arising from quarks that take part in superconductivity depend both on the condensate functions in quark-antiquark channel (ϕ^i) as well as in quark-quark channel (f, f_1). Further, the thermal functions $\sin^2\theta_\pm^{ia}$, as we shall see later, will be related to the number density distribution functions.

Next, for the nonsuperconducting blue up quarks, the contribution to the scalar condensate is given by

$$I_s^{13} = -\sum_n \alpha_n \frac{|q^{13}|B}{(2\pi)^2} \int dp_z \cos\phi^{13}(1 - \sin^2\theta_-^{13} - \sin^2\theta_+^{13}). \quad (24)$$

Let us note that in the limit of vanishing of the color superconducting condensate functions ($f, f_1 \to 0$), the contributions given in Eq. (21) reduce to Eq. (24) as they should [24].

Similarly, scalar condensate contribution from the charged strange quarks (red, green) is given by

$$I_s^{3a} = -\sum_n \alpha_n \frac{|q^{3a}|B}{(2\pi)^2} \times \int dp_z \cos\phi^{3a}(1 - \sin^2\theta_-^{3a} - \sin^2\theta_+^{3a}) \quad (a = 1,2). \quad (25)$$

Finally, for the uncharged quarks, i.e., blue down and blue strange quarks, the contributions to the scalar condensates are given by, for flavor i ($i = 2, 3$),

$$I_s^{i3} = -\frac{2}{(2\pi)^3} \int d\mathbf{k} \cos\phi^i (1 - \sin^2\theta_-^{i3} - \sin^2\theta_+^{i3}). \tag{26}$$

Next, we write down the condensate in the superconducting channel which is given as

$$\begin{aligned} I_D &= \langle \bar{\psi}_c^{ia} \gamma^5 \psi^{jb} \rangle \epsilon^{ij} \epsilon^{3ab} \\ &= \sum_n \alpha_n \frac{|q_i B|}{(2\pi)^2} \int dp_z \cos\left(\frac{\phi_1 - \phi_2}{2}\right) \\ &\quad \times [\sin 2f (1 - \sin^2\theta_-^1 - \sin^2\theta_-^2) \\ &\quad + \sin 2f_1 (1 - \sin^2\theta_+^1 - \sin^2\theta_+^2)]. \end{aligned} \tag{27}$$

Let us note that the superconducting condensate also depends upon the chiral condensate functions $\phi(p_z)$ through the function $\cos(\frac{\phi_1 - \phi_2}{2})$ apart from the thermal distribution functions $\sin^2\theta_\pm^{ia}$. Further, this dependence vanishes when the u and d quark scalar condensates or equivalently the corresponding masses of the quarks are equal.

The other quantity that we wish to investigate is the axial fermion current density that is induced at finite chemical potential including the effect of temperature. The expectation value of the axial current density is given by

$$\langle j_5^3 \rangle \equiv \langle \bar{\psi}_i^a \gamma^3 \gamma^5 \psi_j^a \rangle.$$

Using the field operator expansion Eq. (10) and Eq. (3) for the explicit forms for the spinors, we have for the ith flavor

$$\langle j_5^{i3} \rangle = \sum_n \frac{N_c}{(2\pi)^2} \int dp_x (I_n^2 - I_{n-1}^2)(\sin^2\theta_-^i - \sin^2\theta_+^i). \tag{28}$$

Integrating over dp_y using the orthonormal condition of Eq. (5), all the terms in the above sum for the Landau levels cancel out except for the zeroth Landau level so that

$$\langle j_5^{i3} \rangle = \frac{N_c |q_i| B}{(2\pi)^2} \int dp_z [\sin^2\theta_-^{i0} - \sin^2\theta_+^{i0}], \tag{29}$$

which is identical to that in Ref. [46] once we identify the functions $\sin^2\theta_\mp^{i0}$ as the particle and the antiparticle distribution functions for the zero modes [see e.g., Eq. (55) in the next section]. In the chiral limit at zero temperature and without superconductivity, one gets the following as the axial current after summing over all three flavors:

$$\langle j_5^0 \rangle = \frac{3eB}{2\pi^2} \left[\mu + \frac{1}{3}\sqrt{\mu^2 - m_s^2}\right]. \tag{30}$$

III. EVALUATION OF THERMODYNAMIC POTENTIAL AND GAP EQUATIONS

As has already been mentioned, we shall consider in the present investigation, the three-flavor Nambu Jona Lasinio model including the Kobayashi-Maskawa-t-Hooft (KMT) determinant interaction. The corresponding Hamiltonian density is given as [24,28,36,47]

$$\begin{aligned} \mathcal{H} &= \psi^\dagger(-i\boldsymbol{\alpha}\cdot\boldsymbol{\Pi}) + \gamma^0 \hat{m})\psi \\ &\quad - G_S \sum_{A=0}^{8} [(\bar{\psi}\lambda^A\psi)^2 - (\bar{\psi}\gamma^5\lambda^A\psi)^2] \\ &\quad + K[det_f[\bar{\psi}(1+\gamma_5)\psi] + det_f[\bar{\psi}(1-\gamma_5)\psi]] \\ &\quad - G_D[(\bar{\psi}\gamma^5\epsilon\epsilon_c\psi^C)(\bar{\psi}^C\gamma^5\epsilon\epsilon_c\psi)], \end{aligned} \tag{31}$$

where $\psi^{i,a}$ denotes a quark field with color "a" ($a = r, g, b$), and flavor "i" ($i = u, d, s$), indices. $\Pi = -i(\nabla - i\tilde{e}\tilde{\boldsymbol{A}}\tilde{Q})$ is the canonical momentum in the presence of the rotated U(1) gauge field $\tilde{A}_\mu$. ϵ is the Levi-Cività tensor in flavor space while ϵ_c is the Levi-Cività tensor in color space. $\psi^C = i\gamma^1\gamma^2\psi$ is the charge conjugate spinor. When there is no superconductivity $A_\mu = \tilde{A}_\mu$ which is the usual massless photon field with the coupling to the quark field being given the electromagnetic charge eQ_f, where Q_f is diagonal matrix $(2/3, -1/3, -1/3)$. As mentioned in the previous section, when the superconducting gap is nonvanishing, the massless gauge field is given by $\tilde{A}_\mu = \cos\alpha A_\mu - \sin\alpha G_\mu^8$, where $\cos\alpha = g/\sqrt{g^2 + e^2/3}$. We have taken here the standard convention of $SU(3)_c$ generators in the adjoint representation [33]. The $\tilde{Q}$ charges of the quarks are given in Table I. It may also be relevant here to mention that, while we are taking into account combination of the photon and gluon field which is massless, the other orthogonal massive component, is either Meissner screened or nucleated into vortices [48].

The matrix of current quark masses is given by $\hat{m} = \mathrm{diag}_f(m_u, m_d, m_s)$ in the flavor space. We shall assume in the present investigation, isospin symmetry with $m_u = m_d$.

TABLE I. Table: List of quarks and their electromagnetic and rotated charges.

Quark	e-charge	$\tilde{e}$-charge
u-red	$\frac{2}{3}$	$\frac{1}{2}$
u-green	$\frac{2}{3}$	$\frac{1}{2}$
u-blue	$\frac{2}{3}$	1
d-red	$-\frac{1}{3}$	$-\frac{1}{2}$
d-green	$-\frac{1}{3}$	$-\frac{1}{2}$
d-blue	$-\frac{1}{3}$	0
s-red	$-\frac{1}{3}$	$-\frac{1}{2}$
s-green	$-\frac{1}{3}$	$-\frac{1}{2}$
s-blue	$-\frac{1}{3}$	0

In Eq. (31), λ^A, $A = 1, \ldots 8$ denote the Gellmann matrices acting in the flavor space and $\lambda^0 = \sqrt{\frac{2}{3}}\mathbf{1}_f$, $\mathbf{1}_f$ as the unit matrix in the flavor space. The four point interaction term $\sim G_S$ is symmetric in $SU(3)_V \times SU(3)_A \times U(1)_V \times U(1)_A$. In contrast, the determinant term $\sim K$ which for the case of three flavors generates a six point interaction which breaks $U(1)_A$ symmetry. In the absence of magnetic field, if the mass term is neglected, the overall symmetry is $SU(3)_V \times SU(3)_A \times U(1)_V$. This spontaneously breaks to $SU(3)_V \times U(1)_V$ implying the conservation of the baryon number and the flavor number. The current quark mass term introduces additional explicit breaking of chiral symmetry leading to partial conservation of the axial current. The last term in Eq. (31) describe a scalar diquark interaction in the color antitriplet and flavor antitriplet channel. Such a form of four point interaction can arise e.g., by Fierz transformation of a four point vector current-current interaction having quantum numbers of a single gluon exchange. In that case the diquark coupling G_D is related to the scalar coupling as $G_D = 0.75 G_S$.

Next we evaluate the expectation value of the kinetic term in Eq. (31) which is given as

$$T = \langle\Omega(\beta,\mu)|\psi^{ia\dagger}(-i\boldsymbol{\alpha}\cdot\nabla - \tilde{q}^{ia}Bx\alpha_2)\psi^{ia}|\Omega(\beta,\mu)\rangle \equiv \sum_{ia} T^{ia}. \tag{32}$$

In the above the sum over the colors a and flavors i is understood. The color flavor dependent charges $\tilde{q}^{ia}$ for the quasiparticles is given in Table I. To evaluate this, for nonvanishing $\tilde{q}$ charges, we use Eq. (10) and the results of spatial derivatives on the functions $I_n(\xi)$ ($\xi = \sqrt{|q_i|B}(x - p_y/(|q_i|B))$):

$$\frac{\partial I_n}{\partial x} = \sqrt{|q^{ia}|B}[-\xi I_n + \sqrt{2n} I_{n-1}],$$
$$\frac{\partial I_{n-1}}{\partial x} = \sqrt{|\tilde{q}^{ia}|B}[-\xi I_{n-1} + \sqrt{2(n-1)} I_{n-2}]. \tag{33}$$

Using the above, a straightforward but somewhat tedious manipulations lead to the contribution arising from the quarks that take part in superconductivity, i.e., for color, flavor indices i, $a = 1, 2$,

$$T^{ia} = -\sum_{n=0}^{\infty} \alpha_n \frac{|\tilde{e}B|}{2(2\pi)^2} \int dp_z (m_i \cos\phi_i + |p_i| \sin\phi_i) \times (1 - F^{ia} - F_1^{ia}), \qquad (i, a = 1, 2), \tag{34}$$

where we have defined $|p_i|^2 = p_z^2 + 2n|\tilde{q}B|$, ($\tilde{q} = \tilde{e}/2$). Here, the quark-antiquark condensate effects are encoded in the function ϕ_i while diquark and di-antiquark condensate effects are encoded in the functions F^{ia} and F_1^{ia} respectively as given in Eqs. (22) and (23).

For the blue u quark, which is charged but does not take part in diquark condensation the corresponding contribution to the kinetic term is given by

$$T^{13} = -\sum_{n=0}^{\infty} \alpha_n \frac{|\tilde{e}B|}{(2\pi)^2} \int dp_z (m_1 \cos\phi_1 + |p_1| \sin\phi_1)(1 - \sin^2\theta_-^{13} - \sin^2\theta_+^{13}). \tag{35}$$

The contribution of the charged strange quarks (with charges $\tilde{e}/2$) to the kinetic energy is given by, with $a = 1, 2$,

$$T^{3a} = -\sum_{n=0}^{\infty} \alpha_n \frac{|\tilde{e}B|}{2(2\pi)^2} \int dp_z (m_3 \cos\phi_3 + |p_3| \sin\phi_3)(1 - \sin^2\theta_-^{3a} - \sin^2\theta_+^{3a}). \tag{36}$$

Finally, the contribution from the $\tilde{e}$ -charge neutral quarks (blue d and blue s) is given as

$$T^{i3} = -\int \frac{d\mathbf{p}}{(2\pi)^3} (m_i \cos\phi_i + p \sin\phi_i)(1 - \sin^2\theta_-^{i3} - \sin^2\theta_+^{i3}) \qquad (i = 2, 3). \tag{37}$$

The contribution to the energy density from the quartic interaction term in Eq. (31), using Eq. (20) turns out to be

$$V_S \equiv -G_S \langle\Omega(\beta,\mu)| \sum_{A=0}^{8} [(\bar{\psi}\lambda^A\psi)^2 - (\bar{\psi}\gamma^5\lambda^A\psi)^2] |\Omega(\beta,\mu)\rangle = -2G_S \sum_{i=1,3} I_s^{i\,2}, \tag{38}$$

where $I_s^i = \langle\bar{\psi}_i\psi_i\rangle$ is the scalar quark-antiquark condensate given in Eq. (20). Further, in the above, we have used the properties of the Gellman matrices $\sum_{A=0}^{8} \lambda_{ij}^A \lambda_{kl}^A = 2\delta_{il}\delta_{jk}$.

Next, let us discuss the contribution from the six quark determinant interaction term to the energy expectation value. There will be six terms in the expansion of the determinant, each involving three pairs of quark operators of different flavors. These are to be "contracted" in all possible manner while taking the expectation value. This means in the present context of having quark-antiquark and diquark condensates, one can contract a ψ with a $\bar{\psi}$

or ψ with a ψ. The former leads to condensates having quark-antiquark condensates $I_s^{(i)}$ while the latter leads to diquark condensates I_D. Further, for the case of quark-antiquark condensate contributions, the contracting ψ and $\bar{\psi}$ having the same color will lead to the dominant contribution while contracting similar operators with different colors will lead to a N_c suppressed contribution. Next, regarding the contributions arising from the diquark, terms which are proportional to strange quark-antiquark condensate $\langle\bar{s}s\rangle$ will be dominant. These will have the contractions of strange quark-antiquarks having the same color. The rest of the four terms will be suppressed at least by a factor N_c. Explicitly these two terms are given by $\sim\sum_h \bar{s}\,O^h s[\bar{u}\hat{O}^h u\times(\bar{d}\hat{O}^h d) - \bar{u}\hat{O}^h d\times(\bar{d}\hat{O}^h u)]$, where $h=\pm$ and $\hat{O}^{\pm}=(1\pm\gamma_5)$. When contracted diquark wise, both terms give identical contributions, except that the contribution of the second term will be of opposite sign as compared to the first term. This is a consequence of the flavor antisymmetric nature of the diquark condensates. This leads to

$$\begin{aligned} V_{\rm det} &= +K\langle \det_f[\bar{\psi}(1+\gamma_5)\psi] + \det_f[\bar{\psi}(1-\gamma_5)\psi]\rangle \\ &= \frac{1}{3}|\epsilon_{ijk}|I_s^{(i)}I_s^{(j)}I_s^{(k)} + \frac{K}{4}I_s^{(3)}I_D^2. \end{aligned}$$

Next, the contribution from the diquark interaction is given by

$$V_D = -\langle G_D[(\bar{\psi}\gamma^5\epsilon\epsilon_c\psi^C)(\bar{\psi}^C\gamma^5\epsilon\epsilon_c\psi)]\rangle = -G_D I_D^2, \tag{39}$$

where the diquark condensate I_D is already defined in Eq. (27).

To calculate the thermodynamic potential (negative of the pressure), we also have to specify the chemical potentials relevant for the system. Here, we shall be interested in the form of quark matter that might be present in compact stars that are older than a few minutes so that chemical equilibration for weak interaction is satisfied. The relevant chemical potentials in such a case are the baryon chemical potential $\mu_B = 3\mu_q$, the chemical potential μ_E associated with the electromagnetic charge, and, the color potentials μ_3 and μ_8. The chemical potential is a matrix that is diagonal in color and flavor space and is given by

$$\mu_{ij,ab} = (\mu\delta_{ij} + Q_{ij}\mu_E)\delta_{ab} + (T^3_{ab}\mu_3 + T^8_{ab}\mu_8)\delta_{ij}. \tag{40}$$

Since red and green color of a given flavor of quark is degenerate and the diquark is in the blue direction in the color space, we can assume $\mu_3 = 0$.

The thermodynamic potetial, Ω, is then given by using Eqs. (32), (38), and (39), with s being the entropy density,

$$\Omega = T + V_S + V_{\rm det} + V_D - \langle\mu N\rangle - \frac{1}{\beta}s, \tag{41}$$

where we have introduced

$$\langle\mu N\rangle = \langle\psi^{ia\dagger}\mu_{ij,ab}\psi^{jb}\rangle = \sum_{i,a}\mu^{ia}\rho^{ia}, \tag{42}$$

where ρ^{ia} is the vector density $\rho^{ia} = \langle\psi^{ia\dagger}\psi^{ia}\rangle$. For the superconducting quarks this is given by

$$\rho^{ia} = \sum_n \alpha_n \frac{\tilde{e}B}{2(2\pi)^2}\int dp_z(F^{ia} - F_1^{ia}), \quad (i,a=1,2), \tag{43}$$

while for the blue u quark, the same is given by

$$\rho^{13} = \sum_n \alpha_n \frac{\tilde{e}B}{(2\pi)^2}\int dp_z(\sin^2\theta_-^{13} - \sin^2\theta_+^{13}). \tag{44}$$

For the charged strange quarks, this density is given by

$$\rho^{3a} = \sum_n \alpha_n \frac{\tilde{e}B}{2(2\pi)^2}\int dp_z(\sin^2\theta_-^{3a} - \sin^2\theta_+^{3a}), \quad (a=1,2). \tag{45}$$

For the $\tilde{e}$-uncharged quarks (blue down and blue strange), the vector density is given by

$$I_v^{i3} = \frac{2}{(2\pi)^3}\int d\mathbf{p}(\sin^2\theta_-^{i3} - \sin^2\theta_+^{i3}). \qquad (i=2,3). \tag{46}$$

Finally, the entropy density is given by $s = \sum_{i,a}s^{ia}$, where s^{ia} is the entropy density for quarks of flavor i and color a. For the quarks with charge $\tilde{q}^{ia}$, the phase space is Landau quantized and we have the entropy density given as [44]

$$s^{ia} = -\sum_n \alpha_n \frac{|q^{ia}|B}{(2\pi)^2}\int dp_z\{(\sin^2\theta_-^{ia}\ln\sin^2\theta_-^{ia} + \cos^2\theta_-^{ia}\ln\cos^2\theta_-^{ia}) + (-\to +)\}. \tag{47}$$

On the other hand, for the uncharged (blue down and blue strange) quarks, the entropy density is given by

$$s^{i3} = -\frac{2}{(2\pi)^3}\int d\mathbf{p}\{(\sin^2\theta_-^{i3}\ln\sin^2\theta_-^{i3} + \cos^2\theta_-^{i3}\ln\cos^2\theta_-^{i3}) + (-\to +)\}, \qquad (i=2,3). \tag{48}$$

Thus, the thermodynamic potential is now completely defined in terms of the condensate functions ϕ^i, $f(k)$ and the thermal distribution functions $\theta_{\mp}^{ia}$ which will be determined through a functional extremization of the thermodynamic potential. Minimizing the thermodynamic potential with respect to the quark-antiquark condensate function $\phi_i(p)$, i.e., $\delta\Omega/\delta\phi_i = 0$, leads to

$$\cot\phi^{ia} = \frac{(m_i - 4G_S I_s^i + K\epsilon^{ijk} I_s^j I_s^k + \delta_{i3}\frac{k}{4} I_D^2)}{|p_{ia}|} \equiv \frac{M_i}{|p_{ia}|}, \tag{49}$$

where, as earlier, we have defined $|p_{ia}| = \sqrt{p_z^2 + 2n|q_{ia}|B}$ and we have defined the constituent quark mass $M_i = m_i - 4G_S I_s^{(i)} + K|\epsilon_{ijk}| I_s^{(i)} I_s^{(j)} I_s^{(k)} + \delta^{i3} I_D^2 \frac{k}{4}$. These expressions are actually self-consistent equations for the constituent quark masses as scalar condensate $I_s^{(i)}$ as given in Eq. (20) involve M_i through their dependence on ϕ_i. Explicitly, these mass gap equations are given as

$$M^u = m^u - 4G_S I_s^{(u)} + 2K I_s^{(d)} I_s^{(s)}, \tag{50}$$

$$M^d = m^d - 4G_S I_s^{(d)} + 2K I_s^{(u)} I_s^{(s)}, \tag{51}$$

$$M^s = m^s - 4G_S I_s^{(s)} + 2K I_s^{(d)} I_s^{(u)} + \frac{K}{4} I_D^2. \tag{52}$$

Let us note that while the color and flavor dependence on the quark-antiquark condensate functions ϕ^{ia} arises *only* from the momentum $|p_{ia}| = \sqrt{p_z^2 + 2n|\tilde{q}_{ia}|B}$ through the color flavor dependent $\tilde{q}$ charges, the constituent quark masses are color singlets and are given by the solutions of the self-consistent equations (50)–(52). Further, the flavor mixing determinant interaction makes the masses of quark of a given flavor dependent upon the condensates of the other flavor quarks. This apart, the strange quark mass explicitly depends upon the diquark condensates through this determinant interaction. Note that for the two flavor superconductivity as considered here, the strange quark mass is affected explicitly by the superconducting gap given by the last term on the right-hand side Eq. (52). Of course, there is implicit dependence on the superconducting gap in the second term through the functions F and F_1 [given in Eqs. (22) and (23)]. Further, when chiral symmetry is restored for the light quarks, i.e., when the scalar condensates for the nonstrange quarks vanish, still, the determinant term gives rise to a density dependent dynamical strange quark mass arising from diquark condensates of the light quarks [47]. Such a mass generation is very different from the typical mechanism of quark mass generation through quark-antiquark condensates [49].

In a similar manner, minimizing the thermodynamic potential with respect to the diquark function $f(k)$ and di-antiquark function $f_1(k)$, i.e., $\frac{\delta\Omega}{\delta f(k)} = 0$ and $\frac{\delta\Omega}{\delta f_1(k)} = 0$, leads to

$$\begin{aligned}\tan 2f(k) &= \frac{2(G_D - \frac{K}{4} I_s^{(3)}) I_D}{\bar{\epsilon}_n - \bar{\mu}} \cos\left(\frac{\phi_1 - \phi_2}{2}\right) \\ &\equiv \frac{\Delta}{\bar{\epsilon}_n - \bar{\mu}} \cos\left(\frac{\phi_1 - \phi_2}{2}\right); \\ \tan 2f_1(k) &= \frac{\Delta}{\bar{\epsilon}_n + \bar{\mu}} \cos\left(\frac{\phi_1 - \phi_2}{2}\right),\end{aligned} \tag{53}$$

where we have defined the superconducting gap Δ as

$$\Delta = 2\left(G_D - \frac{K}{4} I_s^{(3)}\right) I_D, \tag{54}$$

and $\bar{\epsilon} = (\epsilon_n^u + \epsilon_n^d)/2$, $\bar{\mu} = (\mu^{ur} + \mu^{dg})/2 = \mu + 1/6\mu_E + 1/\sqrt{3}\mu_8$, where we have used Eq. (40) for the chemical potentials. Further, ϵ_n^i is the nth Landau level energy for the ith flavor with constituent quark mass M_i given as $\epsilon_n^i = \sqrt{p_z^2 + 2n|q_i|B + M_i^2}$. It is thus seen that the diquark condensate functions depend upon the *average* energy and the *average* chemical potential of the quarks that condense. We also note here that the diquark condensate functions depend upon the masses of the two quarks which condense through the function $\cos((\phi_1 - \phi_2)/2)$. The function $\cos\phi_i = M_i/\epsilon_n^i$ can be different for u,d quarks, when the charge neutrality condition is imposed. Such a normalization factor is always there when the condensing fermions have different masses as has been noted in Ref. [50] in the context of the CFL phase.

Finally, the minimization of the thermodynamic potential with respect to the thermal functions $\theta_{\pm}^{ia}(\mathbf{k})$ gives

$$\sin^2\theta_{\pm}^{ia} = \frac{1}{\exp(\beta(\omega_{i,a} \pm \mu_{ia})) + 1}. \tag{55}$$

Various ω^{ia}'s $(i, a \equiv \text{flavor, color})$ are explicitly given as

$$\omega_{n\pm}^{11} = \omega_{n\pm}^{12} = \bar{\omega}_{n\pm} + \delta\epsilon_n \pm \delta_\mu \equiv \omega_{n\pm}^u, \tag{56}$$

$$\omega_{n\pm}^{21} = \omega_{n\pm}^{22} = \bar{\omega}_{n\pm} - \delta\epsilon_n \mp \delta_\mu \equiv \omega_{n\pm}^d, \tag{57}$$

for the quarks participating in condensation. Here, $\bar{\omega}_{n\pm} = \sqrt{(\bar{\epsilon}_n \pm \bar{\mu})^2 + \Delta^2 \cos^2(\phi_1 - \phi_2)/2}$. Further, $\delta\epsilon_n = (\epsilon_n^u - \epsilon_n^d)/2$ is half the energy difference between the quarks which condense in a given Landau level and $\delta\mu = (\mu_{ur} - \mu_{dg})/2 = \mu_E/2$ is half the difference between the chemical potentials of the two condensing quarks. For the charged quarks which do not participate in the superconductivity,

$$\omega_{n\pm}^{ia} = \epsilon_n^i \pm \mu^{ia}. \tag{58}$$

In the above, the upper sign corresponds to antiparticle excitation energies while the lower sign corresponds to the particle excitation energies.

Let us note that when the charge neutrality conditions are not imposed, the masses of u and d quarks will be almost the same but for the effect of the (rotated) magnetic field as the magnitude of the charges for red and green quarks are the same and that of the blue color is different. Since the chemical potentials of all the quarks are the same when charge neutrality is not imposed, all four quasiparticles taking part in diquark condensation will have (almost) the same energy $\bar{\omega}_{n-}$. On the other hand, when charge neutrality condition is imposed, it is clear from the dispersion relations given in Eqs. (56) and (57) that it is possible to have zero modes, i.e., $\omega^{ia}=0$ depending upon the values of $\delta\epsilon_n$ and $\delta\mu$. So, although we shall have nonzero order parameter Δ, there will be fermionic zero modes or the gapless superconducting phase [51,52].

Substituting the solutions for the quark-antiquark condensate function ϕ^i of Eq. (49), we have the solutions for the different quark-antiquark condensates, i.e., I_s^{ia} given by, using Eqs. (21), (24), and (25),

$$I_s^{ia} = -\sum_n \alpha_n \frac{\tilde{e}B}{2(2\pi)^2}\int dp_z \frac{M_i}{\sqrt{p_z^2+2n(\tilde{e}B/2)+M_i^2}}(1-F^{ia}-F_1^{ia}), \qquad (i,a=1,2), \tag{59}$$

$$I_s^{13} = -\sum_n \alpha_n \frac{\tilde{e}B}{(2\pi)^2}\int dp_z \frac{M_1}{\sqrt{p_z^2+2n(\tilde{e}B)+M_1^2}}(1-\sin^2\theta_-^{13}-\sin^2\theta_+^{13}), \tag{60}$$

$$I_s^{3a} = -\sum_n \alpha_n \frac{\tilde{e}B}{2(2\pi)^2}\int dp_z \frac{M_3}{\sqrt{p_z^2+2n(\tilde{e}B/2)+M_3^2}}(1-\sin^2\theta_-^{3a}-\sin^2\theta_+^{3a}), \qquad (a=1,2), \tag{61}$$

for the $\tilde{e}$ charged quarks while for the uncharged quarks (blue down and blue strange quarks),

$$I_s^{i3} = -\frac{2}{(2\pi)^3}\int d\mathbf{p}\frac{M_i}{i\sqrt{\mathbf{p}^2+M_i^2}}(1-\sin^2\theta_-^{i3}-\sin^2\theta_+^{i3}), \qquad (i=2,3). \tag{62}$$

Similarly, substituting the solutions for the diquark/di-antiquark condensate functions from Eq. (53) in Eq. (27), we have, with the usual notations, $\bar{\xi}_{n\pm}=\bar{\epsilon}_n\pm\bar{\mu}$ and $\bar{\omega}_{n\pm}=\sqrt{\bar{\xi}_{n\pm}^2+\Delta^2\cos^2(\phi_1-\phi_2)/2}$,

$$I_D = \frac{2}{(2\pi)^2}\sum_n \alpha_n|\tilde{e}B/2|\int dp_z\Delta\cos^2\left(\frac{\phi_1-\phi_2}{2}\right)\left[\frac{1}{\bar{\omega}_{n-}}(1-\sin^2\theta_-^1-\sin^2\theta_-^2)+\frac{1}{\bar{\omega}_{n+}}(1-\sin^2\theta_+^1-\sin^2\theta_+^2)\right]. \tag{63}$$

Thus Eqs. (50)–(52) for the mass gaps, Eq. (54) for the superconducting gap and Eqs. (59)–(63) define the self-consistent mass gap equation for the ith quark flavor and the superconducting gap.

Next we discuss the thermodynamic potential. We substitute the solutions for the condensate functions [Eqs. (49) and (53)] in the expression for the thermodynamic potential [Eq. (41)] and use the gap equations [Eqs. (50)–(52) and (54)]. The thermodynamic potential is then given by

$$\Omega_q = \Omega_{1/2}^{sc}+\Omega_{1/2}^{s}+\Omega_0+\Omega_1+4G_s\sum_i I_s^{i^2}-4KI_s^uI_s^dI_s^s+\frac{\Delta^2}{4G_D'}-\frac{K}{4}I_s^sI_D^2, \tag{64}$$

where we have defined an effective diquark coupling $G_D'=G_D-\frac{K}{4}I_s^s$ in the presence of the determinant term which mixes the flavors. Let us now discuss each of the terms in Eq. (64). The first term is the contribution from the quarks that take part in superconductivity, i.e., the red and blue, u,d quarks. This contribution is given by

$$\begin{aligned}\Omega_{1/2}^{sc} &= -2\sum_n\alpha_n\frac{\tilde{e}B}{2(2\pi)^2}\int(\epsilon_n^u+\epsilon_n^d)dp_z+2\sum_n\alpha_n\frac{\tilde{e}B}{2(2\pi)^2}\int((\bar{\xi}_{n-}+\bar{\xi}_{n+})-(\bar{\omega}_{n-}+\bar{\omega}_{n+}))\\ &\quad -2\sum_n\sum_{i=u,d}\alpha_n\frac{\tilde{e}B}{(2\pi)^2\beta}\int dp_z[\log(1+\exp(-\beta(\omega_{n-}^i-\mu_{ir})))+\log(1+\exp(-\beta(\omega_{n+}^i+\mu_{ir})))]\\ &\equiv \Omega_{1/2,0}^{sc}(T=0,\mu=0)+\Omega_{1/2,med}^{sc}(T,\mu),\end{aligned} \tag{65}$$

where we have separated the contribution of the medium $\Omega_{1/2,med}^{sc}$ from $T=0$, $\mu=0$ contribution. Similarly, the ($\tilde{e}$) charged strange quark contribution to the thermodynamic potential is given by

$$\Omega^s_{1/2} = -2\sum_n \alpha_n \frac{\tilde{e}B}{2(2\pi)^2}\int dp_z \epsilon^s_n - \sum_n \sum_{a=1,2}\sum_{s=\pm1}\alpha_n \frac{\tilde{e}B}{2(2\pi)^2\beta}\int dp_z[\log(1+\exp(-\beta(\omega_{3a}+s\mu_{ia})]$$
$$\equiv \Omega^s_{1/2,0} + \Omega^s_{1/2,\mathrm{med}}. \tag{66}$$

The term Ω_1 in Eq. (64) arises from the blue colored u quark with charge $\tilde{e}$ and is given as

$$\Omega_1 = -\sum_n \alpha_n \frac{\tilde{e}B}{(2\pi)^2}\int (\epsilon^u_n) - \sum_n\sum_{s=\pm1}\alpha_n \frac{\tilde{e}B}{(2\pi)^2\beta}\int dp_z[\log(1+\exp(-\beta(\omega_{33}+s\mu_{33})] \equiv \Omega^u_{1,0}+\Omega^u_{1,\mathrm{med}}.$$

Finally, the $\tilde{e}$ uncharged quarks' contributions to the thermodynamic potential Ω_0 are given by

$$\Omega_0 = -2\sum_{i=2,3}\int \frac{d\mathbf{p}}{(2\pi^3)}\epsilon^i(\mathbf{p}) - \frac{2}{(2\pi)^3\beta}\int d\mathbf{p}\sum_{s=\mp1}[\log(1+\exp(-\beta(\omega_{23}+s\mu_{33})]. \tag{67}$$

Now, all the zero temperature and zero chemical potential contributions of the thermodynamic potential in Eqs. (65)–(67) are ultraviolet divergent. This divergence also gets transmitted to the gap equations through the quark-antiquark as well as diquark condensates in Eqs. (59), (60), (61), and (63). For the chargeless case, these can be rendered finite through a regularization with a sharp cutoff in the magnitude of three momentum as is usually done in the NJL models. However, it is also seen that a sharp cutoff in the presence of magnetic field for charged particles suffers from cutoff artifacts since the continuous momentum dependence in two spatial dimensions are replaced by the sum over discrete Landau levels. To avoid this, some calculations use a smooth parametrization for the cutoff as e.g., in Ref. [17]. In the present work however we follow the elegant procedure that was followed in Ref. [23] by adding and subtracting a vacuum (zero field) contribution to the thermodynamic potential which is also divergent. This manipulation makes e.g., the Dirac vacuum contribution in the presence of magnetic field to a physically more appealing form by separating the same to a zero field vacuum contribution and a finite field contribution written in terms of the Riemann-Hurwitz ζ function. The vacuum contribution to the energy density arising from a charged quark can be written as [23,24]

$$-\sum_{n=0}^{\infty}\frac{\alpha_n|q_iB|}{(2\pi)^2}\int dp_z\sqrt{p_z^2+2n|q_i|B+M_i^2}$$
$$= -\frac{2}{(2\pi)^3}\int d\mathbf{p}\sqrt{\mathbf{p}^2+M_i^2}$$
$$-\frac{|q_iB|^2}{2\pi^2}\left[\zeta'(-1,x_i)-\frac{1}{2}(x_i^2-x_i)\ln x_i+\frac{x_i^2}{4}\right], \tag{68}$$

where we have defined the dimensionless quantity, $x_i = \frac{M_i^2}{2|q_iB|}$, i.e., the mass parameter in units of the magnetic field. Further, $\zeta'(-1,x) = d\zeta(z,x)/dz|_{z=1}$ is the derivative of the Riemann-Hurwitz zeta function [53].

Using Eq. (68), the quark-antiquark condensate of $(\tilde{q})$ charged quarks can be written as

$$\langle\bar{\psi}^{ia}\psi^{ia}\rangle = -\frac{2}{(2\pi)^3}\int d\mathbf{p}\frac{M_i}{\sqrt{\mathbf{p}^2+M_i^2}}$$
$$-\frac{M_i|q_iB|}{2\pi^2}\left[x_i(1-\ln x_i)+\ln\Gamma(x_i)+\frac{1}{2}\ln\left(\frac{x_i}{2\pi}\right)\right]$$
$$+I^{ia}_{s\,\mathrm{med}}$$
$$\equiv I^{ia}_{s\,\mathrm{vac}}+I^{ia}_{s\,\mathrm{field}}+I^{ia}_{s\,\mathrm{med}}. \tag{69}$$

The first term, $I^{ia}_{s\,\mathrm{vac}}$ can be explicitly evaluated with a cutoff Λ as

$$I^{ia}_{s\,\mathrm{vac}} = \frac{M_i}{2\pi^2}\left[\Lambda\sqrt{\Lambda^2+M_i^2}-M_i^2\log\left(\frac{\Lambda+\sqrt{\Lambda^2+M_i^2}}{M_i}\right)\right]. \tag{70}$$

The medium contribution to the scalar condensate from the superconducting part is

$$I^{ia}_{s\,\mathrm{med}} = \sum_n \alpha_n \frac{\tilde{e}B}{2(2\pi)^2}\int dp_z\frac{M_i}{\epsilon^i_n}(F^{ia}-F^{ia}_1), \tag{71}$$

while, for the nonsuperconducting blue u quarks,

$$I^{13}_{s\,\mathrm{med}} = \sum_n \alpha_n \frac{\tilde{e}B}{(2\pi)^2}\int dp_z\frac{M_1}{\epsilon^1_n}(\sin^2\theta^{13}_- - \sin^2\theta^{13}_+). \tag{72}$$

Similarly, the contribution of the medium to the $(\tilde{q})$ charged strange quark-antiquark condensate is

$$I^{3a}_{s\,\mathrm{med}} = \sum_n \alpha_n \frac{\tilde{e}B}{2(2\pi)^2}$$
$$\times\int dp_z\frac{M_3}{\epsilon^3_n}(\sin^2\theta^{3a}_- - \sin^2\theta^{3a}_+), \quad (a=1,2). \tag{73}$$

In what follows, we shall focus our attention to zero temperature calculations. Using the relation $\lim_{\beta\to\infty}\frac{1}{\beta}\ln(1+\exp(-\beta\omega)) = -\omega\theta(-\omega)$ and using Eqs. (65) and (68), we have the zero temperature thermodynamic potential for the color superconducting quarks given as

$$\Omega^{sc}_{1/2}(T=0,\mu,B) = \Omega^{sc}_{1/2,0}(T=0,\mu=0) + \Omega^{sc}_{1/2,\mathrm{med}}(T=0,\mu), \quad (74)$$

with

$$\Omega^{sc}_{1/2,0}(T=0,\mu=0) = -2\times 2\sum_{i=u,d} G(\Lambda,M_i) - 2\sum_{i=u,d} F(x_i,B), \quad (75)$$

where we have defined the function $G(\Lambda,M)$ as

$$G(\Lambda,M) = \frac{1}{(2\pi)^3}\int\sqrt{\mathbf{p}^2+M^2}d\mathbf{p} = \frac{1}{16\pi^2}\left[\Lambda\sqrt{\Lambda^2+M^2}(2\Lambda^2+M^2) - M^4\log\left(\frac{\Lambda+\sqrt{\Lambda^2+M^2}}{M}\right)\right]. \quad (76)$$

The prefactors in the first term correspond to color and spin degeneracy factors while the same in the second term corresponds to the color degeneracy factor. The magnetic field dependent function, $F(x_i,B)$ with $x_i = M_i^2/|q_iB|$,

$$F(x_i,B) = \frac{|q_iB|^2}{2\pi^2}\left[\zeta'(-1,x_i) - \frac{1}{2}(x_i^2-x_i)\ln x_i + \frac{x_i^2}{4}\right]. \quad (77)$$

The medium contribution from the superconducting quarks is given as

$$\Omega^{sc}_{1/2,\mathrm{med}}(T=0,\mu) = 2\sum_{n=0}^{n_{\max}}\alpha_n\frac{\tilde{e}B}{2(2\pi)^2}\int_0^{p_{z,n}^{\max}} dp_z[\bar{\xi}_{n-}+\bar{\xi}_{n+}-(\bar{\omega}_{n-}+\bar{\omega}_{n+})] + 2\sum_{n=0}^{n_{\max}}\sum_{i=u,d}\alpha_n\frac{\tilde{e}B}{2(2\pi)^2}\int_0^{p_{z,n}^{\max}} dp_z i[\omega^i_{n-}\theta(-\omega^i_{n-}) + \omega^i_{n+}\theta(-\omega^i_{n+})]. \quad (78)$$

The three momentum cutoff Λ for the magnitude of momentum in the absence of magnetic field leads to the sum over the Landau level up to $n_{\max} = \frac{\Lambda^2}{\tilde{e}B}$. Further, the positivity of the magnitude of p_z restricts the cutoff in $|p_z|$ as $p_{z,n}^{\max} = \sqrt{\Lambda^2 - n\tilde{e}B}$ for a given value of n of the Landau level.

The contribution of the blue up quark to the thermodynamic potential $\Omega_1 = \Omega_{1,0} + \Omega_{1,\mathrm{med}}$ with

$$\Omega_{1,0}(T=0,\mu=0) = -2G(\Lambda,M_u) - F(x_u,B), \quad (79)$$

and

$$\Omega_{1,\mathrm{med}}(T=0,\mu) = \sum_{n=0}^{n^u_{\max}}\alpha_n\frac{\tilde{e}B}{(2\pi^2)}\left[\mu_{ub}\sqrt{\mu_{ub}^2-M_{nu}^2} + M_{nu}^2\log\left(\frac{\mu_{ub}+\sqrt{\mu_{ub}^2-M_{nu}^2}}{M_{nu}}\right)\right], \quad (80)$$

where $M_{nu} = \sqrt{M_u^2+2n\tilde{e}B}$ is the nth Landau level mass for up quark and $n^u_{\max} = Int[\frac{\mu_{ub}^2-M_u^2}{2\tilde{e}B}]$ is the maximum number of Landau level consistent with the zero temperature distribution function.

The $\tilde{e}$ charged strange quark contribution to the thermodynamic potential $\Omega^s_{1/2} = \Omega^s_{1/2,0} + \Omega^s_{1/2,med}$, with

$$\Omega^s_{1/2,0}(T=0,\mu=0) = -2\times 2G(\Lambda,M_s) - 2F(x_s,B), \quad (81)$$

and

$$\Omega_{1/2,\mathrm{med}}(T=0,\mu) = 2\sum_{n=0}^{n^s_{\max}}\alpha_n\frac{\tilde{e}B}{2(2\pi^2)}\left[\mu_{sr}\sqrt{\mu_{sr}^2-M_{ns}^2} + M_{ns}^2\log\left(\frac{\mu_{sr}+\sqrt{\mu_{sr}^2-M_{ns}^2}}{M_{ns}}\right)\right], \quad (82)$$

where $M_{ns} = \sqrt{M_s^2+2n\tilde{e}B}$ is the nth Landau level mass for the s quarks. Further, the sum over the Landau levels is restricted to $n^s_{\max} = \mathrm{Int}[\frac{\mu_{sr}^2-M_s^2}{\tilde{e}B}]$ arising from the distribution function at zero temperature $\theta(\mu-\epsilon_n)$.

For the uncharged quarks, i.e., blue down and strange quarks, we have $\Omega_0 = \Omega_{0,0} + \Omega_{0,\mathrm{med}}$ with

$$\Omega_{0,0}(T=0,\mu=0) = -2\sum_{i=d,s} G(\Lambda, M_i), \tag{83}$$

and for the medium part, with $p_{fi} = \sqrt{\mu_i^2 - M_i^2}$,

$$\Omega_{0,\mathrm{med}}(T=0,\mu) = 2\sum_{i=d,s} H_i(\mu_{i3}, p_{fi}). \tag{84}$$

In the above H_i is the medium contribution from a single chargeless flavor given as

$$H_i(\mu, p_f) = \frac{1}{16\pi^2}\left[p_{fi}\mu_i(p_{fi}^2 + \mu_i^2) - M_i^4 \log\left(\frac{\mu^i + p_{fi}}{M^i}\right)\right]. \tag{85}$$

Next, we write down the expressions for the condensates at zero temperature, which are needed to compute the thermodynamic potential in Eq. (64). This is already given by Eq. (69). Here, we write down explicitly the zero temperature limit for the same. The scalar condensate for, say, u quarks is given as

$$I_s^u = I_{s\,\mathrm{vac}}^u + I_{s\,\mathrm{med}}^{ur} + I_{s\,\mathrm{med}}^{ug} + I_{s\,\mathrm{med}}^{ub} + \sum_{a=1}^{3} I_s^{\mathrm{field}-u}(x_{ua}). \tag{86}$$

The vacuum contribution $I_{s\,\mathrm{vac}}^u$ is already given in Eq. (70).

The scalar condensate medium contribution from the superconducting red up and green up quarks is given as

$$I_{s\,\mathrm{med}}^{ur} = I_{s\,\mathrm{med}}^{ug} = -\sum_{n=0}^{n_{\max}} \alpha_n \frac{(\tilde{e}B)}{2(2\pi)^2}\int dp_z \frac{M_u}{\epsilon_n^u}(F^{ur} + F_1^{ur}). \tag{87}$$

The expressions for the distribution functions F^{ia} and F_1^{ia} are already given in Eqs. (22) and (23) in terms of the diquark condensate functions and the thermal distribution functions. In the zero temperature limit, the distribution functions for e.g., u quarks become

$$F^{ur} = \frac{1}{2}\left(1 - \frac{\bar{\xi}_{n-}}{\bar{\omega}_{n-}}\right)(1 - \theta(-\omega^d)), \tag{88}$$

and

$$F_1^{ur} = \frac{1}{2}\left(1 - \frac{\bar{\xi}_{n+}}{\bar{\omega}_{n+}}\right). \tag{89}$$

The blue up quark contribution to the scalar condensate is given by

$$I_{s\,\mathrm{med}}^{ub} = -\sum_{n=0}^{n_{\max}^u} 2M\alpha_n \frac{\tilde{e}B}{(2\pi)^2}\log\left(\frac{p_z^{\max} + \sqrt{p_z^{\max 2} + M_{nu}^2}}{M_{nu}}\right). \tag{90}$$

As in Eq. (80) here we have defined the nth Landau level mass for the blue up quark as $M_{nu}^2 = M_u^2 + 2n|\tilde{e}B|$. The magnetic field contribution to the scalar condensate for the up quarks of a given color "a" is given by

$$I_s^{\mathrm{field}-u}(x_{ua}) = -M_u\frac{|q_aB|}{2\pi^2}\left[x_a(1 - \ln x_a) + \ln\Gamma(x_a) + \frac{1}{2}\frac{x_a}{2\pi}\right], \tag{91}$$

where $x_a = M_u^2/2|q_aB|$ and $q_a = \tilde{e}/2$ for red and green colors and $q_a = \tilde{e}$ for blue color up quarks.

In an identical manner, the scalar condensates for the down and strange quarks I_s^d, I_s^s can be written down with appropriate changes for the charges and the masses. The diquark condensate $4I_D$ is given in Eq. (63) where the zero temperature limit can be taken by replacing the distribution functions $\sin^2\theta^i = \theta(-\omega^i)$, $(i = u, d)$. Thus the thermodynamic potential, Ω_q given in Eq. (64) gets completely defined for the quark matter in the presence of a magnetic field.

In the context of neutron star matter, the quark phase that could be present in the interior consists of the u,d,s quarks as well as electrons, in weak equilibrium,

$$d \to u + e^- + \bar{\nu}_{e^-}, \tag{92a}$$

$$s \to u + e^- + \bar{\nu}_{e^-}, \tag{92b}$$

and

$$s + u \to d + u, \tag{92c}$$

leading to the relations between the chemical potentials μ_u, μ_d, μ_s, μ_E as

$$\mu_s = \mu_d = \mu_u + \mu_E. \tag{93}$$

The neutrino chemical potentials are taken to be zero as they can diffuse out of the star. So there are *two* independent chemical potentials needed to describe the matter in the neutron star interior which we take to be the quark chemical potential μ_q and the electric charge chemical potential μ_e in terms of which the chemical potentials are given by $\mu_s = \mu_q - \frac{1}{3}\mu_e = \mu_d$, $\mu_u = \mu_q + \frac{2}{3}\mu_e$ and $\mu_E = -\mu_e$. In addition, for a description of the charge neutral matter, there is a further constraint for the chemical potentials through the following relation for the particle densities given by

$$Q_E = \frac{2}{3}\rho_u - \frac{1}{3}\rho_d - \frac{1}{3}\rho_s - \rho_E = 0. \tag{94}$$

The color neutrality condition corresponds to

$$Q_8 = \frac{1}{\sqrt{3}} \sum_{i=u,d,s} (\rho^{i1} + \rho^{i2} - 2\rho^{i3}) = 0. \tag{95}$$

In the above, ρ^{ia} is the number density for quarks of flavor i and color a. In particular, the number densities of the condensing quarks are given as

$$\rho^{ia} = \sum_n \frac{\tilde{e}B}{2(2\pi)^2} \int dp_z (F^{ia} - F_1^{ia}), \quad (i, a = 1, 2), \tag{96}$$

where F^{ia}, F_1^{ia} are defined in Eqs. (22) and (23) respectively in terms of the condensate functions and e.g., for zero temperature is given explicitly in Eq. (88) for up red quarks. For the blue colored quarks, the same for the up blue quarks is given by

$$\rho^{ub} = \sum_{n=0}^{n^u_{\max}} \alpha_n \frac{\tilde{e}B}{2\pi^2} \sqrt{\mu_{ub}^2 - M_u^2 - 2n\tilde{e}B}, \tag{97}$$

while for the $\tilde{e}$ uncharged d quarks

$$\rho^{db} = \frac{(\mu_{db}^2 - M_d^2)^{3/2}}{3\pi^2}. \tag{98}$$

For the charged strange quarks the number densities are given by

$$\rho^{sr} = \rho^{sg} = \sum_{n=0}^{n^s_{\max}} \alpha_n \frac{\tilde{e}B}{(2\pi)^2} \sqrt{\mu_{sr}^2 - M_s^2 - n\tilde{e}B}, \tag{99}$$

while for the $\tilde{e}$ uncharged blue strange quarks

$$\rho^{sb} = \frac{(\mu_{sb}^2 - M_s^2)^{3/2}}{3\pi^2}. \tag{100}$$

The electron number density is given by

$$\rho_E = \sum_n^{n_{maxe}} \alpha_n \frac{\tilde{e}B}{\pi^2} \left(\sqrt{\mu_E^2 - 2n\tilde{e}B} \right). \tag{101}$$

To discuss the pressure in the context of matter in the core of the neutron star, one also has to add the contribution of the electrons to the thermodynamic potential. Since we shall describe the system as a function of $\tilde{e}B$, we shall take the approximations $\tilde{e} \sim e, A_\mu \sim \tilde{A}_\mu$ to a good approximation as the mixing angle is small. The corresponding thermodynamic potential for the electrons is given by

$$\Omega_e = \sum_{n=0}^{n^e_{\max}} \alpha_n \frac{eB}{(2\pi)^2} \left[\mu_E \sqrt{\mu_E^2 - 2neB} - 2neB \log\left(\frac{\mu_E + \sqrt{(\mu_E^2 - 2neB)}}{\sqrt{2neB}} \right) \right], \tag{102}$$

where $n^e_{\max} = \frac{\mu_E^2}{2|\tilde{e}B|}$. Clearly in Eqs. (101) and (102) we have neglected the electron mass ($m_E \sim 0.5$ MeV), which is small compared to μ_E which is few tens of MeV. Thus the total thermodynamic potential or the negative of the pressure is given as, with Ω_q given in Eq. (64)

$$\Omega = \Omega_q + \Omega_e. \tag{103}$$

The thermodynamic potential [Eq. (103)], the mass and superconducting gap equations [Eqs. (50)–(52) and (54)], along with the charge neutrality conditions [Eq. (94) and (95)] are the basis for our numerical calculations for various physical situations that we shall discuss in detail in the following section.

IV. RESULTS AND DISCUSSIONS

We begin the discussions with the parameters of the NJL model. The model parameters are the three current masses of quarks, namely m_u, m_d and m_s and the couplings G_S, G_D and the determinant coupling K. This apart, one additional parameter, the momentum cutoff Λ, is also required to regularize the divergent integrals which are characteristic of the four point interaction of NJL models. Except for the diquark coupling G_D, there are several parameter sets for the couplings derived from fitting of the meson spectrum and chiral condensate [54–56]. The diquark coupling is not known from fitting since one does not have a diquark spectrum to fit with. The Fierz transforming quark-antiquark term from one gluon exchange term gives the relation $G_D = 0.75\ G_S$. Although not precise, many other references use this value [47,57,58]. However some other references [59,60] also consider the case of stronger diquark coupling $G_D = G_S$ apart from $G_D = 0.75\ G_S$. In the following we shall limit ourselves only to the case of $G_D = 0.75\ G_S$. For a nice discussion on this we refer the interested reader to Sec. 4.2.2 of Ref. [61]. The parameters used in our calculations are $m_u = 5.5$ MeV, $m_d = 5.5$ MeV, $m_s = 140.7$ MeV for the current quark masses, the momentum cutoff $\Lambda = 602.5$ MeV and the couplings $G_s \Lambda^2 = 1.835$ and $K\Lambda^5 = 12.36$ as have been chosen in Ref. [56]. After choosing the light current quark mass $m_u = m_d = 5.5$ MeV, the remaining four parameters are chosen to fit vacuum values of pion decay constant f_π, masses of pion, kaon and η'. With this set of parameters the η meson mass is underestimated by about 6 percent and leads to u and d constituent mass in vacuum to be about 368 MeV. The strange mass is about 549 MeV at zero temperature and density. The determinant interaction is responsible for $U(1)_A$ anomaly and getting the correct eta mass. Further, this interaction also mixes the various gap equations and affects the superconducting gap significantly as we shall see. However, we must point out that there is a large discrepancy in the determination of this six fermion interaction coupling K. For example, in Ref. [54] the parameter $K\Lambda^5$ differs by as

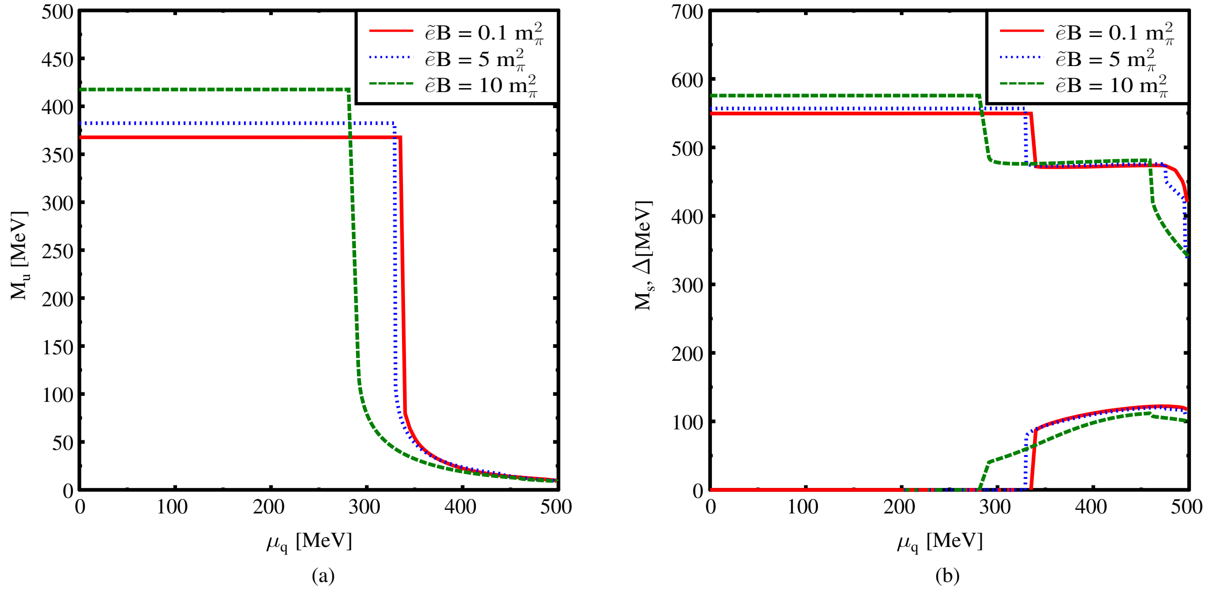

FIG. 1. Constituent quark masses and superconducting gap when charge neutrality conditions are not imposed. Part (a) shows the M_u at zero temperature as a function of quark chemical potential for different values of the magnetic field. Part (b) shows the same for the strange quark mass M_s and the superconducting gap.

large as 30 percent as compared to the value chosen here. This discrepancy is due to the difference in the treatment of η' mesons with a high mass [28]. In fact, this leads to an unphysical imaginary part for the corresponding polarization diagram in the η' meson channel. This is unavoidable because NJL is not confining and is unrealistic in this context. Within the above-mentioned limitations of the model and the uncertainty in the value of the determinant coupling, we proceed with the present parameter set which has already been used for phase diagram of dense matter in Refs. [28,59] and for neutron star matter in Ref. [62].

We begin our discussion for the simpler case where the charge neutrality conditions are not imposed. In this case, the electrical and color charge chemical potential are set to zero so that all the quarks have same potential μ_q. In this case we have to solve four gap equations, three for the constituent masses [Eqs. (50)–(52)] and the fourth for the superconducting gap [Eqs. (54) and (63)]. For given values of quark chemical potential and magnetic field we solve the gap equations self-consistently. A few comments regarding solving these gap equations may be in order. Although the gap equations and the thermodynamic potential has been written down for a given T and μ, we confine our attention to the case of zero temperature only in the present investigation. Second, for nonvanishing magnetic fields, all the Landau levels for the medium part up to a cutoff, $n_{\max} = \frac{\sqrt{\mu^2 - M_i^2}}{2\tilde{e}B}$ for each flavor i, are taken into account. Near the μ_c, the critical chemical potential for chiral transition for light quarks, there can be multiple solutions for the gap equations. We have chosen the solutions which have the lowest thermodynamic potential.

In Fig. 1, we have shown the variation of the masses as a function of quark chemical potential μ_q for three different values of magnetic fields, $\tilde{e}B = 0.1\ \mathrm{m}_\pi^2$, $5\ \mathrm{m}_\pi^2$, $10\ \mathrm{m}_\pi^2$. The results for $\tilde{e}B = 0.1\ \mathrm{m}_\pi^2$ reproduce the vanishing magnetic field results. As the chemical potential increases, the masses remain constant up to a critical value of quark chemical potential μ_c and the superconducting gap remains zero. At the critical chemical potential there is a first order phase transition and the constituent masses drop sharply from their vacuum values and the superconducting gap becomes nonzero. For vanishing magnetic field, the isospin symmetry for the light quarks is unbroken and the constituent masses of u and d quarks are degenerate. The critical chemical potential, μ_c, is about 340 MeV for (almost) vanishing magnetic field. In this case, the up and the down quark masses decrease from their vacuum values of about 368 MeV to about 80 MeV. The strange mass being coupled to other gaps via determinant interaction also decreases from 549 to 472 MeV when this first order transition happens for the light quarks. However, since this μ_c is still less than the strange mass its density remains zero. The superconducting gap rises from 0 to 88.0 MeV at μ_c. As the chemical potential is increased beyond μ_c, the superconducting gap shows a mild increase reaching a maximum value of 122 MeV at around $\mu_q \sim$ 475 MeV beyond which the gap shows a mild decrease with μ.

Such a decrease of the gap with chemical potential could be due to two reasons. First, at higher chemical potentials, beyond $\mu = 475$ MeV, the strange quark mass starts decreasing rapidly. This leads to a decrease of the effective diquark coupling $G_D' = G_D + \frac{K}{4}\langle\bar{s}s\rangle$ resulting in a decrease

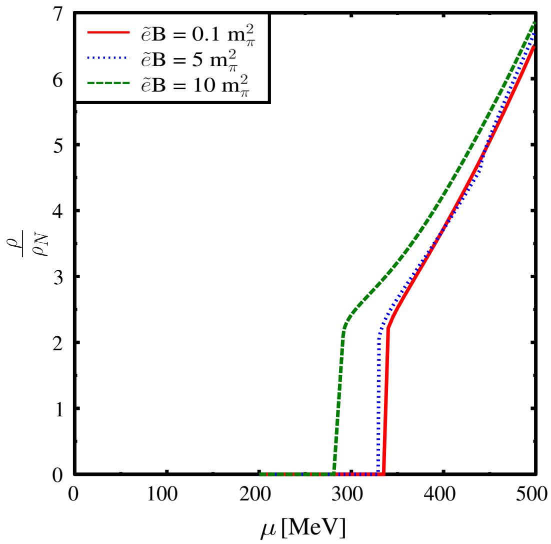

FIG. 2. Baryon number density in units of nuclear matter density as a function of chemical potential for different strengths of magnetic field at zero temperature.

in the superconducting gap with increasing chemical potential. Second, such a behavior of decreasing superconducting gap with μ for large μ could also be a manifestation of a finite cutoff in the momentum integration in e.g., Eq. (78). One may note that the first term in Eq. (78) is the contribution from the medium. Indeed, for $T = 0$, $\mu = 0$ the contributions of the two terms in the integrand here cancel out unlike the term in Eq. (68) which is a genuine vacuum contribution and is divergent. The second term in Eq. (78) in any case gives a contribution from the medium when $\delta\mu \neq 0$. For both terms the upper limit of p_z integration, $p_{z,n}^{\max}$, has a Λ dependence. Therefore, it is expected that there will be a cutoff dependence in the contribution of this term to the thermodynamic potential. This effect of finite cutoff therefore will be more pronounced at large μ. Thus the decrease of the superconducting gap at large μ in Fig. 1(b) could also be a reflection of this effect. Therefore the decreasing behavior of Δ can be both due to the decrease of effective diquark coupling G_D', and the effects of a finite cutoff.

In Fig. 2, we have plotted the total baryon number density in units of nuclear matter density ($\rho_N = 0.17/\mathrm{fm}^{-3}$) as a function of quark chemical potential. For vanishing magnetic field, at the critical chemical potential $\mu_c \sim 340$ MeV, the baryon density jumps from 0 to 0.38 fm^{-3} which is about 2.2 times the nuclear matter density.

Upon increasing the magnetic field, as seen in Fig. 1, the vacuum constituent quark masses increase due to magnetic catalysis at zero density. It may also be observed here that the μ_c for chiral transition for the light quarks decreases with the magnetic field. Such a phenomenon is known as inverse magnetic catalysis at finite chemical potential [63]. Let us note that in the superconducting phase the $\tilde{e}$ charges of the u and d quarks are identical in magnitude while that of the unpaired blue quark are different for u and d quarks. This results in the color summed scalar condensate I_s^u and I_s^d to be different in the presence of a magnetic field. This leads to the difference in constituent masses for the light quarks. For $\tilde{e}B = 10\ m_\pi^2$ the u mass in the chiral symmetry broken phase increases by about 13.6 percent and strange mass by about 4.7 percent. The critical chemical potential decreases from about 340 MeV to about 291 MeV. As seen in the plot, the superconducting gap decreases and the peak value decreases from 122 to 111 MeV. As may be seen from Eqs. (54) and (63), the superconducting gap depends upon the effective diquark coupling $G_D' = G_D\text{-}\frac{K}{4}I_s^s$. With an increase in magnetic field the effective coupling G_D' has a slight increase in magnitude as the strange quark condensate increases with magnetic field. Therefore, one would have expected an increase in Δ with magnetic field. However, the variation in Δ due to the magnetic field is essentially decided by Eq. (63). From here also one would have expected an increase in Δ with magnetic field as $\tilde{e}B$ occurs in the numerator in Eq. (63). In fact, this behavior is actually seen for high magnetic field, where only the lowest Landau level contributes to the integral in Eq. (63). For moderately strong magnetic fields, contributions of the higher Landau levels become relevant for the behavior of gap with magnetic field. As long as the contribution of higher Landau levels are nonvanishing, the gap equation can support the solution for the gap that decreases with magnetic field. We may point out that $\tilde{e}B = 5\ m_\pi^2$ and $10\ m_\pi^2$ the cutoff for Landau levels $n_{\max}$ equals 3 and 1 respectively. For $\tilde{e}B \geq 20\ m_\pi^2$ only the lowest Landau level contributes to the integral in Eq. (63) and the gap increases with magnetic field. One may also note that at higher magnetic fields the charge asymmetry between the u and d quark becomes apparent in their masses as expected. At $10\ m_\pi^2$ the difference is about 3.4 percent and at $15\ m_\pi^2$ its about 5.7 percent at lower chemical potentials.

One may note that below the critical chemical potential μ_c the u quarks have higher mass compared to d quarks as all the three colors are charged for u quarks while for the d quarks, the blue color is chargeless. However, beyond the critical chemical potential the u quark has a lower mass compared to d quarks. This is because with magnetic field the medium contribution to chiral condensate increases. This increase is the same for the condensing pairs of u and d quarks but different for the blue quarks. The blue up quark has charge $\tilde{e} = 1$ whereas it is zero for the down blue quark. Therefore the medium contribution from the up quark is more than the down quark and it reduces the condensate for the up quark and consequently its mass too. As we shall see later, imposing charge neutrality requires the d quark chemical potential to be much higher compared to u quarks to balance their larger positive charge. This forces the d quark mass to be smaller compared to u quark mass above critical chemical potential. This results in an opposite

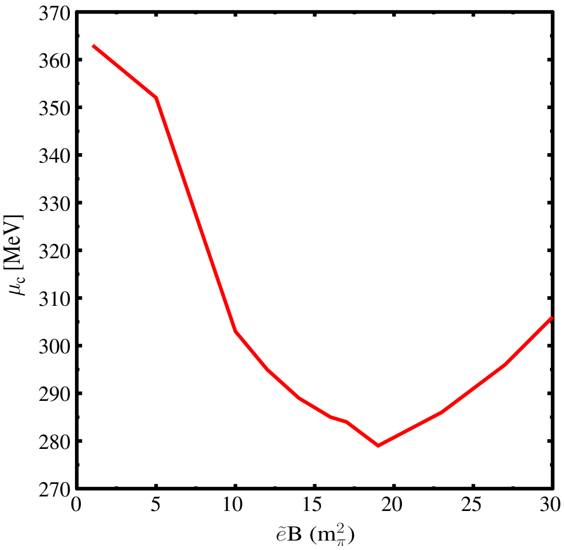

FIG. 3. Critical chemical potential for chiral transition at zero temperature as a function of magnetic field.

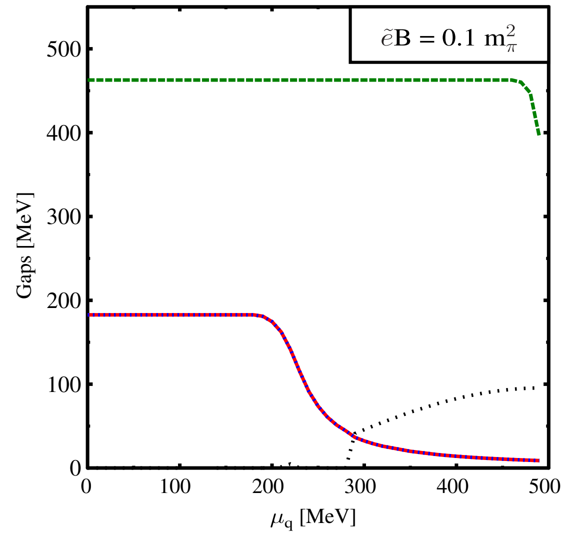

FIG. 4. Gaps without determinant interaction at zero temperature as a function of quark chemical potential. The solid curve refers to masses of u-d quarks, the dashed curve refers to the mass of strange quark and the dotted curve corresponds to the superconducting gap.

behavior for the u and d quark masses with chemical potential, beyond μ_c when the charge neutrality condition is imposed *vis-à-vis* when such a condition is not imposed.

As may be observed from Fig. 2, the baryon number density increases with magnetic field for a given chemical potential. This is because for the magnetic fields considered here, the symmetry is restored for lower chemical potential at higher magnetic field. Thus for a given chemical potential beyond the critical chemical potential the masses become smaller for higher magnetic field leading to larger baryon number density. This is consistent with inverse magnetic catalysis. One may note however that for very large fields, there is magnetic catalysis of chiral symmetry breaking in the sense that critical chemical potential increases with magnetic field. In Fig. 3 we show the behavior of μ_c as a function of magnetic field. It is observed that μ_c is minimum for $\tilde{e}B = 19\ m_\pi^2$.

To examine the effect of flavor mixing determinant interaction, we show in Fig. 4 the variation of the masses and the superconducting gap without the determinant interaction. As expected, without the mixing of flavors the strange mass remains unaffected when u and d quark masses decrease. This is significantly different behavior compared to Fig. 1 where the strange mass decreases by about 74 MeV beyond μ_c when there is a first order transition for the light quarks. This also affects the superconducting gap. The superconducting gap is smaller as the effective diquark coupling decreases without the determinant interaction term.

In Fig. 5 we show the variation of the gaps as a function of the magnetic field for $\mu = 200$ MeV and $\mu = 400$ MeV. $\mu = 200$ MeV is less than the critical μ_c for any value of magnetic field considered here. Hence the constituent masses are high and the superconducting gap is zero. We find that the masses increase monotonically with the magnetic field. At $\tilde{e}$B $= 10\ m_\pi^2$, the u mass increases by 14 percent of its zero field value while strange mass increases by 5 percent. Similarly for $\mu = 400$ MeV which is larger than the critical chemical potential for magnetic fields considered here, one also has finite superconducting gap. However, in this case it is observed that the u and d masses decrease slowly and monotonically with magnetic field while strange quark mass remains almost constant. The superconducting gap shows an oscillatory behavior with increase in magnetic field. The oscillatory behavior is associated with the discontinuous changes in the density of states due to Landau quantization and is similar to de Hass van Alphen effects for magnetized condensed matter system.

Finally, in Fig. 6 we have plotted the axial current density normalized to the same for three flavor without any condensates as given in Eq. (30) as a function of baryon density for values of magnetic field 5 and 10 m_π^2. For smaller chemical potentials but above the chiral transition this ratio is about 0.75 since strange quarks do not contribute as their masses are larger than these values of chemical potential. For μ_q about 480 MeV the strange quarks contribution to the axial current density becomes nonvanishing and the ratio approaches to the value when there are no condensates. Let us note that while quark masses decrease with chemical potential, the superconducting gap increases with chemical potential. This leads to a nearly constant value for this ratio for the range of chemical potential below the strange quark mass. Above $\mu_q = 480$ MeV, the ratio shows a monotonic increase with chemical potential as the strange quark mass starts decreasing.

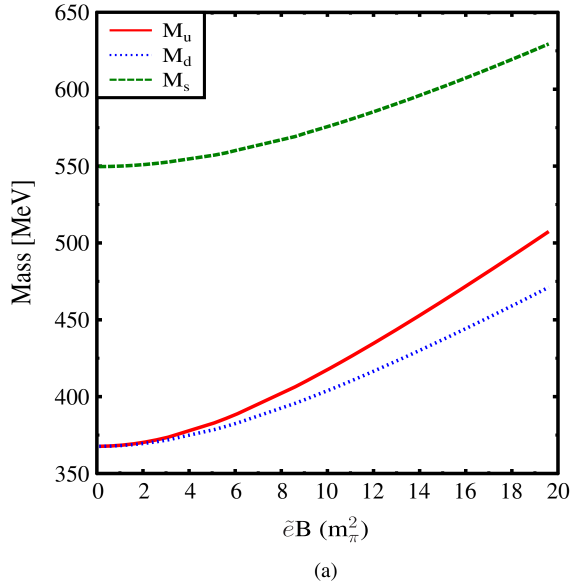

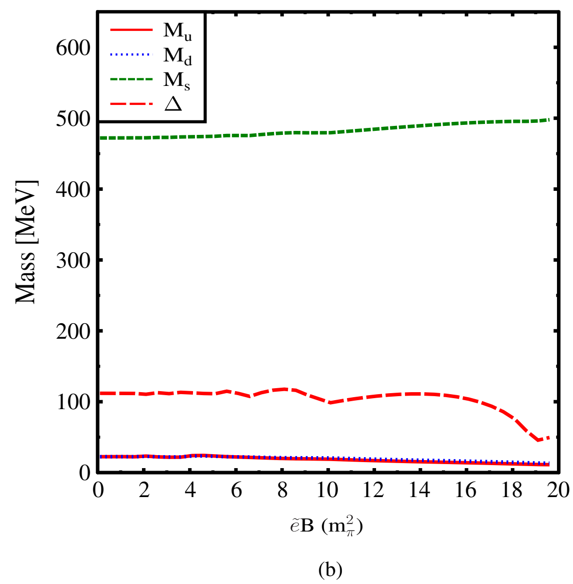

FIG. 5. Constituent quark masses as a function of magnetic field for $T = 0$. Part (a) shows the masses of the three quarks below the chiral transition for $\mu = 200$ MeV. Part (b) shows the same for the masses along with the superconducting gap above the chiral transition for $\mu_q = 400$ MeV.

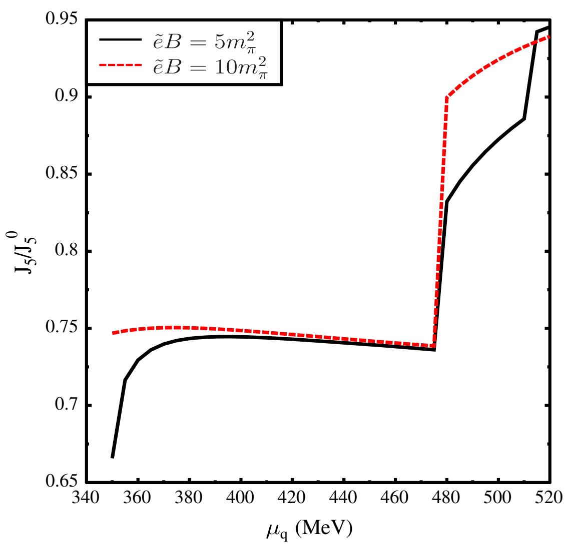

FIG. 6. Axial current density for $\tilde{e}B = 5$ m_π^2 (black solid line) and $\tilde{e}B = 10$ m_π^2 (red dashed line).

A. Charge neutral magnetized quark matter

Next we discuss the consequences of imposing charge neutrality conditions ($Q_E = 0, Q_8 = 0$). In Fig. 7 we show the results for the masses and the superconducting gaps for strength of the external magnetic field $\tilde{e}B = 0.1$ m_π^2 [Fig. 7(a)] and $\tilde{e}B = 10$ m_π^2 [Fig. 7(b)]. For small magnetic field ($\tilde{e}B = 0.1$ m_π^2) the masses in the symmetry broken phase are the same as before but the critical chemical potential is now shifted to around $\mu_c = 364$ MeV as compared to $\mu_c = 335$ MeV when the condition is not imposed. At the transition point with neutrality the u-quark mass decreases from 367 to 111 MeV and the down quark mass from 367 to 87 MeV. Charge neutrality requires d quark number densities to be higher as compared to u quarks. Let us note that near the critical chemical potential there are multiple solutions of the gap equations. The solution which is thermodynamically preferred when the charge neutrality condition is not imposed may no longer be the preferred solution when the constraint of charge neutrality is imposed [36]. The strange quark mass is higher than the chemical potential at the chiral restoration so its density is zero. However due to the determinant interaction the strange mass decreases at the chiral restoration from 549 to 472 MeV. At still higher chemical potential the strange quark density becomes nonzero and strange quark also helps in maintaining charge neutrality.

The critical baryon density when charge neutrality is imposed is however similar to the case when neutrality is not imposed. Specifically $\rho_c \sim 2.25\rho_0$ with charge neutrality while $\rho_c \sim 2.26\rho_0$ without charge neutrality despite the fact that μ_c is higher ($\mu_c = 364$ MeV) for the charge neutral matter compared when such charge neutrality condition is not imposed ($\mu_c = 335$ MeV). This is because the constituent masses at the transition is large ($M_u \sim 111$ MeV and $M_d \sim 87$ MeV) for charge neutral case compared to ($M_u \sim M_d \sim 85$ MeV) without the charge neutrality condition. For $\tilde{e}B = 0.1$ m_π^2, at the chiral transition $\mu_c = 364$ MeV the superconducting gap increases from zero to 69 MeV. As the chemical potential is further increased the superconducting gap increases to 80 MeV until $\mu = \mu_1 \sim 420$ MeV where it shows a sudden jump to 106 MeV. This happens when the gapless modes cease to exist as explained below. As magnetic field is increased to $\tilde{e}B = 10$ m_π^2, as

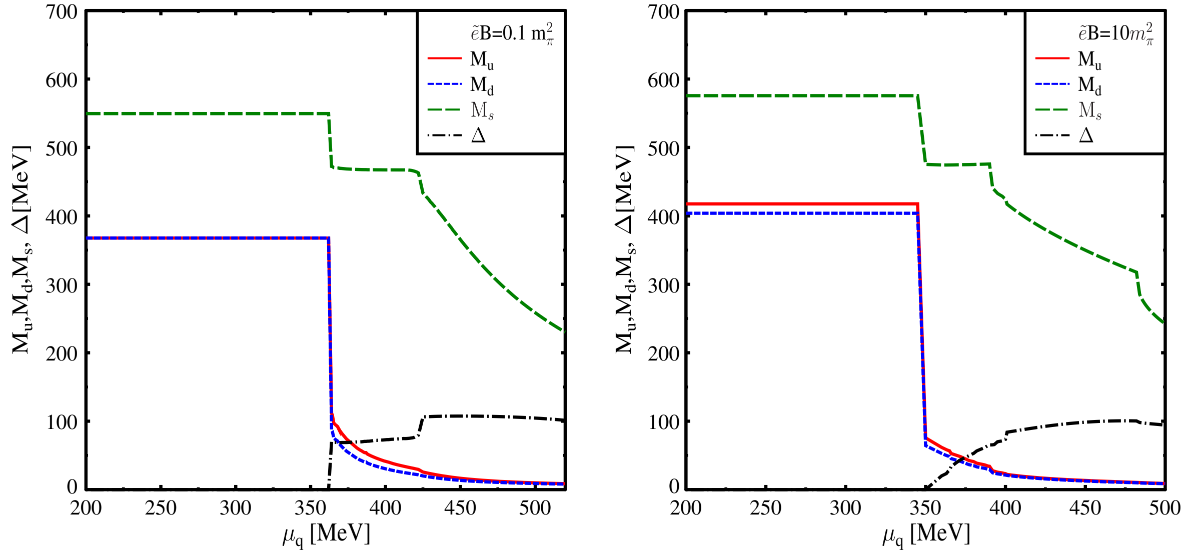

(a) (b)

FIG. 7. Constituent quark masses and superconducting gap when charge neutrality conditions are imposed. Part (a) shows the masses and superconducting gap at zero temperature as a function of quark chemical potential for magnetic field $\tilde{e}B = 0.1\ \mathrm{m}_\pi^2$. Part (b) shows the same for $\tilde{e}B = 10\ \mathrm{m}_\pi^2$.

may be observed in Fig. 6(b), the critical chemical potential μ_c for the charge neutral matter decreases to 350 MeV similar to the case without the charge neutrality condition with inverse magnetic catalysis. The superconducting gap on the other hand becomes smaller. One can also observe that unlike the vanishingly small magnetic field case, the superconducting gap increases smoothly with chemical potential from zero initial value to 73 MeV at $\mu = \mu_1 \sim 400$ MeV where it again jumps to a value of 83 MeV.

B. Gapless modes

In the region between μ_c and μ_1 the system shows gapless mode which we discuss now in some detail. Without magnetic field this has earlier been seen for charge neutral matter [35,36,64].

As discussed earlier, from the dispersion relations for Landau levels for the superconducting matter as given in Eqs. (56) and (57), it is possible to have zero modes depending upon the values of $\delta\mu$ and $\delta\epsilon_n$. These quantities are not independent parameters but are dependent dynamically on the charge neutrality condition and the gap equations. For charge neutral matter, near μ_c, the d-quark number density is larger so that $\delta\mu = \mu_E/2$ is negative. This renders $\omega_n^u(p_z) > 0$ for any value of momentum p_z. On the other hand, for $\delta\mu$ negative, ω_n^d can vanish for some values of p_z. This defines the Fermi surfaces for the superconducting d quarks. It is easy to show that the excitation energy of nth Landau level ω_n^d for the condensing d quarks vanishes for momenta $|p_{zn}| = \sqrt{\mu_\pm^2 - 2n\tilde{e}B}$. Here $\mu_\pm = (\bar{\mu} \pm \sqrt{\delta\mu^2 - \Delta^2})\theta(\delta\mu - \Delta)$. Thus higher Landau levels can also have gapless modes so long as $\sqrt{\mu_\pm^2 - 2n\tilde{e}B}$ is non-negative. Gapless modes occur when the chemical potential difference $\delta\mu$ is greater than the superconducting gap. In Fig. 8(a), we have plotted the dispersion relation i.e., the excitation energy as a function of momentum for the lowest Landau level for the condensing quarks for $\mu_q = 340$ MeV and magnetic field $\tilde{e}B = 10\ \mathrm{m}_\pi^2$. The superconducting gap turns out to be $\Delta = 35.3$ MeV and $\delta\mu = -74.5$ MeV. The dispersion for the d quarks is given as $\omega_{0-}^d = \bar{\omega}_{0-} - \delta\epsilon + \delta\mu$ while the same for the u quark is given as $\omega_{0-}^u = \bar{\omega}_{0-} + \delta\epsilon - \delta\mu$. The average chemical potential is $\bar{\mu} = 366$ MeV. Far from the pairing region, $|p_z| \sim \bar{\mu} = 366$ MeV the spectrum looks like the usual BCS-type dispersion relation. Of the two excitation energies, ω_0^u shows a minimum at $p_z = \bar{\mu}$ with a value $\omega_{0-}^u(|p_z| = \bar{\mu}) \sim \Delta - \delta\mu = 110$ MeV. On the other hand, ω_{0-}^d vanishes at momenta $|p_z| = \mu_\pm$. In this breached pairing region one has only unpaired d quarks and no u quarks. This can be seen explicitly as below.

The number densities of u quarks participating in condensation is given by

$$\rho_{sc}^u = \rho^{ur} + \rho^{ug}$$
$$= \sum_n \frac{\alpha_n \tilde{e}B}{(2\pi)^2} \int dp_z \left[\frac{1}{2}\left(1 - \frac{\bar{\zeta}_{n-}}{\bar{\omega}_{n-}}\right)(1 - \theta(-\omega_n^d)) - \frac{1}{2}\left(1 - \frac{\bar{\zeta}_{n+}}{\bar{\omega}_{n+}}\right)\right], \tag{104}$$

where $\bar{\zeta}_{n-} = \bar{\epsilon}_n - \bar{\mu}$, $\mu = \frac{\mu_1 1 + \mu_2 2}{2}$ and $\bar{\epsilon} = \frac{\epsilon_u + \epsilon_d}{2}$. This is because $\omega_{n_-}^u = \bar{\omega}_{n_-} - \delta\mu + \delta\epsilon$ is always positive as $\delta\mu = \frac{\mu^u - \mu^d}{2}$ is negative and the theta function $\theta(-\omega_n^u)$ does not

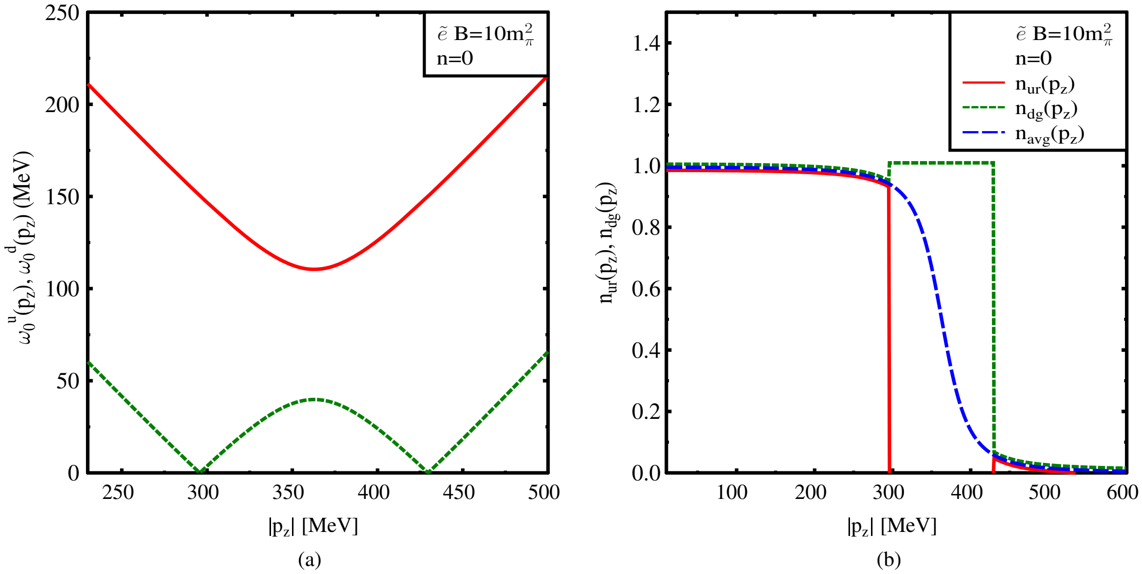

FIG. 8. Dispersion relation and the occupation number for condensing quarks at T $= 0$, $\mu_q = 340$ MeV. Part (a) shows the dispersion relation for the condensing quarks for zeroth Landau level. The upper curve is for u quark and the lower curve corresponds to d quark dispersion relation. Part (b) shows the occupation number as a function of momentum for $\tilde{e}B = 10$ m$_\pi^2$.

contribute. Similarly the density of d quarks participating in condensation is given by

$$\rho_{sc}^d = \rho^{dr} + \rho^{dg}$$
$$= \sum_n \alpha_n \frac{\tilde{e}B}{(2\pi)^2} \int dp_z \left[\theta(-\omega_n^d) + \frac{1}{2}\left(1 - \frac{\bar{\zeta}_{n-}}{\bar{\omega}_{n-}}\right)(1 - \theta(-\omega_n^d)) - \frac{1}{2}\left(1 - \frac{\bar{\zeta}_{n+}}{\bar{\omega}_{n+}}\right)\right]. \tag{105}$$

For positive ω_{n-}^d, the θ-function contributions vanishes and the distribution functions are the BCS distribution function. On the other hand, when $|p_z| \in [P_{n-}, P_{n+}]$, ω_n^d is negative leading to ρ_{sc}^u to vanish but for the antiparticle contribution. In this region of momenta, ρ_{sc}^d is unity. We have plotted in Fig. 8(b) the occupation number of the up and down quarks that take part in condensation as a function of the magnitude of momentum p_z i.e., the integrands of Eqs. (104) and (105) respectively for the lowest Landau level. It is easy to see from Eqs. (104) and (105) e.g., for the lowest Landau level that, except for the interval (μ_-, μ_+), the distribution function is like the BCS distribution function. This is shown by the blue long-dashed line. The u-quark distribution is shown by the red solid line while the d-quark distribution is shown by the green short dashed line. Indeed, except for the interval (μ_-, μ_+), all three curves overlap with each other. In the "gapless" momentum region, the u-quark occupation vanishes while d-quark occupation is unity. This leads to the fact that the momentum integrated distribution function for the condensing u and d quarks is not the same for the gapless region unlike the usual BCS phase. We have plotted the number densities for the u and d quarks in Fig. 9 which shows a fork structure in the gapless region.

Gapless modes have been considered earlier for two flavor quark matter both with [37,38] and without magnetic field [35,36]. However it has been shown [65,66] that in QCD at zero temperature the gapless 2SC phases are unstable. This instability manifests itself in imaginary Meissner mass of some species of the gluons. Finite temperature calculations [67] show that at some critical value of temperature the instability vanishes. This value

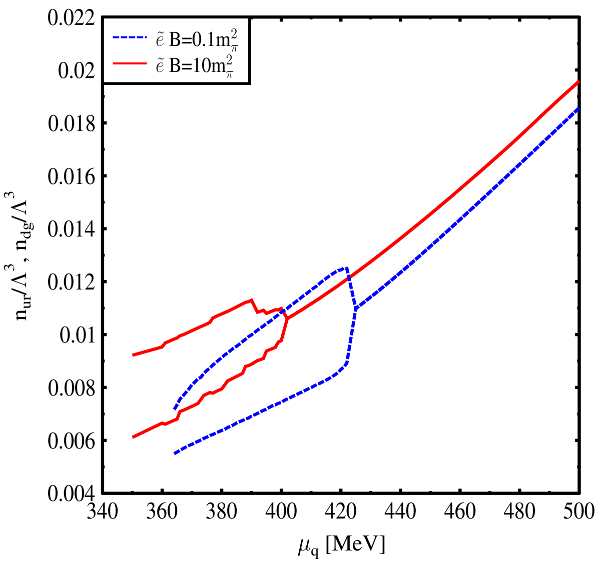

FIG. 9. Number densities of up and down quarks participating in the superconductivity for $\tilde{e}B = 0.1$ m$_\pi^2$ (dashed line) and $\tilde{e}B = 10$ m$_\pi^2$ (solid line).

may range from few MeV to tens of MeV. The instability of the gapless phases indicates that there should be other phases of quark matter breaking translational invariance e.g., inhomogenous phase of quark matter like crystalline color superconductivity [68,69]. One may note that these considerations apply to the case without magnetic field and may change in the presence of a strong magnetic field.

In Fig. 10, we have plotted the electric and color chemical potentials μ_E and μ_8 to maintain the electric and color charge neutrality conditions given in Eqs. (94) and (95) as a function of quark chemical potential. For $2+1$ flavor matter, strange quarks play an important role in maintaining charge neutrality. As the quark chemical potential increases, $|\mu_E|$ increases to maintain charge neutrality. When the chemical potential becomes large enough for strange quarks to contribute to densities, they also help in maintaining charge neutrality. This leads to a decrease in electron density or the corresponding chemical potential $|\mu_E|$. This behavior is reflected in Figs. 10(a) and 10(b) as the initial slow rise of the $|\mu_E|$. However, as $|\mu_E|$ increases, the difference $\delta\mu = -\mu_E/2$ also increases and at μ_1, the condition $\delta\mu > \Delta$ for gapless modes to exist ceases to be satisfied. At the gapless to BCS transition point, the u-quark number density increases while that of d quarks

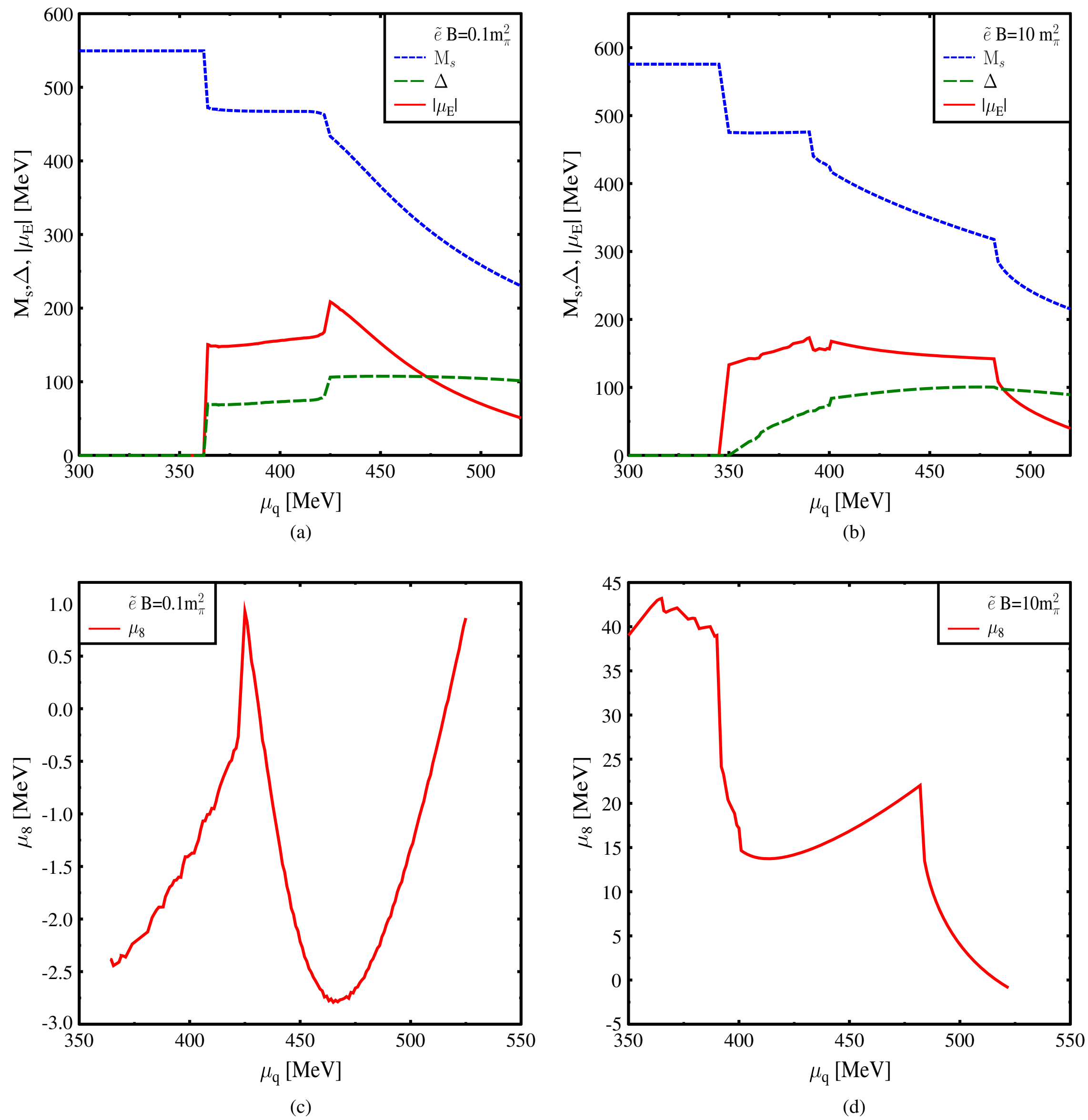

FIG. 10. Chemical potential μ_E and μ_8 for charge neutral quark matter. $|\mu_E|$ is plotted as a function of quark chemical potential μ_q for magnetic field $\tilde{e}B = 0.1\ m_\pi^2$ (a) and for $\tilde{e}B = 10\ m_\pi^2$ (b). In (a) and (b) we have also plotted the mass of strange quarks and superconducting gap as a function of quark chemical potential to highlight the dependence of charge chemical potential on these two parameters. In the lower two plots, the color chemical potential μ_8 is plotted as a function μ_q for $\tilde{e}B = 0.1\ m_\pi^2$ (c) and for $\tilde{e}B = 10\ m_\pi^2$ (d).

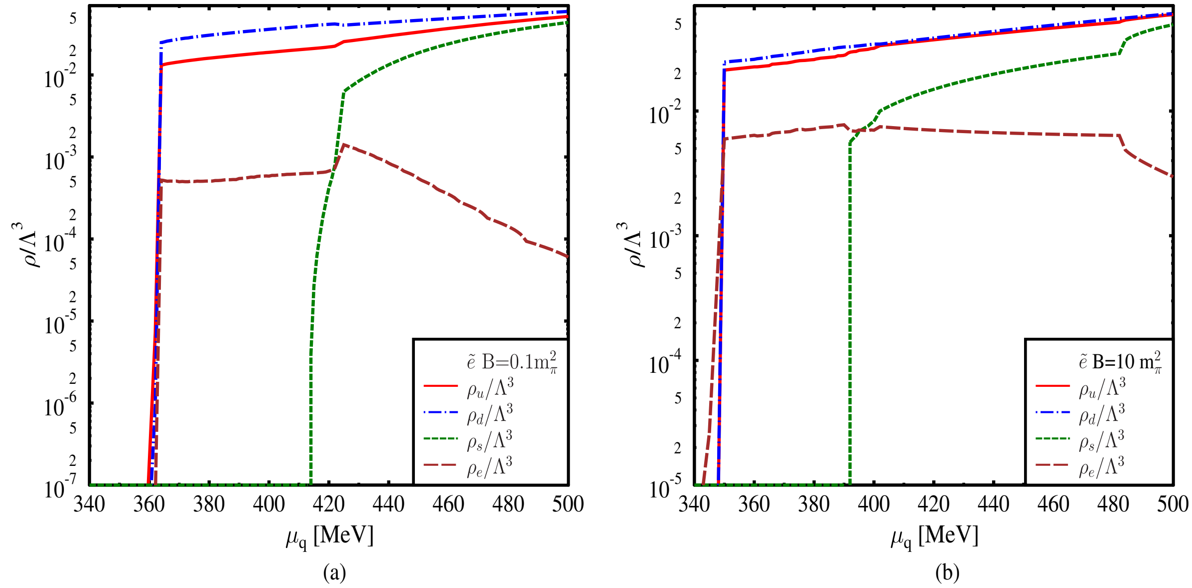

FIG. 11. Population of different species for charge neutral quark matter for $\tilde{e}B = 0.1\ \mathrm{m}_\pi^2$ (a) and for $\tilde{e}B = 10\ \mathrm{m}_\pi^2$ (b).

decreases and both become equal as in the usual BCS pairing phase. This leads to an increase in the positive electric charge density. To maintain electrical charge neutrality, the electron density increases at this point. Therefore gapless to BCS transition is accompanied with an increase in $|\mu_E|$. On the other hand, at higher densities when strange quarks start contributing to the density, it is accompanied with a drop in $|\mu_E|$ as strange quarks help in maintaining the charge neutrality along with the electrons. It turns out that for $\tilde{e}B = 0.1\ \mathrm{m}_\pi^2$, the strange quark densities become nonvanishing after the gapless to BCS transition. This leads to the continuous decrease in the $|\mu_E|$ in the BCS phase as seen in Fig. 10(a). On the other hand, for larger fields, e.g., $\tilde{e}B = 10\ \mathrm{m}_\pi^2$, chiral transition occurs at a lower μ_c due to magnetic catalysis and the strange quark density starts becoming nonvanishing at lower chemical potential. This leads to a decrease in $|\mu_E|$ at $\mu = 392$ MeV as may be seen in Fig. 10(b). At $\mu = 400$ MeV, there is the transition from the gapless to BCS phase and is accompanied with a rise in $|\mu_E|$ as discussed above. Beyond $\mu = 400$ MeV, $|\mu_E|$ starts decreasing monotonically as strange quark density increase.

In Figs. 10(c) and 10(d), we have plotted the color chemical potential μ_8. For the weak field case, μ_8 is rather small (few MeVs) compared to both the electric chemical potential as well as the quark chemical potential which are 2 orders of magnitude larger. For the small field, the difference in densities of red and green quarks and the blue quarks essentially arises because of the difference in the distribution functions. This results in a small but finite net color charge. To maintain color neutrality one needs a small μ_8. On the other hand, at the large magnetic field, the net color charge difference becomes larger as the $\tilde{e}$ charges of red and green quarks and that of blue quarks are different. This requires a somewhat larger μ_8 to maintain color neutrality as seen in Fig. 10(d). In Fig. 11 we have plotted the number densities of each species for the charge neutral matter for two different magnetic fields. As may be clear from both plots the electron number densities get correlated with the strange quark number densities.

Finally, we discuss the equation of state (EOS) for different magnetic fields. In Fig. 12 we have plotted pressure as a function of energy for $\tilde{e}\mathrm{B} = 0.1\ \mathrm{m}_\pi^2$ and $10\ \mathrm{m}_\pi^2$. One can observe that the EOSs become stiffer with increase in magnetic field. This can be understood as follows. For $\mu < \mu_c$, the thermodynamic potential contribution from the

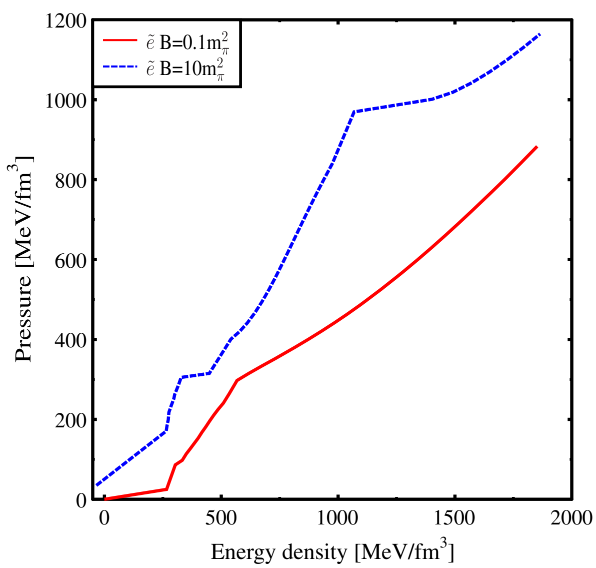

FIG. 12. Equation of state for $\tilde{e}B = 0.1\ \mathrm{m}_\pi^2$ (dashed line) and $\tilde{e}B = 10\ \mathrm{m}_\pi^2$ (solid line).

field as in Eqs. (75), (79), and (81) is dominant and decreases with an increase in magnetic field. This leads to a higher pressure for higher magnetic field. As the chemical potential increases, for $\mu > \mu_c$, the medium contribution becomes dominant. As the masses decrease with magnetic field, the medium contribution increases with magnetic field. Moreover, the field contributions also lead to an increase in pressure. Both these effects make the resulting EOS stiffer at higher magnetic field as may be seen in Fig. 12.

V. SUMMARY

We have analyzed here the effect of magnetic field and neutrality conditions on the chiral as well as diquark condensates within the framework of a three-flavor NJL model. This essentially generalizes the results of Ref. [24] to include the u-d superconductivity in the presence of a magnetic field. The methodology uses an explicit variational construct for the ground state in terms of quark-antiquark pairing for all three flavors as well as diquark pairing for the light quarks. A nice feature of the approach is that the four component quark field operator in the presence of a magnetic field could get expressed in terms of the ansatz functions that appear for the description of the ground state. Apart from the methodology being different, we also have new results. Namely, the present investigations have been done in a three-flavor NJL model along with a flavor mixing six quark determinant interaction at finite temperature and density and fields within the same framework. In that sense it generalizes the two flavor color superconductivity in the presence of a magnetic field considered earlier in Refs. [19,37,38]. The gap functions and the thermal distribution functions could be determined self-consistently for given values of the temperature, the quark chemical potential and the strength of magnetic field.

For the charge neutral matter the chiral transition is a first order transition and we observe inverse magnetic catalysis at finite density. The chiral condensate for strange quark affects the u-d superconductivity through the flavor mixing determinant interaction. The effective diquark coupling increases in the presence of strange quark condensates. On the other hand the diquark condensates contribute to the mass of the strange quark through the determinant interaction. Inverse magnetic catalysis is observed for magnetic fields up to 19 m_π^2. Beyond it magnetic catalysis is observed for chiral symmetry breaking [63].

At finite densities, the effects of Landau quantization get manifested in the oscillation of the order parameters similar to the de Hass van Alphen effect for magnetization in metals. However, in the present case of dense quark matter, the order parameters, the masses and the superconducting gap themselves are dependant on the strength of magnetic fields which leads to a nonperiodic oscillation of the order parameter.

Imposition of charge neutrality condition for the quark matter leads to gapless modes even in presence of magnetic field. The superconducting gaps in gapless modes are smaller compared to the gaps in the BCS phase. The transition from gapless to BCS phase is a sharp transition. The difference in the gap in the two phases at this transition decreases with magnetic field. For charge neutral matter the strange quark plays an important role in maintaining the charge neutrality. This leads to a depletion of electron density at higher chemical potential where strange quarks start to contribute to the densities. The resulting equation of state becomes stiffer with magnetic field.

We have considered here quark-antiquark pairing and diquark pairing in the ansatz for ground state which is homogeneous with zero total momentum. However it is possible that the condensates be spatially inhomogeneous [70] with a net total momentum [71–74]. Indeed, the gapless modes for the charge neutral matter leads to instability arising from imaginary Meissner masses for some of the gluons when $\delta\mu > \Delta$ [66]. This can be suggestive of having inhomogeneous superconducting phases [68,69] which are not considered here. The phase structure here would be nontrivial and interesting in the presence of two vectors, the magnetic field and nonzero momentum of the condensate. Furthermore, the equation of state derived for charge neutral quark matter combined with the same for hadronic matter can be used to study structural properties of neutron star with quark matter core. It will be interesting to see the compatibility of such an equation of state which is constrained by astrophysical observations like GW170817 [75]. Some of these investigations are in progress and will be reported elsewhere.

ACKNOWLEDGMENTS

The authors would like to thank Amruta Mishra for many discussions.

APPENDIX: EVALUATION OF OPERATOR EXPECTATION VALUES OF SOME OPERATORS

We give here some details of the evaluation of some operators at finite T, μ and B in the state given in Eq. (18). As the state is obtained from $|0\rangle$, one can calculate the expectation values of different operators, e.g.,

$$\langle q_r^{ia\dagger}(n,k_\chi), q_{r'}^{jb}(n',k'_\chi)\rangle = \delta^{ij}\delta^{ab}\delta_{rr'}\delta_{nn'}\delta(\mathbf{k}_\chi - \mathbf{k}'_\chi)F^{ia}(\mathbf{k}_\chi), \tag{A1}$$

where

$$F^{ia}(\mathbf{k}_\chi) = \sin^2\theta_-^{ia} + \sin^2 f(1 - \sin^2\theta_-^{ia} - |\epsilon^{ij}\epsilon^{ab}|\sin^2\theta_-^{jb}) \times (1-\delta^{a3})(1-\delta^{i3}). \tag{A2}$$

Similarly for the expectation values for the operators involving antiquarks, we have

$$\langle \tilde{q}_r^{ia\dagger}(n,k_\chi), \tilde{q}_{r'}^{jb}(n',k'_\chi)\rangle = \delta^{ij}\delta^{ab}\delta_{rr'}\delta_{nn'}\delta(\mathbf{k}_\chi - \mathbf{k}'_\chi)(1 - F_1^{ia}(\mathbf{k}_\chi)), \tag{A3}$$

where

$$F_1^{ia}(\mathbf{k}_\chi) = \sin^2\theta_+^{ia} + \sin^2 f_1(1 - \sin^2\theta_+^{ia} - |\epsilon^{ij}\epsilon^{ab}|\sin^2\theta_+^{jb})(1-\delta^{a3})(1-\delta^{i3}). \tag{A4}$$

Using the field operator expansion of Eq. (10) and Eqs. (A1) and (A3), one can evaluate

$$\langle \psi_\alpha^{ia\dagger}(\mathbf{x})\psi_\beta^{jb}(\mathbf{y})\rangle = \sum_n \frac{|q_i B|}{(2\pi)^2}\int dk_\chi e^{ik_\chi\cdot(\mathbf{x}-\mathbf{y})}\Lambda_-^{ia,jb}{}_{\beta\alpha}(n,k_\chi) \tag{A5}$$

with

$$\Lambda_-^{ia,jb} = \delta^{ij}\delta^{ab}[F^{ia}(n,k_z)U_{\beta r}(n,k_\chi)U_{r\alpha}(n,k_\chi)^\dagger + (1 - F_1^{ia}(n,k_z))V_{\beta r}(n,-k_\chi)V_{r\alpha}(n,-k_\chi)^\dagger]. \tag{A6}$$

Explicitly,

$$\begin{aligned} U_r(n,\boldsymbol{p}_\chi)U_r^\dagger(n,\boldsymbol{p}_\chi) &= \frac{1}{2}\begin{pmatrix} (1+\cos\phi)I_n^2 & 0 & \hat{p}_z\sin\phi I_n^2 & i\hat{p}_\perp \sin\phi I_n I_{n-1} \\ 0 & (1+\cos\phi)I_{n-1}^2 & -i\hat{p}_\perp\sin\phi I_n I_{n-1} & -\hat{p}_z\sin\phi I_{n-1}^2 \\ \hat{p}_z\sin\phi I_n^2 & i\hat{p}_\perp\sin\phi I_n I_{n-1} & (1-\cos\phi)I_n^2 & 0 \\ -i\hat{p}_\perp\sin\phi I_n I_{n-1} & -\hat{p}_z\sin\phi I_{n-1}^2 & 0 & (1-\cos\phi)I_{n-1}^2 \end{pmatrix}. \\ &= \frac{1}{2}\Big[I_n^2(1+\gamma^0\cos\phi)\Pi^+ + I_{n-1}^2(1+\gamma^0\cos\phi)\Pi^- + \frac{\hat{p}_z}{2}\sin\phi(\gamma_0\gamma^3(I_n^2+I_{n-1}^2) + \gamma^5(I_n^2 - I_{n-1}^2)) \\ &\quad - \hat{p}_\perp\sin\phi\gamma^2\gamma^0\Big], \end{aligned} \tag{A7}$$

where we have defined $\Pi^\pm = (1 \pm i\gamma^1\gamma^2)/2$, $\hat{p}_z = \frac{p_z}{|p|}$, $\hat{p}_\perp = \frac{\sqrt{2nqB}}{|p|}$ with $|p| = \sqrt{p_z^2 + 2nqB}$.

Similarly for the antiquark spinors

$$\begin{aligned} V_r(n,-\boldsymbol{p}_\chi)V_r^\dagger(n,-\boldsymbol{p}_\chi) &= \frac{1}{2}\begin{pmatrix} (1-\cos\phi)I_n^2 & 0 & -\hat{p}_z\sin\phi I_n^2 & -i\hat{p}_\perp \sin\phi I_n I_{n-1} \\ 0 & (1-\cos\phi)I_{n-1}^2 & i\hat{p}_\perp\sin\phi I_n I_{n-1} & \hat{p}_z\sin\phi I_{n-1}^2 \\ -\hat{p}_z\sin\phi I_n^2 & -i\hat{p}_\perp\sin\phi I_n I_{n-1} & (1+\cos\phi)I_n^2 & 0 \\ i\hat{p}_\perp\sin\phi I_n I_{n-1} & \hat{p}_z\sin\phi I_{n-1}^2 & 0 & (1+\cos\phi)I_{n-1}^2 \end{pmatrix}. \\ &= \frac{1}{2}\Big[I_n^2(1-\gamma^0\cos\phi)\Pi^+ + I_{n-1}^2(1-\gamma^0\cos\phi)\Pi^- - \frac{\hat{p}_z}{2}\sin\phi(\gamma_0\gamma^3(I_n^2+I_{n-1}^2) + \gamma^5(I_n^2 - I_{n-1}^2)) \\ &\quad + \hat{p}_\perp\sin\phi\gamma^2\gamma^0\Big]. \end{aligned} \tag{A8}$$

This leads to, e.g., for the expectation value of chiral condensate for a given flavor as

$$I_s^i = \langle\bar{\psi}^i\psi^i\rangle = -\frac{1}{(2\pi)^2}\sum_n\sum_a\int dp_y dp_z(1 - F^{ia} - F_1^{ia})\cos\phi_n^i(I_n^2 + I_{n-1}^2). \tag{A9}$$

One can integrate over dp_y to obtain the contribution for the quarks that are charged as

$$I_s^i = \sum_a\sum_n \frac{\alpha_n}{(2\pi)^2}|q_i B|\int dp_z(1 - F^{ia} - F_1^{ia})\cos\phi_n^i. \tag{A10}$$

On the other hand, the contribution to the scalar condensate from the quarks that are neutral (down blue and strange blue) is given as

$$I_s^i = \frac{2}{(2\pi)^3} \int d\mathbf{p} \cos\phi^i (1 - \sin^2\theta_-^{i3} - \sin^2\theta_+^{i3}) \qquad (i = 2, 3). \tag{A11}$$

Next, we discuss about the contributions to diquark condensates. Similar to Eq. (A12), we have

$$\begin{aligned} \langle q_r^{ia}(n, k_{\not{z}}), q_{r'}^{jb}(n', k'_{\not{z}}) \rangle &= r\delta_{r,-r'} \epsilon^{ij} \epsilon^{3ab} \delta_{nn'} \delta(\mathbf{k}_{\not{z}} + \mathbf{k}'_{\not{z}}) \sin 2f(n, k_z)(1 - \sin^2\theta_-^{ia} - \sin^2\theta_-^{jb}) \\ &\equiv r\delta_{r,-r'} \epsilon^{ij} \epsilon^{3ab} \delta_{nn'} \delta(\mathbf{k}_{\not{z}} + \mathbf{k}'_{\not{z}}) G(k_z, n) \end{aligned} \tag{A12}$$

and, for antiquark operators

$$\begin{aligned} \langle \tilde{q}_r^{ia}(n, k_{\not{z}}), \tilde{q}_{r'}^{jb}(n', k'_{\not{z}}) \rangle &= r\delta_{r,-r'} \epsilon^{ij} \epsilon^{3ab} \delta_{nn'} \delta(\mathbf{k}_{\not{z}} + \mathbf{k}'_{\not{z}}) \sin 2f(n, k_z)(1 - \sin^2\theta_-^{ia} - \sin^2\theta_-^{jb}) \\ &\equiv r\delta_{r,-r'} \epsilon^{ij} \epsilon^{3ab} \delta_{nn'} \delta(\mathbf{k}_{\not{z}} + \mathbf{k}'_{\not{z}}) G_1(k_z, n). \end{aligned} \tag{A13}$$

For the diquark condensates we have

$$\langle \psi_\alpha^{ia}(\mathbf{x}) \psi_\beta^{jb}(\mathbf{y}) \rangle = \epsilon^{ij} \epsilon^{3ab} \sum_n \frac{|q_i B|}{(2\pi)^2} \int dk_{\not{z}} e^{ik_{\not{z}} \cdot (\mathbf{x}-\mathbf{y})} [P_u C\gamma^5 G(k_z, n) + P_v C\gamma^5 G_1(k_z, n)]_{\beta\alpha}, \tag{A14}$$

where $P_u C\gamma^5 = \sum_r r U_{\alpha r} U'_{-r\beta}$ and $P_v C\gamma^5 = \sum_r r V_{\alpha r} V'_{-r\beta}$ and the prime on the spinors denotes a spinor with opposite charge and momentum corresponding to the unprimed spinors. Explicitly,

$$P_u = \frac{1}{2} \begin{pmatrix} \cos\frac{\phi}{2}\cos\frac{\phi'}{2} I_n^2 & 0 & \hat{p}_z \cos\frac{\phi}{2}\sin\frac{\phi'}{2} I_n^2 & i\hat{p}_\perp \cos\frac{\phi}{2}\sin\frac{\phi'}{2} I_n I_{n-1} \\ 0 & \cos\frac{\phi}{2}\cos\frac{\phi'}{2} I_{n-1}^2 & -i\hat{p}_\perp \cos\frac{\phi}{2}\sin\frac{\phi'}{2} I_n I_{n-1} & -\hat{p}_z \cos\frac{\phi}{2}\sin\frac{\phi'}{2} I_{n-1}^2 \\ \hat{p}_z \cos\frac{\phi'}{2}\sin\frac{\phi}{2} I_n^2 & i\hat{p}_\perp \cos\frac{\phi'}{2}\sin\frac{\phi}{2} I_n I_{n-1} & \sin\frac{\phi}{2}\sin\frac{\phi'}{2} I_n^2 & 0 \\ -i\hat{p}_\perp \sin\frac{\phi}{2}\cos\frac{\phi'}{2} I_n I_{n-1} & -\hat{p}_z \sin\frac{\phi}{2}\cos\frac{\phi'}{2} I_{n-1}^2 & 0 & \sin\frac{\phi}{2}\sin\frac{\phi'}{2} I_{n-1}^2 \end{pmatrix} \tag{A15}$$

and

$$P_v = \frac{1}{2} \begin{pmatrix} -\sin\frac{\phi}{2}\sin\frac{\phi'}{2} I_n^2 & 0 & \hat{p}_z \sin\frac{\phi}{2}\cos\frac{\phi'}{2} I_n^2 & i\hat{p}_\perp \sin\frac{\phi}{2}\cos\frac{\phi'}{2} I_n I_{n-1} \\ 0 & -\sin\frac{\phi}{2}\sin\frac{\phi'}{2} I_{n-1}^2 & -i\hat{p}_\perp \sin\frac{\phi}{2}\cos\frac{\phi'}{2} I_n I_{n-1} & -\hat{p}_z \sin\frac{\phi}{2}\cos\frac{\phi'}{2} I_{n-1}^2 \\ \hat{p}_z \cos\frac{\phi}{2}\sin\frac{\phi'}{2} I_n^2 & i\hat{p}_\perp \cos\frac{\phi}{2}\sin\frac{\phi'}{2} I_n I_{n-1} & -\cos\frac{\phi}{2}\cos\frac{\phi'}{2} I_n^2 & 0 \\ -i\hat{p}_\perp \cos\frac{\phi}{2}\sin\frac{\phi'}{2} I_n I_{n-1} & -\hat{p}_z \cos\frac{\phi}{2}\sin\frac{\phi'}{2} I_{n-1}^2 & 0 & -\cos\frac{\phi}{2}\cos\frac{\phi'}{2} I_{n-1}^2 \end{pmatrix}. \tag{A16}$$

This leads to, e.g., for expectation value of the diquark condensate as

$$\begin{aligned} I_D &= \langle \bar{\psi}_c^{ia} \gamma^5 \psi^{jb} \rangle \epsilon^{ij} \epsilon^{3ab} \\ &= \frac{2}{(2\pi)^2} \sum_n \alpha_n |q_i B| \int dp_z \cos\left(\frac{\phi_1 - \phi_2}{2}\right) [\sin 2f(1 - \sin^2\theta_-^1 - \sin^2\theta_-^2) + \sin 2f_1(1 - \sin^2\theta_+^1 - \sin^2\theta_+^2)]. \end{aligned} \tag{A17}$$

[1] For reviews see K. Rajagopal and F. Wilczek, arXiv:hep-ph/0011333; D. K. Hong, Acta Phys. Pol. B 32, 1253 (2001); M. G. Alford, Annu. Rev. Nucl. Part. Sci. 51, 131 (2001); G. Nardulli, Riv. Nuovo Cimento 25, 1 (2002); S. Reddy, Acta Phys. Pol. B 33, 4101 (2002); T. Schaefer, arXiv:hep-ph/0304281; D. H. Rischke, Prog. Part. Nucl. Phys. 52, 197

(2004); H. C. Ren, arXiv:hep-ph/0404074; M. Huang, Int. J. Mod. Phys. E **E14**, 675 (2005); I. Shovkovy, Found. Phys. **35**, 1309 (2005).
[2] D. Kharzeev, L. McLerran, and H. Warringa, Nucl. Phys. **A803**, 227 (2008); K. Fukushima, D. Kharzeev, and H. Warringa, Phys. Rev. D **78**, 074033 (2008).
[3] V. Skokov, A. Illarionov, and V. Toneev, Int. J. Mod. Phys. A **24**, 5925 (2009).
[4] D. E. Kharzeev, J. Liao, S. A. Voloshin, and G. Wang, Prog. Part. Nucl. Phys. **88**, 1 (2016); D. Kharzeev, Ann. Phys. (N.Y.) **325**, 205 (2010); K. Fukushima, M. Ruggieri, and R. Gatto, Phys. Rev. D **81**, 114031 (2010).
[5] M. D'Elia, S. Mukherjee, and F. Sanflippo, Phys. Rev. D **82**, 051501 (2010).
[6] A. J. Mizher, M. N. Chenodub, and E. Fraga, Phys. Rev. D **82**, 105016 (2010).
[7] D. Bandyopadhyaya, S. Chakrabarty, and S. Pal, Phys. Rev. Lett. **79**, 2176 (1997); S. Chakrabarty and S. Mandal, Phys. Rev. C **75**, 015805 (2007).
[8] R. C. Duncan and C. Thompson, Astrophys. J. **392**, L9 (1992).
[9] C. Thompson and R. C. Duncan, Astrophys. J. **408**, 194 (1993).
[10] C. Thompson and R. C. Duncan, Mon. Not. R. Astron. Soc. **275**, 255 (1995).
[11] C. Thompson and R. C. Duncan, Astrophys. J. **473**, 322 (1996).
[12] C. Y. Cardall, M. Prakash, and J. M. Lattimer, Astrophys. J. **554**, 322 (2001).
[13] A. E. Broderick, M. Prakash, and J. M. Lattimer, Phys. Lett. B **531**, 167 (2002).
[14] D. Lai and S. L. Shapiro, Astrophys. J. **383**, 745 (1991).
[15] E. J. Ferrer, V. Incera, J. P. Keith, and P. Springsteen, Phys. Rev. C **82**, 065802 (2010).
[16] X. G. Huang, M. Huang, D. H. Rischke, and A. Sedrakian, Phys. Rev. D **81**, 045015 (2010).
[17] K. Fukushima, M. Ruggieri, and R. Gatto, Phys. Rev. D **81**, 114031 (2010).
[18] E. V. Gorbar, V. A. Miransky, and I. Shovkovy, Phys. Rev. C **80**, 032801(R) (2009); , Phys. Lett. B **695**, 354 (2011).
[19] Sh. Fayazbakhsh and N. Sadhooghi, Phys. Rev. D **82**, 045010 (2010); **83**, 025026 (2011).
[20] V. P. Gusynin, V. Miranski, and I. Shovkovy, Phys. Rev. Lett. **73**, 3499 (1994); Phys. Lett. B **349**, 477 (1995); Nucl. Phys. **B462**, 249 (1996); E. J. Ferrer and V. de la Incerra, Phys. Rev. Lett. **102**, 050402 (2009); Nucl. Phys. **B824**, 217 (2010).
[21] D. Ebert and K. G. Klimenko, Nucl. Phys. **A728**, 203 (2003).
[22] J. K. Boomsma and D. Boer, Phys. Rev. D **81**, 074005 (2010).
[23] D. P. Menezes, M. Benghi Pinto, S. S. Avancini, and C. Providencia, Phys. Rev. C **80**, 065805 (2009); D. P. Menezes, M. Benghi Pinto, S. S. Avancini, A. P. Martinez, and C. Providencia, Phys. Rev. C **79**, 035807 (2009).
[24] B. Chatterjee, H. Mishra, and A. Mishra, Phys. Rev. D **84**, 014016 (2011).
[25] M. Alford, K. Rajagopal, and F. Wilczek, Phys. Lett. B **422**, 247 (1998); Nucl. Phys. **B537**, 443 (1999).
[26] M. Alford, C. Kouvaris, and K. Rajagopal, Phys. Rev. Lett. **92**, 222001 (2004).
[27] K. Rajagopal and A. Schimitt, Phys. Rev. D **73**, 045003 (2006).
[28] M. Buballa, Phys. Rep. **407**, 205 (2005).
[29] S. P. Klevensky, Rev. Mod. Phys. **64**, 649 (1992).
[30] E. J. Ferrer, V. de la Incera, and C. Manuel, Phys. Rev. Lett. **95**, 152002 (2005); E. J. Ferrer and V. de la Incera, Phys. Rev. Lett. **97**, 122301 (2006); Phys. Rev. D **76**, 114012 (2007).
[31] J. Noronah and I. Shovkovy, Phys. Rev. D **76**, 105030 (2007).
[32] K. Fukushima and H. J. Warringa, Phys. Rev. Lett. **100**, 032007 (2008).
[33] E. V. Gorbar, Phys. Rev. D **62**, 014007 (2000).
[34] M. G. Alford, J. Berges, and K. Rajagopal, Nucl. Phys. **B571**, 269 (2000).
[35] M. Huang and I. Shovkovy, Nucl. Phys. **A729**, 835 (2003).
[36] A. Mishra and H. Mishra, Phys. Rev. D **71**, 074023 (2005).
[37] T. Mandal, P. Jaikumar, and S. Digal, arXiv:0912.1413; T. Mandal and P. Jaikumar, Phys. Rev. C **87**, 045208 (2013); Phys. Rev. D **94**, 074016 (2016).
[38] M. Coppola, P. Allen, A. G. Grunfeld, and K. N. N. Scoccola, Phys. Rev. D **96**, 056013 (2017).
[39] A. Mishra and H. Mishra, Phys. Rev. D **69**, 014014 (2004).
[40] H. Mishra and S. P. Misra, Phys. Rev. D **48**, 5376 (1993).
[41] H. Mishra and J. C. Parikh, Nucl. Phys. **A679**, 597 (2001).
[42] K. Bhattacharya, arXiv:0705.4275; M. de J. Anguiano-Galicia, A. Bashir, and A. Raya, Phys. Rev. D **76**, 127702 (2007).
[43] A. Mishra and S. P. Misra, Z. Phys. C **58**, 325 (1993).
[44] H. Umezawa, H. Matsumoto, and M. Tachiki, *Thermofield Dynamics and Condensed States* (North-Holland, Amsterdam, 1982); P. A. Henning, Phys. Rep. **253**, 235 (1995).
[45] A. Mishra and H. Mishra, J. Phys. G **23**, 143 (1997).
[46] M. A. Metlitsky and A. R. Zhitnitsky, Phys. Rev. D **72**, 045011 (2005).
[47] A. Mishra and H. Mishra, Phys. Rev. D **74**, 054024 (2006).
[48] M. Alford and A. Sedrakian, J. Phys. G **37**, 075202 (2010).
[49] A. W. Steiner, Phys. Rev. D **72**, 054024 (2005).
[50] F. Gastineau, R. Nebauer, and J. Aichelin, Phys. Rev. C **65**, 045204 (2002).
[51] A. A. Abrikosov and L. P. Gorkov, Sov. Phys. JETP **12**, 1243 (1961).
[52] M. G. Alford, J. Berges, and K. Rajagopal, Phys. Rev. Lett. **84**, 598 (2000).
[53] E. Elizalde, J. Phys. A **18**, 1637 (1985).
[54] T. Hatsuda and T. Kunihiro, Phys. Rep. **247**, 221 (1994).
[55] M. Lutz, S. Klimt, and W. Weise, Nucl. Phys. **A542**, 521 (1992).
[56] P. Rehberg, S. P. Klevansky, and J. Huefner, Phys. Rev. C **53**, 410 (1996).
[57] M. Buballa and M. Oertel, Nucl. Phys. **A703**, 770 (2002).
[58] A. W. Steiner, S. Reddy, and M. Prakash, Phys. Rev. D **66**, 094007 (2002).
[59] S. B. Ruester, V. Werth, M. Buballa, I. Shovkovy, and D. H. Rischke, Phys. Rev. D **72**, 034004 (2005); S. B. Ruester, I. Shovkovy, and D. H. Rischke, Nucl. Phys. **A743**, 127 (2004).
[60] D. Blaschke, S. Fredriksson, H. Griogorian, A. M. Oztas, and F. Sandin, Phys. Rev. D **72**, 065020 (2005).
[61] M. Buballa, Phys. Rep. **407**, 205 (2005).
[62] K. Schertler, S. Leupold, and J. Schaffner-Bielich, Phys. Rev. C **60**, 025801 (1999).

[63] F. Preis, A. Rebhan, and A. Schmitt, J. High Energy Phys. 03 (2011) 033; Lect. Notes Phys. **871**, 51 (2013).
[64] W. V. Liu and F. Wilczek, Phys. Rev. Lett. **90**, 047002 (2003); E. Gubankova, W. V. Liu, and F. Wilczek, Phys. Rev. Lett. **91**, 032001 (2003).
[65] I. Giannakis and H.-C. Ren, Phys. Lett. B **611**, 137 (2005).
[66] M. Huang and I. Shovkovy, Phys. Rev. D **70**, 094030 (2004).
[67] K. Fukushima, Phys. Rev. D **72**, 074002 (2005).
[68] K. Rajagopal and R. Sharma, Phys. Rev. D **74**, 094019 (2016).
[69] J. A. Bowers and K. Rajagopal, Phys. Rev. D **66**, 065002 (2002).
[70] S. Sarkar and R. Sharma, Phys. Rev. D **96**, 094025 (2017).
[71] D. Nickel, Phys. Rev. D **80**, 074025 (2009).
[72] G. Baser, G. Dunne, and D. Kharzeev, Phys. Rev. Lett. **104**, 232301 (2010).
[73] H. Abuki, Phys. Rev. D **98**, 054006 (2018).
[74] I. E. Frolov, V. Ch. Zhukovsky, and K. G. Klimenko, Phys. Rev. D **82**, 076002 (2010).
[75] F. J. Fattoyev, J. Piekarewicz, and C. J. Horowitz, Phys. Rev. Lett. **120**, 172702 (2018).

Spin Polarization and Chiral Condensation in 2+1 flavor Nambu-Jona-Lasinio model at finite temperature and baryon chemical potential

Aman Abhishek*
Theory Division, Physical Research Laboratory, Navrangpura, Ahmedabad 380 009, India and Indian Institute of Technology Gandhinagar, Gandhinagar 382355, Gujarat, India

Arpan Das† and Hiranmaya Mishra‡
Theory Division, Physical Research Laboratory, Navrangpura, Ahmedabad 380 009, India

Ranjita K. Mohapatra§
Department of Physics, Indian Institute of Technology Bombay, Powai, Mumbai 400076, India

We investigate the ferromagnetic (spin polarization) condensation in (2+1) flavor Nambu Jona-Lasinio(NJL) model with non-zero current quark masses at finite temperature and density which may be relevant in the context of neutron stars. The spin polarization condensation arises due to a tensor type interaction that may be generated due to non- perturbative effects in Quantum Chromodynamics(QCD). In this investigation we study the interplay between chiral condensate and spin polarization condensation for different values of tensor coupling. Spin polarization in the case of 2+1 flavor is different from two flavor case because of an additional F_8 condensate associated with λ_8^f flavor generator. We find non-zero values of the two spin condensates in the chirally restored phase. Beyond a certain temperature the spin polarization condensates vanish for any value of quark chemical potential. The spin condensates affect the chiral phase transition, quark masses and the quark dispersion relation. Thermodynamic behavior of F_3 and F_8 are found to be different and they affect the quark masses differently.

PACS numbers: 25.75.-q, 12.38.Mh

I. INTRODUCTION

One of the recent interests in high energy physics is to study the phase diagram of strongly interacting matter. QCD phase diagram has been studied extensively in the temperature (T) - baryon chemical potential (μ_B) plane [1, 2]. The first principle lattice QCD (LQCD) simulations give a reliable prediction about the nature of QCD phases and phase transitions at zero baryon chemical potential and finite temperature [3–5]. Although LQCD calculations can be trusted at small baryon chemical potential $\mu_B \simeq 0$ using extrapolation, at relatively large baryon chemical potential the "fermion sign problem"[6]in LQCD prevents one from making reliable estimates. LQCD calculations predict that at $\mu_B = 0$, the nature of the transition from confined hadronic phase to deconfined quark gluon plasma (QGP) phase is not a thermodynamic phase transition rather it is a smooth crossover with a transition temperature $T_c \in [149 - 163]$ MeV [7]. On the other hand, QCD inspired effective field theory models e.g. Nambu-Jona-Lasinio model (NJL) etc., indicate that the phase transition from the hadronic phase to QGP phase at large baryon chemical potential and small temperature is first order in nature with physical quark masses. This indicates the presence of a critical endpoint at the end of the first order chiral phase transition line in the QCD phase diagram. Apart from the confined hadronic phase and deconfined QGP phases, QCD phase diagram has a very rich structure at a low temperature and high baryon chemical potential. In this region of the phase diagram, possibility of various exotic phases has been investigated such as the color superconducting phase[8–10], quarkyonic phase[11], inhomogeneous chiral condensed phase [12–14], etc.

Heavy ion collision experiments e.g. relativistic heavy ion collider (RHIC) and large hadron collider (LHC), give us a unique opportunity to explore the QCD phase diagram. Strongly interacting QGP produced in these experiments at relativistic energies recreates the physical conditions of the microsecond old universe just after the big bang. The strongly interacting plasma produced in these high energy collisions can be characterized as high temperature and

*Electronic address: aman@prl.res.in
†Electronic address: arpan@prl.res.in
‡Electronic address: hm@prl.res.in
§Electronic address: ranjita@iitb.ac.in

low baryon chemical potential QGP. At high densities relative to nuclear saturation density and low temperature exotic phases of QCD can exist, e.g. two flavor color superconducting phase (2SC), color-flavor locked phase (CFL), crystalline color superconductor, etc. Some of these high density QCD phases can also be explored in the upcoming heavy ion collision experiments at moderate center of mass energies at FAIR and NICA. Apart from these terrestrial experiments, the interior astrophysical ultra compact objects like neutron stars provide an ideal condition to indirectly explore these high density QCD phases. Due to very low temperature and high baryon density, in the interior of a neutron star various QCD phases may be realized, e.g. deconfined quark matter [15, 16], meson condensation in hadronic phase[17], two flavor color superconducting phase, color-flavor locked phase [8–10] etc.

Further, compact objects like neutron stars can be strongly magnetized. Observations indicate that the magnetic field strength at the surface of pulsars can be of the order of $10^{12} - 10^{13}$ Gauss [18]. Strongly magnetized neutron stars (magnetars) may have even stronger magnetic fields $\sim 10^{15} - 10^{16}$ Gauss [19–25]. Using virial theorem and comparing the magnetic field energy and gravitational energy, one can estimate the physical upper bound on the strength of the magnetic field for a gravitationally bound star to be of the order 10^{18} Gauss[18]. For self bound objects like quark stars this bound can be even higher [26]. The physical origin of the very strong magnetic field in the magnetars require reconsideration of the common understanding that the magnetic field of a neutron star is originated from the progenitor star [27]. Since quark matter can possibly be present at high densities, inside the neutron stars, presence of quark ferromagnetic phase in high density quark matter has also been suggested as possible explanation of large magnetic field associated with magnetars [28–30]. As a possible solution to this problem, author in Ref.[28] examined the possible existence of spin-polarized deconfined quark matter using one gluon exchange interaction between quarks in Fermi liquid theory within Hartree-Fock approximation. Taking the idea as proposed in the Ref.[28], spin polarization in the quark matter has been well explored in the subsequent literature. In general, a collective spin polarization of charged quarks can give rise to ferromagnetic nature of quark matter at high density, hence the spin of the fermions play the crucial role in determining the possibility of ferromagnetic nature of dense quark matter. It has been shown that in non-relativistic framework there is no possibility of spin polarization in normal nuclear matter[31]. On the contrary, using relativistic Hartree-Fock approximation, possibility of spin polarization at asymptotic high density has been suggested in Ref.[32, 33]. It is important to note that the relativistic framework may be more suitable than the non-relativistic approach to understanding the existence of spin polarization. But in any case to explore spin polarization in quark matter at a high density or baryon chemical potential a relativistic approach is very natural.

In relativistic framework "spin density" can be expressed in two different ways, first by the spatial component of the axial vector (AV) mean field, $\psi^\dagger \Sigma^i \psi \equiv -\bar{\psi}\gamma_5\gamma^i\psi$, constructed out of the fermionic field (quarks)ψ and axial vector combination of Dirac gamma matrices; second by tensor Dirac bilinear (T) $\psi^\dagger\gamma^0\Sigma^i\psi \equiv -\bar{\psi}\sigma^{12}\psi$. Although AV and T type mean fields are different in the massless limit of fermions, it has been shown that they are equivalent in nonrelativistic approximation [29]. Coexistence of the spin polarization and color superconductivity has been studied using the AV interaction for quark matter in NJL model [30]. The interplay between the spin polarization and chiral symmetry breaking at finite density for a single quark flavor using AV mean field has also been studied within NJL model in Ref.[34]. In Ref.[34], it has been shown that for one flavor, spin polarization is possible at finite density and zero temperature provided the ratio of the couplings of the axial vector channel and the pseudo scalar channel satisfies some lower bound. It has been argued in Ref.[34] that due to the interplay between spin polarization and chiral symmetry for a certain value of chemical potential, spin polarization appears due to the large dynamical quark masses generated by spontaneous chiral symmetry breaking. Interestingly it was also shown that spin polarization plays an important role in changing the value of the dynamical mass and at a very high density, both dynamical quark mass and spin polarization vanish in the chiral symmetric phase. Although in Ref.[28] author introduced the idea of quark spin polarization using one gluon exchange interaction, in the NJL model studies, AV mean field has been used. Due to the Fierz transformation, one can get AV channel interaction between quarks from one gluon exchange interaction, but the tensor Dirac bilinear representation of "spin density" operator does not appear in the Fierz transformation of the one gluon exchange interaction. Hence at asymptotically high densities where one gluon exchange interaction in perturbative QCD is applicable, spin polarization cannot be studied using the T channel interaction. But for moderate densities near chiral phase transition density perturbative QCD is not applicable and one can use QCD inspired low energy effective models e.g. NJL model. NJL model is not directly related to perturbative one gluon exchange interaction. In this model AV or T channel interactions are not written keeping in mind the perturbative nature of QCD and some nonperturbative effects can give rise to tensor channel interaction. Hence spin polarization in the tensor channel, which can be different from the AV channel can be studied within the NJL model. In fact, the tensor channel opens up a completely different point of view in looking into the spin polarization problem of quark matter at moderate densities e.g. in two flavour NJL model spin-polarized phase can be shown to be present in the chiral restored phase where the dynamical quark mass is zero [35, 36]. This result is different than the result obtained in Ref.[34], where spin polarization is not present in chiral restored phase. Since the manifestation of the AV and T channel interaction is different, the interplay between the AV and T type spin-polarized phases becomes interesting to study along with the other phases expected to arise in high baryon density region of the QCD phase diagram

[12, 30, 34, 35, 37–41].

In the present work we discuss the interplay between the spin polarization condensate ($\langle\bar{\psi}\Sigma^i\psi\rangle$) and the scalar chiral condensate ($\langle\bar{\psi}\psi\rangle$) in (2+1) flavor NJL model using only tensor(T) type interaction for spin polarization. Most of the earlier works used some simplified approximation to study the interplay between spin polarization and other high density phases, which includes single flavor NJL model [34], SU(2) flavor NJL model [35, 40], SU(3) flavor NJL model [42] with zero current quark mass etc. However, for a more realistic situation one should consider (2+1) flavor NJL model with different current quark mass of strange and non-strange quarks. This apart, the structure of ferromagnetic condensation for (2+1) flavor NJL model is qualitatively different from that of two flavor NJL model as inherently two different kinds of spin polarizations are possible which are associated with the diagonal generators of the SU(3) flavour group. Behaviour of these spin polarization condensates as function of temperature and quark chemical potential (μ) has been discussed extensively. Since the spin polarization condensates are also related to the quark-antiquark scalar condensates, it is evident that the spin polarization condensates affect the constituent mass of the quarks. In this work spin polarization condensates due to the tensor type interaction appear in the chiral symmetry restored phase and the quark masses, specifically strange quark masses, are strongly affected by the spin polarization condensates in the chiral symmetric phase.

This paper is organized in the following manner. We first discuss the formalism of 2+1 flavour NJL model in the presence of tensor type interactions in Sec.(II). In Sec.(II) derivation of the thermodynamic potential is discussed in a mean field approach. Once the thermodynamic potential is derived one can get the gap equations to solve for the condensates. After the formalism important results and the corresponding discussion are given in Sec.(III). Finally in Sec.(IV) we summarize our work.

II. FORMALISM

In order to study the spin polarization due to tensor channel interaction for realistic $(2+1)$ flavor and $SU(3)$ color quarks we start with the following NJL Lagrangian density [39, 43],

$$\mathcal{L} = \bar{\psi}\left(i\partial\!\!\!/ - \hat{m}\right)\psi + \mathcal{L}_{sym} + \mathcal{L}_{det} + \mathcal{L}_{tensor} + \mu\bar{\psi}\gamma^0\psi, \tag{1}$$

where $\psi = (u, d, s)^T$ is the three flavor quark field and the diagonal current quark matrix is $\hat{m} = \mathrm{diag}_f(m_u, m_d, m_s)$. In this work we have assumed that due to isospin symmetry in the non strange quark sector $m_u = m_d$. Strange quark mass m_s is different from the other light quark masses. Difference between the strange and non strange quark masses explicitly breaks the $SU(3)$ flavor symmetry. μ is the quark chemical potential. In literature different chemical potential for the strange and nonstrange quarks have been considered, but the phase diagram has no qualitative difference. In this case we are assuming that the quark chemical potential of the strange and nonstrange quarks are same. Following the representations of different interaction terms as given in Ref.[43], in general one considers,

$$\mathcal{L}_{sym} = g\sum_{a=0}^{a=8}\left[\left(\bar{\psi}\lambda_a\psi\right)^2 + \left(\bar{\psi}i\gamma_5\lambda_a\psi\right)^2\right]. \tag{2}$$

This term has been constructed keeping in mind the $U(3)_L \times U(3)_R$ chiral symmetry for three flavor case and it can be generalized to any number of flavours N_f. The interaction term $\mathcal{L}_{sym}$ represents four point interaction, where $\lambda_0 = \sqrt{2/3}I_f$ and λ_a, $a = 1, ...(N_f^2 - 1)$ are the generators of $SU(N_f)$. In the present case I_f is 3×3 identity matrix and λ_a for $a = 1, ...8$ are the Gell-Mann matrices.

The interaction term $\mathcal{L}_{det}$ in Eqn.(1) is ‘t Hooft determinant interaction term. This term breaks $U(1)$ axial symmetry explicitly and also successfully describes the nonet meson properties[44–46]. It can be expressed as,

$$\mathcal{L}_{det} = -K\mathrm{det}_f[\bar{\psi}(1+\gamma_5)\psi + h.c] \tag{3}$$

In this interaction term determinant is taken in the flavour space. This term represents maximally flavour-mixing $2N_f$ point interaction for N_f quark flavours. For two flavour NJL model this term does not introduce any new dynamics because for two flavour case it gives four Fermi interaction which is already there. But for three or more flavours this term generates new type of interaction, e.g. for three flavour case it gives rise to six point interaction term. The tensor interaction which is responsible for spin polarization is given as [39, 42],

$$\mathcal{L}_{tensor} = \frac{G_T}{2}\sum_{a=3,8}\left(\bar{\psi}\Sigma_z\lambda_a\psi\right)^2, \qquad \Sigma_z = \begin{pmatrix} \sigma_z & 0 \\ 0 & \sigma_z \end{pmatrix}, \tag{4}$$

where σ_z is the third Pauli matrix. Here we have assumed polarization along the z-axis. Note that $\mathcal{L}_{tensor}$ is not invariant under chiral symmetry, rather one requires to add a similar term with γ^5 matrix to make the tensor interaction symmetric under chiral symmetry. Since we are not considering any condensation involving γ^5, we have omitted the term which ensures chiral invariance for the tensor interaction. Thus the total Lagrangian with finite chemical potential becomes,

$$\mathcal{L} = \bar{\psi}\left(i\partial\!\!\!/ - \hat{m}\right)\psi + g\sum_{a=0}^{a=8}\left(\bar{\psi}\lambda_a\psi\right)^2 - K\det{}_f[\bar{\psi}(1+\gamma_5)\psi + h.c] + \sum_{a=3,8}\frac{G_T}{2}\left(\bar{\psi}\Sigma_z\lambda_a\psi\right)^2 + \mu\bar{\psi}\gamma^0\psi. \tag{5}$$

In the mean field approximation expanding the operators around their expectation values and neglecting higher order fluctuations, we obtain,

$$\begin{aligned}
&\left(\bar{u}u\right)^2 \simeq 2\langle\bar{u}u\rangle\bar{u}u - \langle\bar{u}u\rangle^2 = 2\sigma_{ud}\bar{u}u - \sigma_{ud}^2 \\
&\left(\bar{d}d\right)^2 \simeq 2\langle\bar{d}d\rangle\bar{d}d - \langle\bar{d}d\rangle^2 = 2\sigma_{ud}\bar{d}d - \sigma_{ud}^2 \\
&\left(\bar{s}s\right)^2 \simeq 2\langle\bar{s}s\rangle\bar{s}s - \langle\bar{s}s\rangle^2 = 2\sigma_s\bar{s}s - \sigma_s^2 \\
&\left(\bar{\psi}\Sigma_z\lambda_3\psi\right)^2 \simeq 2\langle\bar{\psi}\Sigma_z\lambda_3\psi\rangle\left(\bar{\psi}\Sigma_z\lambda_3\psi\right) - \langle\bar{\psi}\Sigma_z\lambda_3\psi\rangle^2 = 2F_3\left(\bar{\psi}\Sigma_z\lambda_3\psi\right) - F_3^2 \\
&\left(\bar{\psi}\Sigma_z\lambda_8\psi\right)^2 \simeq 2\langle\bar{\psi}\Sigma_z\lambda_8\psi\rangle\left(\bar{\psi}\Sigma_z\lambda_8\psi\right) - \langle\bar{\psi}\Sigma_z\lambda_8\psi\rangle^2 = 2F_8\left(\bar{\psi}\Sigma_z\lambda_8\psi\right) - F_8^2,
\end{aligned} \tag{6}$$

where the chiral condensates or the quark-antiquark condensates are $\langle\bar{u}u\rangle = \langle\bar{d}d\rangle \equiv \sigma_{ud}$, $\langle\bar{s}s\rangle \equiv \sigma_s$ and the spin polarization condensates are $F_3 = \langle\bar{\psi}\Sigma_z\lambda_3\psi\rangle$ and $F_8 = \langle\bar{\psi}\Sigma_z\lambda_8\psi\rangle$. We can write the mean field Lagrangian as,

$$\begin{aligned}
\mathcal{L} = \bar{\psi}\left(i\partial\!\!\!/ - \hat{M} + G_TF_3\Sigma_z\lambda_3 + G_TF_8\Sigma_z\lambda_8 + \mu\gamma^0\right)\psi - 2g\left(\sigma_{ud}^2 + \sigma_{ud}^2 + \sigma_s^2\right) + 4K\sigma_{ud}^2\sigma_s \\
- \frac{G_T}{2}F_3^2 - \frac{G_T}{2}F_8^2,
\end{aligned} \tag{7}$$

where, $\hat{M} \equiv \mathrm{diag}(M_u, M_d, M_s)$, with effective masses,

$$\begin{aligned}
M_u &= m_u - 4g\sigma_{ud} + 2K\sigma_{ud}\sigma_s \\
M_d &= m_d - 4g\sigma_{ud} + 2K\sigma_{ud}\sigma_s \\
M_s &= m_s - 4g\sigma_s + 2K\sigma_{ud}^2.
\end{aligned} \tag{8}$$

For a given system at finite temperature and finite chemical potential most important quantity for the understanding of the thermodynamic behaviour or the phase structure, is the thermodynamic potential. Once the thermodynamic potential for this model is known, thermodynamic quantities can be extracted using Maxwell relations. The thermodynamic potential for the Lagrangian as given in Eqn.(7) in the grand canonical ensemble at a finite temperature and finite chemical potential can be given as:

$$
\begin{aligned}
\Omega(T,\mu,\sigma_{ud},\sigma_s,F_3,F_8) =& -N_c\sum_{f=u,d,s}\int\frac{d^3p}{(2\pi)^3}\Bigg[\left(E_{f+}+E_{f-}\right)+T\ln\left(1+e^{-\beta(E_{f+}-\mu)}\right)\\
&+T\ln\left(1+e^{-\beta(E_{f+}+\mu)}\right)+T\ln\left(1+e^{-\beta(E_{f-}-\mu)}\right)\\
&+T\ln\left(1+e^{-\beta(E_{f-}+\mu)}\right)\Bigg]\\
&+2g(\sigma_{ud}^2+\sigma_{ud}^2+\sigma_s^2)-4K\sigma_{ud}^2\sigma_s+\frac{G_T}{2}F_3^2+\frac{G_T}{2}F_8^2,\\
=& -\frac{6}{4\pi^2}\sum_{f=u,d,s}\int_0^{\Lambda}dp_T\int_0^{\sqrt{\Lambda^2-p_T^2}}p_Tdp_z\Bigg[\left(E_{f+}+E_{f-}\right)+T\ln\left(1+e^{-\beta(E_{f+}-\mu)}\right)\\
&+T\ln\left(1+e^{-\beta(E_{f+}+\mu)}\right)+T\ln\left(1+e^{-\beta(E_{f-}-\mu)}\right)\\
&+T\ln\left(1+e^{-\beta(E_{f-}+\mu)}\right)\Bigg]\\
&+2g(\sigma_{ud}^2+\sigma_{ud}^2+\sigma_s^2)-4K\sigma_{ud}^2\sigma_s+\frac{G_T}{2}F_3^2+\frac{G_T}{2}F_8^2
\end{aligned}
\tag{9}
$$

where $N_c=3$ is the number of colors, transverse momentum $p_T=\sqrt{p_x^2+p_y^2}$ and the single particle energies are,

$$
\begin{aligned}
E_{u+}=&\sqrt{p_z^2+\left(\sqrt{p_T^2+M_u^2}+G_T\left(F_3+\frac{F_8}{\sqrt{3}}\right)\right)^2}\\
E_{u-}=&\sqrt{p_z^2+\left(\sqrt{p_T^2+M_u^2}-G_T\left(F_3+\frac{F_8}{\sqrt{3}}\right)\right)^2}\\
E_{d+}=&\sqrt{p_z^2+\left(\sqrt{p_T^2+M_d^2}+G_T\left(F_3-\frac{F_8}{\sqrt{3}}\right)\right)^2}\\
E_{d-}=&\sqrt{p_z^2+\left(\sqrt{p_T^2+M_d^2}-G_T\left(F_3-\frac{F_8}{\sqrt{3}}\right)\right)^2}\\
E_{s+}=&\sqrt{p_z^2+\left(\sqrt{p_T^2+M_s^2}+G_T\frac{2F_8}{\sqrt{3}}\right)^2}\\
E_{s-}=&\sqrt{p_z^2+\left(\sqrt{p_T^2+M_s^2}-G_T\frac{2F_8}{\sqrt{3}}\right)^2}
\end{aligned}
\tag{10}
$$

Thermodynamic behaviour of the condensates can be found by solving the gap equations, which can be found from the stationary conditions (for details see Appendix),

$$
\frac{\partial\Omega}{\partial\sigma_{ud}}=\frac{\partial\Omega}{\partial\sigma_s}=\frac{\partial\Omega}{\partial F_3}=\frac{\partial\Omega}{\partial F_8}=0 \tag{11}
$$

Gap equations can have several roots, but the solution with the lowest value of thermodynamic potential is taken as the stable solution.

NJL model Lagrangian in (3+1) dimension has operators which have mass dimension more than four, thus it can shown to be a non-renormalizable theory [47]. Thus the divergence coming from the three momentum integral of the vacuum part can not be removed by the renormalization prescriptions. The model predictions inevitably depend on the regularization procedures and parameter dependence in each regularization method has been reported in Ref.[48, 49]. In this work we have considered the most frequently used 3D momentum cutoff regulation scheme to regularize the divergence in Eq.(9) for thermodynamic potential.

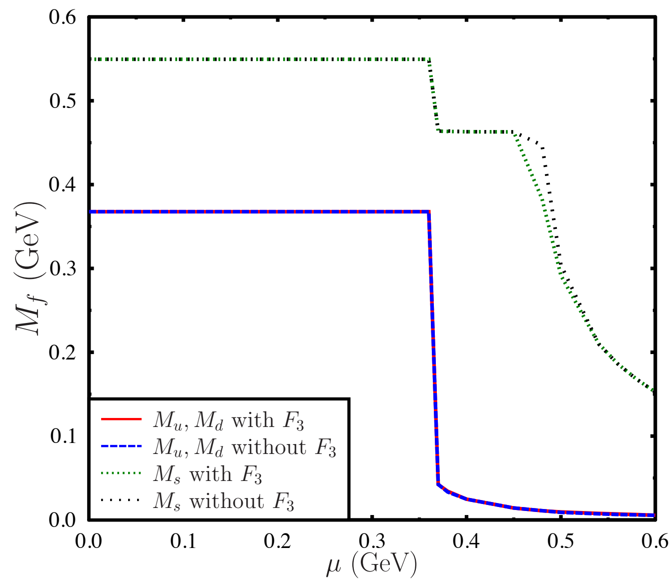

FIG. 1: Constituent quark mass as a function of quark chemical potential at zero temperature in the presence and absence of spin polarization condensation. Red-solid line and green-dotted line represent non strange and strange quark mass in the presence of spin polarization condensate F_3. Blue-dashed line and black-dotted line represents non strange and strange quark constituent mass in the standard 2+1 flavor NJL model in the absence of any spin polarization condensate. Sharp jump in the value of M_u and M_s near $\mu = 0.360$ GeV indicates the first order chiral phase transition. In this case we have considered the tensor interaction coupling to be $G_T = 2g$. Comparing green and the black lines for strange quark it is clear that non zero value of spin condensate affects strange quark mass. However, the non strange quark masses are almost unaffected due to the presence of spin polarization condensate. For $G_T = 2g$ non zero value of F_3 appears only near 0.480 GeV which is away from the chiral phase transition critical chemical potential, hence in this case the chiral phase transition is unaffected by the presence of spin polarization.

In the study of spin polarization in NJL model, the parameter which plays the crucial role is the tensor channel interaction G_T. If one considers only vector current interaction, e.g. one gluon exchange interaction in perturbative QCD processes, then such a tensor interaction can not be generated by Fierz transformation. However, such a tensor interaction can be generated from two gluon exchange diagrams [39]. It is relevant to point out that one can also get tensor channel interaction by Fierz transformation from scalar and pseudo scalar interaction [35],

$$g\left[(\bar{\psi}\psi)^2 + (\bar{\psi}i\gamma_5\lambda_a\psi)^2\right] = \frac{g}{4}\left[(\bar{\psi}\psi)^2 - \frac{1}{2}(\bar{\psi}\gamma^\mu\gamma^\nu\lambda_a\psi)^2 + ...\right], \tag{12}$$

which gives $|g/G_T| = 2$. In the present investigation we can take G_T as a free parameter to study the inter relationship between scalar and tensor condensates. It may also be noted that the parameters g and G_T may be considered independently to derive mesonic properties [50–52]. It has been shown that $SU(2)$ NJL model with both positive and negative tensor couplings can describe the phenomenology of mesons. Indeed $SU(2)$ Lagrangian has been considered with vector, axial vector and tensor interaction in Ref. [52] where, the gap equations are solved in the usual Hartree approximation while mesons are described in the random phase approximation [52]. In this work we have only considered G_T as a free parameter with positive values only i.e. G_T and g are of same sign. In the literature various values have been considered e.g. $G_T = 2g, 1.5g$ [39] as well as $G_T = 4.0g$ [52]. We have also obtained our results taking different values of G_T. Results with some specific parameter sets have been mentioned in the result and discussion section.

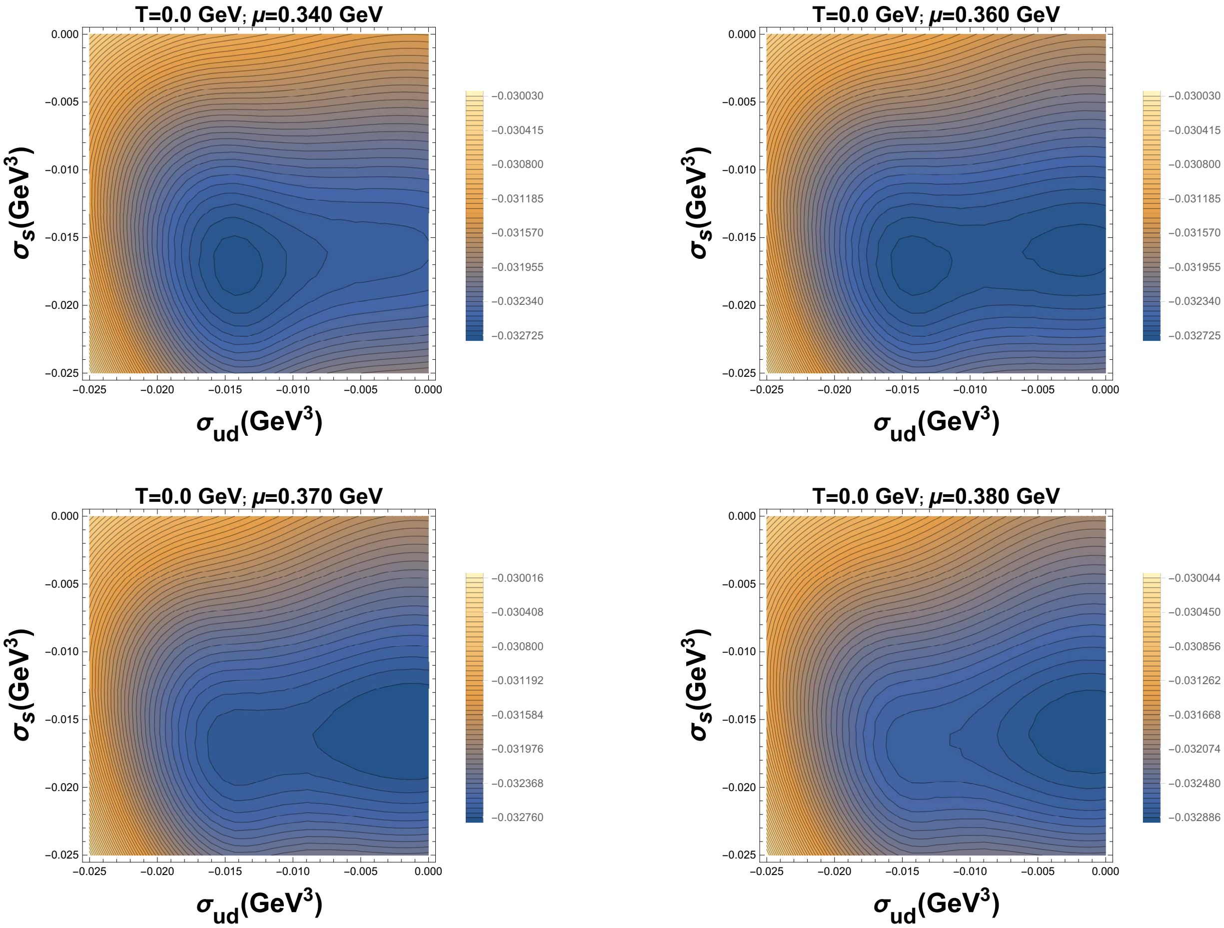

FIG. 2: The figure shows the contour maps of the thermodynamics potential with the set of parameters in table(I) and $G_T = 2g$ at $T = 0.0$ GeV for different values of μ. The darker region in the plots show the lower value of the thermodynamic potential. The horizontal and vertical axes represents the non strange quark condensate σ_{ud} and strange quark condensate σ_s respectively. Existence of almost degenerate vacuum is clear from the figure near $\mu = 0.360$ GeV. Hence the chiral phase transition near $\mu = 0.360$ is a first order phase transition. Spin polarization condensation F_3 has no effect on the chiral phase transition. As we have shown in Fig.(3) non zero value of F_3 occurs near $\mu = 0.480$ GeV at $T = 0.0$GeV for $G_T = 2g$, which is far away from the critical quark chemical potential for the chiral phase transition.

III. RESULTS AND DISCUSSIONS

We begin the discussion with the parameterization of the model. The parameters to be fixed are the three current quark masses (m_u, m_d, m_s), the scalar coupling (g), the determinant coupling K, the tensor coupling(G_T) and the three momentum cut-off Λ to regularize divergent integrals. Except for the tensor coupling G_T, there are several parameter sets available for NJL model [43]. These fits are obtained using low energy hadronic properties such as pion decay constant and masses of pion, kaon and η' [45, 53, 54]. The determinant interaction is important as it breaks $U(1)_A$ symmetry and gives correct η mass. One may note that there is discrepancy in determination of the determinant coupling K. For example in Ref. [45] the value of the coupling differs by as much as 30 percent compared to value used in present work. This discrepancy arises due to difference in treatment of η' mesons with a high mass [43]. In fact, this leads to a nonphysical imaginary part for the corresponding polarization diagram in the η' meson channel. This is unavoidable because NJL is not confining and is unrealistic in this context. Within the above mentioned limitations of the model and the uncertainty in the value of the determinant coupling, we proceed with the present parameter set as given in Table (I) [43].

Let us first note that there are four condensates, σ_{ud}, σ_s, $F_3 \equiv \langle \bar{u}\Sigma_z u\rangle - \langle \bar{d}\Sigma_z d\rangle$ and $F_8 \equiv \frac{1}{\sqrt{3}}\left(\langle \bar{u}\Sigma_z u\rangle + \langle \bar{d}\Sigma_z d\rangle - 2\langle \bar{s}\Sigma_z s\rangle\right)$, to be determined from the solution of the gap Eq.(11). However for simplicity we shall first consider $F_8 = \frac{F_3}{\sqrt{3}}$, so that the spin polarization condensate for d quarks and s quarks are treated at the

Parameter Set	
Parameters and couplings	**Value**
Three momentum cutoff (Λ)	$\Lambda = 602.3 \times 10^{-3}$ (GeV)
u quark mass (m_u)	$m_u = 5.5 \times 10^{-3}$ (GeV)
d quark mass (m_d)	$m_d = 5.5 \times 10^{-3}$ (GeV)
s quark mass (m_s)	$m_s = 140.7 \times 10^{-3}$ (GeV)
Scalar coupling (g)	$g = 1.835/\Lambda^2$
Determinant interaction (K)	$K = 12.36/\Lambda^5$

TABLE I: Parameter set considered in this work for 2+1 NJL model apart from the tensor coupling G_T.

same footing i.e. $\langle \bar{d}\Sigma_z d\rangle \equiv \langle \bar{s}\Sigma_z s\rangle$ [42]. The results in such a scenario is determined below.

A. Results with $F_8 = \frac{F_3}{\sqrt{3}}$

1. *Chiral phase transition and the behavior of quark masses for $G_T = 2g$ at zero temperature*

Let us consider the thermodynamic potential at zero temperature as a function of quark chemical potential (μ) along with the condition $F_8 = F_3/\sqrt{3}$ [42]. For quantitative analysis we consider the tensor coupling $G_T = 2g$. Fig.(1) shows the behavior of the constituent quark masses as a function of quark chemical potential at zero temperature in the presence as well as in the absence of spin polarization condensate F_3.

From Fig.(1) it is clear that the vacuum masses ($T = 0, \mu = 0$), for the non strange quarks are 0.368 GeV and the strange quark mass is 0.549 GeV. The vacuum masses for the constituent quarks remain the same as the case with $G_T = 0$, as the tensor condensates appear only at large chemical potential. This is chiral symmetry broken phase where constituent quark masses are generated dynamically. Close to $\mu = \mu_c = 0.360$ GeV there is sudden drop in the masses of u, d quarks $M_u = M_d$. Because of the flavour mixing due to the determinant interaction the strange quark mass also changes at $\mu = \mu_c$. This sudden change in the constituent mass indicates a first-order phase transitions. It is also expected that chiral phase transition should occur in the 2+1 flavor NJL model near $\mu = 0.360$ GeV at zero temperature in the absence of spin polarization. Using the gap equations it can be shown that at zero temperature and zero chemical potential $F_3 = 0$ is a solution. It turns out that at zero temperature and zero chemical potential $F_3 = 0$ is also a stable solution, hence F_3 does not affect the constituent quark masses at low chemical potential at zero temperature. As the chemical potential is increased beyond the chiral restoration for the light quarks, it is observed that the spin polarized condensate develops for a range of chemical potential. In particular, as shown in Fig. (3) for zero temperature, a non zero F_3 starts to develop at $\mu \simeq 0.480$ GeV and increases slightly with μ, becoming a maximum around $\mu \simeq 0.510$ GeV, beyond which it decreases and eventually vanishes at $\mu \simeq 0.600$ GeV. Therefore we observe here in Fig.(1) that the chiral transition for the light quarks is not affected by the spin polarization condensates as the latter exist at μ larger than μ_c for $G_T = 2g$. It is important to mention that both $\bar{\psi}\psi$ and $\bar{\psi}\gamma^\mu\gamma^\nu\psi$ break the chiral symmetry, but their thermodynamic behavior is quite opposite. At zero temperature and zero chemical potential non zero value of scalar condensation is thermodynamically stable, while the tensor condensate vanishes. However at high chemical potential when the tensor condensate takes non zero value the chiral condensate vanishes but for small current quark mass. The non invariance of the tensor interaction under chiral symmetry can be manifested in the change of quark masses even if the scalar condensate vanishes for the light quarks.

We can also understand the behavior of the constituent quark masses $M_u = M_d$ and M_s in the presence and absence of the spin polarization condensation by looking into the behaviour of thermodynamic potential as a function of quark-antiquark condensates σ_{ud}, σ_s and spin polarization condensate F_3 for different values of temperature (T) and chemical potential μ. Contour plots of thermodynamic potential in the $\sigma_{ud} - \sigma_s$ plane for different value of chemical potential (μ) at zero temperature have been shown in Fig.(2) with the set of parameters given in table(I) and $G_T = 2g$. The darker regions in the plots show the lower value of the thermodynamic potential. The horizontal and vertical axes represent the nonstrange quark-antiquark condensate σ_{ud} and strange quark-antiquark condensate σ_s. As may be observed in Fig.(2), for zero temperature and $\mu < \mu_c \sim 0.360$ GeV minimization of the thermodynamic potential gives us a unique nonzero value of the quark-antiquark condensate. This nonzero value of both σ_{ud} and σ_s indicates chiral symmetry broken phase at zero temperature and $\mu \leq 0.360$ GeV. At $\mu = 0.360$ GeV one can see the existence of almost degenerate vacua in the thermodynamic potential one for $\sigma_{ud} \sim -0.015$ GeV^3 and the other at $\sigma_{ud} \sim 0.0$ GeV^3. As the chemical potential is increased this degeneracy is lifted and the vacuum with σ_{ud}

is close to zero has the minimum value for the thermodynamic potential. At $\mu = 0.4$ GeV the value of σ_{ud} as well as M_u is very small and is close to the current quark mass value. This indicates that at chemical potential larger than $\mu_c = 0.360$GeV chiral symmetry is restored. This chiral symmetry restoration is partial in nature in the sense that while the scalar condensate $\sigma_{ud} \simeq 0$, but for the current quark masses $(m_u, m_d \neq 0)$, the strange condensate σ_s is rather large as can be seen in Fig.(1) and Fig.(2) . As μ is further increased beyond μ_c, σ_s also approaches its (approximate) chiral limit continuously. Degeneracy in the thermodynamic potential and a sharp jump in the order parameter (σ_{ud}) indicates first order phase transition. Hence the chiral transition at zero temperature is of first order in nature. This first order nature of the chiral phase transition can also be seen at finite temperature, however, at relatively larger temperature chiral phase transition does not remain as a first order phase transition. In fact, the end of the first order transition to the crossover defines the critical end point. At higher temperatures, beyond the critical temperature quark-antiquark condensate changes smoothly across the critical chemical potential.

When we take $G_T = 2g$, the value of F_3 is not large enough near $\mu = 0.360$ GeV and the chiral phase transition is unaffected by the spin polarization. Since quark-antiquark condensates σ_{ud} and σ_s are intimately connected with the F_3, non zero value of F_3 can change the quark dynamical mass (see Fig.(1)). Strange quark mass is more affected by the presence of the spin polarization condensate (F_3), because dynamical mass of u quark becomes very small just after the chiral phase transition, however, strange quark has a substantial mass even after the chiral phase transition. Similar to the result at zero temperature, for $G_T = 2g$ chiral phase transition is almost unaffected in the presence of spin polarization at finite temperature also.

2. Behavior of F_3 for $G_T = 2g$

Next let us focus our attention to the thermodynamic behavior of F_3. Fig.(3) shows the contour plots of the thermodynamic potential in $\sigma_s - F_3$ plane at zero temperature with increasing value of the chemical potential (μ) for $G_T = 2g$. As before the darkest regions in the contour plots show the global minimum of the thermodynamic potential and the corresponding values of σ_s and F_3 are correct condensation value. It is clear from the Fig.(3) that spin polarization is possible within the small range of chemical potential $\mu \simeq 0.480 - 0.570$ GeV at zero temperature. From this figure it is clear that with increase in chemical potential σ_s decreases. In this work, we have kept the value of $\mu \leq \Lambda$, because Λ is the cut-off of the theory. When the chemical potential is close to 0.6 GeV both σ_s and F_3 becomes zero. For large chemical potentials($\mu > 570$ MeV), spin polarization condensate completely melts along with the other condensates. Presence of spin polarization condensation can affect the QCD phase diagram in many different ways. As we have already mentioned that the spin polarization condensate coming from the tensor interaction also breaks the chiral symmetry, an obvious effect of a large value of spin polarization condensate should be seen in the chiral phase transition. We have also observed that F_3 decreases with increasing temperature and vanishes at few tens of MeV. Therefore such condensates do not affect the critical end point.

3. Quark masses and ferromagnetic condensate for larger tensor coupling

The left plot and the right plot in Fig.(4) are for quark masses and ferromagnetic condensate respectively, for the tensor coupling $G_T = 2.5g$ and $G_T = 2.8g$. One may note that for larger tensor coupling the u and d quark masses are not affected but the strange quark mass is significantly affected. Ferromagnetic condensate is stronger for larger value of tensor coupling and survives for a longer range of quark chemical potential. It is important to mention that for tensor couplings greater than $G_T = 3g$ the chiral transition itself is affected. However the requirement of baryon matter stability places a upper bound on the value of tensor coupling.

4. Finite temperature effect on the spin polarization condensate F_3 for $G_T = 2g$

After demonstrating the behavior of the spin polarization condensate as a function of chemical potential at zero temperature for different values of the tensor coupling, let us look into the temperature behavior of F_3 for a fixed value of $G_T = 2g$. Temperature behavior of spin polarization condensate as well as σ_s is shown in Fig.(5). Fig.(5) shows the contour plots of thermodynamic potential in the plane of $\sigma_s - F_3$ for different values of temperature and chemical potential. Each row shows the behavior of thermodynamic potential as a function of increasing chemical potential for a fixed temperature. On the other hand, each column shows the behavior of the thermodynamic potential as a function of temperature for a fixed value of chemical potential. From the first two row in Fig.(5), for temperature $T = 0.02$ GeV and 0.04 GeV, it is clear that as the chemical potential increases non zero value of spin polarization develops. It attains a maximum value at an intermediate value of the chemical potential and as the chemical potential becomes very high F_3 becomes zero. However, each column shows that with increasing temperature the formation of the spin polarization becomes difficult and the maximum value of F_3 also decreases with temperature. The third row in Fig.(5) shows that when the temperature is $T = 0.06$ GeV, value of the spin polarization condensate F_3 is almost zero. Hence one can conclude that as the temperature increases the range of chemical potential within which spin polarization can exist decreases. Further there exists a temperature beyond which spin polarization cannot occur irrespective of the value of chemical potential for a given value of G_T. Also note that with increase in temperature and chemical potential strange quark condensate (σ_s) decreases.

5. *Threshold coupling for existence of* F_3

The existence of spin polarization inevitably depends on the value of G_T. G_T determines the strength of the spin polarization condensation. The dependence of F_3 on the tensor coupling has been shown in the Fig(6). Fig.(6) shows the thermodynamic potential in $\sigma_s - F_3$ plane as a function of chemical potential for three different values of tensor couplings $G_T = 2g, 1.8g$ and $1.5g$ at zero temperature. Along each row in Fig.(6) the contours of thermodynamic potential have been shown for different values of the chemical potential but keeping G_T fixed. On the other hand in each column of Fig.(6) contours of thermodynamic potential have been shown for various values the tensor coupling constant G_T for a given chemical potential. Value of the spin polarization condensate decreases with decreasing value of G_T. When $G_T = 2g$, F_3 has a substantial non zero value at zero temperature and $\mu = 0.510$ GeV, however for $G_T = 1.8g$ this value starts to decrease and for $G_T = 1.5g$ spin polarization condensate F_3 almost vanishes. This result for zero temperature can be easily extended to a non zero temperature. For finite temperature one requires a larger value of G_T, for the spin polarization to exist. As G_T increases, the threshold μ above which F_3 starts becoming nonvanishing decreases, and the critical μ above which F_3 vanishes increases. Both these behavior lead to a larger range of μ that supports a non vanishing F_3 as G_T increases. Further the magnitude of F_3 increases with G_T.

B. Results for independent F_3, F_8

We have already discussed the variation of F_3 and F_8 with chemical potential where we have considered $F_8 = F_3/\sqrt{3}$ in the thermodynamic potential. However for more general situation we have to consider F_3 and F_8 simultaneously. In Fig.(7)(a), Fig.(7)(b), Fig.(7)(c) we have shown the variation of F_3 and F_8 with chemical potential at zero temperature for $G_T = 2g, 2.5g, 2.8g$ respectively. It is clear from the Fig.(7) that non zero F_3 appears at relatively smaller μ than F_8. Since F_8 is associated with strange quark-antiquark condensate it survives even at larger chemical potential relative to the F_3 condensate. It is also important to notice that with larger tensor coupling spin condensates appear at relatively smaller quark chemical potential.

C. Magnetic field due to spin polarization

The spin polarization condensate implies a alignment of spin of quarks. This will lead to a magnetic field due to quark magnetic moment. We estimate the strength of the effective magnetic field (B_{eff}) due to spin polarization condensate as [35]:

$$\bar{\mu}_q B_{eff} = G_T F, \quad \bar{\mu}_q = \frac{\mu_u + \mu_d}{2}, \quad \bar{\mu}_u = \frac{(\frac{2}{3}e)}{2m_q}, \quad \bar{\mu}_d = \frac{(-\frac{1}{3}e)}{2m_q} \tag{13}$$

Here F denotes the spin polarization condensate and $\bar{\mu}_q$ is the average magnetic moment of the light quarks. For an estimation of B_{eff} we take $F \sim 0.018$ GeV^3 (at quark chemical potential ~ 510 MeV) and $G_T = 2g$. Using these value we get $eB_{eff} \sim \mathrm{m}_\pi^2$ or 10^{18} Gauss. The value of the magnetic field on the surface of the magnetars is of the order of 10^{15} Gauss, but in the center the strength of the magnetic field can be higher. It is interesting to note that even this crude estimation of the magnetic field due to the spin polarized phase of the deconfined quark matter leads to a correct order of magnitude estimation of the magnetic field in the core of the magnetars.

IV. CONCLUSIONS

In this work, we have considered the 2+1 flavor NJL model in the presence of tensor interaction with non zero current quark masses. The original idea of the presence of spin polarization in quark liquid was motivated considering one gluon exchange interactions in perturbative QCD processes [28]. Ferromagnetic quark matter can arise due to both axial vector and tensor type interaction. Although the axial vector type interaction can be generated from the one gluon exchange QCD interaction by Fierz transformation, the tensor type interactions cannot be generated using Fierz transformation. Thus at very high densities where perturbative QCD processes are relevant, tensor type of interaction will not be suitable to study spin polarization in quark matter. More importantly at moderate densities close to the chiral phase transition one expects nonperturbative effects to play an important role. In the present investigation within the ambit of NJL model applied to moderate densities, we have considered only the tensor type four point interaction. We might note here that the coupling constant of the tensor interaction is related to the scalar and pseudo scalar channel. However in general, this tensor coupling constant can be independent. We take the coupling constant of the tensor interaction G_T as a parameter of the model. We have taken various values of the tensor couplings G_T, e.g. $G_T = 2.0g$ and lower as well as relatively larger values of G_T, e.g. $G_T = 2.5g, 2.8g$ etc.

For 2+1 flavor NJL model, tensor type interaction at the mean field level leads to two types of spin polarization condensates, $F_3 = \langle\bar{\psi}\Sigma_z\lambda_3\psi\rangle$ and $F_8 = \langle\bar{\psi}\Sigma_z\lambda_8\psi\rangle$. Since we have various condensates in 2+1 flavor NJL model in the presence of tensor interaction we take a rather simplified approximation, where F_3 and F_8 are not independent rather $F_8 = F_3/\sqrt{3}$. One may note that in general F_3 and F_8 are independent due to the fact that F_8 is associated with the strange quark spin polarization condensate, on the other hand F_3 contains only u, d quark spin polarization condensates. Therefore we have also considered the case where F_3 and F_8 are treated independently. Generically spin polarization for moderate tensor coupling (e.g. $G_T = 2g$) does not appear at zero temperature and zero chemical potential, rather it appears at high μ in the chiral restored phase. At large chemical potential and small temperature the generic feature of such spin polarized condensate lies in affecting the strange quark mass rather than the non-strange quark masses for moderate tensor coupling. Such spin polarized condensate vanishes for temperatures of the order of few tens of MeV and thus can be relevant for neutron stars and proto neutron stars. We also find that there is a threshold tensor coupling, below which the spin polarization condensates do not develop.

Unlike superconducting diquark condensate, the spin polarization condensate is not a monotonic function of chemical potential and as the chemical potential is increased the magnitude becomes a maximum beyond which it vanishes when μ is increased further. The range of chemical potential for which such condensate exists as well as the magnitude of the condensate, increases with the strength of the tensor coupling. We estimate the magnitude of the magnetic field corresponding to the ferromagnetic condensate in high density quark matter to be of the order of $\sim m_\pi^2 \sim 10^{18}$ Gauss. It is important to mention that although spin polarization condensate was thought as a source of magnetic field in magnetars, magnetic field can also be present in the neutron stars originated from the progenitor star. External magnetic field can affect the formation of spin condensates. In this context it has been shown recently that one can have non vanishing spin polarization condensate for quark matter in the presence of magnetic field [55].

Acknowledgement

We would like to thank Robert Pisarski for important comments on this work. RKM would like to thank Theoretical Physics Division of Physical Research Laboratory, Ahmedabad for support and local hospitality for her visit, during which this problem was initiated. Also RKM would like to thank Basanta K. Nandi and Sadhana Dash for constant support and encouragement.

Appendix

The gap equations for four independent condensates, two chiral condensates σ_{ud}, σ_s and two spin polarization condensates F_3, F_8 are as follow,

$$\frac{\partial\Omega}{\partial\sigma_{ud}} = -N_c\int\frac{d^3p}{(2\pi)^3}\Bigg[\frac{M_u}{E_{u_+}}\left(1+\frac{G_T(F_3+F_8/\sqrt{3})}{\sqrt{p_T^2+M_u^2}}\right)(-4g+2K\sigma_s)\left\{1-\frac{1}{1+e^{\beta(E_{u_+}-\mu)}}-\frac{1}{1+e^{\beta(E_{u_+}+\mu)}}\right\}$$
$$+\frac{M_u}{E_{u_-}}\left(1-\frac{G_T(F_3+F_8/\sqrt{3})}{\sqrt{p_T^2+M_u^2}}\right)(-4g+2K\sigma_s)\left\{1-\frac{1}{1+e^{\beta(E_{u_-}-\mu)}}-\frac{1}{1+e^{\beta(E_{u_-}+\mu)}}\right\}$$
$$+\frac{M_d}{E_{d_+}}\left(1+\frac{G_T(F_3-F_8/\sqrt{3})}{\sqrt{p_T^2+M_d^2}}\right)(-4g+2K\sigma_s)\left\{1-\frac{1}{1+e^{\beta(E_{d_+}-\mu)}}-\frac{1}{1+e^{\beta(E_{d_+}+\mu)}}\right\}$$
$$+\frac{M_d}{E_{d_-}}\left(1-\frac{G_T(F_3-F_8/\sqrt{3})}{\sqrt{p_T^2+M_d^2}}\right)(-4g+2K\sigma_s)\left\{1-\frac{1}{1+e^{\beta(E_{d_-}-\mu)}}-\frac{1}{1+e^{\beta(E_{d_-}+\mu)}}\right\}$$
$$+\frac{M_s}{E_{s_+}}\left(1+\frac{2G_TF_8/\sqrt{3}}{\sqrt{p_T^2+M_s^2}}\right)(4K\sigma_{ud})\left\{1-\frac{1}{1+e^{\beta(E_{s_+}-\mu)}}-\frac{1}{1+e^{\beta(E_{s_+}+\mu)}}\right\}$$
$$+\frac{M_s}{E_{s_-}}\left(1-\frac{2G_TF_8/\sqrt{3}}{\sqrt{p_T^2+M_s^2}}\right)(4K\sigma_{ud})\left\{1-\frac{1}{1+e^{\beta(E_{s_-}-\mu)}}-\frac{1}{1+e^{\beta(E_{s_-}+\mu)}}\right\}\Bigg]+8g\sigma_{ud}-8K\sigma_{ud}\sigma_s=0 \tag{14}$$

$$\frac{\partial\Omega}{\partial\sigma_s} = -N_c\int\frac{d^3p}{(2\pi)^3}\Bigg[\frac{M_u}{E_{u_+}}\left(1+\frac{G_T(F_3+F_8/\sqrt{3})}{\sqrt{p_T^2+M_u^2}}\right)(2K\sigma_{ud})\left\{1-\frac{1}{1+e^{\beta(E_{u_+}-\mu)}}-\frac{1}{1+e^{\beta(E_{u_+}+\mu)}}\right\}$$
$$+\frac{M_u}{E_{u_-}}\left(1-\frac{G_T(F_3+F_8/\sqrt{3})}{\sqrt{p_T^2+M_u^2}}\right)(2K\sigma_{ud})\left\{1-\frac{1}{1+e^{\beta(E_{u_-}-\mu)}}-\frac{1}{1+e^{\beta(E_{u_-}+\mu)}}\right\}$$
$$+\frac{M_d}{E_{d_+}}\left(1+\frac{G_T(F_3-F_8/\sqrt{3})}{\sqrt{p_T^2+M_d^2}}\right)(2K\sigma_{ud})\left\{1-\frac{1}{1+e^{\beta(E_{d_+}-\mu)}}-\frac{1}{1+e^{\beta(E_{d_+}+\mu)}}\right\}$$
$$+\frac{M_d}{E_{d_-}}\left(1-\frac{G_T(F_3-F_8/\sqrt{3})}{\sqrt{p_T^2+M_d^2}}\right)(2K\sigma_{ud})\left\{1-\frac{1}{1+e^{\beta(E_{d_-}-\mu)}}-\frac{1}{1+e^{\beta(E_{d_-}+\mu)}}\right\}$$
$$+\frac{M_s}{E_{s_+}}\left(1+\frac{2G_TF_8/\sqrt{3}}{\sqrt{p_T^2+M_s^2}}\right)(-4g)\left\{1-\frac{1}{1+e^{\beta(E_{s_+}-\mu)}}-\frac{1}{1+e^{\beta(E_{s_+}+\mu)}}\right\}$$
$$+\frac{M_s}{E_{s_-}}\left(1-\frac{2G_TF_8/\sqrt{3}}{\sqrt{p_T^2+M_s^2}}\right)(-4g)\left\{1-\frac{1}{1+e^{\beta(E_{s_-}-\mu)}}-\frac{1}{1+e^{\beta(E_{s_-}+\mu)}}\right\}\Bigg]+4g\sigma_s-4K\sigma_{ud}^2=0 \tag{15}$$

$$\frac{\partial\Omega}{\partial F_3} = -N_c\int\frac{d^3p}{(2\pi)^3}\Bigg[G_T\frac{\sqrt{p_T^2+M_u^2}+G_T(F_3+F_8/\sqrt{3})}{E_{u_+}}\left\{1-\frac{1}{1+e^{\beta(E_{u_+}-\mu)}}-\frac{1}{1+e^{\beta(E_{u_+}+\mu)}}\right\}$$
$$-G_T\frac{\sqrt{p_T^2+M_u^2}-G_T(F_3+F_8/\sqrt{3})}{E_{u_-}}\left\{1-\frac{1}{1+e^{\beta(E_{u_-}-\mu)}}-\frac{1}{1+e^{\beta(E_{u_-}+\mu)}}\right\}$$
$$+G_T\frac{\sqrt{p_T^2+M_d^2}+G_T(F_3-F_8/\sqrt{3})}{E_{d_+}}\left\{1-\frac{1}{1+e^{\beta(E_{d_+}-\mu)}}-\frac{1}{1+e^{\beta(E_{d_+}+\mu)}}\right\}$$
$$-G_T\frac{\sqrt{p_T^2+M_d^2}-G_T(F_3-F_8/\sqrt{3})}{E_{d_-}}\left\{1-\frac{1}{1+e^{\beta(E_{d_-}-\mu)}}-\frac{1}{1+e^{\beta(E_{d_-}+\mu)}}\right\}\Bigg]$$
$$+G_TF_3=0 \tag{16}$$

$$
\begin{aligned}
\frac{\partial\Omega}{\partial F_8} = -N_c \int \frac{d^3p}{(2\pi)^3} \Bigg[& \frac{G_T}{\sqrt{3}} \frac{\sqrt{p^2+M_u^2}+G_T(F_3+F_8/\sqrt{3})}{E_{u_+}} \left\{ 1 - \frac{1}{1+e^{\beta(E_{u_+}-\mu)}} - \frac{1}{1+e^{\beta(E_{u_+}+\mu)}} \right\} \\
& - \frac{G_T}{\sqrt{3}} \frac{\sqrt{p^2+M_u^2}-G_T(F_3+F_8/\sqrt{3})}{E_{u_-}} \left\{ 1 - \frac{1}{1+e^{\beta(E_{u_-}-\mu)}} - \frac{1}{1+e^{\beta(E_{u_-}+\mu)}} \right\} \\
& - \frac{G_T}{\sqrt{3}} \frac{\sqrt{p^2+M_d^2}+G_T(F_3-F_8/\sqrt{3})}{E_{d_+}} \left\{ 1 - \frac{1}{1+e^{\beta(E_{d_+}-\mu)}} - \frac{1}{1+e^{\beta(E_{d_+}+\mu)}} \right\} \\
& + \frac{G_T}{\sqrt{3}} \frac{\sqrt{p^2+M_d^2}-G_T(F_3-F_8/\sqrt{3})}{E_{d_-}} \left\{ 1 - \frac{1}{1+e^{\beta(E_{d_-}-\mu)}} - \frac{1}{1+e^{\beta(E_{d_-}+\mu)}} \right\} \\
& + 2\frac{G_T}{\sqrt{3}} \frac{\sqrt{p^2+M_s^2}+2G_TF_8/\sqrt{3}}{E_{s_+}} \left\{ 1 - \frac{1}{1+e^{\beta(E_{s_+}-\mu)}} - \frac{1}{1+e^{\beta(E_{s_+}+\mu)}} \right\} \\
& - 2\frac{G_T}{\sqrt{3}} \frac{\sqrt{p^2+M_s^2}-2G_TF_8/\sqrt{3}}{E_{s_-}} \left\{ 1 - \frac{1}{1+e^{\beta(E_{s_-}-\mu)}} - \frac{1}{1+e^{\beta(E_{s_-}+\mu)}} \right\} \Bigg] + G_T F_8 = 0 \qquad (17)
\end{aligned}
$$

[1] D.H. Rischke, Prog. Part. Nucl. Phys. **52**, 197 (2004).
[2] K. Rajagopal and F. Wilczek, arXiv:hep-ph/0011333, in *At the frontier of particle physics*, Vol.**3**, M. Shifman(Ed.) a, World Scientific, 2061-2151.
[3] F. Karsch, arXiv:hep-lat/0106019, Lect. Notes. Phys. 583:209, (2002).
[4] E. Laerman and O. Philipsen, Ann. Rev. Nucl. Part. Sci. **53**, 163, (2003).
[5] M. Cheng et al, Phys. Rev. D **77**, 014511, (2008).
[6] Z. Foder, S. Katz, JHEP **203**, 014 (2002); Ph. de Forcrand and O. Phillipsen, Nucl. Phys B **642**, 290 (2002); M.P. Lombardo and M. DElia, Phys. Rev. D **67**, 014505 (2003); C. Alton et. al., Phys. Rev. D **66**, 074507 (2002);ibid Phys. Rev. D **68**, 014507 (2002).
[7] H.T.Ding, Nucl. Phys. **A 931**, 52, (2014).
[8] M. G. Alford, A. Schmitt, K. Rajagopal and T. Schafer, Rev. Mod. Phys. **80**, 1455 (2008) and references therein.
[9] M. Alford, K. Rajagopal and F. Wilczek, Nucl. Phys. B **537**, 443 (1999).
[10] K. Iida and G. Byam, Phys. Rev. D **63**, 074018 (2001).
[11] L. McLerran and R. D. Pisarski, Nucl. Phys. A **796**, 83 (2007).
[12] E. Nakano and T. Tatsumi, Phys. Rev. D **71**,114006 (2005).
[13] D. Nickel, Phys. Rev. Lett. **103**, 072301 (2009).
[14] M. Buballa and S. Carignano, Prog. Part. Nucl. Phys. **81**, 39 (2015) and references therein.
[15] G. Baym, T. Hatsuda, T. Kojo, P. D. Powell, Y. Song, T. Takatsuka, Rep. Prog. Phys. 81, 056902 (2018).
[16] N. Itoh, Progress of Theoretical Physics 44, Issue 1, July 1970, 291.
[17] T. Kunihiro, T. Muto, T. Takatsuka, R. Tamagaki and T. Tatsumi, Prog. Theor. Phys. Suppl. **112**, 1(1993).
[18] D. Bandyopadhyaya, S. Chakrabarty, and S. Pal, Phys.Rev. Lett. 79, 2176 (1997); S. Chakrabarty and S. Mandal, Phys. Rev. C 75 , 015805 (2007).
[19] R. C. Duncan and C. Thompson, Astrophys. J.392,L9 (1992).
[20] C. Thompson and R. C. Duncan, Astrophys. J. 408, 194 (1993).
[21] C. Thompson and R. C. Duncan, Mon. Not. R. Astron. Soc. 275, 255 (1995).
[22] C. Thompson and R. C. Duncan, Astrophys. J. 473, 322 (1996).
[23] C. Y. Cardall, M. Prakash, and J. M. Lattimer, Astrophys.J. 554, 322 (2001).
[24] A. E. Broderick, M. Prakash, and J. M. Lattimer, Phys. Lett. B 531, 167 (2002).
[25] D. Lai and S. L. Shapiro, Astrophys. J.383, 745 (1991).
[26] E. J. Ferrer, V. Incera, and J. P. Keith, I. Portillo, and P. Springsteen, Phys. Rev. C 82, 065802 (2010).
[27] G. Chanmugam, Annu. Rev. Astron. Astrophys. **30**, 143 (1992).
[28] T. Tatsumi, Phys. Lett. B **489**, 280 (2000).
[29] T. Maruyama and T. Tatsumi, Nucl. Phys. A. **693**, 710 (2001).
[30] E. Nakano, T. Maruyama and T. Tatsumi, Phys. Rev. D **68**, 105001 (2003).
[31] V.R. Pandharipande, V.K. Garde, J.K. Srivastava, Phys. Lett. B **38** 485 (1972).
[32] R. Niembro, S. Marcos, M.L. Quelle, J. Navarro, Phys. Lett. B 249 (1990) 373.
[33] S. Marcos, R. Niembro, M.L. Quelle, Phys. Lett. B 271 (1991) 277.
[34] S. Maedan, Prog. Theor. Phys.**118**, no. 4, 729 (2007).
[35] Y. Tsue, J. de. Providencia, C. Providencia and M. Yamamura, Prog. Theor. Phys. **128**, 507 (2012).
[36] T. Maruyama, E. Nakano and T. Tatsumi, *"Horizons inWorld Physics (Nova Science, NY, 2011)*,Vol.276, Chap.7
[37] Y. Tsue, J. de. Providencia, C. Providencia and M. Yamamura, H. Bohr, PTEP **2013**, 103 D01 (2013).

[38] Y. Tsue, J. de. Providencia, C. Providencia and M. Yamamura, H. Bohr, PTEP **2013**, 103 D02 (2015).
[39] H. Matsuoka, Y. Tsue, J. da Providencia, C. Providencia and M. Yamamura, Phys. Rev. D **95**, 054025 (2017).
[40] H. Matsuoka, Y. Tsue, J. da Providencia, C. Providencia, M. Yamamura and H. Bohr, PTEP **2016**, 053 D02 (2016).
[41] M. Morimoto, Y. Tsue, J. da Providencia, C. Providencia and Y. Yamamura, IJMP E, Vol.27, No.4, 1850028 (2018).
[42] H. Bohr, P. K. Panda, C. Providencia, J. D. Providencia, Int. J. Mod. Phys. E 22, No.4, 1350019 (2013).
[43] M. Buballa, Phys.Rept. **407**, 205-376 (2005).
[44] U. Vogl, W. Weise, Prog. Part. Nucl. Phys. 27 (1991) 195.
[45] T. Hatsuda, T. Kunihiro, Phys. Rep. 247 (1994) 221.
[46] P. Rehberg, S.P. Klevansky, J. Hufner, Phys. Rev. C 53 (1996) 410.
[47] S. P. Klevansky, Rev. Mod. Phys. 64, 649 (1992).
[48] H. Kohyama, D. Kimura, T. Inagaki, Nucl. Phys. **B906** 524548 (2016).
[49] H. Kohyama, D. Kimura, T. Inagaki, Nucl.Phys. **B896** 682-715 (2015).
[50] M. Jaminon, E. Ruiz Arriola, Phys. Lett. **B443** 33 (1998).
[51] M. Jaminon, M. C. Ruvio and C. A. de Sousa, Int. J. Mod. Phys. A **17**, 4903 (2002).
[52] O. A. Battistel, T. H. Pimenta and G. Dallabona, Phys. Rev. D **94**, 085011 (2016).
[53] M. Lutz, S. Klimt and W. Weise, Nucl Phys. **A 542**, 521, 1992.
[54] P. Rehberg, S.P. Klevansky and J. Huefner, Phys. Rev. **C 53**, 410 (1996).
[55] S. Mao, D. H. Rischke, Phys.Lett. B792 (2019) 149-155.

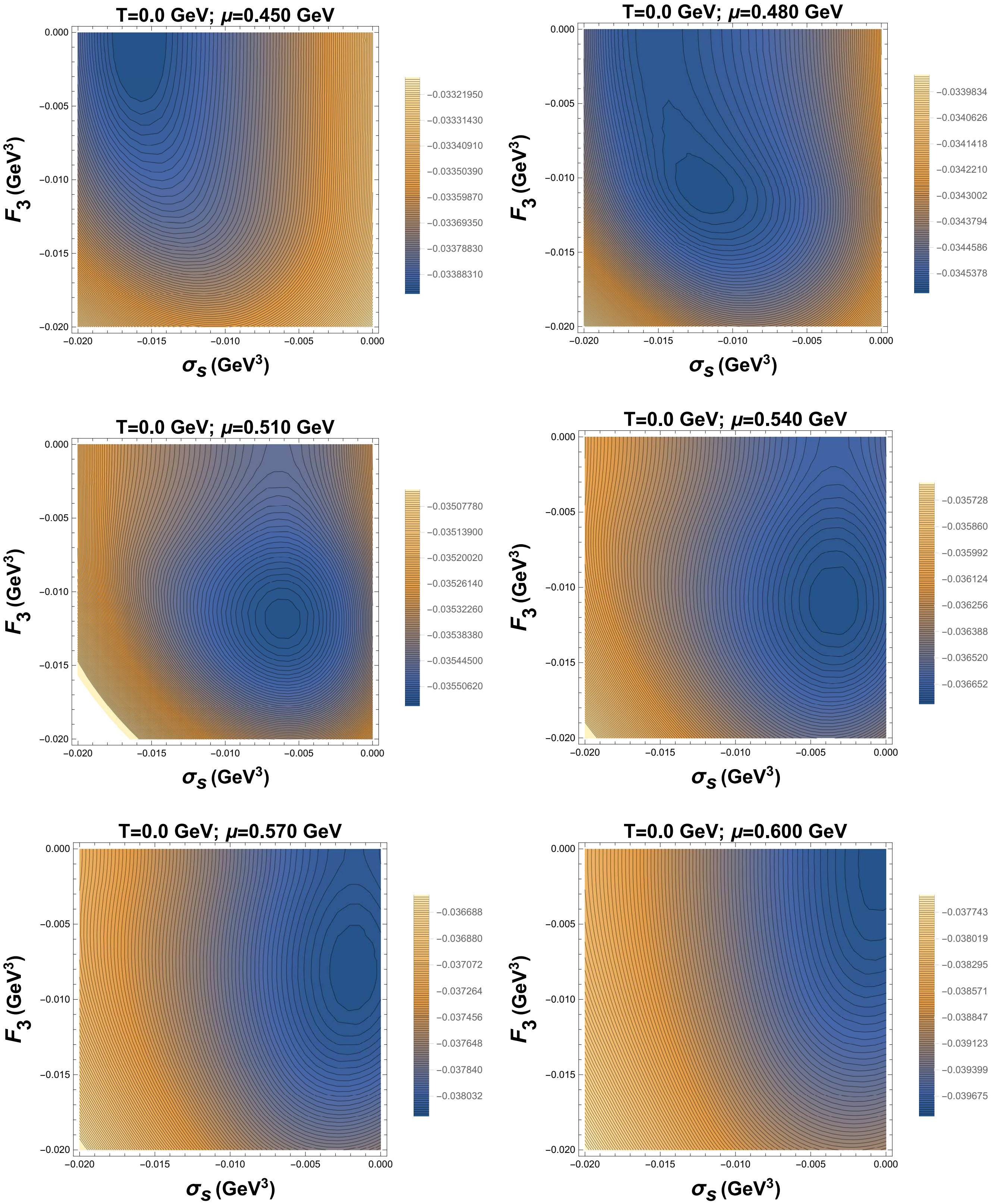

FIG. 3: This figure shows the contour plots of the thermodynamic potential in $\sigma_s - F_3$ plane at zero temperature with different values of quark chemical potentials (μ) for the case of $G_T = 2g$ and $F_8 = F_3/\sqrt{3}$. It is clear from the plots that non zero spin polarization appears at $\mu = 0.480$ GeV, reaches its maximum value near $\mu = 0.510$ GeV and it completely melts near $\mu = 0.600$ GeV.

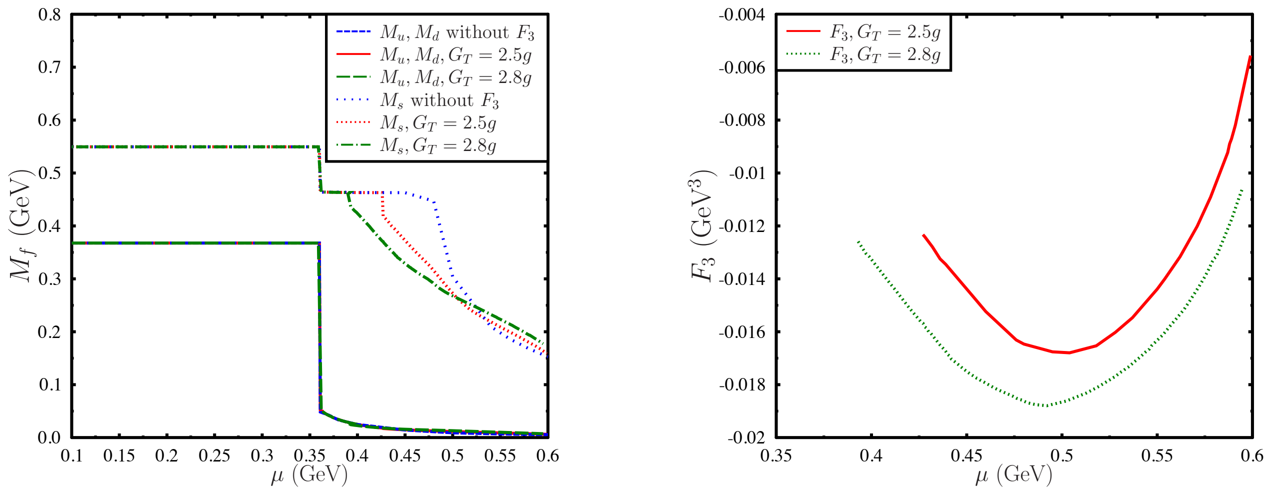

FIG. 4: Left Plot: Dependence of constituent quark mass on the quark chemical potential at zero temperature in the presence as well as in the absence of spin polarization condensation for different values of tensor couplings for $F_8 = F_3/\sqrt{3}$. Sharp jump in the value of M_u and M_s near $\mu = 0.360$ GeV in both plots indicates the first order chiral phase transition which is expected for standard 2+1 flavour NJL model. Right plot: Variation of spin polarization condensate with quark chemical potential at zero temperature with different values of tensor couplings $G_T = 2.5g$ and $G_T = 2.8g$. For larger tensor coupling tensor condensate form at relatively smaller chemical potential and it remains non zero for a wide range of chemical potential.

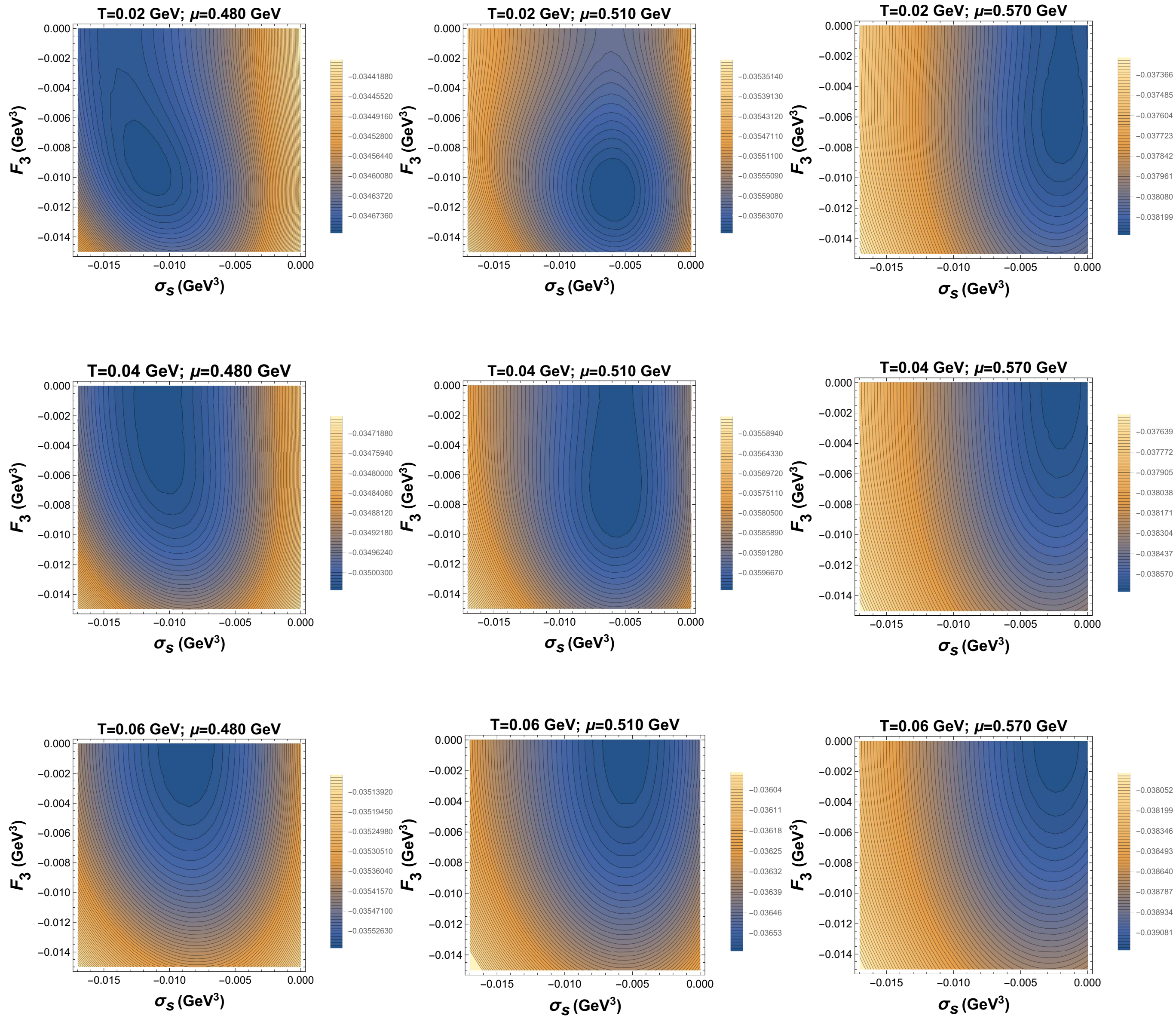

FIG. 5: This figure shows the contour plots of the thermodynamic potential in $\sigma_s - F_3$ plane for finite temperature (T) and finite chemical potential (μ) with $G_T = 2g$ and $F_8 = F_3/\sqrt{3}$. Along each row as we move from left to the right, temperature has been kept fixed but μ is increasing, similarly along each column μ has been kept fixed with T increasing. Darker regions in these contour plots show the global minimum of the thermodynamic potential. It is clear from the plots that at small temperature non zero value of the spin polarization starts to appear at smaller value of the chemical potential and it also melts at higher chemical potential. Thus for smaller temperature the domain of μ where one can get non zero spin polarization is larger. This domain of existence for the spin polarization condensate becomes smaller with increasing temperature T for a given value of G_T. In fact when the temperature is $T = 0.06$ GeV we cannot get spin polarization for any value of μ.

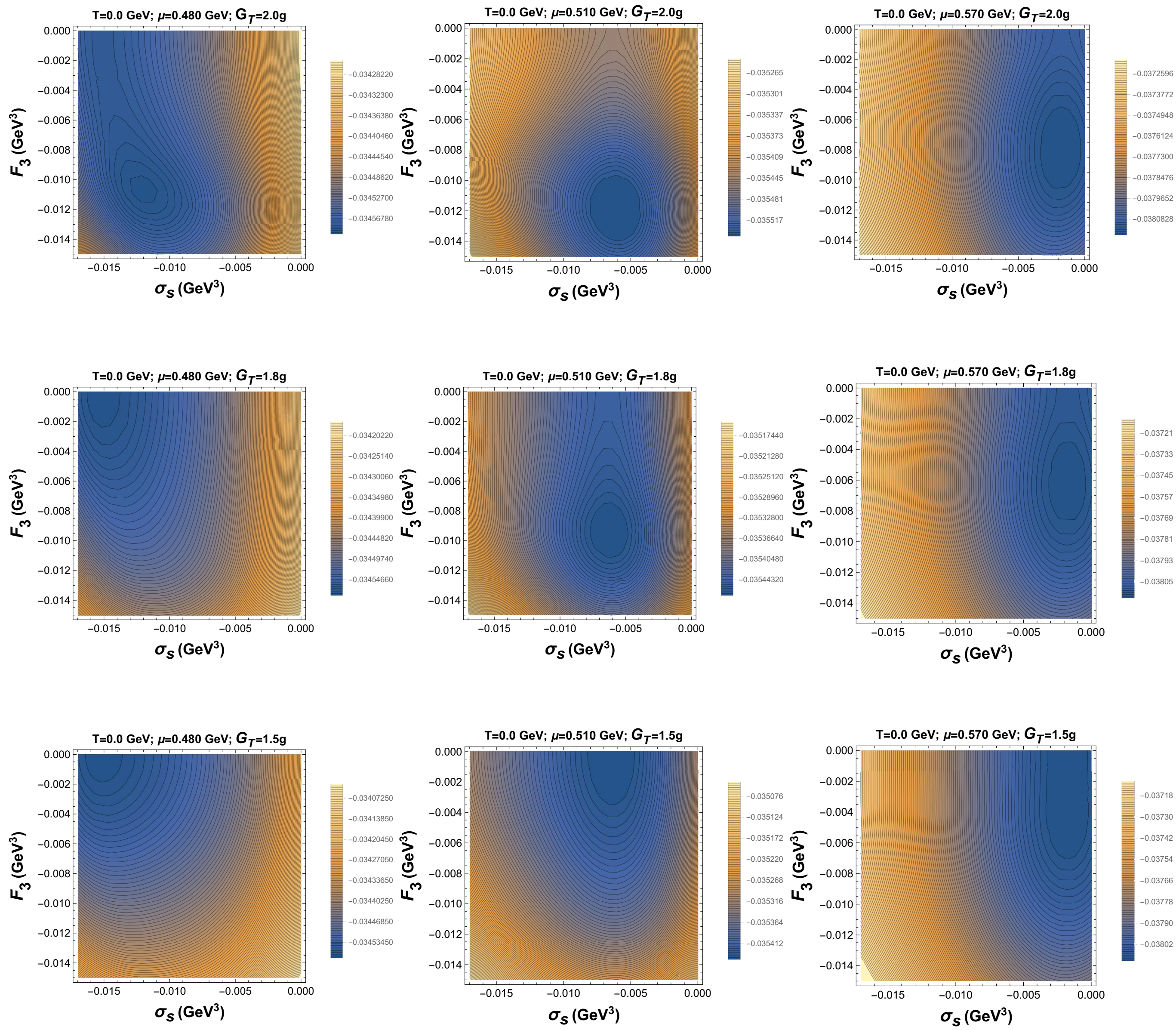

FIG. 6: This figure shows the contour plots of the thermodynamic potential in $\sigma_s - F_3$ plane for zero temperature (T) and finite chemical potential (μ) with different values of tensor coupling G_T and $F_8 = F_3/\sqrt{3}$. In the first, second and the third row the tensor couplings are taken as $G_T = 2g, 1.8g$ and $1.5g$ respectively. Along each row temperature and G_T has been kept fixed but μ is increasing, similarly along each column μ and T has been kept fixed with G_T decreasing. Darker regions in these contour plots shows the global minimum of the thermodynamic potential. It is clear from the plots that at zero temperature, for larger value of tensor coupling spin polarization can exist for a relatively wide range of chemical potential. With the decreasing value of tensor coupling e.g. for $G_T = 1.5g$ spin polarization almost vanishes. This result can be easily extended to finite temperature. For non zero temperature existence of spin polarization requires lager value of G_T.

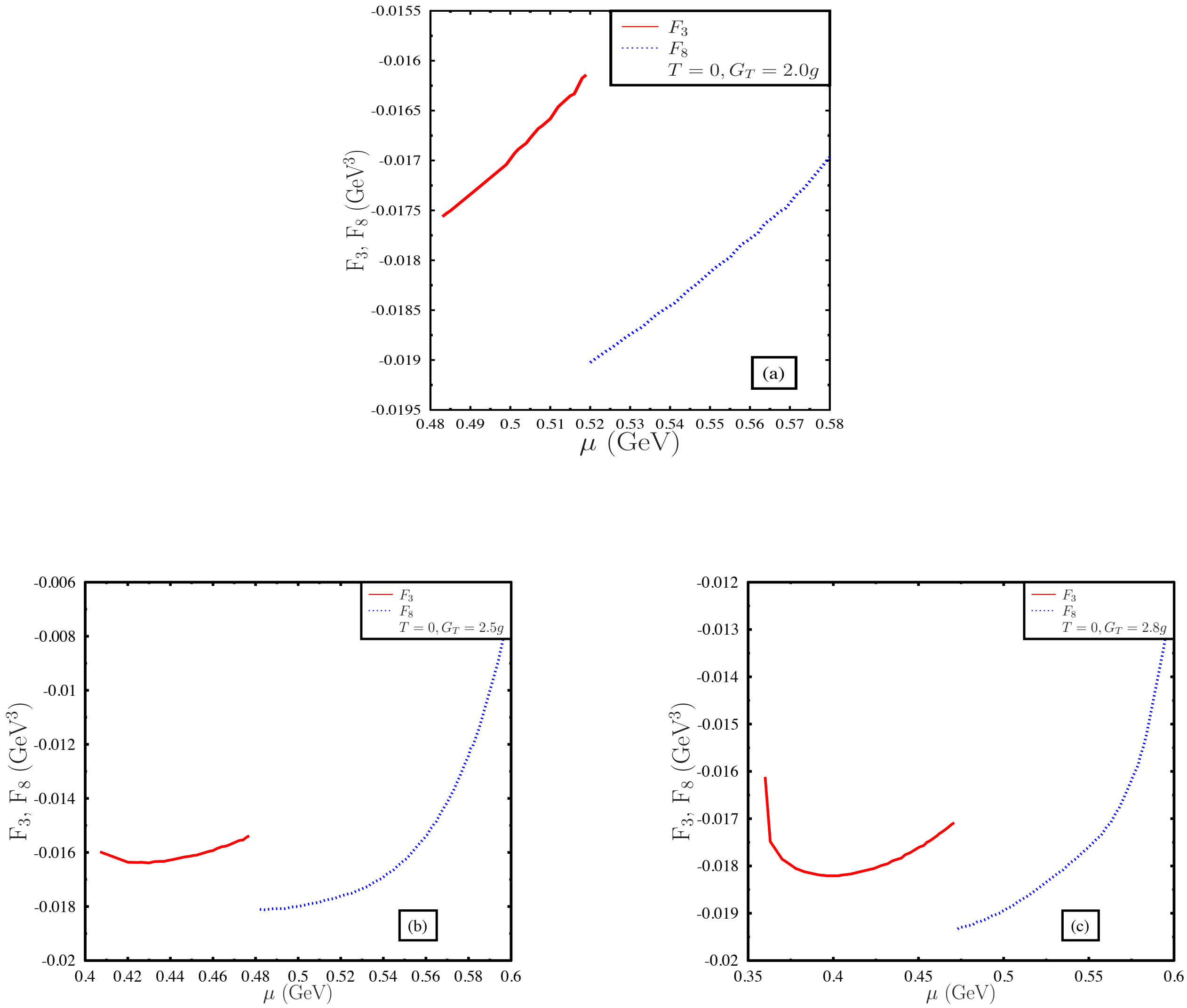

FIG. 7: Plot (a), (b) and (c) show the variation of F_3 (red solid line) and F_8 (blue dotted line) with chemical potential where F_3 and F_8 considered simultaneously in the thermodynamic potential at zero temperature for $G_T = 2g, 2.5g, 2.8g$ respectively. It is clear from the Fig.(7) that non zero F_3 appears at relatively smaller μ than F_8. Since F_8 is associated with strange quark-antiquark condensate it survives even at larger chemical potential relative to the F_3 condensate. It is also important to notice that with larger tensor coupling spin condensates appear at relatively smaller quark chemical potential.